The endocannabinoid system and cognition

Dissertation

zur

Erlangung des Doktorgrades (Dr. rer. nat.)

der

Mathematisch-Naturwissenschaftlichen Fakultät

der

Rheinischen Friedrich-Wilhelms-Universität Bonn

vorgelegt von

Joanna Agnieszka Komorowska-Müller

aus

Szczecin, Polen

Bonn, Juni 2021

Angefertigt mit der Genehmigung der Mathematisch-Naturwissenschaftlichen Fakultät der Rheinischen Friedrich-Wilhelms-Universität Bonn

1. Gutachter: Prof. Dr. Andreas Zimmer
2. Gutachter: Prof. Dr. Gerhard von der Emde

Tag der Promotion: 17.12.2021

Erscheinungsjahr: 2022

Parts of this thesis are included in the following publications:

Komorowska-Müller, J. A., Rana, T., Olabiyi, B. F., Zimmer, A., & Schmöle, A. C. (2021). Cannabinoid receptor 2 alters social memory and microglial activity in an age-dependent manner. Molecules, 26(19), 1–19. https://doi.org/10.3390/molecules26195984

Komorowska-Müller, J. A., Ravichandran, K. A., Zimmer, A., & Schürmann, B. (2021). Cannabinoid receptor 2 deletion influences social memory and synaptic architecture in the hippocampus. Scientific Reports, 11(1), 1–10. https://doi.org/10.1038/s41598-021-96285-9

Komorowska-Müller, J. A., & Schmöle, A. C. (2021). CB2 receptor in microglia: The guardian of self-control. International Journal of Molecular Sciences, 22(1), 1–27. https://doi.org/10.3390/ijms22010019

For all my loved ones. Family and friends.

Abbreviations

Abbreviation	Explanation
2-AG	2-arachidonoylglycerol
ACEA	Arachidonyl-2'-chloro- ethylamide
2P	2-photon
3D	Three-dimensional
A.U.	Arbitrary unit
AD	Alzheimer's disease
AEA	Arachidonoylethanolamine
AF+	Autofluorescence positive
AMPAR	α-amino-3-hydroxy-5-methyl-4-isoxazolepropionic acid receptor
ANOVA	Analysis of variance
Arp2/3	Actin-related protein 2/3 complex
ATP	Adenosine triphosphate
Aβ	Amyloid-β
BDNF	Brain-derived neurotrophic factor
bp	Base pair
BSA	Bovine serum albumin
CA	Cornu Ammonis
cAMP	Cyclic adenosine monophosphate
$CB_1^{-/-}$	Cnr1 knockout mice
CB_1R	Cannabinoid receptor 1
$CB_2^{-/-}$	Cnr2 knockout mice
CB_2R	Cannabinoid receptor 2
CCL	CC-chemokine ligand
CD	Cluster of differentiation
Cnr1	Cannabinoid receptor 1 (gene)
Cnr2	Cannabinoid receptor 2 (gene)
CNS	Central nervous system
CO	Carbon monoxide
Creb	Cyclic AMP response element binding protein
CX3CR1	C-X3-C Motif Chemokine Receptor 1 (fractalkine receptor)
DAGLα	Diacylglycerol lipase α
DAPI	4',6-diamidino-2-phenylindole
DG	Dentate gyrus
DNA	Deoxyribonucleic acid
dNTP	Deoxyribose nucleoside triphosphate
DPSS	Yellow-green diode-pumped solid-state
DSE	Depolarisation-induced suppression of excitation
DSI	Depolarisation-induced suppression of inhibition
E/I	Excitatory/inhibitory balance
ECM	Extracellular matrix
ECS	Endocannabinoid system
ECs	Endocannabinoids
EDTA	Ethylenediaminetetraacetic acid

Abbreviation	Explanation
eGFP	Enhanced green fluorescent protein
EtBr	Ethidium bromide
FAAH	Fatty acid amid hydrolase
GABA	g-aminobutyric acid
GFP	Green fluorescent protein
GPCR	G protein coupled receptor
GPR55	G protein-coupled receptor 55
HeNe	Helium-neon
IBA1	Ionized calcium-binding adapter molecule 1
ID	Identifier
IFNγ	Interferon alpha
IGF1	Insulin-like growth factor 1
IHC	Immunohistochemistry
IL-33	Interleukin 33
IL1R1	ST2, Interleukin 1 receptor-like 1
ITI	Inter-trial interval
i.p.	Intraperitoneal
LD test	Light-dark test
LPS	Lipopolysaccharide
LTD	Long-term depression
LTP	Long-term potentiation
MAGL	Monoacyl glycerol lipase
MGV	Mean grey value
MRI	Magnetic resonance imaging
mRNA	Messenger RNA
mTOR	Mammalian Target of Rapamycin
MWM	Morris water maze
n	Number of stacks/images/cells
N	Number of mice
NA	Numerical aperture
NAPE-PLD	NAPE-phospholipase D
NGS	Normal goat serum
NMDA	N-methyl-D-aspartate
NOLR	Novel object location recognition
o-maze	Elevated zero maze
PBS	Phosphate-buffered saline
PCR	Polymerase chain reaction
PFC	Prefrontal cortex
PKA	Protein kinase A
PR	Partner recognition
PSD	Postsynaptic density
qPCR	Real time quantitative PCR
RGS14	Regulator Of G Protein Signaling 14
RM	Mixed-effects model (REML)
RNA	Ribonucleic acid
ROI	Region of interest
RT	Room temperature

Abbreviation	Explanation
RT-PCR	Reverse-transcription polymerase chain reaction
SEM	Standard error of the mean
s.c.	Subcutaneous
TAE	Tris-acetate-EDTA
TBS	Tris-buffered saline
TE	Tris EDTA
THC	Δ^9-tetrahydrocannabinol
TNFa	Tumor necrosis factor alpha
Tris	Tris (hydroxymethyl) aminomethane
TrkB	Tropomyosin receptor kinase B
TRPV1	Vanilloid receptor type 1
UV	Ultraviolet
vGAT	Vesicular GABA transporter
vGLUT1	Vesicular glutamate transporter 1
VTA	Ventral tegmental area
WAVE1	Wiskott-Aldrich syndrome protein family verprolin homologous protein 1
WRC	WAVE1 regulatory complex
WT	Wild type

STATEMENT: PROJECTS IN THE THESIS

The main project of my thesis, “THC-treatment differentially alters spines dynamics in old and young mice”, involved work with aged mice (18-month old mice). While waiting for mice to age and animal permission to get accepted as well as training in cranial window surgeries and imaging, I engaged in a separate project “Cannabinoid receptor 2 and cognition”. This gave me an opportunity me to become proficient in other techniques including a variety of behavioural tests and immunohistochemical stainings.

Both aforementioned projects are presented here as individual parts of my PhD thesis.

Summary

“THC-treatment differentially alters spines dynamics in old and young mice.”

The endocannabinoid system (ECS) is a neuromodulatory system involved in cognitive processes. Increasing the ECS tone with low-dosage THC - a potent agonist of two main cannabinoid receptors (CB_1R and CB_2R) – has been shown to restore the diminished cognitive abilities of old mice back to the levels of young mice. In contrast, the same treatment in young mice had an opposite or no effect. In old mice, changes in cognition were accompanied by altered gene expression profile. Among others, upregulation of genes encoding synaptic proteins. Thus, pending the question how does THC treatment influences synapses and their dynamics.

We examined the effects of chronic low-dose THC treatment on synapses by following up on the same dendritic spines before, during, and after the THC treatment using in vivo chronic imaging in 3-month and 18-month old mice. Subsequently, in 18-month old animals we investigated THC-evoked changes in microglia activity as a possible mechanism behind observed changes in the spine dynamics.

We found that the timing and direction of the THC effect was age-dependent. In 18-month old mice, THC treatment increased spine density and spine stability, while decreasing spine dynamics. Investigation of microglia activity revealed that THC treatment decreased microglia phagocytic activity and contacts between microglia and neurons. In contrast, in 3-month old mice THC treatment only temporarily increased spine dynamics and thus decreased spine stability.

Taken together, our investigations indicate that THC treatment differentially alters spine dynamics in young and old mice possibly through the modulation of microglial activity.

Summary

“Cannabinoid receptor 2 and cognition”

Although the cannabinoid receptor 2 (CB_2R) is often thought to play a role mainly outside the brain, several publications have comfirem the presence of CB_2R on hippocampal principal neurons. Activation of CB_2R produces a long-lasting membrane potential hyperpolarization, alters the input/output function of CA2/3 principal neurons and produces alterations in gamma oscillations. However, other cellular, molecular and behavioral consequences of hippocampal CB_2R signaling have not been studied in detail.

Here, we investigated the role of CB_2R in cognition in two different aspects. First, we focused on age-related changes in the CB_2R knockout mice ($CB_2R^{-/-}$) using a series of behavioural paradigms testing memory and anxiety-like behaviour. Second, we investigated gender-specific alterations in $CB_2R^{-/-}$ mice in the context of social memory and synaptic architecture using immunohistochemical stainings of synaptic proteins. Our investigation covered synapsin-I, vesicular GABA transporter (vGAT) and vesicular glutamate transporter (vGLUT1).

We found that $CB_2R^{-/-}$ mice had only a minor age-dependent alteration in social memory. In the partner recognition task, 3-month and 12-month old mice performed worse and 18-month old mice preformed better than their age-matched controls. At the same time, we noticed that $CB_2R^{-/-}$ mice exhibited an age-independent decrease in anxiety-like behaviours. Furthermore, we found that the deletion of CB_2R lead to increased synapsin-I signal and particle density, as well as increased vGAT signal in the hippocampus. This phenotype was restricted to females. We confirmed an impairment of social memory in 6-month old CB_2R deficient mice, observed in both genders. Our results thus demonstrate that the lack of CB_2R leads to changes in the hippocampal synaptic landscape and reveals an important gender-specific difference in endocannabinoid signaling.

Our studies support a significant role of the CB_2R in modulation of different types of memory despite its low expression levels in the brain and provides more insight into a gender-specific role of CB_2R in synaptic architecture.

Contents

1. INTRODUCTION: "THC treatment differentially alters spine dynamics in old and young mice"..... 1

1.1. Dendritic spines..... 1

1.1.1. Dendritic spine dynamics..... 3

1.1.2. Dendritic spines in aging..... 5

1.1.3. Microglia regulate spine dynamics..... 5

1.2. Endocannabinoid system..... 7

1.3. Aging..... 10

1.3.1. Brain aging..... 10

1.3.2. Counter-acting the effects of aging by targeting the ECS..... 12

1.4. Aim of the thesis..... 14

2. MATERIALS AND METHODS: "THC treatment differentially alters spine dynamics in old and young mice"..... 15

2.1. Chemicals..... 15

2.2. Solutions..... 16

2.3. Antibodies..... 18

2.4. Medications..... 19

2.5. Mice..... 20

2.5.1. Experimental groups..... 20

2.6. Genotyping..... 20

2.6.1. DNA isolation..... 20

2.6.2. DNA amplification by polymerase chain reaction (PCR)..... 20

2.6.3. Gel electrophoresis..... 21

2.7. Surgeries, 2-photon imaging, and data quantification..... 22

2.7.1. Cranial Window Implantation..... 22

2.7.2. Osmotic pump preparation..... 23

2.7.3. Osmotic pump implantation surgery..... 24

2.7.4. 2-photon imaging..... 24

2.7.5. 2-photon imaging: finding the same dendritic segment..... 25

2.7.6. Dendritic spine analysis..... 26

2.8. Behavioural experiments 28
2.8.1. Partner recognition test (PR) 28
2.8.2. Olfaction test 29
2.8.3. Nestlet test 29
2.8.4. Vision test 30
2.9. Transcardial perfusion 30
2.10. Immunohistochemistry (IHC) 30
2.10.1. Iba1, GFP, CD68 co – staining (prTHC) 30
2.10.2. Image acquisition 31
2.11. Image analysis 32
2.11.1. MOTIQ, 3-dimentional (3D) microglia morphology analysis 32
2.11.2. Microglia soma size and Iba1/CD68 in the soma 33
2.11.3. Microglia density and Iba1/CD68 in whole cells 33
2.11.4. Colocalization of Iba1 and GFP 34
2.12. Statistical analysis and data presentation 34
3. RESULTS: "THC treatment differentially alters spine dynamics in old and young mice" 36
3.1. THC treatment alters spines and their dynamics 36
3.1.1. In vivo imaging: Experimental setup and basic behaviour 36
3.1.2. Long-term low-dosage THC-treatment increases spine density in 18-month old, but not in 3-month old mice 38
3.1.3. Long-term low-dosage THC-treatment differently alters spine dynamics in 18-month and 3-month old mice 40
3.1.4. Long-term effects of THC treatment 42
3.1.5. THC treatment decreases spine stability in 3-month old mice 43
3.1.6. THC treatment increases spine stability in 18-month old mice. 46
3.1.7. THC treatment changes the distribution of spine sizes 49
3.1.8. THC effect does not depend on the initial spine density and weight 50
3.1.9. THC treated 18-month old mice resemble 3-month old mice on the level of spine dynamics. 52
3.2. THC treatment influences microglia activity in old mice 55
3.2.1. THC decreases microglial CD68 levels 55
3.2.2. THC treatment changes microglia morphology in old mice 57
3.2.3. THC treatment does not change microglia density in old mice 59
3.2.4. THC-induced alteration of Iba1 and CD68 levels is brain area-dependent 61
3.2.5. THC treatment decreased microglia-neuron interaction 63

3.3. Evaluation of cognition and other behaviours of THC-treated mice 66

3.3.1. Repeated imaging and testing decreased mice sociability and thus prevented a proper assessment of memory performance 66

4. DISCUSSION: "THC-treatment differentially alters spine dynamics in old and young mice" 70

4.1.1. THC treatment increases spine density in old mice 70

4.1.2. THC treatment in young mice transiently increases spine dynamics and destabilizes synaptic connections 73

4.1.3. THC treatment in old mice decreases spine dynamics and promotes synaptic stability 75

4.1.4. Aging alters spine dynamics 76

4.1.5. THC treated old mice resemble young mice on the level of spine dynamics 77

4.1.6. Cognitive abilities of the animals could not be assessed in chronic imaging paradigm 78

4.1.7. What are the possible mechanisms of THC action on spine dynamics? 79

4.1.8. THC influences microglial regulation of spine dynamics 80

4.1.9. Conclusion and outlook 85

5. INTRODUCTION: "Cannabinoid receptor 2 and cognition" 86

5.1.1. Cannabinoid receptor 2 (CB_2R) 86

5.1.2. CB_2R in cognition 88

5.1.3. CB_2R in anxiety 89

5.1.4. CB_2R in aging 89

5.2. Aim of the thesis 90

6. MATERIALS AND METHODS: "Cannabinoid receptor 2 and cognition" 91

6.1. Mice 91

6.1.1. Experimental groups 91

6.2. Genotyping 92

6.2.1. DNA isolation 92

6.2.2. DNA amplification by polymerase chain reaction (PCR) 92

6.2.3. Gel electrophoresis 93

6.3. Behavioural experiments 93

6.3.1. Partner recognition test (PR) 93

6.3.2. Home - cage activity measurement 94

6.3.3. Olfaction test 94

6.3.4. y-maze 94

6.3.5. Novel object location recognition test (NOLR). 95

6.3.6. Morris water maze (MWM) 95

6.3.7. Light-dark test (LD test) 96
6.3.8. Elevated zero maze (o-maze) 96
6.3.9. Nestlet test 97
6.4. Transcardial perfusion 97
6.5. Immunohistochemistry (IHC) 97
6.5.1. Syn1, RGS14, vGLUT1, vGAT stainings (prCB2b) 97
6.5.2. Image acquisition 98
6.5.3. Image analysis 98
6.6. Statistical analysis and data presentation 99
7. RESULTS: "Cannabinoid receptor 2 and cognition" 100
7.1. "CB_2R in aging" 100
7.1.1. Age-dependent alterations in basic behaviours after $CB_2R^{-/-}$ deletion 100
7.1.2. CB_2R deletion decreases anxiety in an age-independent manner 102
7.1.3. CB_2R deletion has a moderate age-dependent effect on cognition 103
7.1.4. CB2R deletion in 3-month old mice does not alter spatial and working memory, but increases the time that mice spent light compartment of the LD test 106
7.1.5. CB_2R deletion decreases social memory in both male and female mice 108
7.1.6. Sex-specific alterations in basic behaviours after CB_2R deletion. 110
7.1.7. Increased synapsin-I levels and puncta size in the hippocampus after CB_2R deletion in females, but not in males 112
7.1.8. CB_2R deletion alters excitatory and inhibitory synapses in a gender-specific manner 115
8. DISCUSSION: "Cannabinoid receptor 2 and cognition" 121
8.1.1. CB_2R plays a role in social memory in an age-dependent and gender-independent manner 121
8.1.2. Possible role of CB_2R in memory consolidation under specific conditions 123
8.1.3. CB_2R effects anxiety-like behaviour 124
8.1.4. CB_2R in inflammaging 125
8.1.5. CB_2R deletion does not alter basic behaviours 126
8.1.6. CB_2R deletion alters synaptic architecture primarily in female mice 127
9. Bibliography 129
10. Appendix 163
10.1. Detailed statistics table 163
10.2. Acknowledgments 175

1. INTRODUCTION: “THC treatment differentially alters spine dynamics in old and young mice”

1.1. Dendritic spines

Dendritic spines are protrusions on the dendrite, where principal cells receive the majority of excitatory inputs (Gray, 1959; Runge et al., 2020; Walker & Herskowitz, 2020). A single dendritic spine consists of a spine head, where the synaptic structures are localized and a narrow spine neck connecting the spine with the dendritic shaft. Due to their structure spines are compartments with their own electrical and biochemical signaling. The spine neck plays an important role in regulating Ca^{2+} diffusion from the spine to the dendritic shaft (Hayashi & Majewska, 2005; Tønnesen et al., 2014; Yuste et al., 2000). Postsynaptic densities (PSD) are usually found on the head of the spine. The head includes receptors, signaling molecules, neurotransmitters, ion channels and more. (Caceres et al., 1983; Matus et al., 1982; Peters & Kaiserman-Abramof, 1970; M. Sheng & Kim, 2011). The spine’s cytoskeleton defines its shape and allows for its dynamical changes (**see 1.1.1**). The volume of the spine head is proportional to the number of receptors localized on a postsynapse and overall size of the PSD (Freire, 1978; Kasai et al., 2003; Matsuzaki et al., 2001; Špaček, 1985).

Initially, spines have been classified into three different groups based on their morphology: thin, stubby and mushroom (**Figure 1.1**). Later on, a fourth category of filopodia-like spines was added, which was found in developing, young animals. Filopodia-like spines are long (up to 10 μm) and highly unstable protrusions. Filopodia-like spines are able to contact neighbouring axons to form synapses and transform to more stable spine types (Grutzendler et al., 2002; Peters & Kaiserman-Abramof, 1970; N. E. Ziv & Smith, 1996; Zuo et al., 2005). Thus, filopodia-like spines are hypothesized to be a spine precursor form. Their number is high in juvenile mice and decreases in adulthood. However, other types of spinogenesis do not require a filopodia-like state. The common prerequisite of spinogenesis is the proximity of an axonal bouton (Dailey & Smith, 1996; Kwon & Sabatini, 2011; Oh et al., 2016). Mushroom spines, as the name indicates, have a mushroom-like shape with a small neck and big spine head. They frequently have a large volume and are considered the most stable spine type with a high density of α-amino-3-hydroxy-5-methyl-4-isoxazolepropionic acid receptors (AMPARs) (Grutzendler et al., 2002; Knott et al., 2006; Matsuzaki et al., 2001;

Pfeiffer et al., 2018; Trachtenberg et al., 2002; Yasumatsu et al., 2008). Thin spines have long, thin necks. Stubby spines are characterized as spines with relatively small volume and a very short neck frequently appearing as merged with spine head (Tønnesen et al., 2014) (**Figure 1.1**). Both thin and stubby spines have been reported to be less stable than mushroom spines, but more stable than filopodia as they can persist for several days (Holtmaat et al., 2005).

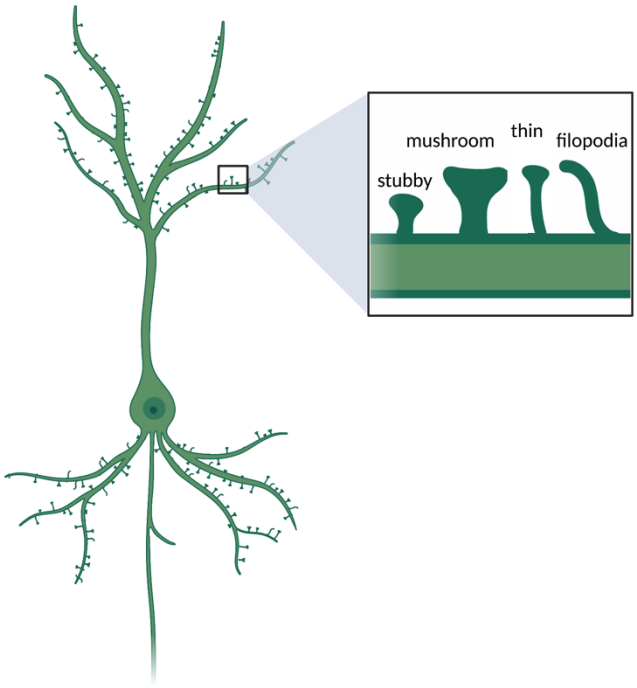

Figure 1.1. Representative illustration of different spine types.

For a long time, spines were only studied in fixed tissue using Golgi staining. It was hypothesized that spines might be plastic as their shape, size and density varied between neurons. Thus, there was a need for new methods enabling a temporal investigation of spines.

The creation of reporter mouse lines having sparse labelling of neurons with fluorescent proteins created a method for a better visual inspection of single dendrites (Feng et al., 2000; Keller-Peck et al., 2001). Subsequent construction of 2-photon (2P) microscopes revolutionized the field as it enabled repeated imaging of the same dendritic segments over a long period of time in live animals (Denk et al., 1990; Grutzendler et al., 2002; Trachtenberg et al., 2002). Follow-up in vivo 2P imaging experiments showed that spines are indeed dynamic structures. Changes occurring at the synapse level resulting in synapse weakening or strengthening subsequently can lead to changes in dendritic spine morphology (Kasai et al., 2003; Matsuzaki et al., 2004; Zhou et al., 2004). For instance, LTP induced by glutamate uncaging near dendritic spines increased their volume and AMPAR current through a mechanism dependent on NMDARs, calmodulin and actin polymerization (Matsuzaki et al., 2004). Conversely, LTD caused dendritic spines shrinkage, also via NMDA-dependent manner and through a mechanism involving cofilin (Zhou et al., 2004). Being highly dynamic structures, the dendritic spines can not only appear or disappear in a site, but may also

change their overall size or even transform from one type to another (Tønnesen et al., 2014). For instance, stimulation of mushroom spines leads to shrinkage of the spine neck, supporting a speculation that stubby spines could be a more active form of mushroom spines (Tønnesen et al., 2014). On the other hand, stimulation of thin spines changes their morphology to more mushroom-like which was interpreted as a creation of more stable synaptic connection (Matsuzaki et al., 2004). In agreement with that, synapses are found more frequently on older spines (Knott et al., 2006). However, there is no straight forward relationship between stability of spines and synapse formation. Transient spines, spines that are appearing and disappearing within a few days, are also able to form functional synapses (Cane et al., 2014).

1.1.1. Dendritic spine dynamics

Dendritic spine dynamics consists of spine loss, gain and stabilization of spines. In adult mice the vast majority (around 80%) of spines are stable and mostly PSD-95 positive (Subramanian et al., 2019). The remaining dynamic spines in mature individuals (around 20%), that are gained and lost, are frequently PSD-95 negative. For a certain dendritic segment, the ‘spine turnover’ represents spine dynamics of the investigated region and is characterized by the amount of lost and gained spines over a fixed period of time (2-3 days) (Grutzendler et al., 2002; Holtmaat & Svoboda, 2009; Majewska et al., 2006; Pfeiffer et al., 2018; Trachtenberg et al., 2002; Zuo et al., 2005).

It was hypothesized that the fraction of dynamic spines might reflect learning capability and plasticity. For example, activity or experience can trigger changes in spine turnover (Dvorkin & Ziv, 2016; Yasumatsu et al., 2008; Zuo et al., 2005). Motor learning increased spine formation and subsequently spine elimination of older spines, thereby maintaining a constant net number of spines (T. Xu et al., 2009; G. Yang et al., 2009). Since learning performance correlated with changes in spine dynamics, it is plausible that plasticity of synapses is the key to memory formation and persistence. In short, memories could be stored as stable synaptic connections.

Changes in spine dynamics are possible through the dynamic rearrangement of actin filaments and transient, activity-dependent entry of microtubules (Bonilla-Quintana et al., 2020; Caceres et al., 1983; Dent, 2017; Hu et al., 2008; Jaworski et al., 2009; Matus et al., 1982). Actin polymerization is a process in which actin monomers (G-actin) polymerize to

form actin filaments (F-actin). Actin polymerization/depolymerization and motility can be regulated via Rho signaling pathways consisting of small G-proteins: RhoA, Rac1 and Cdc42. Of particular interest, the downstream protein complex Wiskott-Aldrich syndrome protein family verprolin homologous protein 1 (WAVE1). WAVE1 plays a key role in actin polymerization and spine maintenance by activating actin-related protein 2/3 complex (Arp2/3) (Walker & Herskowitz, 2020).

The rate of spine dynamics and spine density depends not only on the species, the age of the individual, or behavioural state. It also depends on the investigated brain area, cell layer, cell-type, or even basal versus apical branches of the same neuron (Attardo et al., 2015; Elston & DeFelipe, 2002; Jacobs et al., 2001; Majewska et al., 2006; Tjia et al., 2017). For example, spines in the visual cortex are less dynamic than the ones in auditory or somatosensory cortex (Holtmaat et al., 2005; Majewska et al., 2006). Furthermore, sleep regulates spine dynamics, since spine elimination exceeded spine formation during sleep, whereas wakefulness had the opposite effect (Maret et al., 2011). Sleep also contributes to memory consolidation as it promoted spine formation after motor learning and structural changes of gained spines (W. Li et al., 2017; G. Yang et al., 2014). Also, differences regarding spine turnover have been reported while using thinned-skull versus more invasive cranial window surgery, where a piece of skull is removed and a cover glass is fixed on top of the brain (Grutzendler et al., 2002; Trachtenberg et al., 2002). The latter had showed higher spine turnover for 20 days post-surgery due to a local inflammation and recruitment of glial cells (H. T. Xu et al., 2007).

Spinogenesis is not yet fully understood, but uncaging experiments have proven that it can be triggered by binding of neurotransmitters: glutamate to NMDA receptors and GABA to GABA-A receptors (Kwon & Sabatini, 2011; Oh et al., 2016). It is believed that glutamate participates in spinogenesis throughout life, whereas GABA participates exclusively during early development. While the vast majority of spines contain excitatory synapses, about 15% of spines also host inhibitory synapses (so called “inhibitory spine synapses”) in the cortical pyramidal neurons (J. L. Chen et al., 2012). Inhibitory synapses can now be imaged using 2P in vivo microscopy and Gephyrin-fused fluorophores (J. L. Chen et al., 2012; Villa et al., 2016). Such novel experiments indicated that inhibitory spines are more dynamic than excitatory and even more dynamic than inhibitory synapses formed on the dendritic shaft. Also, not only neurotransmitters, but also neuromodulators have been shown to affect spine

dynamics, since dopamine and serotonin was found to induce structural changes in spines (Bijata et al., 2017; Yagishita et al., 2014).

1.1.2. Dendritic spines in aging

Since aging does not cause neuronal loss, changes in dendritic spine density and dynamics were believed to be associated with age-related cognitive decline (Mitchell & Cusack, 2018). Moreover, dendritic spine loss correlates with impairment in Alzheimer’s Disease (AD) patients and preceded neuronal loss (Boros et al., 2017; DeKosky & Scheff, 1990; Terry et al., 1991). Initial studies have shown that aging caused a decreased synaptic densities in the prefrontal cortex which might primarily be due to the loss of more dynamic, thin spines (Boros et al., 2019; Dickstein et al., 2007; Dumitriu et al., 2010; Young et al., 2014). The remaining thin spines have been shown to have larger heads, which correlated negatively with cognitive performance both in humans and monkeys (Boros et al., 2019; Dumitriu et al., 2010; Young et al., 2014). Thus, it was speculated that spine turnover decreases with age, especially creation of new spines, which would result in the remaining spines being “older” and bigger (Dumitriu et al., 2010). However, all the studies were done ex vivo and thus allowed only for examination of static parameters (like density or morphology) and only hinted what may be the underlying age-related changes in spine dynamics.

Strikingly, recent investigatings using chronic in vivo imaging in the mouse motor and somatosensory cortex showed that aging is associated with an increased spine density and spine dynamics with both gain and loss of spines increased in old mice (Davidson et al., 2020; Mostany et al., 2013). In contrast, another group showed that learning-induced spine plasticity of motor cortex is reduced with age, alongside with spine density (Huang et al., 2020). This warrants more studies to understand age-related changes in spine dynamics under different conditions.

1.1.3. Microglia regulate spine dynamics

Apart from neuronal mechanisms controlling spine dynamics, multiple studies implicated that glia cells can participate in this process (Miyamoto et al., 2013). Under pathological conditions, microglia are capable of removing dysfunctional synapses in a process called

synaptic stripping (Blinzinger & Kreutzberg, 1968; Z. Chen et al., 2014; Kettenmann et al., 2013). This way microglia aid in the healing process and help to restore brain homeostasis.

On the other hand, during development, microglia regulate growth and maintenance of dendritic spines (Nguyen et al., 2020; Paolicelli et al., 2011). As mentioned above, spine density decreases between early life and adulthood alongside the number of filopodia-like spines. Microglia actively participate in spine removal by engulfment of synapses. This process has been named synaptic pruning. Decreasing microglial function by decreasing autophagy or deleting the CX3CR1 or complement receptor, impaired synaptic pruning and increased the number of immature synaptic connections (Kim et al., 2017; Paolicelli et al., 2011; Schafer et al., 2012). On the behavioural level, it resulted in an autism spectrum disorder-like phenotype with social deficits and repetitive behaviours (Kim et al., 2017; Zhan et al., 2014). Furthermore, many studies confirmed the role of microglia in proper circuit formation and maturation as lack of the mentioned components resulted in hyperexcitability (Chu et al., 2010; Schafer et al., 2012; Zhan et al., 2014). Aside from synaptic pruning, other studies have shown that microglia can elicit Ca^{2+} transients and also participate in filopodia formation (Miyamoto et al., 2016).

Microglial engulfment of synapses decreased significantly after postnatal day 5 and continued to do so as mice matured (Schafer et al., 2012). Despite that, microglia unequivalently play a role in synaptic plasticity and remodelling in adult mouse brain. Firstly, microglia are frequently found in close proximity to dendritic spines and microglia activity and spatial localization is modulated by experience (Ying Li et al., 2012; M. Ě. Tremblay et al., 2010; Wake et al., 2009). Microglia were frequently found near small, unstable, and transient spines with average lifetime of less than 2 days (M. Ě. Tremblay et al., 2010). Another study confirmed a negative correlation of microglia proximity and spine stability (Iida et al., 2019). Similarly, increasing the duration of microglia-neuron interactions elevated spine turnover and spine-head filopodia formation (Cangalaya et al., 2020). Secondly, microglia have been shown to participate in learning-induced synapse formation through a mechanism involving brain-derived neurotrophic factor (BDNF) signaling (Parkhurst et al., 2013). Mice that were depleted of microglia had decreased spine dynamics as both loss and gain of spines were reduced. Moreover, microglia depletion caused learning capability to deterioratate in mice and decreased their learning-induced spine formation. In agreement with that, a recent investigation has further proven that microglia are key players in enabling spine dynamics by

phagocytosing extracellular matrix components after learning (Nguyen et al., 2020). Also, another study suggested that microglia phagocytose synapses selectively and partially, rather than entirely through a process named “trogocytosis” (Weinhard et al., 2018). This process is rapid, therefore it can be rarely identified in fixed tissue. Both studies showed that microglia take part in spine-head filipodia induction, which is interpreted as an increase in plasticity (Nguyen et al., 2020; Weinhard et al., 2018). Another recent investigation showed that microglia participate in forgetting of remote memories by engulfing synaptic components (C. Wang et al., 2020). Lastly, activity of synapses increased after direct microglial contact (Akiyoshi et al., 2018). All of these discoveries collectively place microglia as a key facilitator of synaptic remodelling.

In adult brains microglia participate in adult neurogenesis (Ekdahl, 2012; Gemma & Bachstetter, 2013; Y. Ziv & Schwartz, 2008). Microglia depletion or deletion of CX3CR1 resulted in reduced spine density and dynamics accompanied by an increased number of contacts between spines and microglia in adult-born-granule-cells (Reshef et al., 2017). Moreover, $CX3CR1^{-/-}$ mice were shown to have memory deficits and impairment of LTP (Rogers et al., 2011). Conversely, LTP induction altered microglia dynamics. LTP increased microglial processes as well as prolonged microglia contacts with potentiated neurons (Pfeiffer et al., 2016).

Taken together, it is evident from previous studies that microglia play a role in both elimination and formation components of spine dynamics and are crucial regulators of neuronal excitability. Although, understanding how microglia regulates spine dynamics in the context of aging is still elusive.

1.2. Endocannabinoid system

ECS is a neuromodulatory system that plays a major role in many vital processes from neuronal activity to immune modulation. It consists of endocannabinoids (ECs), their receptors, and synthesizing and degrading enzymes. The most abundant ECs are small lipophilic molecules: 2-arachidonoylglycerol (2-AG) and arachydonoylethanolamide (AEA, anandamide) that are produced from membrane phospholipids through an enzymatic reaction (William Devane et al., 1992; Mechoulam et al., 1995). The main 2-AG synthesizing enzyme is diacylglycerol lipase-α (DAGLα), whereas for AEA it is N-acyl phosphatidylethanolamine phospholipase D (NAPE-PLD) (**Figure 1.2**). The main hydrolysing

enzyme of cannabinoids is fatty acid amid hydrolase (FAAH) and monoacyl glycerol lipase (MAGL) degrading AEA and 2-AG, respectively. The exogenous cannabinoids such as cannabidiol or (-)-Δ9-trans-Tetrahydrocannabinol (THC) are well known and are the ligands of both cannabinoid receptors (Gaoni & Mechoulam, 1964; Pertwee, 2008). The two main cannabinoid receptors are the cannabinoid receptor 1 (CB_1R, encoded by *Cnr1* gene) and cannabinoid receptor 2 (CB_2R, encoded by *Cnr2* gene) (**Figure 1.2**, (WA Devane et al., 1988; Munro et al., 1993)). Both cannabinoid receptors are G-protein-coupled receptors (GPCRs). In the brain, CB_1R is one of the most abundant GPCRs (Herkenham et al., 1990). CB_1R is expressed on a high level in hippocampus, cerebellum and cortex, which conveys into its role in cognition, movement and emotional behaviour (Eggan & Lewis, 2007; Herkenham et al., 1990; Mechoulam & Parker, 2013). CB_1R was found on both g-aminobutyric acid (GABA)ergic and glutamatergic neurons, although its expression in the latter was three to ten times lower (Kawamura et al., 2006; Uchigashima et al., 2007). Apart from the main two types of cannabinoid receptor, other known types include vanilloid receptor type 1 (TRPV1) and G protein-coupled receptor 55 (GPR55) (A. J. Brown, 2007).

In the CNS, ECs are produced on demand from membrane lipids in an activity-dependent manner. ECs production is triggered by the activation of $G_{q/11}$-coupled metabotropic glutamate receptors or the mobilization of Ca^{2+} in the postsynapse. Subsequently, ECs are released into the synaptic cleft and in a retrograde fashion bind to the presynaptic CB_1R (**Figure 1.2**, (Howlett et al., 2002; Kano et al., 2009)). CB_1R is linked to $G_{i/o}$ protein, acting through the inhibition of the adenyl cyclase activity and subsequent downregulation of the cyclic adenosine monophosphate/protein kinase A (cAMP/PKA) pathway. That in turn leads to a decrease in neurotransmitter release (Chevaleyre et al., 2007; Heifets & Castillo, 2009; Mechoulam & Parker, 2013). Alternatively, for short-term plasticity, G-protein can directly inhibit voltage-gated Ca^{2+} channels and thus decrease Ca^{2+} influx to the presynapse (S. P. Brown et al., 2003; Kreitzer & Regehr, 2001; Rachel I. Wilson et al., 2001). This phenomenon is called depolarization-induced suppression of inhibition (DSI) and depolarization-induced suppression of excitation (DSE), for inhibitory and excitatory synapses respectively (Kreitzer & Regehr, 2001; Ohno-Shosaku et al., 2001; R. I. Wilson & Nicoll, 2001). However, evidence have also suggested that aside from their retrograde signaling, ECs can also function in an autocrine fashion by binding to the CB_2R receptors localized on the postsynaptic site and thus regulate the excitability of the

postsynapse (**see 5.1.1**). Moreover, the ECs has been also reported to participate in the induction of long-term potentiation (LTP) and long-term depression (LTD) (Chevaleyre et al., 2007; Singla et al., 2007). Although CB_1R is mostly localized on the cell membrane, its expression was also detected on the mitochondrial membrane regulating respiration and mitochondrial signaling (Melser et al., 2017).

In the brain, CB_1R has also been found on other cell types including astrocytes and microglia, but its expression at baseline was rather low (Castillo et al., 2012; Stella, 2009). It has been hypothesized that the ECS can play a role in microglia-neuron communication. For instance, we have previously shown that CB_1Rs on GABAergic neurons play a role in neuron–microglia communication via fractalkine/CX3CR1 (Ativie et al., 2018). Moreover, AEA (and possibly 2-AG as well) can be secreted via microglial extracellular membrane vesicles and can inhibit synaptic transmission of GABAergic neurons by activating CB_1R (Gabrielli et al., 2015).

In the periphery, ECS is present in a variety of systems including cardiovascular system, gastrointestinal system, immune system, muscles, bones, skin and reproductive system (Maccarrone et al., 2015).

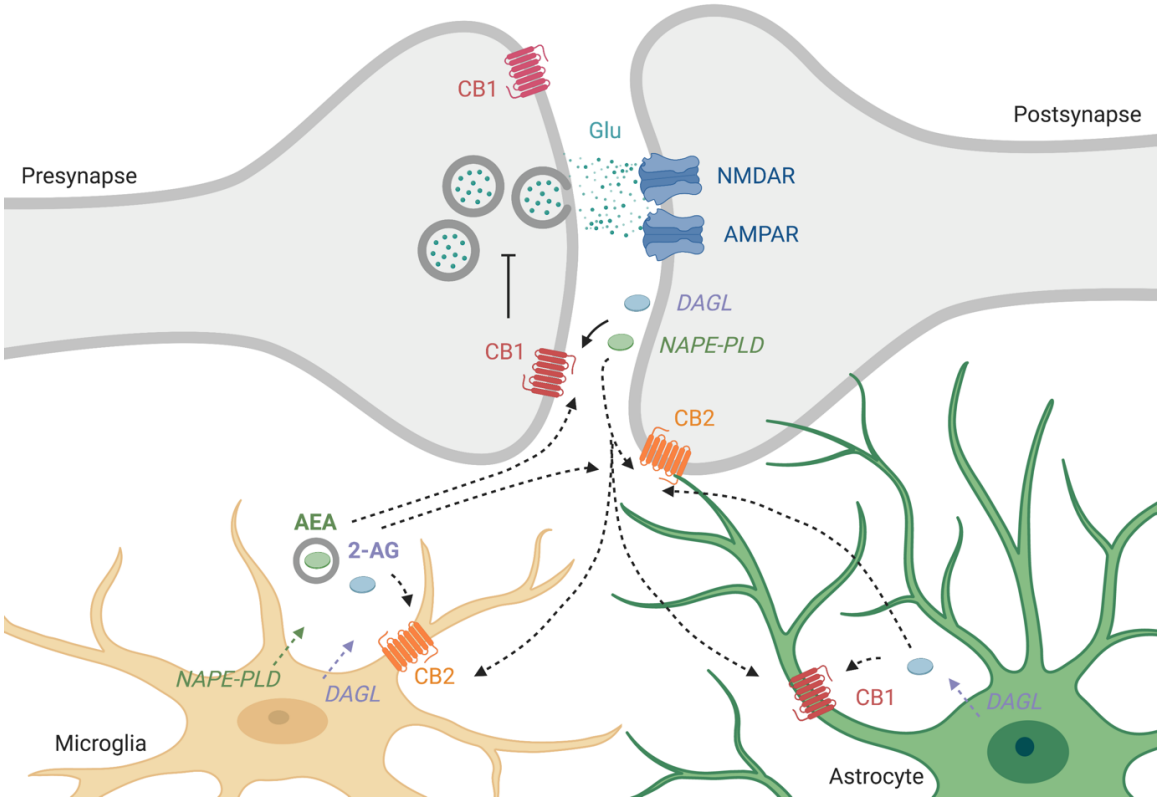

Figure 1.2. ECS components are expressed by microglia, astrocytes and neurons. (A) Overview showing ECS components in both pre- and postsynaptic sites of neurons, in microglia and astrocytes. Full lines represent interactions supported by evidence, whereas dotted lines represent putative interactions. CB_2R — cannabinoid receptor 2, CB_1R — cannabinoid receptor 1, DAGL — diacylglycerol lipase-α, NAPE-PLD — N-acyl phosphatidylethanolamine phospholipase D, 2-AG — 2-arachidonoylglycerol, AEA — arachidonoylethanolamide. (modified from Komorowska-Müller & Schmöle, 2021)

1.3. Aging

1.3.1. Brain aging

Although aging is a natural process, it shares some of the characteristics with pathologies. Aging is also a risk factor for many diseases including cancer (Gems & Partridge, 2013; White et al., 2014). Cellular processes accompanying aging have been categorized into hallmarks and pillars of aging (Kennedy et al., 2014; López-Otín et al., 2013). Lopez-Otin described nine hallmarks of aging fitting into three main categories (López-Otín et al., 2013). The first category includes the primary hallmarks that are believed to be causative regarding cellular damage. Primary hallmarks were: telomere attrition, epigenetic alterations, genomic instability, and loss of proteostasis. The second group included antagonistic hallmarks described as a response to the damage. Such response can be beneficial at small magnitude, but devastating at a larger scale or after longer duration. Antagonistic hallmarks included: cellular senescence, deregulated nutrient sensing, and mitochondrial dysfunction. The last category consisted of integrative hallmarks. Integrative hallmarks were called culprits of the phenotype due to their direct functional impact. This group included stem cell exhaustion and altered cellular communication. Kennedy on the other hand identified seven pillars of aging: epigenetics, inflammation, adaptation to stress, macromolecular damage, proteostasis, stem cell regeneration, and metabolism (Kennedy et al., 2014).

In the brain many of these hallmarks and pillars can be uniquely affected. For instance, neurons are mostly postmitotic cells. This indicates that primary hallmarks, such as telomere attrition and genomic instability, which occur mostly due to repeated cell division, are not predominantly affecting neurons. However, glial cells are known to actively divide. Therefore, glial cells might be mainly affected by these two processes. Similarly, cellular senescence has been shown to primarily affect glial cells as well as neural stem cells (Flanary & Streit, 2004; Nicaise, Willis, Crocker, & Pluchino, 2020; Streit & Xue, 2014 and more). Senescence is a permanent arrest of the cell cycle accompanied by a unique secretory profile with increased expression of extracellular matrix degrading enzymes and inflammatory mediators (Campisi, 2005; Campisi & D'Adda Di Fagagna, 2007; Deleidi et al., 2015). It is believed to be a cell protective mechanism against cancer development (Collado et al., 2007). Arrest of the cell cycle prevented the cells from further division and thus limiting the spread of damaged cells. Strikingly, senescence has been shown to spread to neighbouring cells (so called "bystander effect") and thus was shown to affect entire tissues (Nelson et al., 2012).

In contrast to previously described hallmarks, stem cell exhaustion primarily affects neurons. Aging was shown to decrease the adult neurogenesis rate and number of neuronal stem cells (Villeda et al., 2011).

Another important hallmark of aging is disrupted cellular communication. In the brain, aging affects the communication between microglia and neurons. Disrupted microglia-neuron communication results in increased inflammatory status of the brain (Kennedy et al., 2014; López-Otín et al., 2013).

Microglia are the resident immune cells of the brain and account for 10–15% of central nervous system (CNS) cells (Lawson et al., 1992). Resting microglia constantly scan their surroundings by extending and retracting numerous protrusions and react to changes in their environment (Nimmerjahn et al., 2005). As soon as microglia detect neuronal damage or an infectious component, they rapidly change their morphology and proliferate. They become very motile, travel to the injury site to actively phagocytose debris and damaged neurons, and trigger an inflammatory response (Fuhrmann et al., 2010). Reactive microglia become very motile, travel to the injury site to actively phagocytose debris and damaged neurons (Fuhrmann et al., 2010). Microglia also release proinflammatory mediators such as different chemokines and cytokines and aid in the recruitment of other inflammatory cells (Hickman et al., 2018). Activation of microglia goes along with an increase of proteins including cluster of differentiation 68 (CD68) and Ionized calcium-binding adapter molecule 1 (IBA1) (Hopperton et al., 2018; Jurga et al., 2020). Once the threat has passed, the microglia switch to the anti-inflammatory phenotype and try to dampen further inflammation and induce the healing process. They express anti-inflammatory mediators including different cytokines (IL-4, IL-10, IL-13), metabolic or tissue remodelling factors (chitinase-3-like protein 3, arginase 1) or tropic factors (insulin-like growth factor 1 (IGF1), transforming growth factor-β). They also facilitate phagocytosis of cell debris (Tang & Le, 2016).

Control of microglia is crucial for maintaining homeostasis due to their protective functions. Lack of an efficient, ongoing bidirectional communication between neurons and microglia might trigger microglia to switch to a reactive phenotype. As a result microglia could potentially cause uncontrollable damage (Eyo & Wu, 2013). Nowadays many possible communication routs are still under investigation. Generally neurons are believed to be the ones controlling microglia and suppressing their offensive functions (Chavarría & Cárdenas, 2013). One possible mechanism through which such a control could take place is via a direct

interaction of surface proteins (Bessis et al., 2007; Cardona et al., 2006; Hoek et al., 2000). An example of such a protein is the neuronally expressed chemokine fractalkine and its receptor C-X3-C Motif Chemokine Receptor 1 (CX3CR1), which is present on microglia (Cardona et al., 2006). Neuronal loss during neurodegeneration and consequent loss of these interacting surface proteins activates microglia, thus CX3CR1 is believed to be neuroprotective in neurodegenerative diseases (Cardona et al., 2006). It was recently shown that microglia lacking CX3CR1 exhibited a transcriptome resembling aged microglia (Gyoneva et al., 2019).

Aging is accompanied by a low-grade inflammation defined as inflammaging (Franceschi et al., 2000; Franceschi & Campisi, 2014). Aged microglia frequently have dystrophic morphology with increased pro-inflammatory and phagocytic activity and decreased neuroprotective functions (DiPatre & Gelman, 1997; J. G. Sheng et al., 1998; Shobin et al., 2017; Sierra et al., 2007). After inflammatory stimulation they elicit an exacerbated immune response. Thus, it is believed that aging and possibly other inflammatory events of past are sufficient to prime microglia. Priming of microglia exacerbated their reaction after assaults including infections or even stress (Cunningham et al., 2005; Niraula et al., 2017). As mentioned above, microglial functions in aged brain are further hindered due to the spreading senescence. Hence, not only microglia respond stronger to previously neutral stimuli, but partly their surveillant and neuroprotective activity is also suppressed. Also, disrupted activity of microglia can further accelerate the progression of the immune-dependent conditions (Deeks, 2011). Moreover, the tightly controlled blood-brain-barrier becomes leakier with age leading to infiltration of the peripheral immune cells to the immune-privileged brain (Banks et al., 2021; Montagne et al., 2015). The infiltration can further increase the ongoing low-grade inflammation.

The different activation states of microglia with their positive and negative aspects are of great importance to keep an inflammatory balance in the brain. Within the last decade, several evidences arose that the endocannabinoid system (ECS) and especially CB_2Rs regulate the activation of microglia (Komorowska-Müller & Schmöle, 2021).

1.3.2. Counter-acting the effects of aging by targeting the ECS

ECS, known for its anti-inflammatory, neuromodulatory, and neuroprotective function, emerged as a possible target in counter-acting brain aging. Especially, taking into

consideration that an accelerated aging phenotype was exhibited in mice lacking CB_1R. Accelerated aging in $CB_1R^{-/-}$ mice have been characterized by a premature cognitive decline, gliosis and increased expression of inflammatory cytokines in the brain (Albayram et al., 2011; Albayram, Bilkei-gorzo, & Zimmer, 2012; Bilkei-Gorzo et al., 2005; Bilkei-Gorzo et al., 2012). At the same time, overall endocannabinoid tone decreased with age as 2-AG level and DAGLα expression declined between 2 and 12-month mice alongside with CB_1R binding to G-protein (Yannick Marchalant et al., 2008; Piyanova et al., 2015; Romero et al., 1998).

Initial trials to counter aging by elevating ECS tone using exogenous ligands were promising. A chronic, low-dosage treatment with WIN-55,212–2, a non-selective cannabinoid receptor agonist, increased hippocampal neurogenesis and restored cognitive abilities in old female rats (Y. Marchalant et al., 2009; Yannick Marchalant et al., 2008). Almost a decade later, another CB_1R/CB_2R agonist - THC was used in old male mice (Bilkei-Gorzo et al., 2017). A chronic low-dosage THC treatment of 18-month old mice restored their cognitive abilities to the level of 2-month old mice. Memory improvement was accompanied by an increase in synaptic proteins. Also, the gene expression pattern of old THC-treated mice resembled more with young mice than with that of age-matched controls. The researchers also observed changes in histone acetylation and an increase in dendritic spine densities in the hippocampus as hinted by a Golgi staining. Together, both studies provide evidence that elevating ECS tone in old individuals can be a valid method for counter-acting the age-related cognitive decline.

In young individuals, on the other hand, THC usage can have detrimental consequences (Ameri, 1999). In humans, THC can produce euphoria and an enhancement of sensory perception, but also tachycardia, attention and cognitive deficits (Solowij et al., 1995). The latter deficits have been reported to persist even after a period of abstinence. Studies done both in humans and animal models suggested that the extent of cognitive deficits depends on the age of initial usage (Dragt et al., 2010). Although, it is unclear if this arises from the age-dependent changes in the biological mechanism or socioeconomical situation as earlier users tend to become more heavily dependent. This in turn impacts their future education opportunities. On the other hand, THC usage in young individuals might cause permanent structural and functional alternations in the still maturing brain (Welch et al., 2011). On a cellular level, THC can prove neurotoxic even at doses comparable to THC plasma concentration after marijuana usage. THC increased apoptosis observed by shrinkage

of neuronal cell bodies and DNA fragmentation (Chan et al., 1998). Thus, it is crucial to further investigate THC effect in different age groups and its impact on the brain.

1.4. Aim of the thesis

The aim of my study was to understand how low-dosage, chronic THC treatment affects spine dynamics in young and old mice. In particular, how spine density, gain, loss, and stability of dendritic spines are influenced by the THC treatment and which changes are long-lasting. Subsequently, I hypothesized that microglial cells play a role in the observed THC-induced spine dynamics changes. Therefore, I aimed to prepare a comprehensive overview of changes in microglia activity, morphology, proliferation, and microglia-neuron interactions after THC treatment in old mice. Finally, I aimed to correlate changes in spine dynamics with altered cognitive abilities during the course of the treatment.

2. MATERIALS AND METHODS: “THC treatment differentially alters spine dynamics in old and young mice”

2.1. Chemicals

Chemical	Company (catalog number)
100 bp DNA ladder	Life Technologies (15628-050)
2-Methylbutane/isopentane	Sigma-Aldrich (320404)
2-Propanol/isopropanol	Carl Roth (6752.4)
4’,6-Diamidino-2-phenylindole dihydrochloride (DAPI)	Sigma-Aldrich (10236276001)
Albumin bovine Fraction V, pH = 7.0 (BSA)	Serva (11930.04)
Citric acid	Promega (H526a)
dNTP mix (10 mM)	Sigma-Aldrich (D7295)
Ethanol (EtOH) absolute	VWR (20821.330)
Ethidium bromide solution (10 mg/ml)	Sigma-Aldrich (E1510)
Ethylenediaminetetraacetic acid (EDTA), disodium salt	Calbiochem (324503)
Ethylene glycol	Honeywell (102466)
Fluoromount-G®	SouthernBiotech (0100-01)
Glycerin	Roth (3783.2)
Hydrochloric acid (HCl) 37%	Carl Roth (X942.1)
Na_2HPO_4	Sigma-Aldrich (S5136)
NaH_2PO_4	Sigma-Aldrich (S0751)
Normal goat serum	Abcam (ab7481)
Paraformaldehyde (PFA)	Sigma-Aldrich (P6148)
Phosphate-buffered saline (PBS) tablets	Gibco (18912014)
Proteinase K	NEB (P8107S)
Sodium chloride (NaCl)	Carl Roth (9265)
Sodium dodecyl sulphate (SDS)	Carl Roth (2326)
Sucrose	Sigma-Aldrich (84100)
Taq Polymerase (10x ThermoPol buffer)	NEB (M0267X)
Tris-(hydroxymethyl)aminomethane (Tris base)	Carl Roth (5429)
Tris-HCl	Carl Roth (9090.3)
Triton™ X-100 detergent	Sigma-Aldrich (T9284)
TWEEN® 20	Sigma-Aldrich (P9416)
UltraPure™ agarose	Invitrogen (15510-027)

2.2. Solutions

Genotyping

Solution/buffer	Composition
Lysis buffer	MilliQ H_2O
	100 mM Tris/HCl pH = 8.0
	5 mM EDTA
	200 mM NaCl
	0.2% (w/v) SDS
	Proteinase K (1 mg/ml) (added last)
EtBr bath solution	TAE buffer
	1.5 µg/ml ethidium bromide
Tris-EDTA (TE) buffer, pH = 7.4	MilliQ H_2O
	10 mM Tris
	1 mM EDTA, pH = 8.0
Tris-acetate-EDTA (TAE) buffer	MilliQ H_2O
	40 mM Tris-acetate
	1 mM EDTA pH = 8.0

Immunohistochemistry

Solution/buffer	**Composition**
4% formaldehyde	PBS + 4% (w/v) PFA, filtered
Cryoprotection solution	PBS
	10-30% (w/v) sucrose
PBS pH = 7.4 (500 ml)	500 ml MilliQ H_2O
	1 PBS tablet
Iba1, GFP, CD68 co–staining	
Blocking solution (prepared freshly before usage)	PBS-T 0.5%
	10% (v/v) NGS
	2% (w/v) BSA
Antibody solution (prepared freshly before usage)	PBS-T 0.1%
	5% (v/v) NGS
	2% (w/v) BSA
Antifreeze (free folating sections) 500 ml	0.785 g NaH_2PO_4
	2.59 g Na_2HPO_4
	200 ml MilliQ water
	150 ml Glycerin
	150 ml Glycol
Syn1, RGS14, vGLUT1, vGAT stainings	
Permeabilization buffer (prepared freshly before usage)	TBS + 0.3% (v/v) Triton X-100
Citrate buffer pH = 6.0 (1 l) (antigen retrieval)	1.92 g citric acid
	0.5 ml Tween-20
	filled to 1 l with MilliQ H_2O
Blocking/Antibody solution (prepared freshly before usage)	TBS-T 0.3%
	10% (v/v) NGS
	2% (w/v) BSA
TBS (1 l) pH = 7.5	6.05g Tris base
	8.76 g NaCl
	filled to 1 l with MilliQ H_2O

2.3. Antibodies

PRIMARY ANTIBODIES						
Antigen	**Conjugate**	**Host**	**Dilution**	**Company**	**Catalog #**	**RRID**
IBA1	-	Rabbit	1 to 1000	FUJIFILM Wako	019-19741	AB_839504
CD68	-	Rat	1 to 1000	Bio-Rad	MCA1957	AB_322219
GFP	-	chicken	1 to 2000	Abcam	ab13970	AB_300798
Synapsin-I	-	rabbit	1 to 250	Abcam	ab64581	AB_1281135
vGLUT1	-	guinea-pig	1 to 1000	Millipore	AB5950	AB_2301751
vGAT	-	guinea-pig	1 to 200	Synaptic Systems	131 004	AB_887873
RGS14	-	mouse	1 to 5	NeuroMab	73-170	AB_10698026
SECONDARY ANTIBODIES						
rabbit IgG	AF 647	goat	1 to 1000	Thermo Fisher Scientific	A21245	AB_2535813
rat IgG	AF 594	goat	1 to 1000	Thermo Fisher Scientific	A11007	AB_10561522
chicken IgG	AF 488	goat	1 to 1000	Thermo Fisher Scientific	A11039	AB_2534096
rabbit IgG	AF 488	goat	1 to 1000	Thermo Fisher Scientific	A11008	AB_143165
guinea pig	AF 647	goat	1 to 1000	Abcam	ab150187	AB_2827756
mouse IgG	AF 568	goat	1 to 1000	Thermo Fisher Scientific	A11031	AB_144696

2.4. Medications

Medications (list of stock solutions and providers)

Mediciation	Company
Atipamezolhydrochlorid (Antisedan®)	Orion Corporation, Espoo, Finland
Buprenorphin	Tensgenic (0.3 mg)
Carprofen (Rimadyl®) Injektionslösung	Zoetis Deutschland GmbH, Berlin
Fentanyl	Janssen-Cilag GmbH
Flumazenil Injetions-/Infusionslösung	Hikma Farmacêutica, Portugal
Ketaminhydrochlorid Injektionslösung	Bela-pharm gmbH & Co. KG, Vechta
Medetomidinhydrochlorid (Cepetor®) Injektionslösung	CP-Pharma, Burgdorf
Midazolam Injektions-/Infusionslösung	PUREN Pharma, München
Naloxonhydrochlorid (Naloxon-ratiopharm®) Injektionslösung	Ratiopharm gmbH, Ulm
Natriumchlorid Isotonische Kochsalzlösung (Saline)	Fresenius Kabi, Bad Homburg
Xylazin (2%)	Bela-pharm gmbH & Co. KG, Vechta

Medications (working solutions)

Working solution	Medication	Amount [ml]
MMSLEEP	Midazolam	2.5
	Medetomidinhydrochlorid	0.5
	Saline	7
MMWAKE	Flumazenil	5
	Atipamezolhydrochlorid	0.5
	Saline	4.5
carprophen	Carprofen	0.1
	Saline	9.9
MMFSLEEP	Midazolam	2.5
	Medetomidinhydrochlorid	0.5
	Fentanyl	1
	Saline	6
MMFWAKE	Flumazenil	5
	Atipamezolhydrochlorid	0.5
	Naloxonhydrochlorid	3
	Saline	1.5
ketamine+xylazine	Ketaminhydrochlorid	2
	Xylazine	1
	Saline	3
buprenorphin	Buprenorphin	1
	Saline	5

2.5. Mice

We used Tg(Thy1-EGFP)MJrs/J (GFP-M) mice ((Feng et al., 2000), IMSR Cat# JAX:007788, RRID:IMSR_JAX:007788). These mice express enhanced green fluorescent protein (eGFP) under Thy1 promoter, which results in a sparse neuronal labelling. Mice were bred in the animal facility of the University of Bonn. After weaning mice were transferred to a mouse storage room in the laboratory. Mice were grouped-housed in standard laboratory cages with automatic ventilation system and *ad libitum* water and food access under 12 hour light-dark cycle (lights on at 07:00 am). Cages were monitored daily and bedding, water, and food were changed weekly.

Care of the animals and conduction of the experiments followed the guidelines of the European Communities Directive 86/609/EEC and the German Animal Protection Law regulating animal research and were approved by the LANUV NRW, Germany (81-02.04.2018.A027).

2.5.1. Experimental groups

Four independent groups were tested. One group with young, 3-month old mice, N = 4-5 mice / treatment) and three groups with 16.5-19-month old animals mice. Old groups were pooled together and treated as a single group for analysis (N = 13-14 mice / treatment).

2.6. Genotyping

Genotyping was mostly performed by technical assistants in the lab.

2.6.1. DNA isolation

Mouse tail biopsies were obtained while tattooing of mice paws at around postnatal day 3. DNA isolation was done with the kit “Plasmid DNA purification” according to manufacturer’s guidelines (Macherey-Nagel, REF 740588.50).

2.6.2. DNA amplification by polymerase chain reaction (PCR)

PCR was used to amplify specific DNA amplicons spanning the deleted sequence. Detailed description and a list of PCR components used are listed below. First master mix was created by mixing MilliQ water, 10x ThermoPol buffer, deoxyribose nucleoside triphosphates

(dNTPs) and Primers. Then Taq-Polymerase was added and the PCR reaction was distributed to PCR tubes. Finally, DNA was added to each tube.

PCR for GFP

PCR reaction for genotyping (GFP-m mice)

37 µl	MilliQ water
5 µl	AP buffer
1.5 µl	dNTP mix (10mM)
1 µl	GFP fwd: 5'-AAG TTC ATC TGC ACC ACC G-3'
1 µl	GFP rev: 5'-TCC TTG AAG AAG ATG GTG CG-3'
1 µl	control fwd: 5'-CTA GGC CAC AGA ATT GAA AGA TCT-3'
1 µl	control rev: 5'-GTA GGT GGA AAT TCT AGC ATC ATC C-3'
1 µl	Taq Polymerase
1,5 µl	DNA (around 100 ng/µl)

PCR program		Temperature	Time
1 x	Initial denaturation	94°C	3 minutes
34 x	Denaturation	92°C	30 seconds
	Annealing	60°C	120 seconds
	Elongation	72°C	60 seconds
1 x	Final elongation	72°C	5 minutes
	Cooling	16°C	stop
	Storage	4°C	∞

2.6.3. Gel electrophoresis

Agarose gel was prepared by dissolving agarose in TAE buffer to achieve concentration of 2%. Afterwards, the gel was left to harden in room temperature for at least 45 minutes and was subsequently transferred to the electrophoresis chamber filled with Tris-acetate-EDTA (TAE) buffer. From each sample, 20 µl of the PCR product was transferred to a new tube containing 2 µl of loading dye. All samples were loaded on the gel into wells. In the first well, 5 µl of 100 bp DNA ladder was loaded to enable the size estimation of the PCR product size. Then, electrophoresis ran at 120 V for 70 minutes. Negatively charged DNA migrates

through the gel to the positive electrode - anode. Since longer DNA fragments migrate slower than shorter fragments, this setup allows for a spatial separation of the PCR products based on their size. Expected band size for GFP-m mice was 200 base pairs (bp) and control band was 324 bp.

After the electrophoresis, gels were transferred to the bath with ethidium bromide (1.5 µg/ml; EtBr) for around 15 minutes. EtBr is a dye that intercalates into DNA and allows for a visualization of the PCR bands. Visualization was done with ChemiDoc MP imaging system (Bio-Rad Laboratories).

2.7. Surgeries, 2-photon imaging, and data quantification

2.7.1. Cranial Window Implantation

Mice were anesthetized with an intraperitoneal (i.p.) injection of MMFSLEEP (0.1 ml / 10 g mouse weight). MMFSLEEP was prepared and stored in room temperature (RT) (**see 2.4**), in the dark prior to usage. After a few minutes carprophen (0.1 ml / 10 g mouse weight) was injected subcutaneously (s.c.). Surgery was started when the reflexes were gone and paw pinch was negative. Mouse hair on the head were epilated. Then the mouse was transferred to a stereotaxic frame on a heating pad and its head was fixed in the frame from the front (using teeth) and from the sides using ear bars. Ointment was put on the mouse eyes to avoid drying (Bepanthen, 5% Dexpanthenol, Bayer). Subsequently, the naked skin on the head was disinfected with ethanol and a single tear - shaped cut was made to remove the skin. Then 7.5% H_2O_2 was applied using a cotton swap and distributed within the exposed area. Remnants of the periosteum were removed using forceps. Skull was cleaned with saline. Mouse head was tilted, so drilling area was placed horizontally. A shallow, circular hole of around 2-3 mm in diameter, was drilled in the skull to mark the margins of the window using a dental drill (HM1 005 – Hager & Meisinger GmbH, Neuss). The window was made over somatosensory cortex. Drilling was continued in a circular fashion using short, weak touches with the side of the drill. Due to the fact that drilling creates heat, cold saline was applied on a skull to avoid heat – induced damage. The drilling was stopped when the bone piece became loose and the bone piece was gently lifted and removed using fine forceps. Cold saline was applied to keep the surface of the brain wet. Cold gel – foam was placed on the window to stop any potential bleeding. Meanwhile, the 5mm cover glass (VWR International, Radnor, U.S.A) was cleaned by immersing it in ethanol and drying on a clean

wipe (Kimtech) tissue. The gel - foam was removed and the window was monitored for any active bleeding. If there was any active bleeding, cold saline and gel – foams were applied to stop it. If there was no active bleeding, a drop of saline was applied on the window and clean cover slip was placed on top of it. The coverslip was kept in place using the blunt side of the drill and glue was applied to fix the coverslip in place. The glue was distributed on the edges of the window and on the whole surface of the exposed skull. Head bar (inhouse made) was fixed with a glue on as far away from the window as possible to allow easy access while imaging. The construction was further fixed using dental cement (Paladur® Pulver mixed with Paladur® Flüssigkeit, Kulzer GmbH, Hanau). Mouse was injected with MMF Wake (equal amount as MMF SLEEP), put back to the cage under a heating lamp and observed until fully awake. MMFWAKE (**see 2.4**) was prepared and stored in RT, in the dark prior to usage. Wet food was placed on a bottom of the cage. The mouse weight and well being was closely monitored for the next three days and once daily carprophen (i.p., 0.1 ml / 10 g mouse weight) and buprenorphine (0.1 mg / kg body weight) was administered. Additional dosage of carprophen was administered one day before the imaging started to clear any residual inflammation. After the cranial window surgery, mice were single-housed in standard laboratory cages under 12 hour light-dark cycle (lights on at 07:00 am).

2.7.2. Osmotic pump preparation

Pumps were prepared more than 24 hours before pump implantation surgery. Osmotic pumps realeasing for 28 days were obtained from alzet (model 1004); release speed: 0.11 µl / h. An average weight of the animals in the experimental group was used to prepare the solutions. For example, for young animals group with an average weight of the group of 25 g, 28.4 mg / ml of THC and vehicle solutions were prepared. To achieve that 284 µl of THC solution (28.4 mg THC diluted in 284 µl EtOH 100%) or 284 µl of EtOH 100% (vehicle) was added to 284 µl of Cremophor. The solution was pipetted up and down to evenly dissolve the THC/vehicle and saline was added to total volume of 1 ml. Then the solutions were transferred to 1 ml syringes and a blend needle (part of the pump set) was inserted. Each pump was placed on an analytical balance individually. Subsequently, the pump was filled with around 0.1 ml of the solution, using previously prepared syringes. Only pumps weighing 0.095 - 0.105 g were used. Filled pump was closed by inserting the releasing cap and placed in a 50 ml tube filled with 40 ml of saline. First all vehicle pumps were filled and placed in a

tube, then all THC pumps were filled and placed in another tube. Both tubes were placed in a holder, light protected and incubated for 26-36 hours in a 37°C oven, lightly shaking for equilibration.

2.7.3. Osmotic pump implantation surgery

Mice were anesthetized using MMFSLEEP (i.p., 0.1 ml / 10 g mouse weight) and carprophen was injected (s.c., 0.1 ml / 10 g mouse weight). Hair on the neck of the animal was epilated. Then animal was placed on a heating pad and eye ointment (Bepanthen, 5% Dexpanthenol, Bayer) was applied. The exposed skin was disinfected with iodine (betaisodona, mundipharma) and around 1-2 cm incision was made. Then, blunt scissors were inserted into the cut and skin was separated from the fascia to create space for the pump implantation. Pump was removed from the saline solution using forceps and inserted into the hole with the realeasing cap facing the back of the animal. Pump was placed at the back of the animal around 4 cm from the incision site. Wound was closed using 1 – 2 wound clips (Fine Science Tools, No. 12032-07) and animal was woken up by injecting equal amount of MMFWAKE. Mouse was put back to the cage under a heating lamp and observed until fully awake. Wet food was placed on a bottom of the cage. The mouse weight and well being was closely monitored for the next two days and once daily carprophen (i.p., 0.1 ml / 10 g mouse weight) was administered. The skin around the pump was massaged for the next 4 days to decrease the risk of scar formation that could hinder the drug release. Wound clips were removed 7 days after the surgery, when the mouse was under anaesthesia for the in vivo imaging (Imaging 4).

2.7.4. 2-photon imaging

Mice were anesthetized using MMSLEEP (i.p., 0.1 ml / 10 g mouse weight). MMSLEEP was prepared (**see 2.4**) and stored in RT, in the dark prior to usage. Imaging was started when the reflexes were gone and paw pinch was negative. Mouse was fixed with the head bar to the imaging plate to stabilize its position and minimalize the breathing artefacts. Eye ointment was administered to avoid eyes drying (Bepanthen, 5% Dexpanthenol, Bayer). The window was cleaned with ethanol to remove any dirt. A circle was made with Vaseline (Fagron GmbH & Co. KG, Barsbüttel) on the cement, around the window to create a barrier for the water. The angle of the mouse head was adjusted that the cranial window was parallel

to the objective. Imaging plate was placed under the microscope and heating was applied to the plate to avoid hypothermia. The breaching of the mouse was observed thought the imaging period.

Scan Image software ((Pologruto et al., 2003), running on MATLAB 2018-2019) alongside with inhouse written code was used to control the 2 – photon (2P) microscope and obtain the images. 2P microscope was inhouse build.

Two different objectives were used: 4x objective (NA 0.1) for overview pictures and 40x objective (NA 0.8, LumPlanFl, Olympus, Hamburg, Germany) to obtain the z-stacks of dendritic segments. To visualize GFP we used a Ti:sapphire Laser (Chameleon Vision-S, Coherent, Santa Clara, CA) at fixed wave length of 910 nm.

For each mouse during the first imaging an overview picture, using a CCD-camera (The Imaging Source Europe GmbH), and a drawing were done to note the vasculature within the window. Blood vessels were used as landmarks to localize the imaging regions. For each mouse 3-5 regions were acquired containing 2-6 dendritic segments each. In each time point from each imaging region one z-stack image was acquired of 1024 x 1024 pixels (0.065 µm/pixel) resolution and 16-bit depth using 0.43 Hz frame rate resulting in a pixel dwell time of 2,000 ns. In the young group step size of 0.51 µm was used, but in old animals it was changed to 0.8 µm to decrease the imaging time. Each frame was acquired 4 times and averaged to increase signal to noise ratio. Frame rate was set to 0.86 Hz and pixel dwell time was 1000 nanoseconds. Dendrites were monitored for phototoxicity and a minimal laser power needed to visualize the dendritic spines was applied. Only apical dendrites from layer V pyramidal neurons were analysed. Overview pictures were done during every imaging session to observe the stability of the window and possible infections. Each imaging lasted 45-90 minutes per mouse. After the imaging, mice were detached from the imaging plate, woken up with MMWAKE (ip., 0.1 ml / 10 g mouse weight), put under a heating lamp and observed until full recovery. MMWAKE was prepared (**see 2.4**) and stored in RT, in the dark prior to usage.

2.7.5. 2-photon imaging: finding the same dendritic segment

In order to use chronic imaging, we first established a reliable approach to image repeatedly the same dendritic segments in vivo. To identify the same imaging regions and thus find the same dendritic segments, we used blood vessels as landmarks (**Figure 2.1**).

Briefly: Imaging regions were marked on a drawing of the vasculature within the cranial window and the microscope was positioned within one of the marked regions. Subsequently, magnification was increased and the shape of the dendritic segments as well as their spatial relation to each other and the neighbouring blood vessels were used to determine the location of the imaging region.

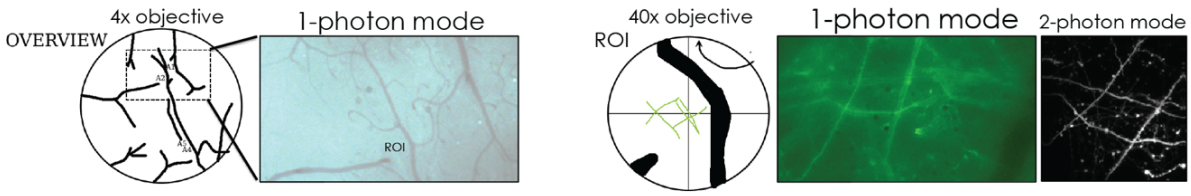

Figure 2.1. Experimental setup for imaging the same dendritic segment in vivo. Method of finding the same dendritic segment in vivo. From left to right. Left panel: drawing of the vasculature within the cranial window and an image taken in 1-photon mode using 4x objective. Imaged region marked both on the drawing and on the image (ROI – region of interest). Right panel: drawing of the imaged region as seen under the 40x objective and a corresponding 1-photon and 2-photon image.

2.7.6. Dendritic spine analysis

Spine analysis was performed using custom MATLAB script "Spine Analysis" provided with Scan Image software (running on Matlab 2012a, 2014a, 2018). Each image was calibrated with the right pixel size and opened in the software; 6-8 images were analysed in the same time. Only images with sufficient quality to visually distinguish dendritic spines were analysed. Around ¼ of the dataset was analysed by Kishore Aravind Ravichandran, with even distribution of treatment groups.

Image analysis consisted of two phases: annotation and correlation. The first one started with annotation of dendritic segments over which spines will be analysed. Only segments that were clearly visible in all the investigated imaging sessions were included. Dendritic segment was annotated from one clear spine to another in characteristic locations to ensure that always the same segment is analysed. Afterwards, each visible spine on the segment was annotated in the most optimal, for this particular spine, frame of the z-stack. A single annotation was a line from the dendritic shaft to the tip of the spine. Only protrusions longer than 0.4 µm were considered as spines (Holtmaat et al., 2009). After annotation, each annotated element was given a unique identifier (ID) in the program. When all the annotations were finished in all the investigated images (time points), then the unique ID allowed for the corelation of annotated elements. Annotated elements could fall into one of

the three different categories: stable, gained, lost (**Figure 3.2)**. Stable when the element was present on both consecutive time points; gained when the element was not there on one time point but appeared on the consecutive one; lost when the element was gone on the consecutive time point. Additionally, program automatically distinguished transient spines that appeared in one timepoint and disappeared on the consecutive time point. If two elements were indicated to be stable their ID was unified.

As an output, a .csv file is generated with one column per time point and single rows representing annotated elements (one ID per row). Data was further analysed using a self-written Python script (together with Daniel Müller-Komorowska). Analysed parameters are summarized in **Table 2.1**. The exact number of analysed stacks per group per timepoint is summarized in **Table 2.2**.

Table 2.1. Analysed parameters of spine dynamics.

Parameter name	Calculation
spine density	total number of spines divided by the total length of analysed dendritic segments
density of dynamic spines	number of gaines and lost spines divided by the total length of analysed dendritic segments
% gained	number of gained spines divided by the number of total spines in the same timepoint multiplied by 100
% stable	number of stable spines divided by the number of total spines in the previous timepoint multiplied by 100
% lost	number of lost spines divided by the number of total spines in the previous timepoint multiplied by 100
% transient	number if spines gained in one timepoint and lost in the consecutive timepoint divded by total number of spines in those two timepoints multiplied by 100
turnover	number of lost and gained spines between two timepoints divided by total number of spines in both timepoints
% surviving spines	Number of spines still present at a certain timepoint divided by the initial number of spines multiplied by 100

Table 2.2. Exact number of zstacks analysed in each timepoint.

3-month old mice																
IMAGING	1	2	3	4	5	6	7	8	9	10	11	12	13	14	15	**Total number of different stacks analysed**
Day	**d-7**	**d-4**	**d-1**	**d7**	**d10**	**d13**	**d16**	**d19**	**d22**	**d25**	**d28**	**d35**	**d42**	**d49**	**d56**	
Vehicle	6	9	8	9	9	9	6	6	6	6	5	5	6	5	4	10
THC	9	7	9	10	10	11	11	10	11	11	10	10	11	12	7	13
18-month old mice																
IMAGING	1	2	3	4	5	6	7	8	9	10	11	12	13	14	15	**Total number of different stacks analysed**
Day	**d-7**	**d-4**	**d-1**	**d7**	**d10**	**d13**	**d16**	**d19**	**d22**	**d25**	**d28**	**d35**	**d42**	**d49**	**d56**	
Vehicle	17	14	17	16	16	16	14	14	15	14	13	12	9	9	9	18
THC	17	21	22	20	17	20	22	20	21	21	19	16	18	12	8	22

2.8. Behavioural experiments

Mice were placed in the test room around 1 hour before the test to allow habituation to the test environment.

2.8.1. Partner recognition test (PR)

PR paradigm was used to assess social memory. The animal activity was analyzed with the Ethiovision XT 13 (Noldus). The test was performed in an open-field box (44 cm x 44 cm) containing a thin (around 1 cm) layer of sawdust. For three consecutive days mice were allowed to explore the arena freely for 10 minutes and were habituated to the environment. On the test day, mice underwent two trials. In trial 1, mice were given 9 minutes to freely explore the arena containing an object (empty grid cage) and a grid cage (diameter around 10 cm, high around 12 cm) with an unfamiliar C57BL6/J male partner mouse. The can and the cage were in opposite corners, each placed around 6-7 cm from the wall. Partner mice were approximately 10 weeks old. Interaction was noted when the mouse nose point was within 2 cm of the cage/can. The time spent on top of any of the objects was deduced from the interaction time. After trial 1 mice were put back to their home - cages for 1 hour. Sociability in trial 1 was calculated as follows:

$$\text{sociability (\%)} = Tp/(Tp+Tc)*100,$$

where Tp is the time of interaction with a partner mouse and Tc is the time of interaction with the object

To detect if the sociability of the group was greater than the chance level, the mean sociability value was tested with a one-sample t-test against a hypothetical mean (50%) which would represent the chance level. Sociability above 50% indicated that the mouse

spent more time interacting with a partner than with an object. In trial 2, an object was replaced by a grid cage with a novel partner mouse and the test mouse was given 3 minutes to freely explore and interact with both partners. Preference for the novel partner was calculated as:

$$\text{preference (\%)} = Tn/(Tf+Tn)*100,$$

where Tf is the time spent with the familiar partner and Tn is the time spent with a novel partner mouse.

If the mouse recognized its previous partner, it should have spent > 50% of interaction time interacting with a novel partner. Therefore, a preference for the new partner is interpreted as learning. To detect learning in each group, we analyzed if the preference for the novel partner statistically deviates from the chance level with a one-sample t-test against a hypothetical mean (50%).

2.8.2. Olfaction test

Olfaction test protocol was modified from “Simple Behavioral Assessment of Mouse Olfaction”; The Olfactory Habituation/Dishabituation Test (M. Yang & Crawley, 2009).

For 30 minutes, mice were habituated to a new cage and a scent-free cotton swab was inserted from the top of the cage, 2-3 cm from the grid top. The test consists of six 1-minute trials with inter-trial interval of 1 minute. In the trials 1-3, 10 µl of water was added to the cotton swab, while in trials 4-6, 10 µl of female urine was added. Interaction time with the cotton swab was measured in each trial. Experiment was recorded with GoPro Hero 5 camera and the interaction times were manually counted using a stopwatch.

If the mice have no olfactory defect, then their interaction time with the water cotton swab (trial 1 to 3) should decrease with each trial. In trial 4, when the female urine cotton swab is first introduced, there should be an increase in the interaction time suggesting that the mice are able to distinguish the novel odor. Subsequently, in trial 5-6, the interaction time should decrease therby showing a proper habituation to the odor.

2.8.3. Nestlet test

This test was used to assess the stress level of the animals as described before (Deacon, 2006). Briefly: nest was removed from the home-cages of the experimental mice and a new nesting material (nestlet) was placed. After 24 hours the nest was scored and the remaining

unshredded nestlet was weighed. The remaining nestlet weight was deduced from initial nestlet weight to obtain the amount of nestlet used in grams. The higher the nest score and % of nestlet used, the better nest building behavior of the animal suggesting a lower stress level.

2.8.4. Vision test

Slow angled-descent forepaw grasping (SLAG) was used to assess vision in tested mice (Gil-Pagés et al., 2013). Shortly: Grid cage is put in an angle of around 45 degrees, under high illumination from the side. Mouse was tail-suspended 15-30 cm above the grid and slowly lowered down, so the grid remained in the mouse field of view without tactile contact. When nearly passing the grid, if the mouse was able to see it, it reaches forward with its paws. Subsequently, the mouse was placed on the grid cage for a few seconds. In the second part, the mouse is turned around by 180 degrees and the test was repeated. Lack of reaching either of the trials indicates vision deficits.

2.9. Transcardial perfusion

Mice were deeply anesthetized with ketamine+xylazine mixture (**see 2.4,** i.p., 0.05 ml / 10 g mouse weight). Then, mice were transcardially perfused with 4% formaldehyde, postfixed for 3.5 – 4 hours in 4% formaldehyde, and cryoprotected by an overnight incubation in 20% sucrose. Brains were frozen in dry-ice cold isopentane and stored in -80°C prior to sectioning.

2.10. Immunohistochemistry (IHC)

2.10.1. Iba1, GFP, CD68 co – staining (prTHC)

Frozen brains were cut into sections 50 µm free-floating, coronal sections on a cryotome and stored in -20°C in a cryoprotectant solution within a 24 - well plate. Prior to the immunohistochemical staining, sections were washed 3 times 10 minutes in PBS to remove the cryoprotectant and refixed in 4% formaldehyde solution for 2 hours with shaking. Then sections were washed 3 times 15 minutes and blocked in a blocking buffer (10% normal goat serum (NGS), 2% bovine serum albumin (BSA), 0.5% Triton-X in PBS) for 4 hours with shaking. Afterwards, sections were incubated with primary antibodies in antibody solution (5% NGS, 2% BSA, 0.1% Triton-X in PBS) for 48 hours at 4 °C, shaking. Primary antibodies:

rabbit anti-ionized calcium-binding adapter molecule 1 (IBA1), chicken anti-green fluorescent protein (GFP) and rat anti-Cluster of Differentiation 68 (CD68) (**see 2.3**). Then, sections were washed 3 times 15 minutes with PBS-T (0.1% Triton X) and were incubated for 4 hours with secondary antibodies in antibody solution at dark and RT with shaking. Secondary antibodies: goat anti-chicken AlexaFluor®488, goat anti-rat AlexaFluor®594, and goat anti-rabbit AlexaFluor®488 (**see 2.3**). Subsequently, sections were washed in PBS-T for 2 times 15 minutes, stained with 4’,6-Diamidin-2-phenylindol (DAPI; 0.1 µg/ml in PBS) for 15 minutes to visualize the nuclei and were washed for 15 minutes in PBS. Then, the slices were briefly rinsed in MilliQ water and were mounted on slides using Fluoromount-G® without DAPI and cover slips No. 1.5H were and stored in the dark at 4 °C.

2.10.2. Image acquisition

IHC stainings were imaged with Leica TCS SP8 confocal microscope. For imaging different fluorophores, the microscope was equipped with an ultraviolet (UV) diode (emission peak at 405 nm), a pulsed argon laser (emission at 458, 476, 488, 514), yellow-green diode-pumped solid-state (DPSS) laser (emission at 561 nm), and two helium-neon (HeNe) lasers (emission at: 594 nm and at 633 nm).

DAPI was excited with a UV Diode; AlexaFluor®488 with argon laser at 488 nm, AlexaFluor®568 with DPSS laser at 561 nm; AlexaFluor®594 with HeNe at 594 nm, and AlexaFluor®647 with HeNe at 633 nm.

Lower magnification images and overview images were obtained using a 20x water – immersion objective (numerical aperture (NA) = 0.75); speed 400. For overview pictures, tile scan was used with fine, slow merging. Higher magnification pictures were obtained with 63x water – immersion objective (NA = 1.2).

The imaging conditions were defined once for each staining and were kept constant thoughtout all the imaging sessions. Imaging conditions included: laser power, gain, frame averaging and signal accumulation, detected emission spectra, pinhole size, resolution of acquired images, imaging speed etc.

For microglia morphology analysis, images were obtained using a 63x objective. 3 z-stacks (around 30 µm; step size 0.5 µm; 0.18 µm/px; resolution 1024 x 1024 px) were acquired per animal from layer 1/2 of the somatosensory cortex. The window area was

avoided to decrease the possibility that the detected differences in microglia arose from local inflammation.

For microglia density analysis and neuron-microglia interaction (low resolution), 3 single plane images of resolution 1024 x 1024, 0.09 µm/px, were taken per animal using 20x objective.

For neuron-microglia interaction analysis in high resolution images, 12 single plane images of resolution 1024 x 1024, 0.18 µm/px, were taken per mouse using 63x objective. Each image contained at least 40 µm of a dendritic segment in focus.

2.11. Image analysis

Image analysis was performed in Fiji (ImageJ v2.1.0/1.53c). Subsequently, the results were exported and further analysed with Microsoft Excel (v 16.43).

If not written otherwise, appropriate threshold per experiment is calculated as an arithmetical average of manually set thresholds. Always the same threshold is used for all the images within an experiment.

2.11.1. MOTIQ, 3-dimentional (3D) microglia morphology analysis

Prior to the analysis Iba1 z-stacks were pre-processed (size reduction 0.5, smoothing, background subtraction: rolling ball). Followed by automated analysis using a custom-written script 'MotiQ' (Plescher et al., 2018). Shortly: the plugin consists of three sub scripts: Cropper, Thresholder and 3D Analyzer. Cropper allows to separate single microglia in a stack and creates a series of roi's containing the chosen microglia as well as a substack. One must manually select the microglia area, thus introducing a possible bias. This function was only used in the later stages of analysis if two or more microglia were detected as one particle in the automated detection due to their close proximity.

Thresholder was used to obtain binary images from the original stacks. The intensity threshold was determined in a 0.5 downscaled maximum-intensity-projection using "MinError" algorithm. Afterwards single cells were detected using 3D Analyzer by signal overlap within the z-stack. Only particles larger than 10,000 voxels were included in the analysis (length calibration: 0.3608 µm/pixel; voxel depth 0.5 µm). Skeleton of the cell was derived from a copy of the input image. Reconstructed cells were inspected visually and cells that were incomplete (cut in x, y or z axes) as well as multiple cells detected as one particle

were excluded from the analysis. If possible, single cells were cropped from multiple cells detected as one particle using MotiQ Cropper and analysed as described above. Measured parameters included: surface area, volume of the cell, ramification index, number of branches, tree length, average branch length.

Ramification index was quantified by dividing cell surface area of the detected microglia by surface of a perfect sphere. Thus, index of 1 indicates that the cell is a perfect sphere – microglia is round and has no processes. The higher the index, the more complexed is the microglia meaning it has a higher branch number.

10-15 cells were analysed per animal from 5-6 animals / treatment, giving a total of 80-125 cells per group.

2.11.2. Microglia soma size and Iba1/CD68 in the soma

All microglial somas were manually delineated based on their optimal frame in the high-resolution z-stacks. The obtained regions of interestes (ROIs) were saved and used for single microglia soma analysis. The size of the ROI was reported as microglia soma size. ROI were used in the same frame to obtain Iba1 intensity measurements using “measure” function in Fiji. For CD68 analysis maximum intensity projection was created from the CD68 z-stacks. CD68 intensity was measure within the ROI’s. Also, the obtained maximum intensity projection images were thresholded with a fixed intensity (mean grey value - MGV) threshold to binarize the images. % of area covered by the CD68 positive signal was measured using “measure” function in the binarized images.

2.11.3. Microglia density and Iba1/CD68 in whole cells

Different layers were delineated manually based on the DAPI image according to the known differences in cell density. Area of each layer were measured using ‘Measure’ function within the selected ROI. Iba1 images were thesholded using fixed % of histogram threshold to correct for differences in the intensity of microglia. 'Analyze Particles' function (minimum punctate size: 20 µm) was used on Iba1 images to detect number and average size of single microglia per layer. In addition, ROI of single microglia detected per image were saved and used in further analysis. Density was calculated as number of cells divided by the investigated area size. Subsequently, corresponding analysis was done using single microglia ROI as using soma microglia ROI (see paragraph above).

2.11.4. Colocalization of Iba1 and GFP

Colocalization of Iba1 and GFP was first assessed using lower magnification images (20x objective; used before for microglia density measurement) and then in the same fashion in high magnification images (63x; single plane dendrites). Both GFP and Iba1 images were binarized using a fixed % of histogram threshold. ROI's we manually delineated around dendritic segments based on GFP signal. Only segments that were in focus and not overlapping with other segments were included into the analysis. Using 'image calculator' binary GFP image was multiplied by binary Iba1 image. As a result, an image was obtained containing only colocalized pixels of Iba1/GFP. Afterwards, 'measure' function was used within ROI to measure the % of area covered on the colocalized image. The % of colocalized pixels was normalized to the size of the dendritic segment. Shortly: the % of colocalized pixels from Iba1/GFP image was divided by the % of GFP positive area from the GFP image within the selected ROI.

Additionally in high magnification images, the dendrite length, width, and number of spines were annotated using 'Spine Analyzer' (**see 2.7.6**). Moreover, to remove single-pixel noise, the images were processed with binary filters (erosion followed by dilation) prior to image multiplication.

2.12. Statistical analysis and data presentation

Microsoft Excel (v 16.43) was used for data analysis followed by statistical analysis and data visualization in GraphPad Prism version 7.0.0 and 9.1.2 for Mac, GraphPad Software, San Diego, California USA, www.graphpad.com. Figures were created in Adobe Illustrator (v 24.0.2). Graphical parts of the figures were prepared using Biorender (biorender.com) and Microsoft PowerPoint (v 16.43). For presentation, representative images were post-processed in Fiji (ImageJ v2.1.0/1.53c) to adjust brightness and contrast. All adjustments were kept consistent among different groups and brain areas. Behavioral data analysis was done using Ethovision XT 13 (Noldus).

Datasets with two independent groups, one dependent variable were first checked for normal distribution using D'Agostino & Pearson normality test. If both datasets distribution did not significantly differ from a normal distribution, then unpaired t-test was

used, otherwise Mann-Whitney test (U-test) was used. For single microglia analysis, outlier test was performed with ROUT = 5% and the detected outliers were excluded.

For time-series experiments with 2 groups and missing values (e.g. Treatment and Time) repeated-measurement ANOVA (Mixed-effects model (REML)) was used followed by Sidak’s multiple comparison test.

For PR, with one-sample t-test the mean of the group was tested against a theoretical mean of 50 to detect significant difference of each group from the chance level.

For correlation analysis normal distribution of the data was checked with the D’Agostino & Pearson normality test. If the data distribution did not significantly differ from the normal distribution Pearson correlation coefficient was used, otherwise Spearman correlation was used.

Statistical significance was stated when p-value < 0.05 at a 95% confidence interval. For the figures including a time-course in which ANOVA was used, the p-values were reported as * $p < 0.05$, ** $p < 0.01$; *** $p < 0.001$; **** $p < 0.0001$. The corresponding exact p-values were reported in the statistics table (**see 10.1**). For all the other figures the exact p-values were reported directly on the graphs. If not possible, then p-values were included in the statistics table (**see 10.1**).

All graphs are presented with standard error of the mean (SEM) unless indicated otherwise.

3. RESULTS: "THC treatment differentially alters spine dynamics in old and young mice"

3.1. THC treatment alters spines and their dynamics

3.1.1. In vivo imaging: Experimental setup and basic behaviour

To investigate how does the THC-treatment affect spine dynamics we used 2-photon microscopy to follow the same dendritic segments in the somatosensory cortex before, during and after the THC treatment (3 mg/ kg body weight / day). Detailed experimental protocol is displayed in **Figure 3.1a**.

Both in 3-month and 18-month-old mice we successfully imaged the same dendritic segments up to 15 consecutive imaging sessions (**Figure 3.1b**). In total, we followed around 1,313 spines over 4,911μm of dendritic segments from 21 regions in 3-month old mice, whereas around 2,287 spines over 6,742μm of dendritic segments from 40 regions in 18-month old mice.

The THC treatment did not cause any gross effect in mice behaviour. We monitored body weight of the mice throughout the experiment and did not observe any significant differences in body weight of THC-treated mice neither in 3-month nor in 18-month old group (**Figure 3.1c**). Although it should be noted that the pattern of time-related changes was different depending on age. In 3-month old group, the weight increased over time, whereas in old mice it decreased. We excluded the possibility that the weight drop in old animals was due to an increased stress-level, since most of the mice had a nest score of 4 – 5 throughout the experiment (**Figure 3.1d**). Also, we did not detect any treatment effect neither in the % of nestlet used nor in the nest score.

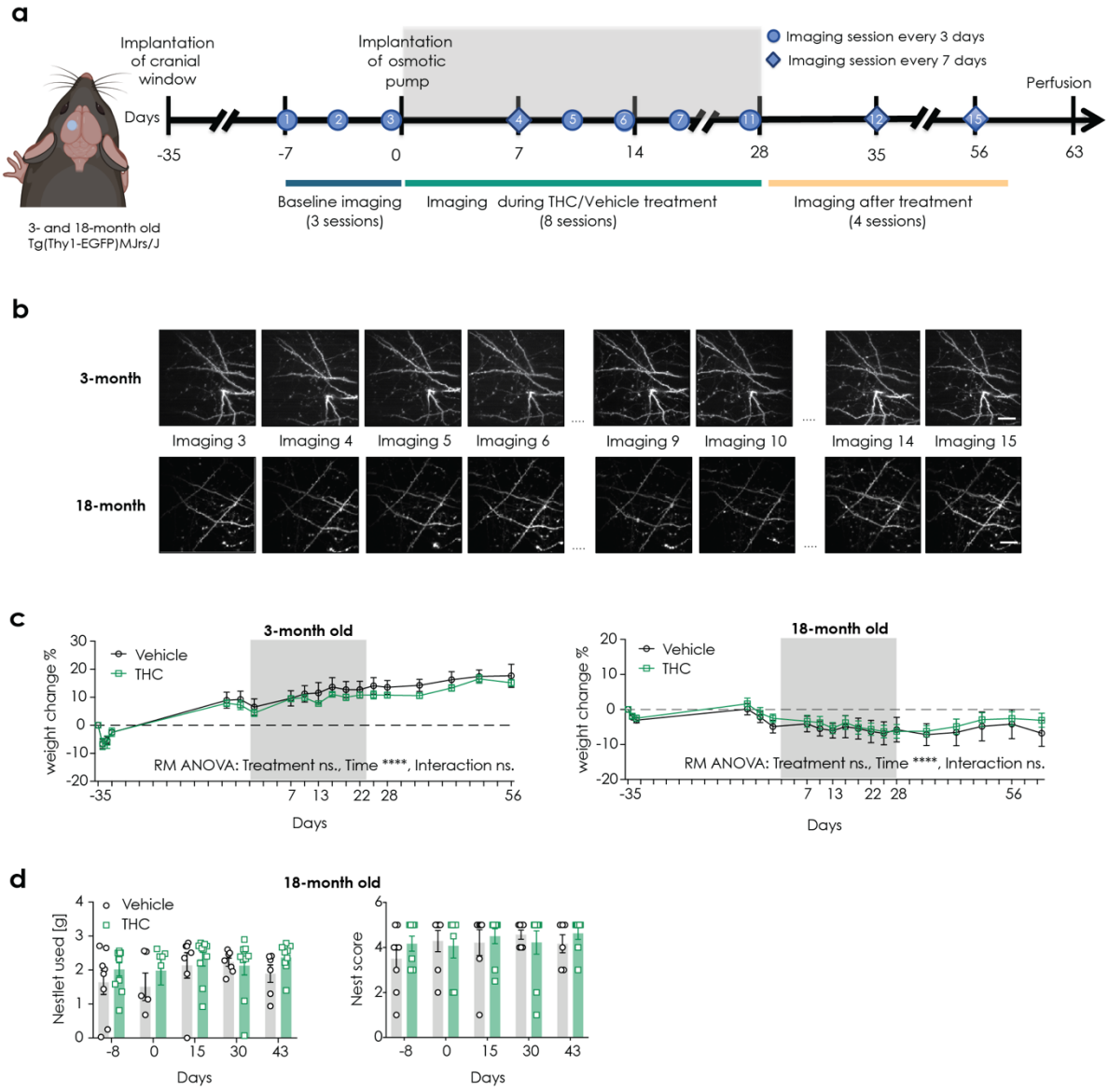

Figure 3.1. Experimental setup and basic behaviours. (**a**) Experimental setup for in vivo imaging before, during and after THC treatment. Each circle and deltoid indicate an imaging session that was done in the interval of 3 and 7 days, respectively. Grey box indicates the treatment duration. (**b**) Example of max z projections of stacks from 3-month and 18-month old mice of the same dendritic segments imaged successfully throughout all 15 imaging sessions. Scaler bar represents 20 μm. (**c**) % of weight change over the course of the experiment. Left panel: 3-month old mice; right panel: 18-month old mice. (**d**) Results of nestlet shredding tests done throughout the experiment from 18-month old mice. Left panel: nestlet used [g]; right panel: nest score; possible nest scores 1-5. Grey box indicates the treatment duration; THC – green; vehicle - black. Young group consisted of 3-month old mice (THC: N=5 mice; vehicle: N=4 mice); old group of around 18-month old mice (THC: N=10 mice; vehicle: N=8 mice). Data shown as mean per group ± SEM. Data was analysed by RM ANOVA (Mixed-effects model (REML)) followed by Sidak’s multiple comparison test; * $p < 0.05$, ** $p < 0.01$; **** $p < 0.0001$.

3.1.2. Long-term low-dosage THC-treatment increases spine density in 18-month old, but not in 3-month old mice

To investigate spine dynamics, we compared images from two consecutive imaging sessions and assigned the detected spines into 4 categories: stable, lost, gained and transient (**Figure 3.2a**). Stable spines (blue arrows) were present on both imaging sessions; lost (red arrow) were present on former imaging session but disappeared on the latter session; gained (green arrow) were novel spines appearing in the latter sessions; whereas transient (yellow arrow) were the novel spines that appeared in one session and disappeared on the consecutive session.

Since a known consequence of altered spine dynamics are the changes in spine density, we first investigated spine density changes induced by THC-treatment (**Figure 3.2b**). In 3-month old mice we did not detect any treatment effect, but we detected a time and interaction effect. Post hoc analysis did not reveal any significant differences. In old mice, we detected a significant treatment and interaction effects. Following post hoc analysis showed significantly increased spine density after THC treatment at day 25, 35, 42, 49, 56 of the experiment. Thus, our results show that THC treatment effect on spine density is age-dependent and rthis esults in a long-term increase in spine density in old mice.

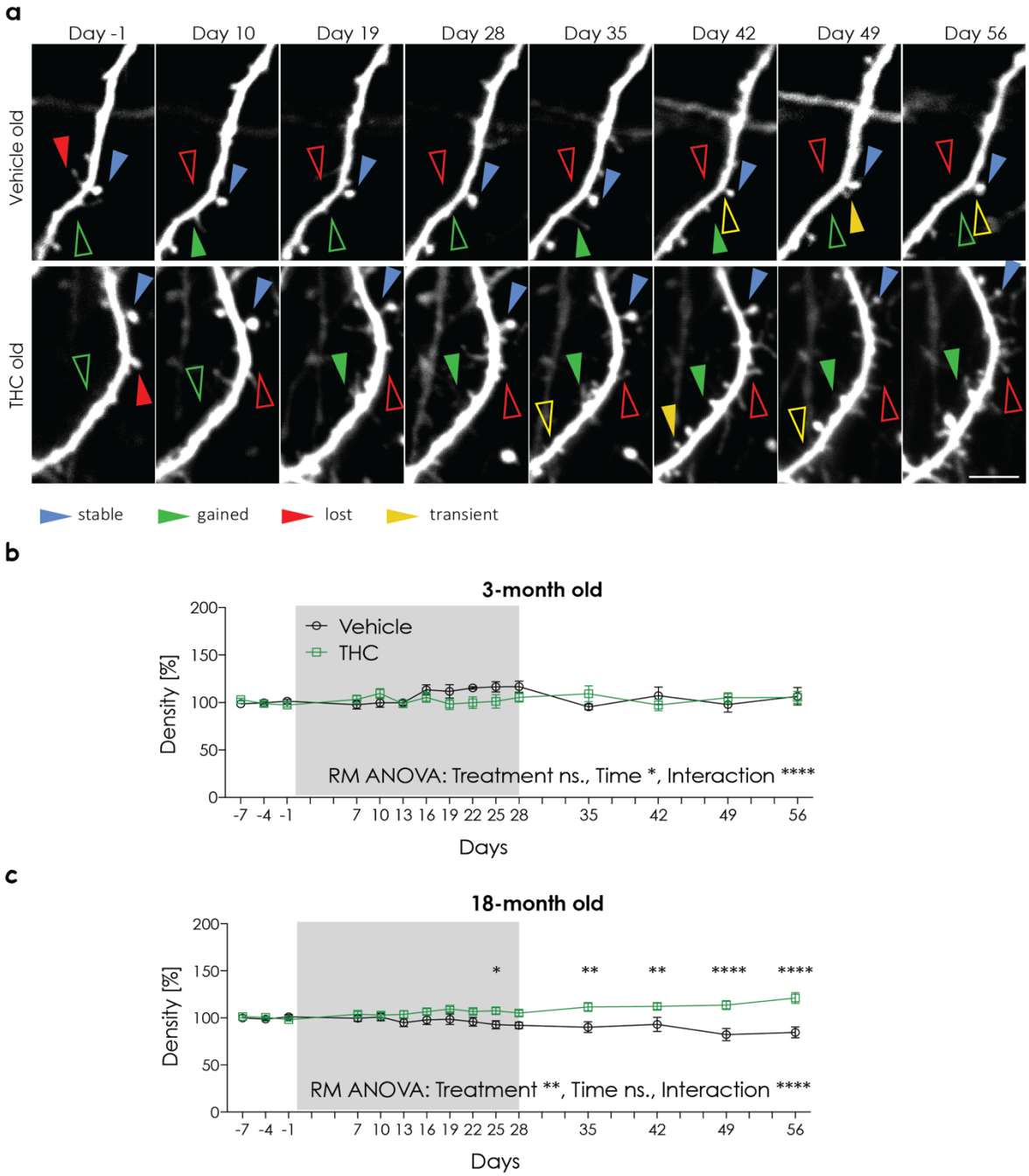

Figure 3.2. Long-term low-dosage THC-treatment increases spine density in old, but not in young mice. (a) representative images of the same dendritic segment acquired during in vivo imaging from old mice treated with vehicle or THC over the course of the experiment. Present spines are represented by filled arrowheads; absent with unfilled arrowhead; stable - blue, gained – green; lost – red; transient – yellow. Scale bar represents 5 μm. (**b**) Spine density in each timepoint. Spine density per stack was normalized to the mean spine density during baseline imaging day -7 to day -1. Grey box indicates the treatment duration; THC – green; vehicle - black. Left panel: 3-month old mice (THC: n = 13 stacks, N = 5 mice; vehicle: n = 10 stacks; N = 4 mice); right panel: around 18-month old mice (THC: n = 22 stacks, N = 10 mice; vehicle: n = 18 stacks; N = 8 mice). Data shown as mean per group ± SEM. Data was analysed by RM ANOVA (Mixed-effects model (REML)) followed by Sidak’s multiple comparison test; * $p < 0.05$, ** $p < 0.01$; **** $p < 0.0001$.

3.1.3. Long-term low-dosage THC-treatment differently alters spine dynamics in 18-month and 3-month old mice

We analysed spine dynamics during the THC treatment (**Figure 3.3**). In 3-month old animals we detected a significant treatment, time and interaction effect in both density of dynamic spines and the turnover ratio (**Figure 3.3a**). Post hoc analysis showed a significant increase at day 7, 10 and 13. Following analysis of changes in % of spines that were lost, gained and stable over the course of the experiment showed a treatment and time effect as well as interaction for % of gained and % of lost spines (**Figure 3.3b**). Post hoc analysis detected a significant increase at day 7 and10 of % of gained and % of transient spines and at day 10 and 13 an increase of % of lost spines. At day 10 and 13 we detected a decrease in % of stable spines (**Figure 3.3b**).

In 18-month old animals we detected a significant treatment and time effect in both density of gained spines and the turnover ratio (**Figure 3.3c**). On a contrary to young mice, in old mice THC treatment significantly decreased the turnover ratio at day 16. We also detected a significant treatment effect in % of lost, % of gained and % of stable spines (**Figure 3.3d**). On day 25, the % of lost spines was decreased, while % of stable spines was increased. On day 28, both % of gained and % of transient spines were decreased.

Taken together our results clearly show that the effect of THC treatment on spine dynamics differs depending on the age. Young mice showed an overall increase in spine dynamics whereas the old mice showed a decrease in spine dynamics.

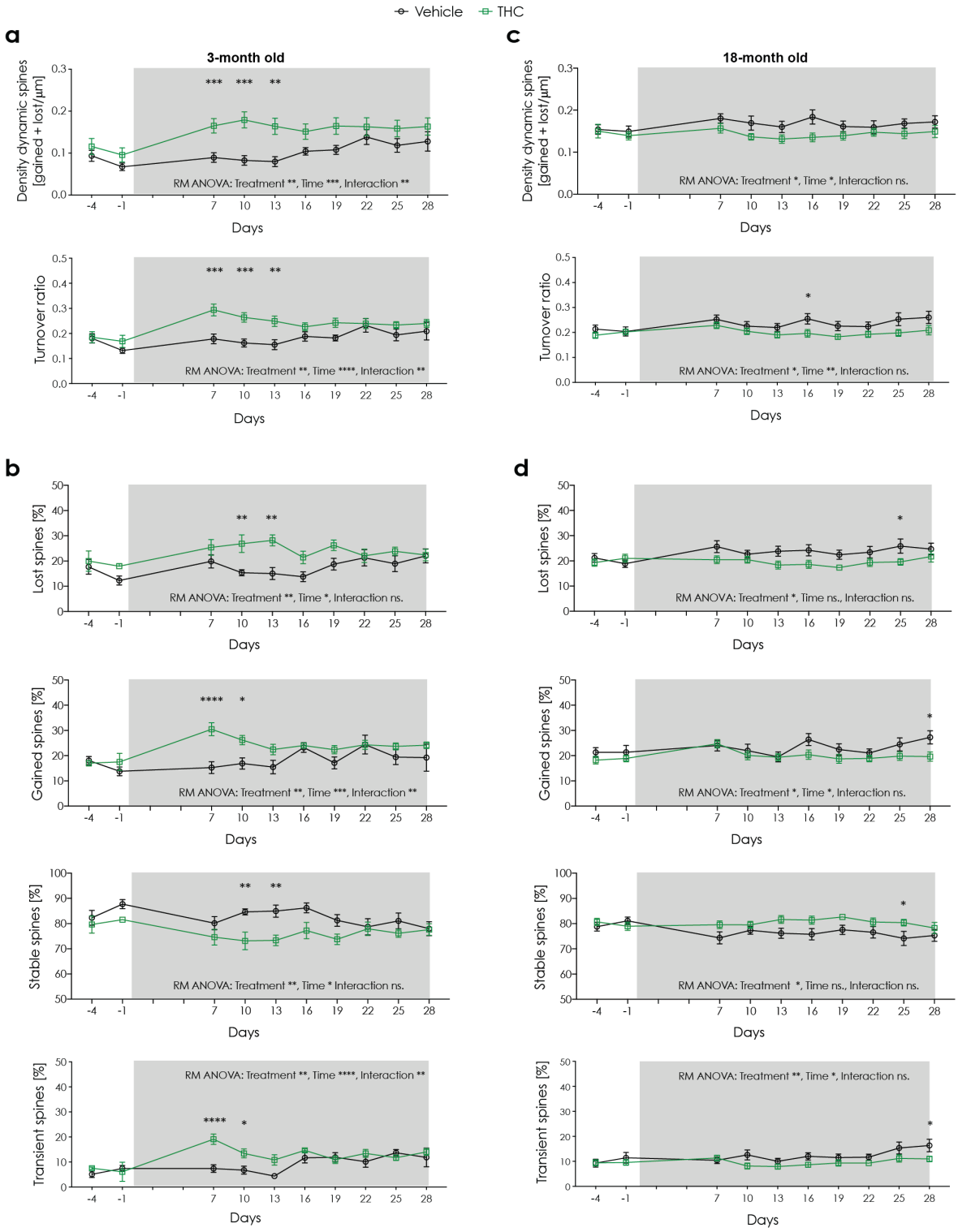

Figure 3.3. Long-term low-dosage THC-treatment differently alters synaptic dynamics in old and young mice. Left panel – young, 3-month old mice (**a, b**); right panel – old, 18-month old mice (**c, d**). (**a, c**) Number of lost and gained spines between two consecutive timepoints per micron (density of dynamic spines) or normalized to total number of spines in both timepoints (turnover ratio). (**b, d**) Percentage of spines that were lost, gained, transient and stable between two consecutive timepoints. Grey box indicates the treatment duration; THC – green; vehicle - black. Left panel: 3-month old mice (THC: n = 13 stacks, N = 5 mice; vehicle: n = 10 stacks; N = 4 mice); right panel: around 18-month old mice (THC: n = 22 stacks, N = 10 mice; vehicle: n = 18 stacks; N = 8 mice). Data shown as mean per group ± SEM. Data was analysed by RM ANOVA (Mixed-effects model (REML)) followed by Sidak’s multiple comparison test; * $p < 0.05$, ** $p < 0.01$; *** $p < 0.001$; **** $p < 0.0001$.

3.1.4. Long-term effects of THC treatment

After terminating the treatment, we continued to follow the same dendritic segments over the course of 4 weeks to investigate long-term effects of the treatment on the spine dynamics. We detected a significant treatment, time and interaction effects for turnover ratio, % of gained and % of lost spines (**Figure 3.4a**). Following post hoc analysis revealed a significant increase in the % of gained spines at day 35.

In 18-month old mice, we detected a treatment and time effects in the turnover ratio and in the % of lost spines (**Figure 3.4b**). For the % of gained spines we exclusively detected a time effect although a post hoc analysis revealed a significant decrease in the % of gained spines in THC treated mice at Day 28. Taken together, we found that even after the treatment termination THC continues to effect spine dynamics.

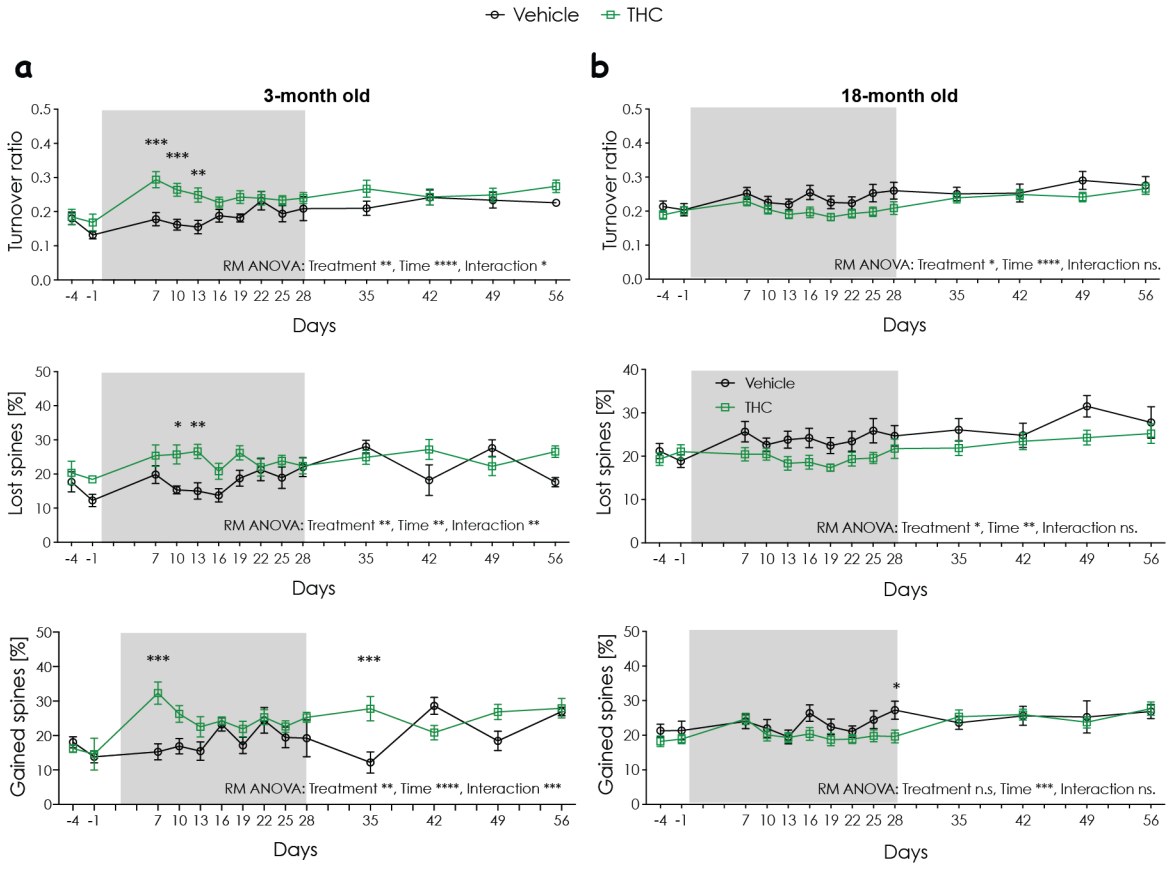

Figure 3.4. Long-term low-dosage THC-treatment differently alters synaptic dynamics in old and young mice even after treatment termination. (**a**) young, 3-month old mice; (**b**) old, 18-month old mice (**b**). Upper panel: Number of lost and gained spines between two consecutive timepoints normalized to total number of spines in both timepoints (turnover ratio); Middle panel: Percentage of spines that were lost; Lower panel: percentage of spine that were gained. Grey box indicates the treatment duration; THC – green; vehicle – black.
3-month old mice (THC: n = 13 stacks, N = 5 mice; vehicle: n = 10 stacks; N = 4 mice); around 18-month old mice (THC: n = 22 stacks, N = 10 mice; vehicle: n = 18 stacks; N = 8 mice). Data shown as mean per group ± SEM. Data was analysed by RM ANOVA (Mixed-effects model (REML)) followed by Sidak's multiple comparison test; * $p < 0.05$, ** $p < 0.01$; *** $p < 0.001$; **** $p < 0.0001$.

3.1.5. THC treatment decreases spine stability in 3-month old mice

Next, we compared spine stability of all spines in 3-month old mice induced by THC treatment. In order to do that, we investigated the survival fraction of spines present at day -1, 7, 10, 13, 16, 28 and 42 (**Figure 3.5**). For all timepoints we detected a significant time effect. Also, we detected a significant treatment effect on the survival of the spines present at day 7 and day 10 and a significant interaction effect on days -1, 7, 10 and 13. Post hoc analysis revealed a significant decrease of the survival of spines present at day 7. The survival of spines present at day -7 was significantly increased up to day 25 of the treatment.

Afterwards, we wanted to know how THC treatment affected the survival of the newborn spines. In order to do that, we investigated the survival of gained spines from day -1, 10, 13, 16, 22, 28 and 42 (**Figure 3.6**). For all the investigated timepoints we detected a significant time effect. Also, we detected a significant treatment effect on the survival of the gained spines from day 10 and 13 and an interaction effect on day 13 and 16. Post hoc analysis revealed that spines gained on day 10 of the THC treatment had a significantly decreased survival on day 13. Also, survival of spines gained on day 13 was decreased from day 22 to 28.

Overall, it was apparent that in 3-month old animals THC treatment decreased spine survival of both stable and gained spines.

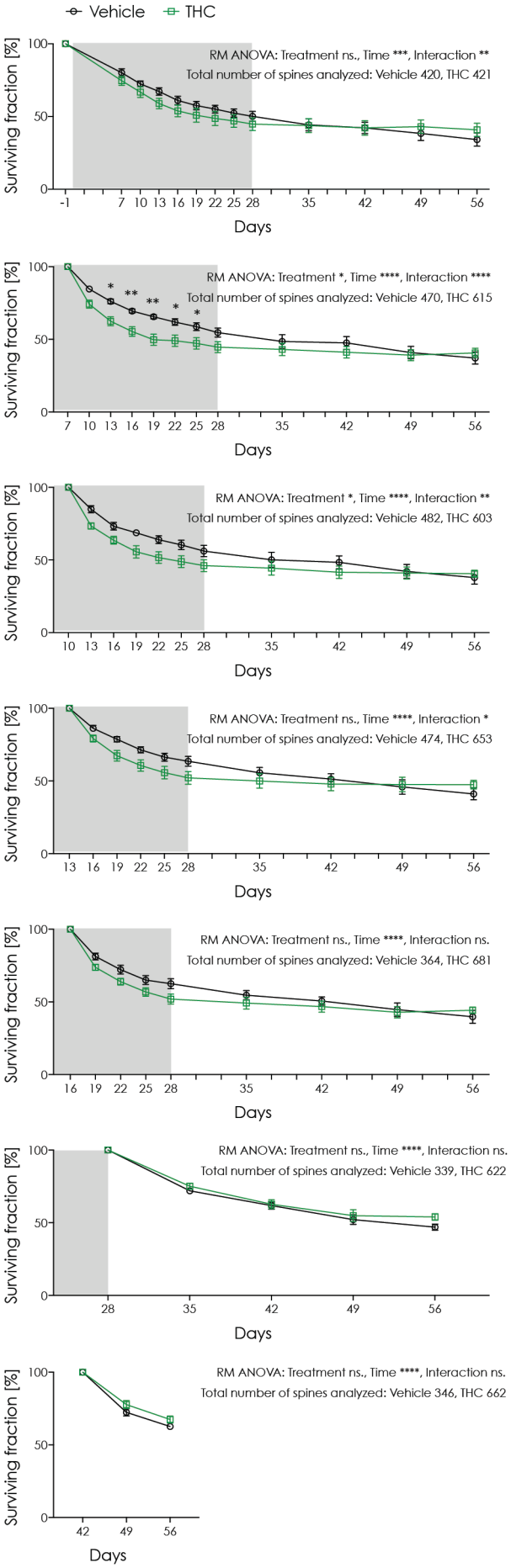

Figure 3.5. THC treatment decreases spine survival in 3-month old mice. Panels from top to bottom: surviving fraction of spines present at day -1; 7; 10; 13; 16; 28; 42. Grey box indicates the treatment duration; THC – green; vehicle – black. 3-month old mice (THC: n = 13 stacks, N = 5 mice; vehicle: n = 10 stacks; N = 4 mice. The exact number of spines analysed in each timepoint is indicated on each graph. Data shown as mean per group ± SEM. Data was analysed by RM ANOVA (Mixed-effects model (REML)) followed by Sidak's multiple comparison test; * $p < 0.05$, ** $p < 0.01$; *** $p < 0.001$; **** $p < 0.0001$.

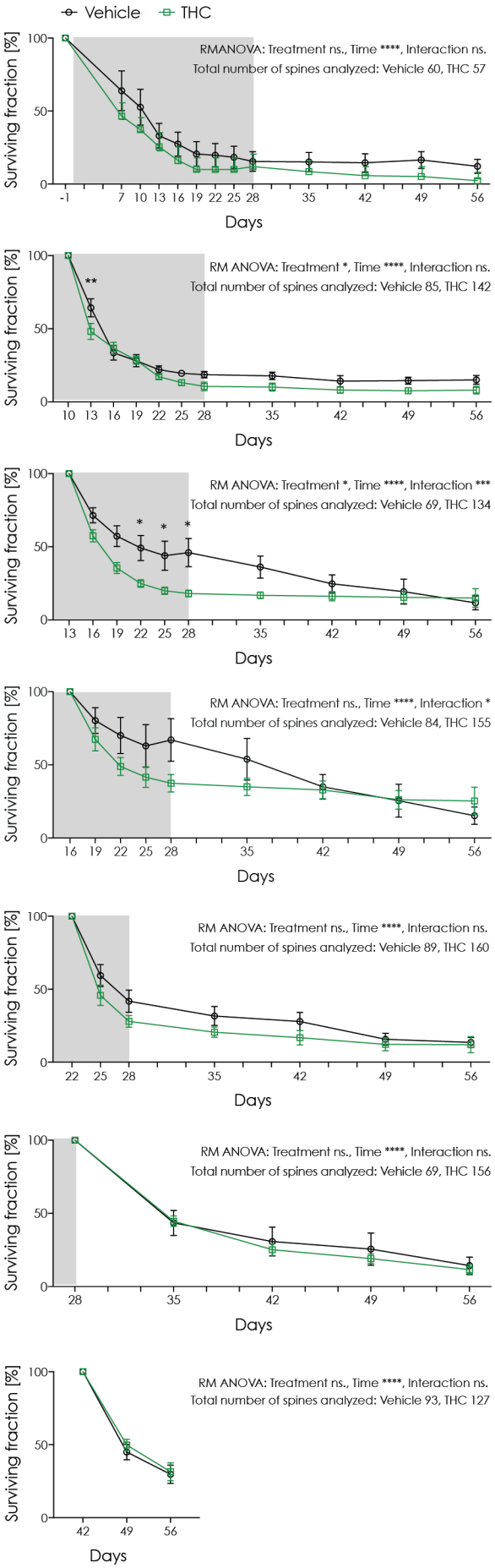

Figure 3.6. THC treatment decreases spine survival of gained spines in 3-month old mice. Panels from top to bottom: surviving fraction of spines gained at day -1; 10; 13; 16; 22; 28; 42. Grey box indicates the treatment duration; THC – green; vehicle – black. 3-month old mice (THC: n = 13 stacks, N = 5 mice; vehicle: n = 10 stacks; N = 4 mice). The exact number of spines analysed in each timepoint is indicated on each graph. Data shown as mean per group ± SEM. Data was analysed by RM ANOVA (Mixed-effects model (REML)) followed by Sidak’s multiple comparison test; * $p < 0.05$, ** $p < 0.01$; *** $p < 0.001$; **** $p < 0.0001$.

3.1.6. THC treatment increases spine stability in 18-month old mice.

We performed the same analysis on the 18-month mice and investigated spine survival of spines present at days -1, 7, 10, 13, 16, 28 and 42 (**Figure 3.7**). In all the investigated timepoints we detected a significant time and treatment effect. Additionally, at day -1, 7, 13, 16 and 28 we also detected a significant interaction effect.

In contrast to young mice, THC treatment increased spine stability in old mice. The treatment affected also the survival of spines that were present before the treatment at day -1, since their survival was significantly increased at day 10 and day 19. Survival of spines present at day 7 was significantly increased at day 19, 25 and 49, whereas survival of spines present at day 16 was increased at day 25. Finally, THC also increased the stability of spines that were present on the last day of the treatment (day 28), since their survival was increased at day 49.

Following that, investigation of the survival of gained spines showed a significant time effect in all investigated timepoints, but treatment and interaction effect were only significant for spines gained at day 10 (**Figure 3.8**). Spines gained on day 10 had a significantly increased survival at day 13 and 16.

In general, THC treatment of 18-month old mice increased spine stability, whereas in 3-month old mice we observed a decrease in spine stability.

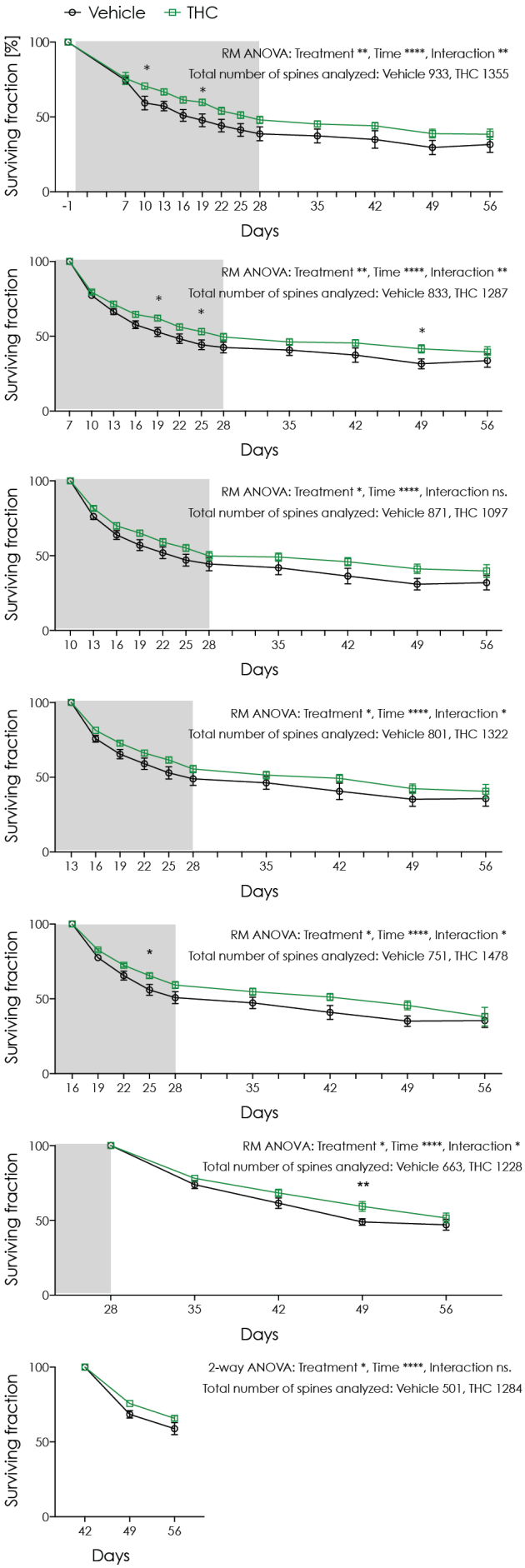

Figure 3.7. THC treatment increases spine survival of present spines in 18-month old mice. Panels from top to bottom: surviving fraction of spines present at day -1; 7; 10; 13; 16; 28; 42. Grey box indicates the treatment duration; THC – green; vehicle – black.
18-month old mice (THC: n = 22 stacks, N = 10 mice; vehicle: n = 18 stacks; N = 8 mice). The exact number of spines analysed in each timepoint is indicated on each graph. Data shown as mean per group ± SEM. Data was analysed by RM ANOVA (Mixed-effects model (REML)) followed by Sidak’s multiple comparison test; * $p < 0.05$, ** $p < 0.01$; *** $p < 0.001$; **** $p < 0.0001$.

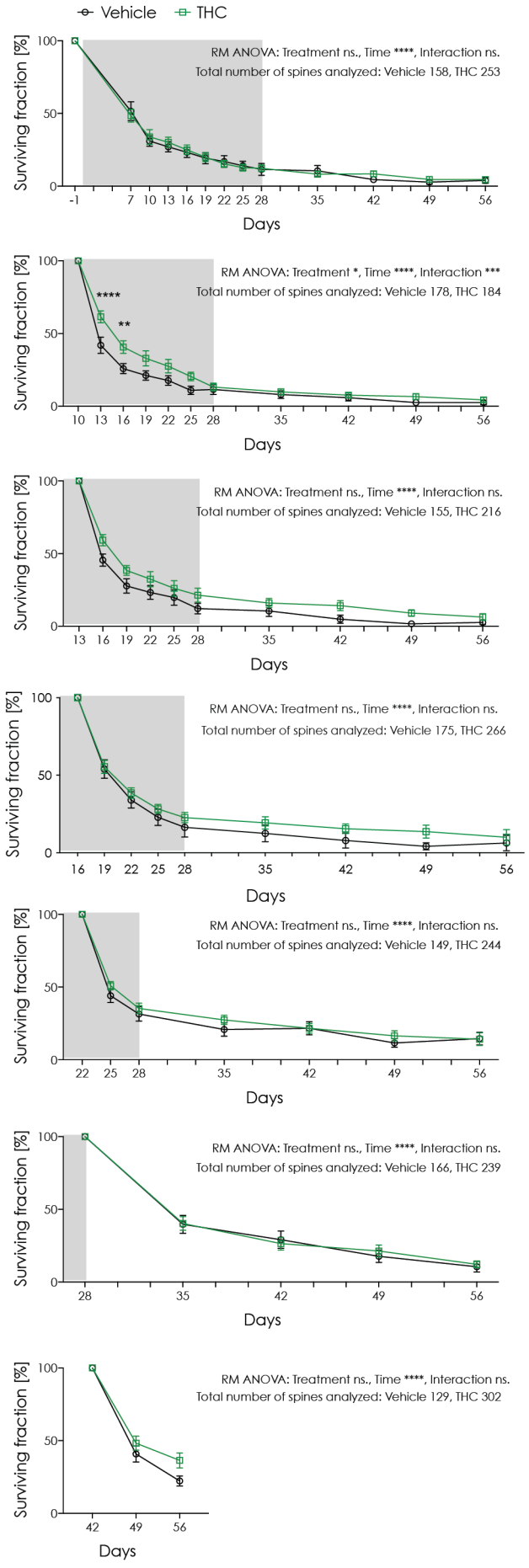

Figure 3.8. THC treatment increases spine survival of gained spines in 18-month old mice. Panels from top to bottom: surviving fraction of spines gained at day -1; 10; 13; 16; 22; 28; 42. Grey box indicates the treatment duration; THC – green; vehicle – black.

18-month old mice (THC: n = 22 stacks, N = 10 mice; vehicle: n = 18 stacks; N = 8 mice). The exact number of spines analysed in each timepoint is indicated on each graph. Data shown as mean per group ± SEM. Data was analysed by RM ANOVA (Mixed-effects model (REML)) followed by Sidak's multiple comparison test; * $p < 0.05$, ** $p < 0.01$; *** $p < 0.001$; **** $p < 0.0001$.

3.1.7. THC treatment changes the distribution of spine sizes

Next, we wanted to determine which population of spines was altered after the THC treatment. To do that, we plotted the distribution of spine lengths from the same mice on day -1 and day 35 (**Figure 3.9**). We binned the data into 0.2 μm bins with the first bin starting at 0.4 μm, since this length was our minimum criterion to classify a protrusion as an existing dendritic spine.

Due to our previous findings that the THC treatment in young mice alters spine dynamics up to 2-3 weeks into the treatment, we also looked at the changes caused by THC during the treatment in 3-month old mice. In order to do that, we compared spine length distributions on day -1 and on day 10 exclusively in 3-month old mice (**Figure 3.9a**). During the treatment, THC increased the number of small and average-sized spines that were 0.6 to 1 μm long (**Figure 3.9a: right panel**), whereas the vehicle treatment slightly increased the number of longer spines that were 1.6 - 1.8 μm long (**Figure 3.9a: left panel**). The overall number of spines in the vehicle group increased from 420 to 482, while in THC treated mice it increased from 332 to 374.

At day 35, THC treatment in 3-month old mice caused a shift of the spine length distribution peak from around 1 μm to 0.8 μm (**Figure 3.9b: right panel**), whereas in vehicle-treated mice there was no visible shift (**Figure 3.9b: left panel**). The total number of spines in the investigated stacks increased after THC treatment from 372 spines on day -1 to 415 at day 35. The vehicle treatment caused a small decrease in the number of spines from 297 to 276 within the same time period. Moreover, THC treatment increased the number of very long protrusions as lengths were binned up to 4.6 μm in contrast to all the other groups in which the last bin was at 4 μm.

In 18-month old mice, neither THC nor vehicle treatment caused any major shifts in the distribution of spine lengths (**Figure 3.9c)**. However, THC treatment increased the number of average-sized spines that were 0.6 to 1 μm long. Also, the overall number of spines was increased in the THC group from 1014 on day -1 to 1128 on day 35 and decreased in vehicle group from 704 to 607. In the vehicle group the decrease probably could not be attributed to spine loss of spines of any specific length, since the decrease was distributed evenly across all bins.

Aging significantly decreased average spine length (**Figure 3.9d**), whereas THC on day 35 did not significantly alter spine length in old mice.

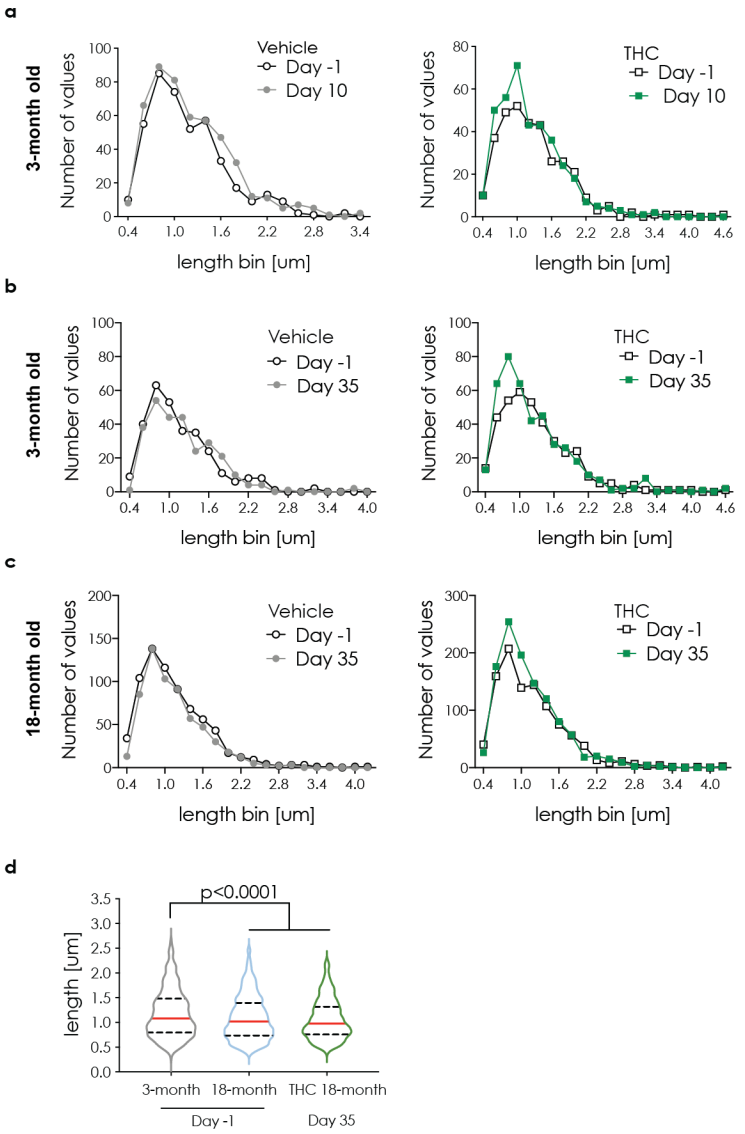

Figure 3.9. THC treatment changes the distribution of dendritic spine lengths. (**a**) Distribution of length of spines in 3-month old mice from the same animals during the treatment; from day -1 and day 10. 3-month old group vehicle n=9, THC n = 7. Distribution of length of spines in 3-month old mice (**b**) and 18-month old mice (**c**) from the same animals after the treatment; at day -1 and day 35. 3-month old group vehicle: n = 5 stacks, THC: n = 7 stacks; 18-month old group vehicle: n = 12 stacks, THC: n = 16 stacks. vehicle-treated mice – left panel; THC-treated mice – right panel. (**d**) Length of spines from young 3-month (grey) and old mice (blue) on day -1 and the effect of THC on day 35 (green). Data displayed as median (red line) with 25 and 75 percentiles (dotted, black lines). n = 740-1675 spines/group. Outliers were identified and removed using ROUT (q = 5 %). Data was checked against normal distribution using D'Augostino &Pearson normality test and significant differences were detected using U-test. The exact p-values are reported on the graph.

3.1.8. THC effect does not depend on the initial spine density and weight

We hypothesized that the effect size of the THC-induced changes could be dependent on the initial spine density as higher spine dynamic rate was reported in regions with high spine density (Tjia et al., 2017). To investigate that for 3-month old mice, we correlated the effect size, represented by turnover ratio at day 7 and 10 with the initial spine density at day -1 (**Figure 3.10a**). The turnover ratio increase was not significantly correlated to the initial spine density, neither at day 7 nor at day 10.

Since it was reported that THC accumulates in fat tissue (Nahas, 2001), we hypothesized if the initial weight of the animal could possibly impact the effect size. Thus, we correlated

weight of the mice at the time of pump implantation (day 0) with the turnover ratio at day 7 (**Figure 3.10b**). We did not detect any significant correlation between the two.

In 18-month old mice we correlated the effect size, this time represented by the relative spine density change (%) at day 35 and 56 to the initial spine density at day -1 (**Figure 3.10c**). As for the 3-month old mice, we did not detect any significant correlation. Subsequently analysed spine density change was also not significantly correlated with the initial weight of the animals at day 0 (**Figure 3.10d**).

Taken together, we have shown that THC effect on dendritic spines is not dependent on the initial spine density or weight of the mice.

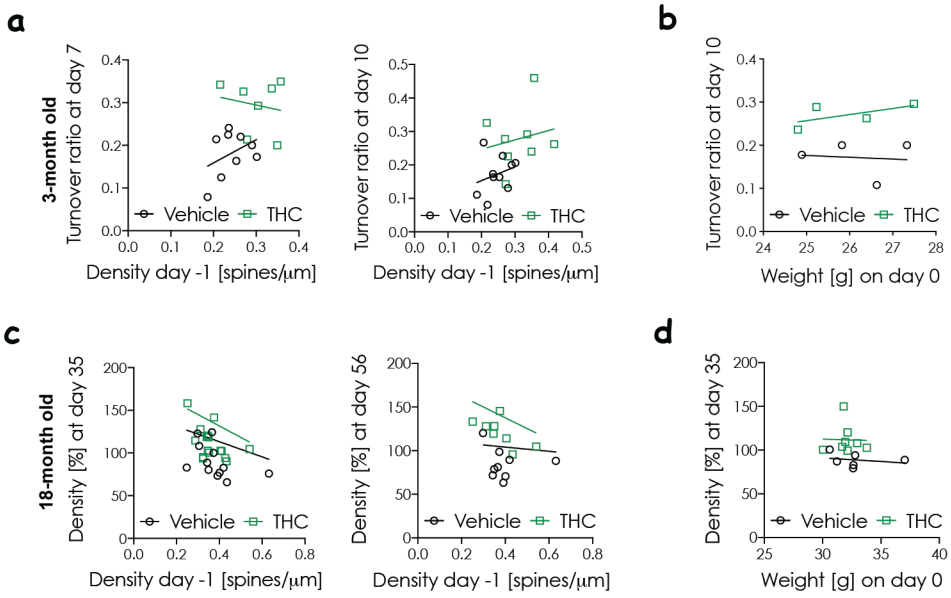

Figure 3.10. THC effect does is not correlated to the initial spine density and weight. (**a**) In 3-month old mice: correlation of the turnover ratio on day 7 (left panel) day 10 (right panel) to the initial spine density before the treatment, at day -1. Vehicle: n = 10 stacks; THC: n = 7 stacks. (**b**) In 3-month old mice: correlation of the mean turnover ratio on day 10 to the initial weight of the mouse before the vehicle/THC treatment (at day 0). Vehicle: N = 4; THC: N = 4 mice. (**c**) In 18-month old mice: correlation of the relative spine density change (%) on day 35 (left panel) and day 56 (right panel) to the initial spine density before the treatment (day -1). Vehicle: n = 9-12 stacks; THC: n = 8-12 stacks. (**d**) In 18-month old mice: correlation of the relative spine density change (%) on day 35 to the initial weight before treatment (day 0). Vehicle: N = 6; THC: N = 7 mice.
THC – green; vehicle – black. Each point represents a single stack (**a, c**) or a single animal (**b, d**). Data was correlated using Pearson or Spearman correlation coefficient.

3.1.9. THC treated 18-month old mice resemble 3-month old mice on the level of spine dynamics

Next, we investigated age-related changes in spine dynamics and how THC-treatment altered those changes. In order to do that, we compared the stacks from all 3-month old mice at baseline (day -7 to day -1) to vehicle and THC treated 18-month old mice (**Figure 3.11**). We calculated different parameters starting with spine density after treatment at day 35 and then following up with the spine dynamics in the middle of the treatment at day 16.

We detected a significant increase in spine density between baseline 3-month old mice and vehicle-treated 18-month old mice (**Figure 3.11a**). This effect was further enhanced by THC as we detected a significant increase in the spine density between THC- and vehicle-treated 18-month old mice at day 35 of the experiment.

The turnover ratio, was increased with age as we detected, since we detected a significant increase between 3-month and 18-month vehicle-treated mice (**Figure 3.11b**). THC treatment at day 16 significantly decreased the turnover ratio in comparison to vehicle treatment. Despite that, the turnover ratio in the THC-treated group was significantly elevated in comparison to the 3-month old group.

The % of lost spines was also increased with age as we detected a significant increase between 3-month and 18-month vehicle-treated mice (**Figure 3.11c**). Here, THC-treatment significantly decreased the percentage of lost spines in comparison to the vehicle treated group. Subsequent comparison between 3-month old and THC-treated 18-month old mice did not show any significant difference between the groups.

Similarly, the % of gained spines also increased with age, since we detected a significant increase between 3-month and 18-month vehicle-treated mice (**Figure 3.11d**). THC treatment did not significantly alter the % of gained spines, but we detected a trend for e decrease between vehicle- and THC-treated 18-month old groups. Also, 18-month old THC treated group had a significantly higher % of gained spines than the 3-month old group.

Subsequent analysis of transient spines did not show any age-related change, but we detected a trend for an increase between 3-month and 18-month vehicle-treated group (**Figure 3.11e**). THC treatment did not significantly decrease the percentage of transient spines, although we detected a trend in this direction. Furthermore, there was no significant difference between 3-month old and THC-treated 18-month old group.

We detected a significant age-related decrease in the % of stable spines as we detected a significant decrease between 3-month and 18-month vehicle-treated mice (**Figure 3.11f**). THC-treatment significantly increased the % of stable spines in comparison to the vehicle-treated group. Moreover, we did not detect any significant difference between 3-month old mice and 18-month old mice from the THC-treated group.

Finally, we looked into age-related changes in spine stability by investigating the survival fraction of spines gained between day 7 and day 10 of the treatment (**Figure 3.11g: top panel**) and all the spines present at day 10 (**Figure 3.11g: bottom panel**). In order to see the aging effect, we first compared the survival curves between young, 3-month old vehicle-treated mice and old, 18-month old vehicle treated mice. We detected a significant time, age and interaction effect in the survival of both gained and present spines. Post hoc analysis showed a significant age-related decrease in the survival of the gained spines on day 13 and in the survival of the present spines on day 25. Then, we investigated the THC effect by comparing 3-month old vehicle group with 18-month old THC-treated group. For the survival of both gained and present spines we only detected a significant time effect. Post hoc analysis did not show any age-related differences.

Collectively, we found that aging increased spine dynamics and decreased spine stability. We also found that THC effect is age dependent and that old THC-treated mice resembled young mice on the level of spine dynamics.

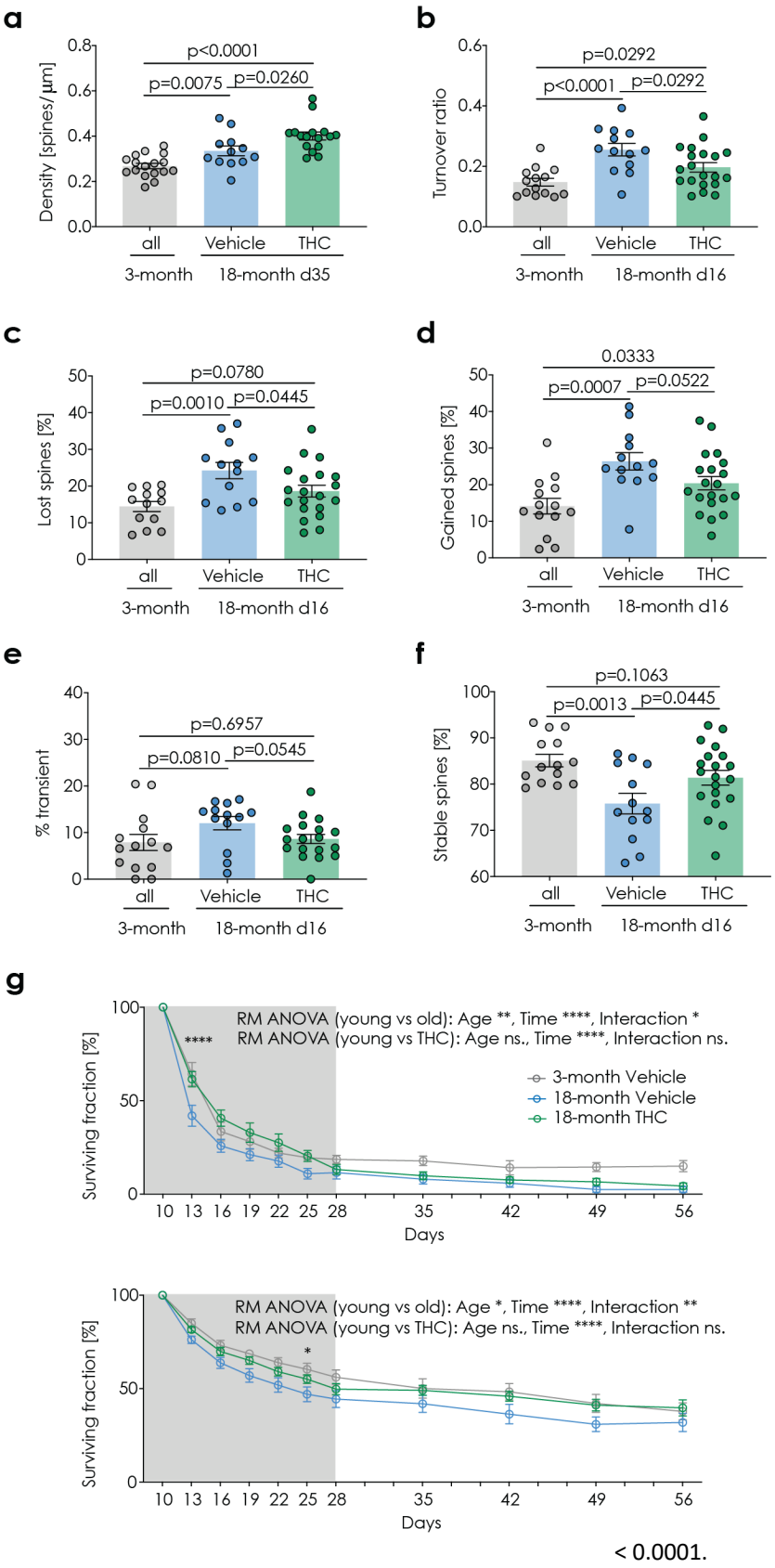

Figure 3.11. THC treated 18-month old mice resemble 3-month old mice on the level of spine dynamics. (**a**) Density of spines – number if spines per micron. d35 – day 35 of the experiment.

(**b**) Turnover ratio – number of lost and gained spines between two consecutive timepoints divided by the total number of spines in both timepoints. The % of spines that were lost (**c**), gained (**d**), transient (**e**) and stable (**f**) between two consecutive timepoints.

3-month old mice, before treatment at day -1 – grey circles (n = 14-17); vehicle-treated 18-month old mice – blue circles (n = 12-13); THC-treated 18-month old mice – green circles (n = 16-20). Each point represents a single stack (**a-f**). Data was checked against normal distribution using D'Augostino &Pearson normality test and columns were compared to each other using unpaired t-test. The exact p-values were placed on each graph.

(**g**) Survival curves from vehicle-treated 3-month (grey circles) and 18-month old mice (blue circles) and THC-treated 18-month old mice (green circles). Top panel – survival curve for spines gained at day 10; bottom panel – survival curve of the spines present at day 10. Data shown as mean per group ± SEM. Data was analysed by RM ANOVA (Mixed-effects model (REML)) followed by Sidak's multiple comparison test between vehicle-treated 3-month and 18-month group; * $p < 0.05$, ** $p < 0.01$; *** $p < 0.001$; **** $p < 0.0001$.

3.2. THC treatment influences microglia activity in old mice

3.2.1. THC decreases microglial CD68 levels

To investigate one of the possible mechanisms of how does THC influence spine dynamics in old mice, we evaluated changes in microglia activity in the somatosensory cortex. Therefore, we performed immunohistochemical staining of brain sections from 18-month old mice treated with either vehicle or THC. We assessed the immunoreactivity of Iba1 – microglial marker and CD68 – microglial phagocytic activity marker (**Figure 3.12a**). Since we used GFP-M mice in our study we were able to visualize neurons using internally expressed eGFP.

First, using high-resolution images we quantified the Iba1 intensity within microglial soma (**Figure 3.12b**), since an increase in Iba1 expression is associated with pro-inflammatory status of microglia. THC treatment caused a significant decrease in somatic Iba1 intensity and shifted the peak of the intensity histogram to lower values: from 40 to 30 mean grey value.

Pro-inflammatory microglia have larger soma and higher phagocytic activity. Thus, next we decided to investigate the soma size and CD68 levels after THC treatment. THC did not alter the soma size of microglia (**Figure 3.12c**), but significantly decreased the CD68 immunoreactivity (**Figure 3.12d**). Due to the fact that CD68 staining is not ubiquitous over the whole soma area, we measured the % of somatic area covered by the CD68 positive signal thereby acquiring a more precise estimation of the CD68 changes (**Figure 3.12e**). We confirmed our previous findings and detected a significant decrease in the % of area covered by CD68 positive puncta after THC treatment. Subsequent analysis of the distribution of values showed that THC treatment significantly increased the number of CD68 negative cells (% of area covered by CD68 positive signal = 0 %). In the vehicle-treated group only 0.65 % of microglial soma area did not contain any CD68, whereas in THC-treated group this number was increased to 4.87 %. Moreover in the vehicle-treated group, the biggest number of microglia had 10-30 % of their soma area covered with CD68 positive signal, whereas in the THC-group it was only 0-10 %.

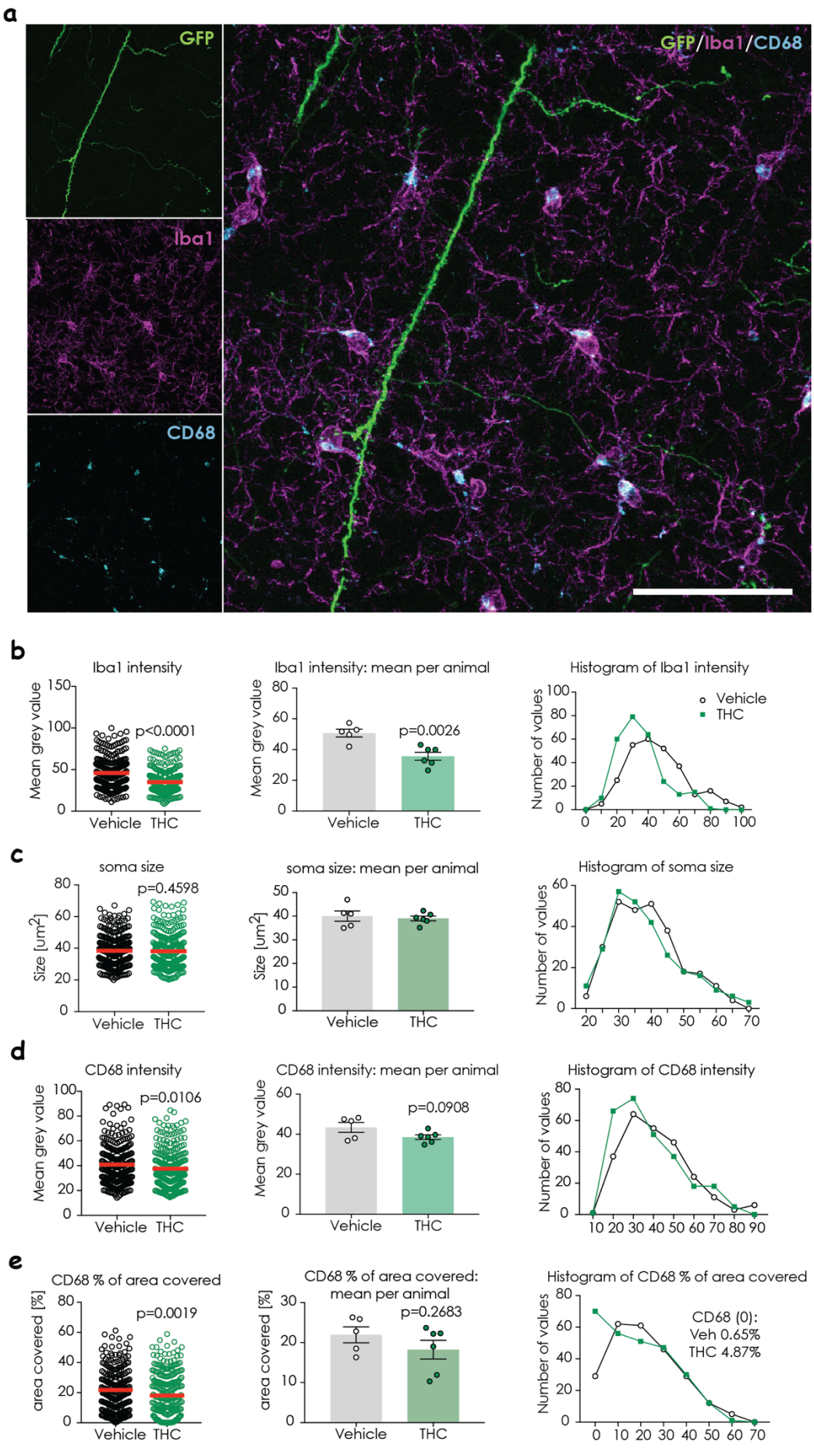
a
GFP
Iba1
CD68
GFP/Iba1/CD68
b
Iba1 intensity
Mean grey value
p<0.0001
Vehicle
THC
Iba1 intensity: mean per animal
p=0.0026
Histogram of Iba1 intensity
Number of values
Vehicle
THC
c
soma size
Size [um2]
p=0.4598
soma size: mean per animal
Histogram of soma size
d
CD68 intensity
p=0.0106
CD68 intensity: mean per animal
p=0.0908
Histogram of CD68 intensity
e
CD68 % of area covered
area covered [%]
p=0.0019
CD68 % of area covered: mean per animal
p=0.2683
Histogram of CD68 % of area covered
CD68 (0):
Veh 0.65%
THC 4.87%

Figure 3.12. Microglial Iba1 and CD68 are decreased after the THC treatment. (**a**) Example images of the GFP/Iba1/CD68 immunoreactivity. Left panel – single channel images. Right panel – merged channel image. Scaler bar represents 50 μm. GFP – green; Iba 1 – magenta; CD68 – cyan. (**b-e**) Left panel – each point represents a single microglial soma. Mean of the group is indicated with a red line. Middle panel – each point represents a mouse. Right panel – histogram of single microglia soma values from the left panel. Vehicle – black/grey; THC – green. Measurement were done within microglial soma ROI: (**b**) Iba1 intensity; (**c**) soma ROI size; (**d**) CD68 intensity; © CD68 % of area covered. N = 278-308 cells/treatment; N = 5-6 animals/treatment. Outliers were identified and removed using ROUT (q = 5 %). Data was checked against normal distribution using D’Augostino &Pearson normality test and groups were compared to each other using unpaired t-test/U-test. The exact p-values are reported on each graph.

3.2.2. THC treatment changes microglia morphology in old mice

Activity of microglia is reflected in changes in their morphology, thus we assessed the microglial morphology to further investigate possible changes in microglia activity. In order to do that we obtained high-resolution z-stacks of whole microglial cells and analysed them with the MOTIQ Fiji plugin. This program automatically traces single cells and generates their 3D reconstructions (**Figure 3.13a**).

Consistently with our previous findings, we found that THC treatment in 18-month old mice significantly decreased Iba1 intensity not only in the soma, but in the whole microglia cell body (**Figure 3.13b**). Simultaneously, THC treatment did not alter microglia volume or surface area, but significantly increased microglia polarity index. Subsequent analysis of the microglia ramification showed that microglia from THC-treated animals had a significantly smaller number of branches and triple points resulting in a lower ramification index (**Figure 3.14c**). However, we did not detect any significant difference in the average branch length.

Taken together, we were able to show that THC treatment caused slight alterations in microglia morphology.

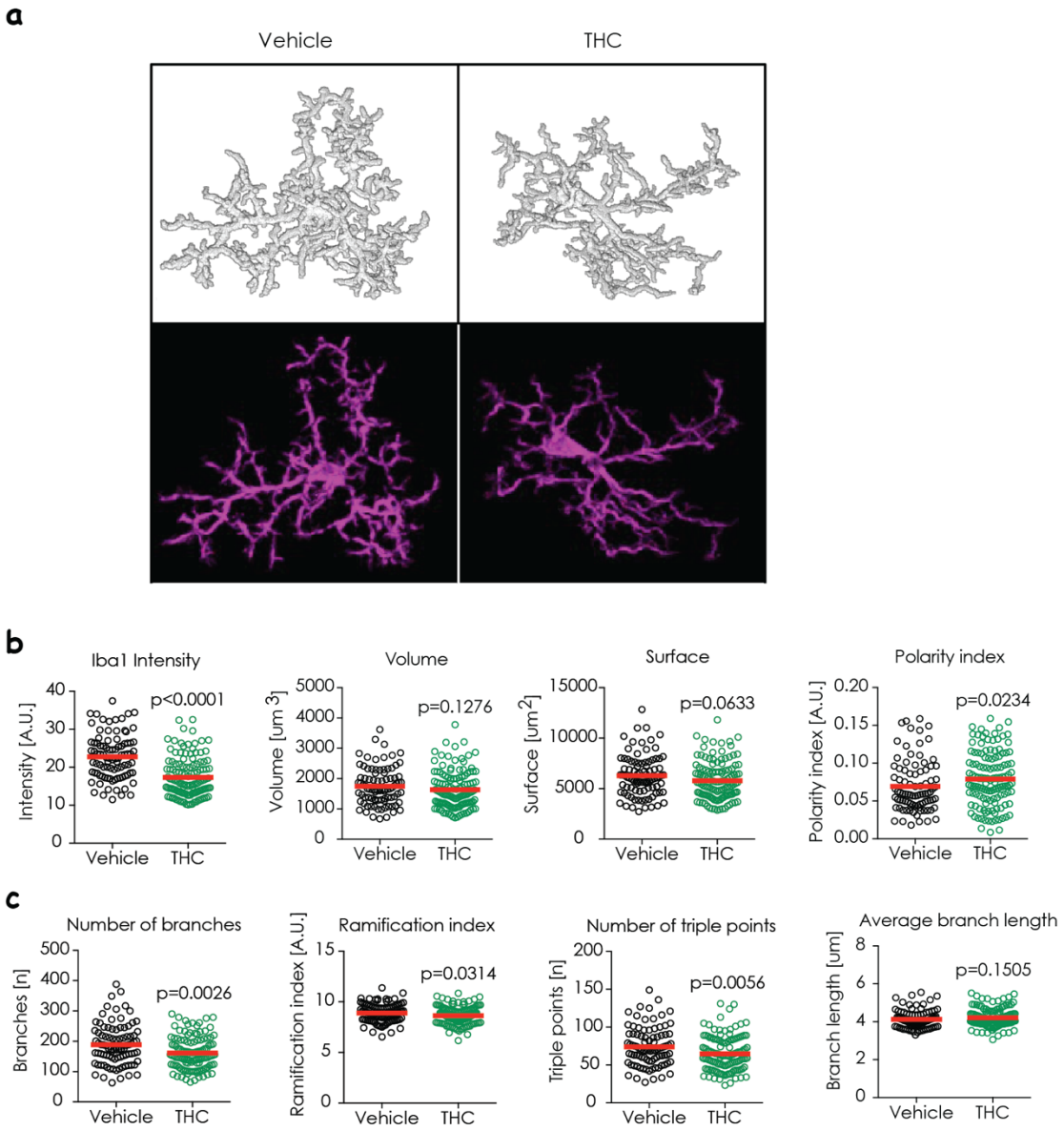

Figure 3.13. THC treatment of old mice changes microglia morphology (**a**) Example images of the microglia cells reconstructions (top panel) and their corresponding maximum z projections (bottom panel). (**b**) General morphological parameters from left to right: Iba1 intensity in the whole cell; volume of the cell; surface of the cell; polarity index of the cell. (**c**) Ramification-related parameters from left to right: number of branches; ramification index; number of triple points; branch length. Each point represents single microglia. Mean of the group is indicated with a red line. Vehicle – black circles; THC – green circles. n = 87-124 cells/treatment/area; N = 5-6 mice/treatment. Outliers were identified and removed using ROUT (q = 5 %). Data was checked against normal distribution using D'Augostino &Pearson normality test and significant differences were detected using U-test. The exact p-values are reported on each graph.

3.2.3. THC treatment does not change microglia density in old mice

Next, we investigated whether THC treatment alters microglia proliferation and if this effect is area-specific. In order to do that, we measured microglia density and % of area covered by the Iba1 signal in the somatosensory cortex and in three hippocampal areas: CA1, CA3 and dentate gyrus (DG) (**Figure 3.14**). For quantification, we used lower magnification, single-plane images. Within each area we distinguished different layers to account for possible layer-specific alterations.

We did not detect any significant treatment or interaction effects in any of the investigated areas, neither for microglia density nor for % of area covered by the Iba1 signal. In the cortex, we detected a layer effect for both microglia density and % of area covered by the Iba1 signal (**Figure 3.14b**). In the CA1, we also detected a layer effect for microglia density, but no effect for % of area covered (**Figure 3.14c**). We did not detect any significant effects in CA3 and DG of the hippocampus, although we detected a trend for a layer effect in the microglia density of the CA3 area (**Figure 3.14d-e**).

Overall, we did not find any effect of the THC treatment neither on the microglia density nor on the % of area covered by microglia. Although, it should be noted that the overall % of area covered was higher in the cortex and DG with means around 4-5 % depending on the layer, while in the CA1 and CA3 it was on the level of 2-3 %.

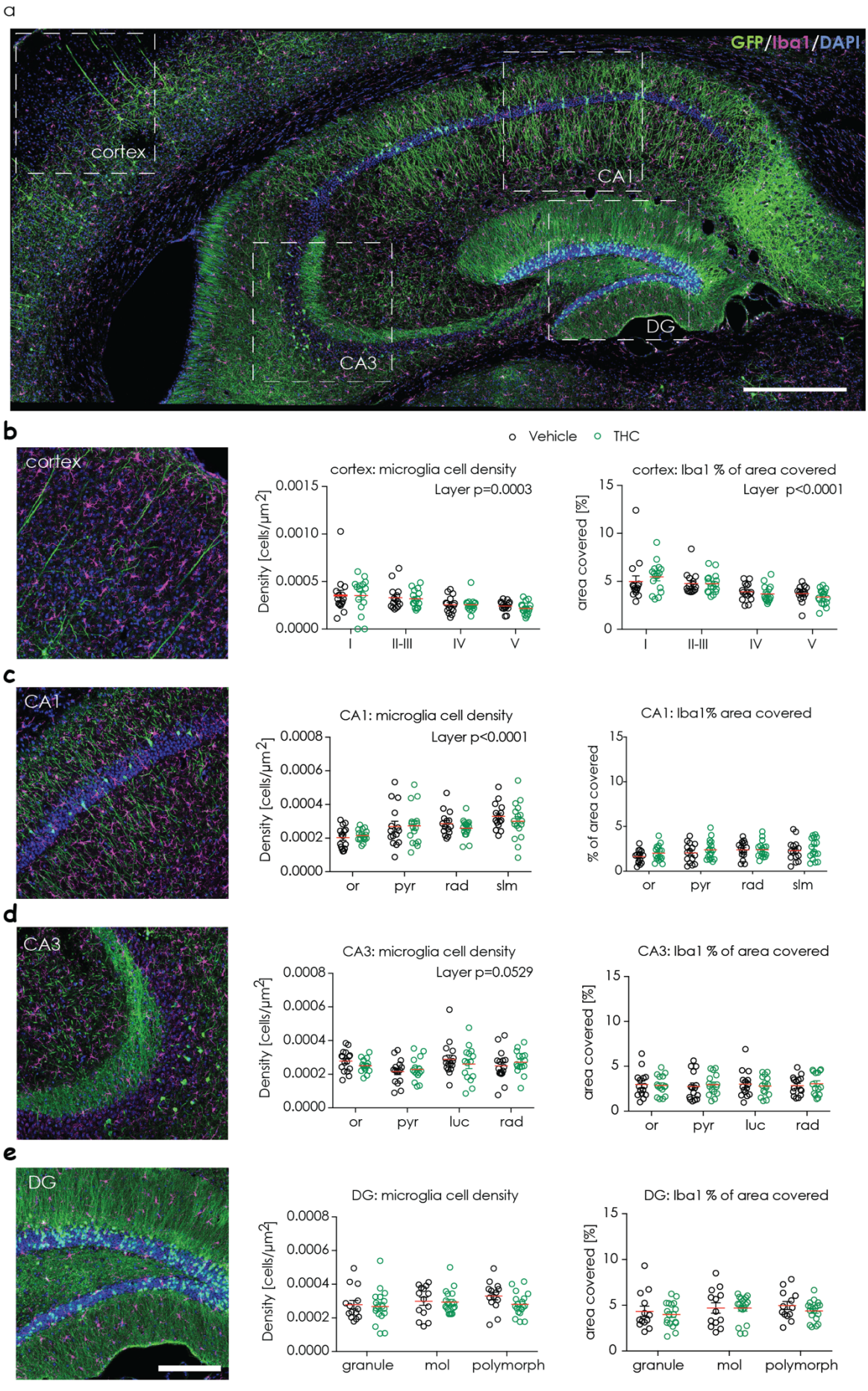
a
GFP/Iba1/DAPI
cortex
CA1
CA3
DG
b
cortex
Vehicle
THC
cortex: microglia cell density
Layer p=0.0003
Density [cells/µm2]
0.0015
0.0010
0.0005
0.0000
I
II-III
IV
V
cortex: Iba1 % of area covered
Layer p<0.0001
area covered [%]
15
10
5
0
c
CA1
CA1: microglia cell density
Layer p<0.0001
0.0008
0.0006
0.0004
0.0002
or
pyr
rad
slm
CA1: Iba1% area covered
% of area covered
d
CA3
CA3: microglia cell density
Layer p=0.0529
luc
CA3: Iba1 % of area covered
e
DG
DG: microglia cell density
granule
mol
polymorph
DG: Iba1 % of area covered

Figure 3.14. THC treatment does not change microglia density. (**a**) Overview image of the GFP/Iba1/DAPI immunohistochemical staining. Scale bar represents 500μm. GFP, neurons – green; Iba 1, microglia – magenta; DAPI, nuclei – blue. (**b-e**) Left panel – a representative image. Scale bar 200 μm. Middle panel – microglia density as number of microglial cells divided by area. Right panel – % of area covered by the Iba1 signal. Each point represents a single image. Mean of the group is indicated with a red line. Vehicle – black circles; THC – green circles. N = 15-18 images/treatment/area; N = 5-6 mice/treatment. Data was analysed by two-way ANOVA. The exact p-values are reported on each graph.

3.2.4. THC-induced alteration of Iba1 and CD68 levels is brain area-dependent

Since THC treatment decreased Iba1 and CD68 intensities in the somatosensory cortex, we next asked whether this is a cortex-specific phenomenon. In order to investigate that, we used the single-plane images from different brain areas to obtain ROI masks of all the detected microglia. Then we measured Iba1 and CD68 intensities within each single microglia ROI mask. Finally, similar to our processing of the high magnification images, we also measured the % of area covered by the CD68 positive signal (**Figure 3.15**).

We were able to confirm our results, since we found once again that THC treatment has significantly decreased Iba1 intensity in the cortex in single microglia (**Figure 3.15a**). The effect was area-dependent, since we detected a similar significant decrease in DG, but not in CA1 or CA3. On a contrary, in CA1 we detected a significant increase in Iba1 intensity.

In agreement with that, both in the cortex and in the DG we detected a significant decrease in CD68 intensity after the THC treatment (**Figure 3.15b**). This effect was not present in CA1 and CA3.

The subsequent analysis of the % of area covered by the CD68 positive signal further confirmed the previous results as THC treatment significantly decreased % of area covered by the CD68 positive signal exclusively in cortex and DG (**Figure 3.15c**).

Since earlier we detected almost a 10-fold increase in CD68 negative cells in the cortex upon THC treatment, we decided to estimate the number of CD68 negative cells in different brain areas (**Figure 3.15d; Table 3.1**). In vehicle-treated group we counted the biggest number of CD68 negative cells in the CA3 (35.81 %) and the lowest number in the DG (23.61 %) and cortex (23.81 %). In all areas we noted an increase in the number of CD68 negative cells after the THC treatment. The biggest increase happened in DG with 11.53 %, similarly in cortex with 10.21 %, a bit smaller in CA3 with 8.44 % and the smallest increase was in CA1 with 4.65 %. Subsequently, we quantified the % of cells expressing low levels of CD68 having less than 5% of area covered by the CD68 positive signal. THC treatment increased the amount of CD68 low-expressing cells by 10-23 % depending on the area. We

detected the highest increase in the DG (23.32 %), a bit lower in CA3 (16.35 %) and lowest in CA1 and cortex (around 10 %).

Taken together we showed that THC treatment decreased Iba1 and CD68 levels similarly in DG and cortex. Also, THC treatment increased the number of CD68 negative and low-expressing microglia in all the investigated brain areas.

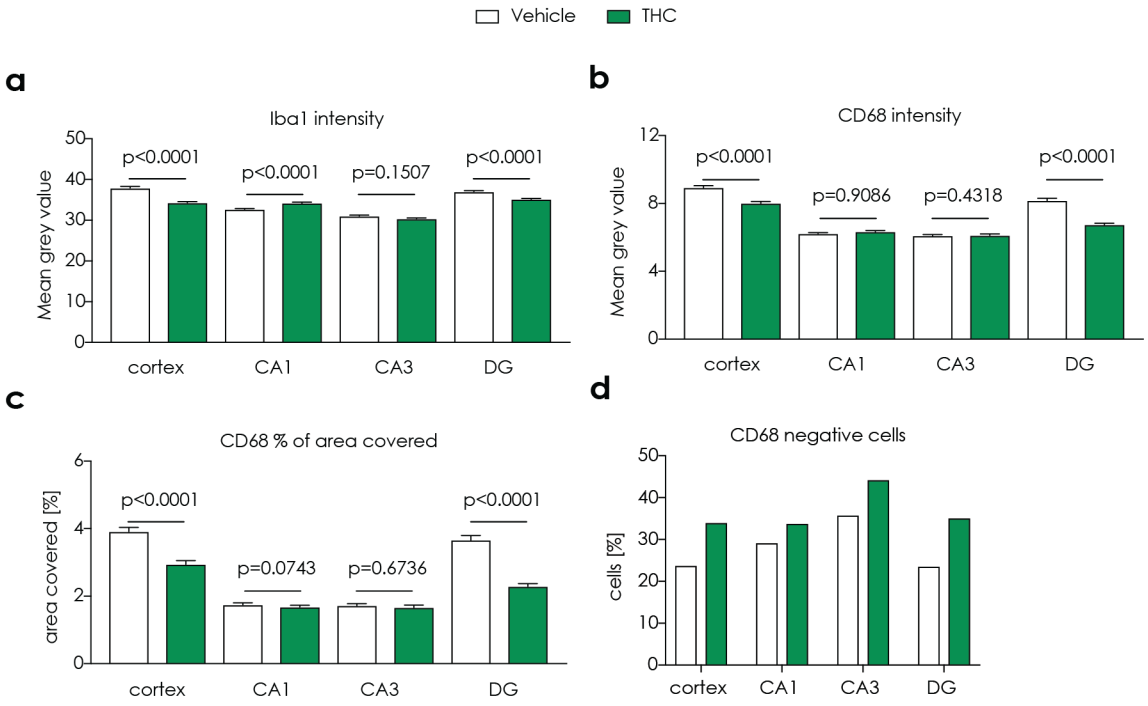

Figure 3.15. THC-induced alteration of Iba1 and CD68 levels is brain area-dependent. (**a**) Iba1 intensity (**b**) CD68 intensity (**c**) % of area covered by CD68 positive signal (**d**) % of all detected microglia that are CD68 negative. Data presented as mean ± SEM. Vehicle – white bars; THC – green bars. N = 916-1436 cells/treatment/area; N = 5-6 mice/treatment. Outliers were identified and removed using ROUT (q = 5 %). Data was checked against normal distribution using D'Augostino &Pearson normality test and groups were compared to each other using unpaired t-test/U-test. Each brain area was analysed independently. The exact p-values are reported on each graph.

Table 3.1. Number of CD68 negative cells in different brain areas after THC treatment. Values presented as a % of all cells.

CD68% = 0%	cortex	CA1	CA3	DG
Vehicle	23.81	29.22	35.81	23.61
THC	34.02	33.87	44.25	35.14
CD68% < 5%	cortex	CA1	CA3	DG
Vehicle	65.63	64.8	72.35	60.11
THC	75.61	74.01	88.7	83.43

3.2.5. THC treatment decreased microglia-neuron interaction

Next, we asked if THC treatment affected the number of microglia-neuron interactions. In order to investigate that, we first used the single plane, lower magnification images that were used previously for microglia density calculation (**Figure 3.16a**).

THC treatment significantly decreased the number of GFP x Iba1 colocalized pixels (**Figure 3.16b**). Due to the high variability of the length and number of dendritic segments that we were able to obtain per animal (2-8) and low-magnification of the images we decided to confirm our findings with an independent experiment. In order to do that we took 10-12 high-magnification single-plane images per animal containing at least 40μm long dendritic segments and repeated the analysis (**Figure 3.16c**). Consistently with our previous finding, we found a significant decrease in the number of GFP x Iba1 colocalized pixels after the THC treatment (**Figure 3.16d**). The difference did not arise from the bias in the imaged dendritic segments as both the % of area covered by the GFP signal per dendritic segment as well as the cumulative length of the investigated segments did not differ between the groups (**Figure 3.16e**).

Then, we asked if the observed decrease comes from a certain type of dendrites or is it a general phenomenon. Thus, we quantified the spine densities on the investigated fragments and measured the corelation between the amount of colocalization and spine density. We found no significant corelation neither in the vehicle nor in the THC-treated groups (**Figure 3.17a**).

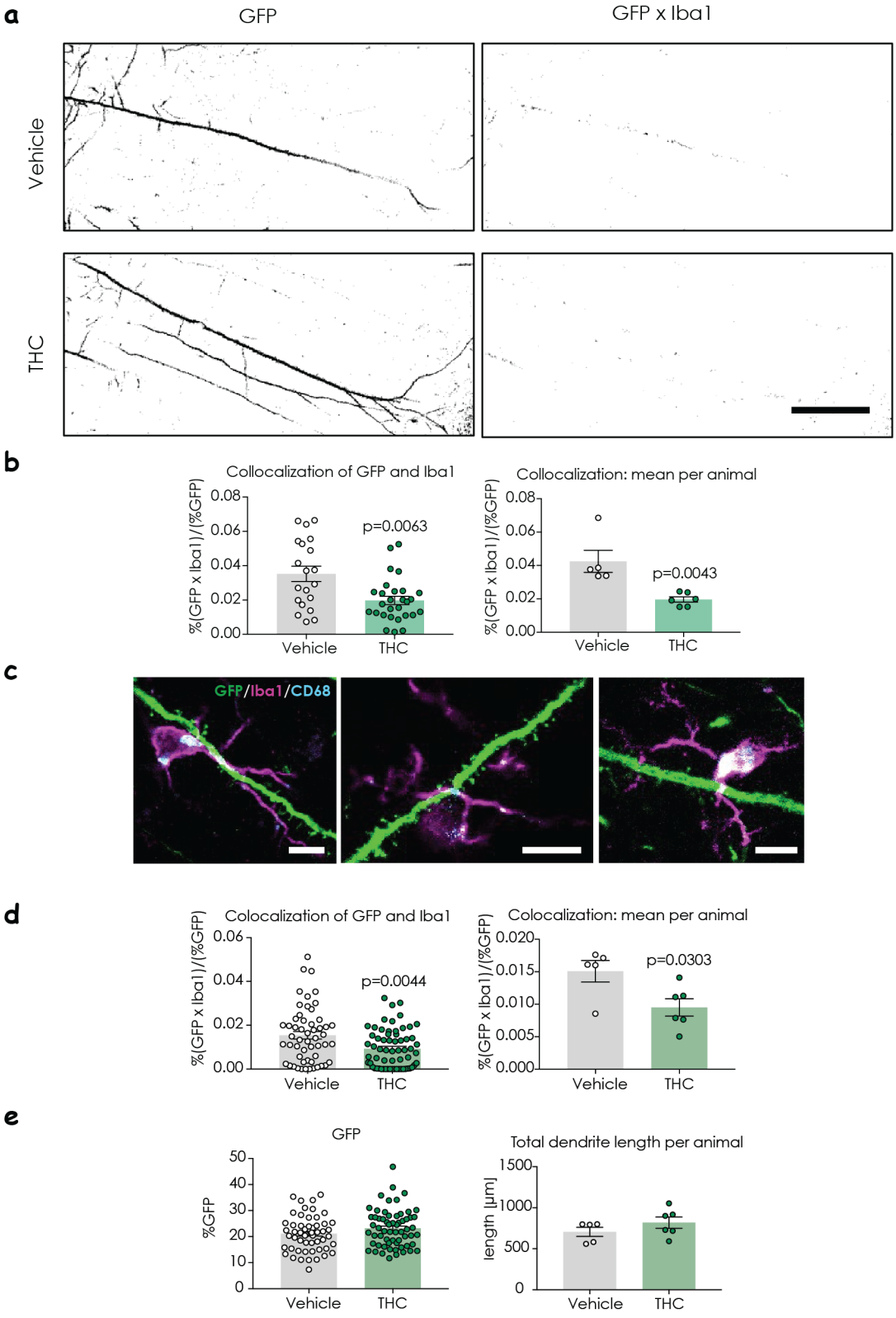

Figure 3.16. THC treatment decreases the interaction between neurons and microglia (**a**) Example binary images of dendritic segment (left panel) and the corresponding binary image of GFPxIba1 colocalized pixels (right panel). Scale bar represents 100 µm. vehicle – top panel; THC – bottom panel. (**b**) Quantification of the % of area occupied by colocalized pixels (GFPxIba1) normalized to the % of area occupied by GFP positive signal from lower resolution images. n = 20-28 dendritic segments/treatment; N = 5-6 mice/treatment. Left panel – all dendritic segments; right panel – mean per animal. (**c**) High magnification example images of colocalization of GFP x Iba1 (white). GFP, neurons – green; Iba 1, microglia – magenta; DAPI, nuclei – blue. Scale bars represent

10 μm. (**d**) Quantification of the % of area occupied by colocalized pixels (GFP x Iba1) normalized to the % of area occupied by GFP positive signal from high-resolution images. n = 60-70 dendritic segments/treatment; N = 5-6 mice/treatment. Left panel – all dendritic segments; right panel – mean per animal. (**e**) Left panel – measured % of area covered by GFP within each segment; Right panel – total length of dendritic segments analysed for high magnification images.
Vehicle – grey circles; THC – green circles. Outliers were identified and removed using ROUT (q = 5 %). Data was checked against normal distribution using D’Augostino &Pearson normality test and groups were compared to each other using unpaired t-test/U-test. The exact p-values are reported on each graph.

Then we binned the data based on spine density (size of the bin = 0.1) and detected a significant treatment effect. Following post hoc analysis showed a significant decrease of the GFP x Iba1 colocalization in dendrites with spine density of 0.6 spines / μm (**Figure 3.17b**). We also detected a trend for a decrease in bins 0.7 – 0.9. Thus, we divided the segments into two groups: with spine density smaller than 0.6 and spine density equal or larger than 0.6 spines / μm. Analysis by Two-way ANOVA showed a significant treatment and interaction effect and the post hoc analysis detected around 60 % decrease in GFP x Iba1 colocalization in dendritic segments with spine density >= 0.6 spines / μm.

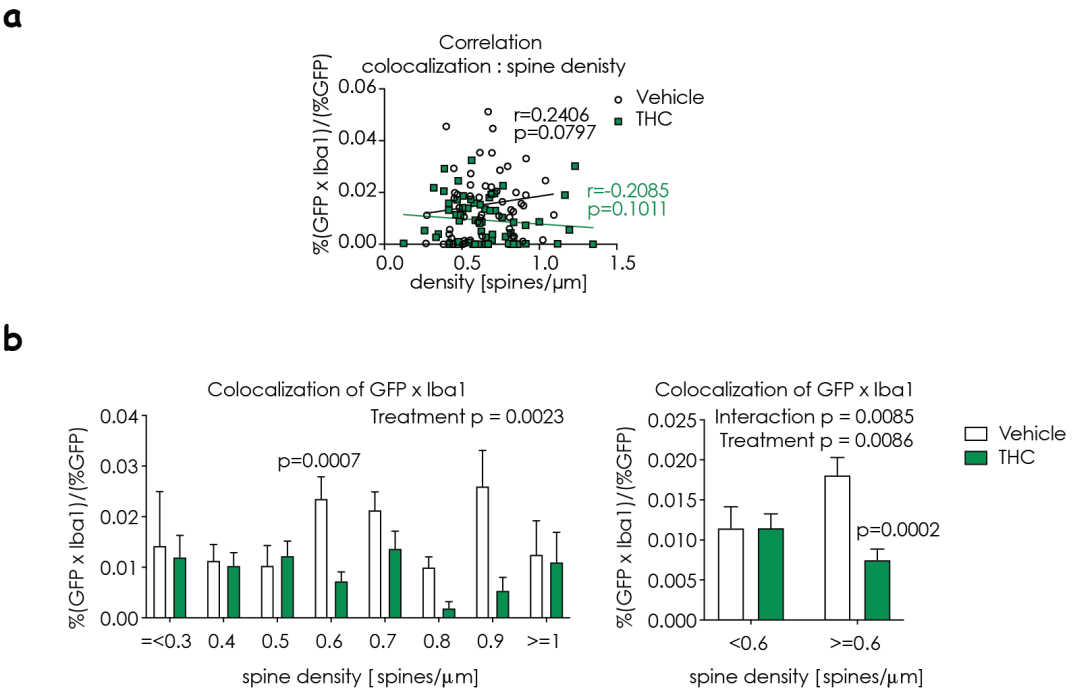

Figure 3.17. THC treatment decreased the colocalization of GFP x Iba1 in dendrites with higher spine density. (**a**) Corelation between colocalization of GFP x Iba1 and spine density. Each point represents a single dendritic segment. n = 60-70 dendritic segments/treatment. Outliers were identified and removed using ROUT (q = 5 %). Sperman r correlation. (**b**) Colocalization of GFP x Iba1 in dendritic segments was binned based on spine density. Left panel – bin size = 0.1, n = 2-15 dendritic segments/treatment/bin; Right panel – divided into two groups. n = 22-35 dendritic segments/treatment/bin. Vehicle – white; THC – green. Data shown as mean per group ± SEM. Data was analysed by two-way ANOVA followed by Sidak’s multiple comparison test. The exact p-values are reported on each graph.

Overall, we were able to show that THC-treatment not only decreased microglial Iba1 and CD68 levels, but also decreased the spatial contacts between microglia and neurons. This effect seemed to be more prominent in dendrites with higher spine density.

3.3. Evaluation of cognition and other behaviours of THC-treated mice

3.3.1. Repeated imaging and testing decreased mice sociability and thus prevented a proper assessment of memory performance

To observe the consequences of THC-treatment on the behavioural level we included a social memory test (partner recognition - PR) (**Figure 3.18a**). We repeated the PR test at different timepoints of the treatment to be able to observe the changes in mice behaviour at baseline (PR1), after the first 3 imaging sessions (PR2), in the middle of the treatment (PR3) and at the end of the treatment (PR4). For the 18-month old groups we also included another PR test two-weeks after the treatment (PR5)**.**

PR test consists of two trials (**Figure 3.18b**). In the first trial we measured the sociability, while in the second one we measured the novelty preference For PR1 and PR2, that took place before the treatment, vehicle and THC groups were pooled together for analysis.

3-month old mice had a sociability above the chance level only in PR1 and 2 and the THC-treated group in PR3, whereas 18-month mice had it only in PR1 (**Figure 3.18c**). Moreover, in PR5, 18-month old THC-treated groups had a significantly lower sociability than the 50% chance level.

The novelty preference of 3-month old mice in PR1 and 2 was above the chance level, which indicates that the mice had an intact social memory (**Figure 3.18d**). However, this was not the case for all the remaining timepoints. Uniformly, 18-month old mice had a novelty preference above chance level also in PR1 and PR2 as well as in PR3 for the vehicle-treated group.

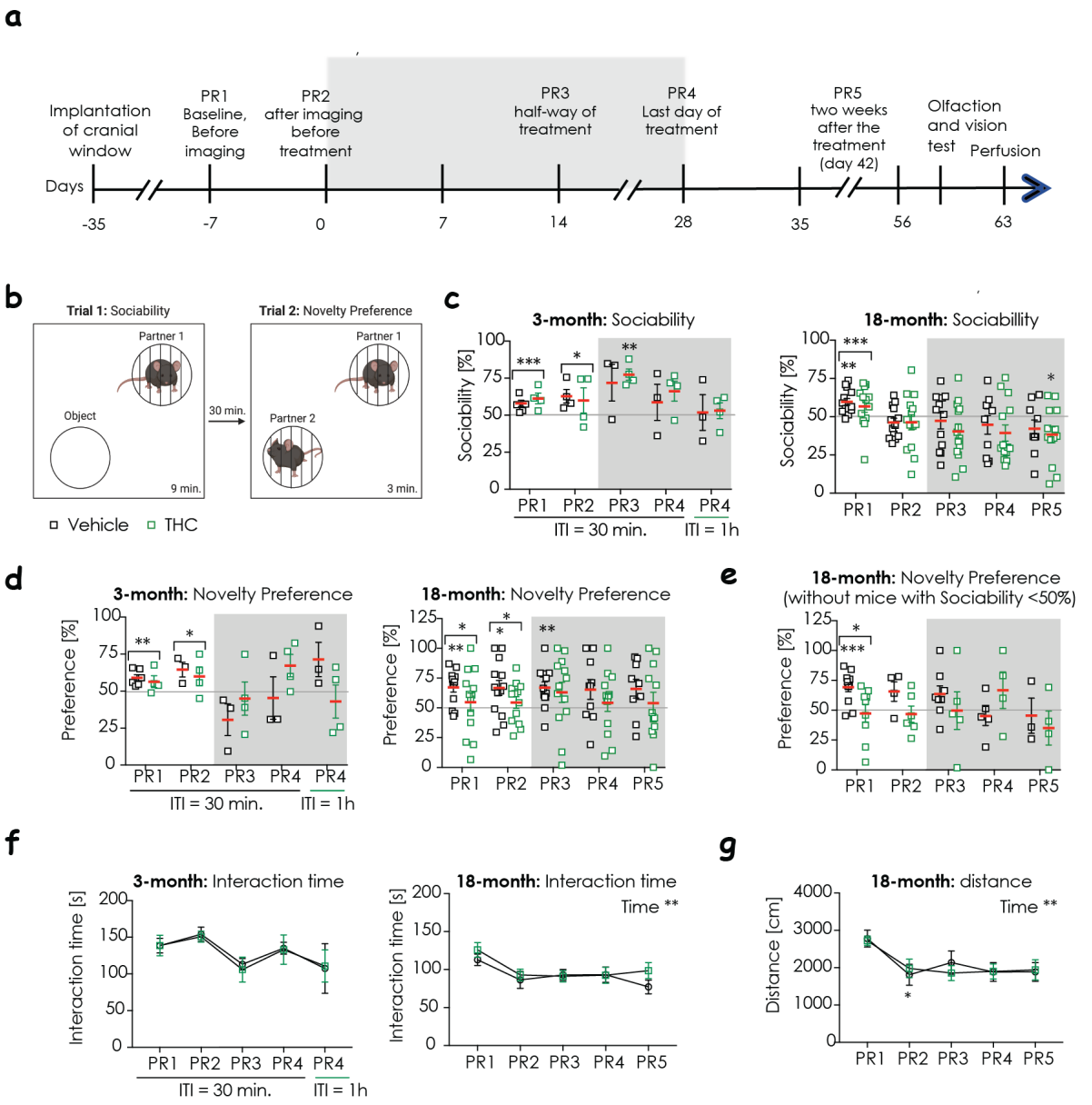

Figure 3.18. Repeated imaging and testing decreased mice sociability and thus prevented a proper assessment of memory performance. (**a**) Experimental setup for behavioural tests before, during and after THC treatment. PR – Partner Recognition test; NOLR – Novel Object Location Recognition Test. Grey box indicates the treatment duration. (**b**) Schematic of the PR test. (**c**) Sociability was calculated as interaction time with a partner mouse over total interaction time. A mean value above 50% indicates that the mice are social. Left panel: 3-month old mice; Right panel: 18-month old mice. (**d**) Preference for the novel partner was calculated as time with the novel partner mouse over total interaction time. Significant difference from the chance level (50%) indicates learning. Left panel: 3-month old mice; Right panel: 18-month old mice. (**e**) Preference for the 18-month old mice with sociability higher than 50%. (**f**) Cumulative interaction time from both trails of the PR test. Left panel: 3-month old mice; Right panel: 18-month old mice. (**g**) Cumulative distance travelled from both trails of the PR test in the 18-month old group. Statistical significance in showed in comparison to PR1.
Vehicle – white squares; THC – green squares. N = 3–14 mice/treatment/age-group. (**c-e**) Each point represents a single mouse. Mean of the group is indicated with a red line. Each group was analysed individually by one-sample t-test (hypothetical mean = 50); * $p < 0.05$, ** $p < 0.01$; *** $p < 0.001$; **** $p < 0.0001$. (**f-g**) Data are displayed as mean value ± SEM. Data was analysed with Two-way ANOVA followed by Sidak’s multiple comparison test; * $p < 0.05$, ** $p < 0.01$; *** $p < 0.001$; **** $p < 0.0001$.

Sociability of mice above 50% chance level is a prerequisite to be able to correctly interpret the results from the novelty preference and draw conclusions about the social memory alterations. Due to a decrease in sociability from PR3 onwards we were not capable to reliably asses the results of the following tests. Thus, we tried an approach in which in 18-month old groups we removed the mice that had a sociability lower than the chance level and looked into the changes in novelty preference of the remaining mice (**Figure 3.18e**). The result showed that the mice had a novelty preference above the chance level only in PR1.

Then we checked if this decrease in sociability is associated with a decrease of the overall interaction time (**Figure 3.18f**). In 3-month old mice we did not detect any significant effect of time, but there was a strong trend suggesting a decrease from PR2 to PR3. On the other hand, in 18-month old mice we did detect a significant time effect. Following post hoc analysis did not show any significant differences between the timepoints, but a trend suggested a decrease between PR1 and PR2.

We also checked if the overall motility of the animals changed with time. In order to do that we measured the distance travelled by the 18-month old mice and detected a significant time effect (**Figure 3.18g**). Post hoc analysis revealed a significant decrease between PR1 and PR2.

Alternatively, we speculated that THC treatment or our repeated imaging could cause a vision or an olfactory impairment that could impact mice performance in smell- and vision-based tests like the PR. In order to test that at the end of our paradigm we included a vision and an olfaction test. We did not detect any vison deficits (data not shown).

To test olfaction, we exposed mice to a cotton swab with either water (trial 1-3) or female urine (trial 4-6) and measured their interaction time. Mice were able to distinguish smells as shown by an increase in interaction time between trial 3 and 4 as well as habituate to the smell as indicated by the decrease of interaction time between trial 4 and 5-6 (**Figure 3.19**).

Taken together, we showed that our experimental paradigm did cause alterations in mice sociability. This in turn made the interpretation of the PR test unreliable. However, the change in sociability did not appear due to sensory deficits, since both vision and olfaction were unaffected by the THC treatment.

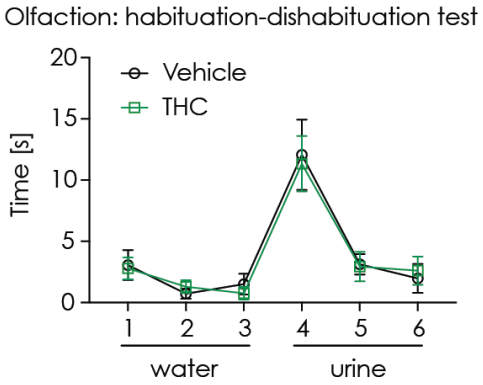

Figure 3.19. THC treatment does not cause any olfactory deficits. Interaction time with a scented cotton swab. Trial 1-3 cotton swab scented with water; trial 4-6 cotton swab scented with female urine. Vehicle – black; THC – green. N = 6-9 mice/treatment/age-group. Data are displayed as mean value ± SEM.

4. DISCUSSION: "THC-treatment differentially alters spine dynamics in old and young mice"

The aim of our study was to examine the age-dependent effect of THC on synapses by following exactly the same dendritic segments before, during and after the THC treatment. Subsequently, we tested the hypothesis that THC might regulate spine dynamics through by altering microglia activity.

We found that timing and direction of the THC effect was age-dependent (**Figure 4.1**). In young mice, THC treatment transiently increased spine dynamics and thus decreased spine stability. In contrast, THC treatment increased spine density and stability in the somatosensory cortex while decreasing the spine dynamics in old mice. Subsequent investigation of microglia activity revealed that THC treatment decreased microglia phagocytic activity and direct contacts between microglia and neurons.

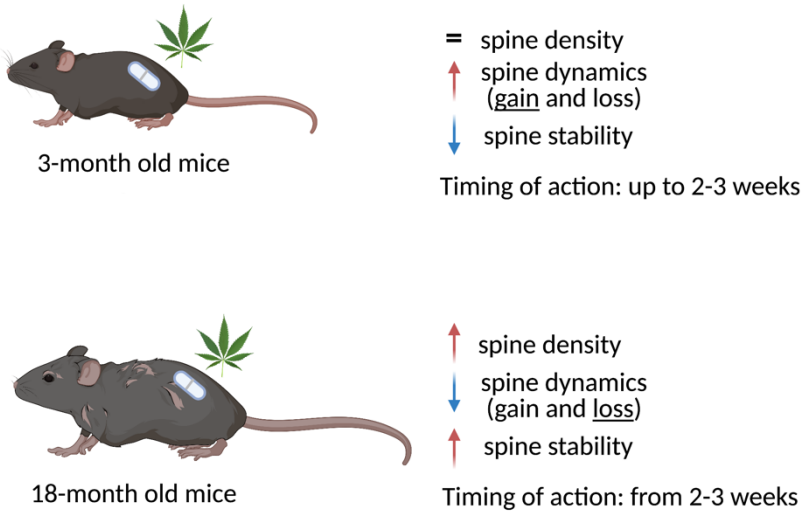

Figure 4.1. Summary of the observed effects on spine dynamics upon THC treatment in young and old mice. Blue arrow – decrease; red arrow – increase.

4.1.1. THC treatment increases spine density in old mice

We observed that THC treatment in young mice did not cause any prominent effects on spine density, whereas THC greatly increased spine density in old mice. This is in agreement with the findings from the original study showing that at day 46, the THC treatment in young mice did not cause any changes in synaptic proteins (Andras Bilkei-Gorzo et al., 2017). On the contrary, researchers observed an increase in pre-synaptic markers synapsin-I and synaptophysin, but surprisingly not in the PSD-95 in old mice (Andras Bilkei-

Gorzo et al., 2017). The findings were further confirmed using a Golgi staining and quantification of synaptic densities in different hippocampal areas. THC treatment increased spine density in CA1 and DG area as well as on interneurons in the CA3 area. Our findings show that this phenomenon is not hippocampus-specific, since we detected an increase of the spine density in layer V apical dendrites of Thy-1 positive cells localized in the somatosensory cortex. Furthermore, we also showed that the increase exceeds day 46 as we detected a significant increase in spine density also at day 49 and 56. We hypothesized that the treatment effects could last further beyond that time as the effect size was stable between day 49 and 56.

It is still not clear how memories are stored in the brain, but one of the hypothesis speculates that memories are stored as synaptic connections. This hypothesis was supported through several findings as learning has lead to the formation of new spines, whereas selective elimination of newly gained spines blocked memory recall (Hayashi-takagi et al., 2016; Holtmaat et al., 2006; T. Xu et al., 2009; G. Yang et al., 2009). Moreover, retention of new spines in motor cortex correlated with memory performance (T. Xu et al., 2009). Hence, long-term memories could be stored as durable neuronal connections. In this view, spine numbers and their stabilization could provide the mechanism for memory storage. Hence, our findings of increased spine density and spine stability in THC-treated old mice are in agreement with the previous reports showing that low-dosage THC treatment improved their cognitive abilities (Andras Bilkei-Gorzo et al., 2017; Y. Marchalant et al., 2009; Yannick Marchalant et al., 2008; Sarne et al., 2018). Also, elevation of the ECS tone using a synthetic CB_1R/CB_2R agonist had similar consequences. A chronic, 21-day treatment in old rats with WIN-55,212–2 (2 mg / kg body weight / day) improved their spatial memory and partially restored neurogenesis in the dentate gyrus (Y. Marchalant et al., 2009; Yannick Marchalant et al., 2008).

Conversely, increased spine density and number of immature spines have been linked to social deficits, repetitive behaviours and autism spectrum disorder (Hutsler & Zhang, 2010; Kim et al., 2017; Zhan et al., 2014). So, the supraphysiological increase in spine density that we observed in old mice could potentially lead to similar effects. While we did observe a decrease in sociability, it was present in all experimental mice. Moreover, observations from behavioural experiments after THC treatment do not support this theory (Andras Bilkei-Gorzo et al., 2017; Y. Marchalant et al., 2009; Yannick Marchalant et al., 2008; Sarne et al.,

2018). It is probable that this is an age-specific observation. The same increase of spine density in young animals could potentially have tremendous consequences on brain function in contrast to beneficial ones in older mice.

In our study, we used a relatively low (3 mg / kg body weight / day) dose THC that should not have any psychotropic effects. Hence, it might be possible that the effects of high-dose of THC on spine dynamics might be different or even opposite to what we observed. For instance, dose-dependent, biphasic effect of THC was shown in case of its anxiolytic/anxiogenic properties, but also in relation to cognition (Childs et al., 2017; Puighermanal et al., 2009).

On the other hand, we also cannot exclude that 3 mg / kg body weight / day is the minimal dose needed to obtain the observed effect on spine dynamics. A study using a single injection of ultralow dose (0.001 mg / kg body weight) of THC in old mice also resulted in improved cognition (Sarne et al., 2018). The single, ultralow dose injection with THC of 24-month old female mice restored their cognitive abilities to the level of 2-month old mice for at least 7 weeks. These behavioural changes were accompanied by an increase in Sirtuin1 as well as volumetric changes detected via magnetic resonance imaging (MRI) in both hippocampus and the prefrontal cortex.

In old, vehicle-treated mice we observed a noticeable decrease in spine density over time. As chronic stress decreases spine density, due to exaggerated spine elimination, we investigated stress-influenced nest building behaviour in our experimental mice (Y. Chen et al., 2008; Liston & Gan, 2011; Radley et al., 2013). We did not detect any apparent differences between the treatment groups. Moreover, removal of stressed mice from the analysis, with nest score 1 - 2, did not diminish the observed decrease in the vehicle group (data not shown). Thus, it is unlikely that the decrease in spine density was caused by stress, but we cannot exclude a negative effect of repeated imaging. It was recently shown that the surgery (exploratory laparotomy) itself and isoflurane anaesthesia in 18-month old mice have inherently decreased the levels of synaptophysin and PSD-95 for at least 7 days (Gao et al., 2021). This in turn, resulted in decreased spatial memory accompanied by an induction of mTOR signalling and decrease in autophagy. Thus, it is possible that we are underestimating the effect of THC as it also possibly compensated for the negative effects of surgery and repeated anaesthesia in old mice.

4.1.2. THC treatment in young mice transiently increases spine dynamics and destabilizes synaptic connections

We have conclusively shown that the THC effect on spine dynamics is age-dependent. In young animals, we observed an increase in the turnover ratio that was significant up to 13 days into the treatment, although the mean turnover ratio was slightly higher also on day 19. Altogether, this suggests that the THC effect lasted only up to 2-3 weeks into the treatment and afterwards spine dynamics came back to the baseline level. One possible explanation of the diminished effect of THC is tolerance development.

In support of that, it is known also from human studies that cannabis effects on cognition are less prominent in frequent users (Colizzi & Bhattacharyya, 2018). Thus, chronic exposure to the drug, as in our experimental design, may lead to long-lasting changes in drug sensitivity. One mechanism of tolerance that was proposed is through an alteration of the enzyme system responsible for the drug metabolism (Costa et al., 1996). Alternatively, most studies suggest a decreased CB_1R availability either via receptor internalization, downregulation or conformational change including a decrease of the G-protein binding to CB_1R (Ameri, 1999; De Fonseca et al., 1994; Feliszek et al., 2016; Oviedo et al., 1993). The speed and extent of CB_1R desensitization are brain-area specific with quick and pronounced responses in CB_1R-dense areas including the hippocampus – a brain area important for learning and memory. This in turn explains, why full tolerance development is frequently observed for cognition, while tolerance develops only partially for a variety of other physiological functions. For instance, frequent users develop tolerance to amnestic effect of THC, but only partial tolerance to its euphoric-effect (D’Souza et al., 2008). We did not test the expression or availability of CB_1R, since we sacrificed the mice 5 weeks after the treatment and it has been reported that CB_1Rs availability starts to recover already after 2 days without THC and is restored to baseline levels within 4 weeks of abstinence (D’Souza et al., 2016).

Within the first 2-3 weeks THC influenced both gain and loss of spines. We observed that percentage of gained spines was increased on day 7 and 10, while percentage of lost spines was increased on day 10, 13. This 3-day shift suggests that the formation of new spines (gain) was the initial process affected by the THC treatment, whereas spine elimination (loss) was a natural consequence occurring in order to bring the system back to balance. In turn, this change in spine dynamics could also reflect developing tolerance in young mice.

Accordingly, we did not observe any major changes in dendritic spine density. Simultaneously, we observed an increase in the % of transient spines on day 7 and day 10 suggesting that most of the gained spines were unstable and were removed within a few days post formation.

Increased spine turnover ratio has been reported after environmental enrichment, sensory stimulation, and learning (Holtmaat et al., 2005; Trachtenberg et al., 2002; G. Yang et al., 2009). For instance, learning rapidly increases spine formation in the motor cortex, which is followed by spine elimination to the baseline levels (T. Xu et al., 2009). Interestingly, the newly formed spines are persistent, whereas pre-existing spines are the ones that are lost. This process is impaired in old mice (Huang et al., 2020). In motor learning this alteration in spine landscape is usually interpreted as an experience-dependent circuit reorganization. However, THC treatment induced loss of the newly gained spines rather than the pre-existing ones. Hence, it is possible that THC caused arbitrary re-wiring of the neuronal circuits that was subsequently corrected after tolerance development. This phenomenon could be responsible for observed increased susceptibility to false memory in young adult cannabis users (Kloft et al., 2020). Moreover, increase in the spine turnover in motor cortex resulted in a diminished motor skill learning in a mice mouse model of Fragile X Syndrome (Padmashri et al., 2013). This suggests further that the increased turnover ratio in young mice can have a negative effect on mice behaviour, including memory. In support of that, treatment of young mice with low-dosage of THC slightly impaired long-term spatial memory (Andras Bilkei-Gorzo et al., 2017). However, it did not affect short-term spatial memory and social memory.

Furthermore, studies on spine dynamics and learning suggest that not the gain of the spines, but subsequent spine stabilization step is a better correlate of a long-term consolidation and storage of new information and skills (T. Xu et al., 2009; G. Yang et al., 2009). In our study, THC decreased spine stability of newly formed spines in young mice. That would indicate a disruption in memory consolidation that could potentially lead to cognitive deficits. Accordingly, it has been demonstrated multiple times that chronic cannabis users show cognitive deficits (Shrivastava et al., 2011). The persistence and scale of the impartment was dependent on the dose as well as the age of the participants supporting an age-related difference in the THC effect.

Other studies using THC treatment in young mice indicated that there might be region-specific differences when it comes to the THC effect on dendritic spines. Repeated administration of THC (0.5 mg / kg body weight) for 11 days altered dendritic arborization and increased spine density in medial PFC and nucleus accumbens (Kolb, 2018). High-dose, repeated THC (10 mg / kg body weight) injection increased spine density on medium spiny neurons in the striatum (Fernandez-Cabrera et al., 2018). However, adolescent treatment with increasing doses of THC for 10 days decreased spine density in the hippocampus and higher-order dendrites and reduced working memory in adult mice (Rubino et al., 2009).

In summary, we have shown that a low-dosage THC treatment transiently increases spine dynamics in young mice. However, this most likely results in a decreased cognitive abilities. Future studies investigating different doses using in vivo imaging and other behavioural paradigms are needed for better understanding of the THC effect on spine dynamics in young mice.

4.1.3. THC treatment in old mice decreases spine dynamics and promotes synaptic stability

In old mice our observations were opposite to the ones made in young mice. Firstly, we did not observe the tolerance development in old mice. On the contrary, the effect of THC on spine density was apparent starting from 2-3 weeks into the treatment and lasted at least until 4 weeks after the treatment termination. In agreement with our findings, it has been shown that tolerance development to THC is impaired in aged mice. THC-induced hypomotility was the same in old mice irrespectively of whether the mice previous received the repeated THC treatment or not (Feliszek et al., 2016). The same pre-treatment in young mice weaken the effect of THC.

Secondly, on the spine dynamics level, we observed that THC caused a decrease in spine dynamics in contrast to the young mice. This decrease was predominantly associated with a reduction in the loss of spines that persisted even after treatment termination. The gain of spines was also slightly reduced during the treatment, but came back to the baseline once the treatment terminated. Decreased loss of spines resulted in an increased spine stability of pre-existing and newborn spines that translated into an increase in spine density.

As discussed above, increased stabilization of newly formed spines is a correlate of learning and memory (Holtmaat et al., 2005; Trachtenberg et al., 2002; T. Xu et al., 2009; G.

Yang et al., 2009). We have shown that THC increased spine stability of both pre-existing and newly formed spines in old mice, which make it a possible mechanism through which THC could have restored the cognitive abilities (Bilkei-Gorzo et al., 2017). Interestingly, the effect was most prominent on spines born around 2-3 weeks into the treatment, but persisted on all the present spines even after treatment terminated. This suggests that THC differently affects spines of different longevity.

The timing of our observed effect, starting from 2-3 weeks into the treatment, coincides with the molecular changes, namely in synapsin-I protein levels (Bilkei-Gorzo et al., 2017). On day 14, there was a small trend for an increase in synapsin-I levels that became significant on day 28 and persisted at least until day 50 (Bilkei-Gorzo et al., 2017). Consistently, first behavioural effects appeared concomitantly. A strong trend for improved spatial memory was detected on day 14 in the THC-treated old mice and a significant improvement was noted on day 28 (Bilkei-Gorzo et al., 2017). This implies that THC increased density of synapses and thus improved cognitive abilities in old mice already after 2-3 weeks when we started to observe first effects on spine dynamics.

4.1.4. Aging alters spine dynamics

Aging is frequently accompanied by age-related cognitive decline. Thus, it is not surprising that aging causes an alteration in spine dynamics. We observed that old mice have higher spine density compared to the young ones as well as higher spine turnover ratio. Increase in spine dynamics was associated with a decrease in the pool of stable spines and increase in the pools of both lost and gained spines. Exactly the same observations were made by Mostany et al. when they compared the synaptic dynamics in juvenile, young, mature, and old mice using in vivo chronic imaging of somatosensory cortex (Mostany et al., 2013). Strikingly, imaging the same mice as mature and a year later as old, further confirmed age-related increase in spine density (Mostany et al., 2013).

Additionally, consistent with previous reports, we saw that the newly gained spines in the somatosensory cortex are less stable than the pre-existing ones. Aging decreased stability of both spine populations as an average half-life of gained and present spines in young animals was 4-5 days and 28 days, respectively. In old animals, it was 2-3 days and 14-19 days. Conversely, Mostany et al., reported that aging increases the probability of spine

stabilization over 30 days, but in the same time reduces their long-term stability (Mostany et al., 2013).

Investigation of axonal boutons showed an age-related increase in bouton density and volume, but not their dynamics (Mostany et al., 2013). Although, we did not include axons in our initial analysis, the regions that we imaged frequently included them, thus in the future it would be possible to perform a corresponding analysis using our dataset. As CB_1R is mostly presynaptic, it might be that the changes that we observed in spines are compensatory effects to changes happening on the presynaptic site. Moreover, Mostany et al. also reported that spines shrink with age which might explain the weaken synapses (Mostany et al., 2013). In agreement with that, we detected an age-related decrease in average spine length. However, THC did not counter-act the decrease in spine length.

Investigation of aging effects in motor cortex showed corresponding effects to the somatosensory cortex suggesting that the age-related changes on spine dynamics might happen similarly in different cortices (Davidson et al., 2020). This, together with a high density of CB_1R in different cortical areas, hippocampus, and cerebellum suggests that the effect of THC on spine dynamics could be uniform among different brain areas (Befort, 2015). Although, it is probable that the timing and the extent of aging-related processes in those brain areas might differ. Thus, we cannot draw brain-wide conclusions of the THC effect on spine dynamics solely based on our results from the somatosensory cortex.

4.1.5. THC treated old mice resemble young mice on the level of spine dynamics

Our data indicates that THC counter-acts the age-related alterations in spine dynamics of old animals. As discussed above, aging is associated with an increase in turnover ratio (both loss and gain of spines) and decrease in spine stability. Strikingly, in old animals, chronic, low-dose THC treatment decreased spine loss and increased spine stability to the level of young mice. The treatment also significantly decreased the overall turnover ratio, although the ratio remained significantly higher than that observed in the young mice. These effects further support the conclusion that a low-dose chronic THC treatment has the capability to partially counter aging-associated changes on the synaptic level (Andras Bilkei-Gorzo et al., 2017). Moreover, THC treatment was also proven to be beneficial in treatment of age-related neurodegenerative diseases. Administration of THC and other cannabinoid receptor agonists have slowed down the progression of AD (Aso et al., 2015; Ramirez et al.,

2005). Also, low-concentration of THC was capable of decreasing Aβ accumulation in a dose-dependent fashion (Cao et al., 2014). Future studies could further explore the positive effects of THC in aged individuals or in age-related diseases of the CNS.

4.1.6. Cognitive abilities of the animals could not be assessed in chronic imaging paradigm

We aimed to correlate the spine dynamics changes with the effect of THC on cognition. To do that, we interspaced PR test throughout our study. Unfortunately, we could not draw any conclusions from the PR test, since we observed that the sociability of the mice declined over the course of the experiment. Average sociability reached a chance level over time. This meant that the mice were no longer social and spent on average equal amount of time with their partner mice and an inanimate object. PR as a memory test has two basic assumptions: 1. mice are social animals and 2. they prefer novelty. Since our mice failed to fulfill the first one, we were not able to confidently interpret the results of the test. Thus, we did not draw any conclusions from the test.

It has been shown before that the sociability of the mice can be affected by the animal being stressed or sick (Lopes et al., 2016; Meerlo et al., 1996). We closely monitored the mice throughtout the experiment on daily basis and did not observe any signs of illness. Since bad state of the mice is frequently accompanied by a drastic and sudden weight loss, we also monitored the weight of the mice. We did not notice any sudden weight changes correlated with sociability decrease. Moreover, we used a nestlet shredding test to assess the stress level of the experimental mice, since nest building is considered a self-caring behaviour and is known to be reduced under severe stress. Mice from both groups built proper nests. Furthermore, THC treatment did not cause any olfactory deficits. Thus, it is unlikely that in our case the decline in mice sociability was a result of stress or illness. On the other hand, we cannot exclude that the imaging paradigm as well as the repetition of the same test influenced the mice sociability or interest in the task. Nevertheless, the change in sociability was not worrisome as the overall interaction time and distance travelled by mice only slightly decreased over time, meaning that all mice were still active and motile.

4.1.7. What are the possible mechanisms of THC action on spine dynamics?

It is currently believed that the binding of neurotransmitters, especially glutamate to NMDA receptors, is the initial trigger for spinogenesis (Kwon & Sabatini, 2011). CB_1R are localized on the presynapse and upon activation, they trigger a G-protein intracellular cascade that results in a decreased neurotransmitter release (Chevaleyre et al., 2006; Heifets & Castillo, 2009; Mechoulam & Parker, 2013). Due to a higher density of CB_1R receptor in GABAergic cells, chronic THC-treatment and subsequent activation could potentially decrease GABAergic transmission in the brain (Kawamura et al., 2006; Uchigashima et al., 2007). This in turn could increase glutamatergic transmission and trigger spine formation and stabilization. Accordingly, THC enhanced the number of vGLUT1 positive puncta in the hippocampus, while decreasing vGAT positive puncta and thus increased the excitatory/inhibitory ratio (Andras Bilkei-Gorzo et al., 2017).

Alternatively, THC can regulate gene expression via epigenetic mechanisms in an age-dependent manner (Andras Bilkei-Gorzo et al., 2017; Prini et al., 2017). In adult and old mice, THC treatment increased H3K9 acetylation, associated with transcriptional activation. The increase preceeded an elevated synapsin-I levels indicating that the epigenetic changes were the underlying mechanism for synaptic alterations (Andras Bilkei-Gorzo et al., 2017). In contrast, THC treatment in adolescence increased H3K9 di- and tri-methylation leading to transcriptional repression (Prini et al., 2017).

Another way of how THC could regulate synaptic dynamics is through the regulation of actin dynamics. It has been shown that spine dynamics are largely dependent on local actin polymerization/depolymerization (Hotulainen & Hoogenraad, 2010). Also, actin enables the structural plasticity of spines - to change their morphology for instance in response to LTP/LTD (Becker et al., 2008; Bosch et al., 2014; Y. Yang et al., 2008). One of the complexes that takes part in actin polymerization is WAVE1 regulatory complex (WRC). CB_1R interacts with WAVE1 Complex and thus plays a role in structural plasticity via the regulation of actin polymerization (Njoo et al., 2015). Activation of the CB_1R with arachidonyl-2’-chloro-ethylamide (ACEA) caused a retraction of dendritic spines and decreased mushroom spine density in vitro by destabilizing F-actin. In adult mice, inflammatory stimuli caused an increase in spine density of spinal cord neurons, whereas AEA administration attenuated activity-dependent remodelling of spines. Actin destabilization might be the underlying mechanism of our observed decrease in spine stability in young mice upon THC treatment.

As CB_1R is mostly presynaptic, the effect that we observe on the postsynaptic spines might be a compensatory response to changes of actin dynamics in axons.

Furthermore, microglial CB_2R activation decreases inflammation by shifting microglia from pro- to anti-inflammatory activation state (Komorowska-Müller & Schmöle, 2021). Since microglia are also involved in regulation of spine dynamics, we hypothesized that THC treatment might alter their activity and thus indirectly affect the stability of dendritic spines.

4.1.8. THC influences microglial regulation of spine dynamics

Microglia can regulate neuronal networks and are able to influence spine dynamics (Choudhury et al., 2020; Parkhurst et al., 2013; M. É. Tremblay, 2012; M. Ě. Tremblay et al., 2010). Microglia either phagocytose inactive spines or, during learning, they phagocytose extracellular matrix components and thus support new spine formation (Choudhury et al., 2020; Nguyen et al., 2020; Weinhard et al., 2018). ECS has been a known regulator of microglia activity and is suggested to play an important role in neuron-microglia communication (Ativie et al., 2018; Komorowska-Müller & Schmöle, 2021).

Both cannabinoid receptors are upregulated on microglia during inflammation (Benito et al., 2003; López et al., 2018; Solas et al., 2013) and CB_2R activation changes microglia activity from pro- to anti-inflammatory. Thus, we speculated that THC treatment might influence spine dynamics by decreasing the microglia pro-inflammatory and phagocytic activity, which has been observed to be frequently increased in aging (DiPatre & Gelman, 1997; J. G. Sheng et al., 1998; Shobin et al., 2017; Sierra et al., 2007). To better understand the possible effect of THC on microglia activity we investigated the changes on four different levels: activity markers, morphological alterations, microglia proliferation, and microglia-neuron direct interactions.

First, we assessed levels of Iba1 and CD68 in the soma of microglia. Both Iba1 and CD68 can be present in resting microglia, but are frequently elevated in microglia upon activation and are considered as pro-inflammatory activation markers (Hopperton et al., 2018; Jurga et al., 2020). In particular, CD68 labels active lysosomes, that are actively storing and digesting waste materials, and thus indicates the phagocytic activity of the cell. As anticipated, THC treatment decreased Iba1 and CD68 levels in the soma of the microglia. Thus, THC treatment reduced overall microglia activity and especially phagocytic activity.

The change in the CD68 was largely due to an increase in the number of CD68 negative cells, which indicates that THC affected a specific subtype of microglia. In agreement with that, a study looking into microglial aging identified two populations of cells in mice and non-human primates: autofluorescence positive (AF+) and negative microglia (Burns et al., 2020). AF colocalized with lysosomal markers and CD68 levels increased in an age-dependent fashion only in AF+ cells. Hence, it is plausible that THC preferentially decreased CD68 levels in AF+ microglia. Also, in agreement with our findings, decreasing the age-related increase in CD68+ cells, rescued synapsin-I levels and cognitive deficits via the inhibition of the prostaglandin receptor (Minhas et al., 2021)

Furthermore, the increase in CD68 negative cells was present in all hippocampal areas as well as in the cortex. However, the magnitude of the effect differened between brain areas. This might reflect differences in transcriptional identities of microglia among brain areas (Grabert et al., 2016; Hart et al., 2012; Olah et al., 2011). Similar observation was made regarding the number of AF+ microglia between cortex, cerebellum and hippocampus with cortex having the highest amount of AF+ cells (Burns et al., 2020). In our experiments, the observed decrease in Iba1 and CD68 levels was only present in cortex and DG, but not in the CA1 and CA3, whereas CA3 had initially the biggest number of CD68 negative cells.

The following 3D morphological analysis in the cortex confirmed that THC decreased Iba1 levels not only in the soma, but in the whole cell body of the microglia. Conversely, THC treatment decreased the number of branches and triple point resulting in a decreased ramification index of the microglia, whereas it increased the polarity index. These changes would rather point to an increased number of ameboid-like, reactive, pro-inflammatory microglia after THC treatment (Olah et al., 2011; Shobin et al., 2017). However, we did not detect any effect of THC on the microglia soma size. While increased microglia reactivity is often associated with a decreased ramification index and increased soma size, there is no clear morphological alteration with change from pro- to anti-inflammatory activity. Hence, just by looking at morphology we are not able to accurately assess the inflammatory status of the microglia.

Taken together, we observed that THC treatment decreased the activity of microglia. THC also altered microglia morphology by decreasing the number of processes and polarizing the cell.

Since microglia activation is not an all-or-none event, it is plausible that THC induced changes in microglia activity and morphology that do not fall into any of the classical categories. In support of that, there is a growing evidence that microglia can have a variety of phenotypes falling between the “classically activated” and “resting” state (Crotti & Ransohoff, 2016; Harry & Kraft, 2012; Olah et al., 2011; Ransohoff, 2016; Wes et al., 2016). For instance, it was shown that mTOR pathway activation leads to a reactive-like microglia morphology and increased phagocytic activity with a decreased pro-inflammatory secretion (X. Zhao et al., 2018). Moreover, these changes resulted in a decreased spine density and development of severe early-onset spontaneous recurrent seizures in mice.

Also, microglia cell density did not change in any of the investigated brain areas and layers suggesting that THC does not alter microglia proliferation. Such an increase is frequently associated with an inflammatory response (Gehrmann et al., 1995). This supports the lack of pro-inflammatory response in THC-treated microglia. Furthermore, low-dose THC treatment did not change the expression of inflammatory genes (Andras Bilkei-Gorzo et al., 2017, inhouse data). Thus, one can speculate that THC does not alter the inflammatory status of the brain, but rather specifically regulates microglia activity. Subsequently, it is plausible that this regulation impacts spine dynamics as it was shown before that hyper ramification of microglia is associated with increased spine loss in the PTSD mouse model (Smith et al., 2019).

Finally, we asked the question if the THC treatment influenced number of microglia-neuron direct interactions. To test that, we conducted two separate investigations using high-resolution and lower-resolution images and quantified the extent of colocalization between dendritic segments and microglia. Consistent with previous findings, both experiments showed a decrease in direct neuron-microglia contacts after THC treatment. This decrease in spatial distribution together with a decrease in microglia activity and decreased microglia branching suggests that microglia had less spatial contacts with neurons. Indeed, it was shown before that microglia proximity is negatively correlated with spine stability (Iida et al., 2019). In agreement with that, spines that were in contact with microglia had a higher chance of being eliminated (M. Ě. Tremblay et al., 2010). Thus, decreased proximity of microglia that we observed could have resulted in increased stability of dendritic spines in old mice. Interestingly, we did not find any significant correlation between the colocalization and spine density. Although when binning the data, we noted that the

decrease in colocalization was specific for denser dendrites. This could indicate that THC primarily influenced microglia interaction with lower order branches or in a specific layer of the cortex. Unfortunately, due to technical limitations we were not able to classify the investigated dendrites into orders, thus we cannot draw any definite conclusions.

Based on our observations, we hypothesize that THC may indirectly influence spine dynamics by regulating microglia activity in the following mechanism (**Figure 4.2**). Aging is known to increase phagocytic activity of microglia (DiPatre & Gelman, 1997; J. G. Sheng et al., 1998; Shobin et al., 2017; Sierra et al., 2007). On the spine dynamics level, we and others have shown that aging increases the loss of spines (Davidson et al., 2020; Huang et al., 2020; Mostany et al., 2013, **Figure 4.2a**). We propose that THC treatment and subsequent activation of the CB_2R decreases phagocytic activity of microglia as well as induces morphological changes including a decrease in branching (**Figure 4.2b**). This in turn results in a decrease in neuron-microglia direct interactions, that hinders phagocytosis of dendritic spines by microglia. Subsequently, it leads to a decrease in the loss of dendritic spines and results in enhanced stability of spines. Lastly, enhanced stability of spines over time increases dendritic spine density.

Recently, interleukin 33 (IL-33) have been reported to be crucial for learning-induced synapse formation mediated by phagocytosis of ECM by microglia (Nguyen et al., 2020). ECS have been shown to be able to affect IL-33/ Interleukin 1 receptor-like 1 (IL1RL1) signaling on two different levels (Du et al., 2020). The CB_1R affected IL-33 levels in neurons, whereas the CB_2R have been shown to independently regulate IL1RL1 levels (Du et al., 2020). As a result, spine gain increase in young mice, could be due to elevated IL-33/IL1RL1 signaling. Although, these dependencies should be further confirmed by an intended study, since the original experiments were done under inflammatory conditions.

Alternatively, microglia could indirectly modulate spine dynamics via BDNF signaling (Parkhurst et al., 2013). Activation of Tropomyosin receptor kinase B (TrkB), that BDNF binds to, was shown to stabilize dendritic spines and increase spine size (Koleske, 2013; Tanaka et al., 2008). In agreement with that, Bilkei-Gorzo et al. noted almost a 50% increase in BDNF expression after THC treatment (Andras Bilkei-Gorzo et al., 2017). Hence, the increased BDNF signaling could explain the increase in spine stability of old mice that we observed in our in vivo experiments. Moreover, BDNF is considered “anti-aging”, since its levels decrease with

age and and increased BDNF signaling offsets some age-related changes including LTP-impairment (Molinari et al., 2020; Rex et al., 2006; Tapia-Arancibia et al., 2008).

It is important to note that all the presented results regarding microglia function after THC treatment were obtained from mice sacrificed five weeks after treatment termination. So, the effect of THC on microglia during the treatment might be completely different. Moreover, by staining microglia we only capture it in a defined, single moment in time. Since microglia are extremely plastic and active cells and spatial contacts of microglia and spines are very transient, it is possible that we are missing some of the crucial observations (Wake et al., 2009). A future study using a double transgenic line visualising not only neurons (using GFP), but also simultaneously microglia (using TdTomato under *Cx3cr1* promoter) would allow for a better temporal view of the neuron-microglia interactions during the THC treatment (Akiyoshi et al., 2018; Cangalaya et al., 2020).

Hence, future studies should address the possible bidirectional communication of neuron and microglia via ECS and its role in spine dynamics in vivo.

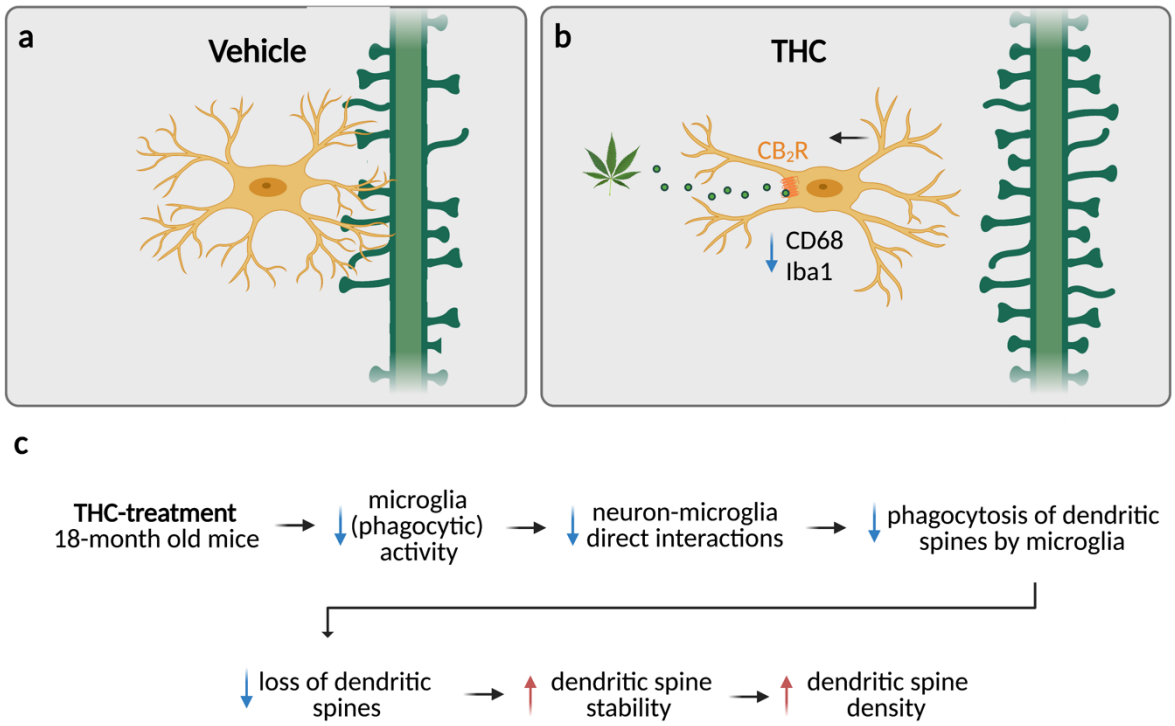

Figure 4.2. Putative mechanism of how THC influences microglia activity and in turn how microglia regulate spine dynamics. (**a**) Microglia removing dendritic spines in Vehicle-treated animals. (**b**) Microglia retracting from dendritic spines after THC treatment and downregulating CD68 and Iba1. (**c**) putative order of events leading to increased spine density after THC treatment. Blue arrow – decrease; red arrow – increase.

4.1.9. Conclusion and outlook

Here, for the first time, we demonstrated that the THC effect on spine dynamics was age-dependent. Using 2P microscopy we were able to follow the same dendritic segment in vivo and quantify changes in spine dynamics before, during and after THC treatment. We showed that in young mice THC has a transient effect on spine dynamics that terminated around 2-3 weeks into the treatment. Primarily, THC treatment in young mice increased gain of spines and subsequently eliminated newly gained spines resulting in no change in net spine density. In contrast, we detected an increased spine density in old mice that lasted at least 4 weeks after treatment was terminated. This increase was due to a stabilization of already pre-existing and new-born spines resulting in decreased spine elimination. However, the mechanism behind those changes was not identified in our current study and should be addressed in the future. Moreover, we did not investigate how the THC-induced supraphysiological increase in spine density in old mice influences neuronal circuits.

Due to a known role of ECS in microglia activity regulation, we hypothesized that microglia played a role in THC-induced changes in spine dynamics. We demonstrated that microglia from THC-treated old mice had decreased activity, altered morphology, and decreased contacts with neurons. Altogether, this indicates that THC-induced a decline in dendritic spine phagocytosis by microglia. However, we cannot exclude that changes observed in microglia are the result of spine dynamics alterations rather than their cause. To address that, future studies could image neuron-microglia interactions in vivo during THC-treatment. This approach would allow for better temporal resolution and enable the investigation during different phases of the treatment.

In summary, we have shown that low-dosage chronic THC treatments differentially alters spine dynamics in old and young mice. Future experiments investigating molecular mechanism, different doses and timing of the treatment are needed to fully understand this observation.

5. INTRODUCTION: “Cannabinoid receptor 2 and cognition”

5.1.1. Cannabinoid receptor 2 (CB_2R)

While CB_1Rs are prominently expressed on neurons, CB_2Rs were long believed to be mainly present on endocrine and immune cells, and regarded as a peripheral cannabinoid receptor. Initial analysis of *Cnr2* knockout ($CB_2R^{-/-}$) mice revealed a weak macrophage phenotype, but essentially normal responses to THC, which supported the idea that CB_2R played a role primarily in the periphery (Buckley et al., 2000).

Over the years mixed reports were published regarding the presence of the CB_2Rs in the healthy brain (Komorowska-Müller & Schmöle, 2021). It was speculated that CB_2Rs are indeed expressed, but at levels that are at the threshold of detection using most conventional methods. It was estimated that brain CB_2R expression is approximately two orders of magnitude lower when compared with spleen tissue (Van Sickle et al., 2005; H.-Y. Zhang et al., 2014). Moreover, characterization of CB_2R in the brain has been a challenge not only due to its low baseline expression, but also the current lack of reliable antibodies (Atwood & MacKie, 2010; Baek et al., 2013; Hai ying Zhang et al., 2019).

While the presence of CB_2Rs was still debated in the healthy brain, many studies detected CB_2Rs under pathological conditions such as neuroinflammation and neurodegeneration. Evidence that macrophages upregulated CB_2Rs upon inflammatory stimuli brought to light that CB_2R upregulation in the brain possibly arises from the activation of residing brain macrophages and immune cells of the brain—microglia (Carlisle et al., 2002). The presence of CB_2R on microglia was confirmed using two reporter mouse lines, in which CB_2R expression was indicated by GFP presence (López et al., 2018; A. C. Schmöle, Lundt, Gennequin, et al., 2015). Thus, the CB_2R receptor appears highly dynamic, but it be upregulated not only in response to inflammation. For instance, fear-conditioning itself exclusively up-regulated CB_2R receptor, but not CB_1R, expression in the hippocampus, and correlated with behaviours including freezing and escape latencies (Robertson et al., 2017).

Further, recent evidence has not only supported the presence of CB_2Rs on microglia, but on neurons in the healthy brain as well. A study reported *Cnr2* mRNA and protein localization on brainstem neurons (Van Sickle et al., 2005). Soon after, an electron microscopy study confirmed its presence in the brain, not only on glial and endothelial cells, but rather unexpectedly on neurons as well (Brusco et al., 2008; Onaivi, 2007). CB_2R was

detected in neuronal cell bodies and on small and medium-size dendrites, but not on axon terminals. Therefore, in contrast to CB_1R, CB_2R was believed to be mainly localized on the postsynaptic neuron (Stempel et al., 2016; Van Sickle et al., 2005) (**Figure 1.1**). Novel techniques such as RNAscope (F. Wang et al., 2012) combined with immunohistochemistry, and flow cytometry with quantitative real-time PCR (qPCR) have provided greater evidence for CB_2R presence in the healthy brain. Such studies showed that CB_2Rs are expressed in glial cells as well as in excitatory and possibly inhibitory neurons in the hippocampus (Y. Li & Kim, 2015; Stempel et al., 2016). Further investigations found neuronal CB_2R expression in midbrain dopaminergic neurons in the ventral tegmental area (VTA), in the prefrontal cortex and cerebellum, with lower levels in the dorsal striatum and nucleus accumbens (Jordan & Xi, 2019; H.-Y. Zhang et al., 2014; H. Y. Zhang et al., 2015; Hai-ying Zhang et al., 2017).

Electrophysiological studies showed that CB_2R can modulate neuronal firing. The activation of the CB_2R decreased neuronal activity and excitability in specific cell populations. In the VTA, administration of a highly selective CB_2R agonist reduced dopaminergic neurons firing, but had no effect on GABAergic neurons (H.-Y. Zhang et al., 2014). Infusion of CB_2R In the hippocampus agonists reduced both glutamate and GABA release (Andó et al., 2012; Sadanandan et al., 2020). Whereas CB_2R deletion resulted in decreased excitatory synaptic transmission and LTP (Yong Li & Kim, 2016b). Furthermore, recent reports showed that CB_2R activation causes long-lasting hyperpolarization through modulation of sodium-bicarbonate co-transporters. This self-inhibitory plasticity, mediated via 2-AG, was detected in the Cornu Ammonis (CA)2/3 area of the hippocampus as well as in the somatosensory cortex (Stempel et al., 2016; Stumpf et al., 2018). Modulation of the neuronal CB_2R altered slow gamma oscillations in vivo, hinting to its possible role in learning and memory (Stempel et al., 2016).

These findings, in addition to electron microscopy data suggest a postsynaptic localization of the CB_2Rs, in contrast to the presynapticaly localized CB_1Rs and point to an autocrine, rather than retrograde function of CB_2Rs. It is possible that CB_1Rs and CB_2Rs offer two different ways of synaptic signal modulation due to their localization – based on the decrease of neurotransmitter release (CB_1R) and dampening of the signal at the post synapse via hyperpolarization (CB_2R) (Jordan & Xi, 2019).

5.1.2. CB_2R in cognition

CB_2Rs have been shown to regulate many different behaviours from feeding to addiction (Agudo et al., 2010; Liu et al., 2017; H.-Y. Zhang et al., 2014). Among others, studies performed in $CB_2R^{-/-}$ mice hinted at an important role of CB_2Rs in learning in and memory, specifically during memory consolidation (García-Gutiérrez et al., 2013; Ratano et al., 2018). It was shown that CB_2R deletion disrupts consolidation of an aversive memory (García-Gutiérrez et al., 2013). Moreover, systemic administration of a CB_2R antagonist impaired aversive memory, while administration of CB_2R agonist had the opposite effect (García-Gutiérrez et al., 2013). In agreement with that, $CB_2R^{-/-}$ mice had an impairment in hippocampus-dependent, long-term contextual fear memory, but not in hippocampus-independent, cued fear memory (Yong Li & Kim, 2016a). These findings were consistent with a decreased synaptic density in the hippocampus that could underly the cognitive deficits (García-Gutiérrez et al., 2013; Yong Li & Kim, 2016b). On the other hand, CB_2R deletion seemed to enhance the working memory, as indicated by an increased percentage of alternations in the y-maze task (Yong Li & Kim, 2016a).

Since both neurons and microglia can express CB_2R, a study investigated if neuronal and microglial CB_2Rs play distinctive roles in the murine dorsal hippocampus. In order to investigate that, the study used the CRISPR-Cas9 genome-editing technique and *Cre*-dependent overexpression, combined with viral injections and transgenic mice to either knockout or overexpress the CB_2R in specific cell types (Yong Li & Kim, 2017). Three different cell types were targeted: pyramidal neurons, GABAergic neurons, and microglia. Manipulation of CB_2Rs on GABAergic neurons did not change any of the investigated behaviours, while CB_2R deletion from pyramidal neurons enhanced working memory, as described before for constitutive knockouts (Yong Li & Kim, 2016a). In contrast, contextual fear memory was enhanced after overexpression of microglial CB_2Rs. Consistently, deletion of microglial CB_2Rs decreased contextual fear memory.

Altogether, the studies showed that both neuronal and microglial CB_2Rs in the hippocampus play a role in learning and memory and that CB_2Rs might differently affect distinctive types of memory. However, up to date little is known of CB_2R role in other types of memory. For instance, recently described CB_2R-dependent long-lasting hyperpolarization pattern was discovered in the CA2/3 neurons. This area of the hippocampus is imported for

social memory (Hitti & Siegelbaum, 2014). Thus, CB_2R could potentially play a role in social memory.

5.1.3. CB_2R in anxiety

CB_2R was shown to play a role in depression and anxiety. In 2011, Ortega-Alvaro et al. reported that constitutive deletion of CB_2R induces “Schizophrenia-related behaviours” (Ortega-Alvaro et al., 2011). Observed behaviour was described by the decreased travelled distance in the open-field test, increased immobility time in the tail suspension test as well as decreased time in open arms and light box in elevated plus-maze and light-dark test, respectively (Ortega-Alvaro et al., 2011). Altogether, the results suggested that $CB_2R^{-/-}$ mice were more sensitive to a stressful stimulus. In agreement with this finding, *Cnr2* overexpression studies done by the same group showed a decreased vulnerability to anxiogenic and depression-like stimuli (García-Gutiérrez & Manzanares, 2011). However, successive investigation done by another group failed to recapitulate this strong anxiety phenotype. Li and Kim detected no change in either the distance travelled in the open-field or time spent in the open arms of the elevated zero maze (Yong Li & Kim, 2016a, 2017). These contradicting findings indicated that there may be other factors involved influencing CB_2R role in anxiety. Recent investigation with DAT-$CB_2R^{-/-}$ mice with CB_2R deleted exclusively in the dopaminergic neurons showed increased motility and even hyperactivity (Liu et al., 2017). These DAT-$CB_2R^{-/-}$ mice also exhibited increased immobility time in both tail suspension and forced swim test suggesting a “depression-like” phenotype. When tested with anxiety paradigms on the other hand, DAT-$CB_2R^{-/-}$ mice spent more time in the lit area during the light-dark test, and more time in open arms of the elevated plus maze, suggesting reduced anxiety. Thus, further studies are needed to fully understand the role that CB_2R plays in anxiety-like behaviours.

5.1.4. CB_2R in aging

Many studies have shown that ECS tone decreases with age (**see 1.3.2**). Deletion of CB_1R resulted in an accelerated aging phenotype, characterized by premature cognitive decline and neuroinflammation (Albayram et al., 2011; Albayram, Bilkei-gorzo, & Zimmer, 2012; Bilkei-Gorzo et al., 2005; Bilkei-Gorzo et al., 2012). However, up to date CB_2R age-related changes were exclusively studied in the context of AD and with regard to its function

in microglia regulation and neuroinflammation (Aso et al., 2013; A.-C. Schmöle et al., 2018; A. C. Schmöle, Lundt, Ternes, et al., 2015). Hence, it is not known if and what role does the CB_2R play in physiological brain aging.

5.2. Aim of the thesis

The aim of my project was to further investigate the role of CB_2R in cognition. Primarily, I aimed to reveal wherever CB_2R plays a role in social memory, and if this role differs depending on the age or gender of the mice. I also aimed to reveal if CB_2R deletion alters basic behaviours and anxiety-like behaviours. I then investigated if CB_2R deletion in female or male mice influences synaptic architecture in the hippocampus.

6. MATERIALS AND METHODS: “Cannabinoid receptor 2 and cognition”

For lists, please refer to the following sections: chemicals (**section 2.1**), solutions (**section 2.2**) and antibodies (**section 2.3**).

6.1. Mice

We used C57BL/6J wild type (WT) and B6.cgCnr2tm1Zim (constitutive CB2 knockout mice, MGI Cat# 2663848, RRID:MGI:2663848) mice. C57BL/6J were originally obtained from a commercial breeder (Charles River). B6.cgCnr2tm1Zim ($CB_2R^{-/-}$) were generated by replacing 3’ region of the coding exon 3 of the *Cnr2* gene with phosphoglycerate kinase PGK - neomycin sequence through homologous recombination in embryonic stem cells (Buckley et al., 2000). This resulted in the 131 amino acid deletion at the C-terminus of the CB_2R eliminating part of intracellular loop 3 and transmembrane domains 6 and 7. Mutant mice were then backcrossed with C57BL/6J for more than ten generations. $CB_2R^{-/-}$ were bred homozygous and backcrossing to C57BL/6J line was done every 6 generations to minimalize the risk of a genetic drift.

Both mouse strains were stored under specific-pathogen-free conditions in the main animal facility of the University of Bonn. After weaning, mice were group-housed in standard laboratory cages with automatic ventilation system and *ad libitum* water and food access under 12 hour light-dark cycle (lights on at 09:00 am). Cages were monitored daily and bedding, water and food were changed weekly.

Care of the animals and conduction of the experiments followed the guidelines of the European Communities Directive 86/609/EEC and the German Animal Protection Law regulating animal research and were approved by the LANUV NRW, Germany (AZ 84-02.04.2017.A231).

6.1.1. Experimental groups

To reveal age-dependent changes using the first test battery (PR, o-maze, MWM) five independent male groups were tested. Two groups with young 3-month and adult 12-month old mice and one old group with 18-month old mice. 3- and 12-month old subgroups were

pooled together for analysis. Using the second test battery (NOLR, LD test, y-maze) two independent 3-month old male groups were tested and subsequently pulled together for analysis. In total 14-15 mice / age group / genotype / test battery were used.

To reveal gender-specific alternations, independent groups of WT and $CB_2R^{-/-}$ were used for behavioral testing and immunohistochemical analysis. For behavioral testing an independent male and female groups were used (N = 11-13 mice / group). For immunohistochemical analysis two independent groups of mice were used. One group included male (N = 3-4 mice / genotype) and female (N = 4 mice / genotype) mice from WT and $CB_2R^{-/-}$. Another group included only female mice (N = 4-5 mice / genotype). Tested mice were between 4 - 6 months old.

6.2. Genotyping

Genotyping was mostly performed by technical assistants.

6.2.1. DNA isolation

Mouse tail tip biopsies were obtained right after weaning. The tissue was lysed overnight in 200 µl of lysis buffer with freshly added 3 µl of proteinase K (1 mg/ml) at 55°C with shaking (550 rpm). The next day, samples were centrifuged (13000 *x g*, 10 min, 4°C) to removed un - lysed tissue remnants, and the supernatant was transferred to a fresh Eppendorf tube. Then 200 µl of isopropanol was added and the tube was gently inverted several times. Samples were subsequently centrifuged to obtain a deoxyribonucleic acid (DNA) pellet. Precipitated DNA pellet was washed twice with 70 % ethanol. The pellet was air-dried and redissolved in 50-100 µl of Tris-EDTA (TE) buffer. Isolated DNA was stored long-term at 4 °C.

6.2.2. DNA amplification by polymerase chain reaction (PCR)

PCR was done as described above (**see section 2.6.2**).

PCR for CB_2R PCR (prCB2ab)

PCR reaction for genotyping ($CB_2R^{-/-}$ mice)

39 µl	MilliQ water
5 µl	10x ThermoPol buffer
1 µl	dNTP mix (10mM)
1 µl	Primer WT: 5´-GTG CTG GGC AGC AGA GCG AAT C -3´
1 µl	Primer KO: 5´-AGC GCA TGC TCC AGA CTG CCT -3´
1 µl	Primer COM: 5’-GTC GAC TCC AAC GCT ATC TTC -3’
1 µl	Taq Polymerase
1 µl	DNA (around 100 ng/µl)

PCR program		Temperature	Time
1 x	Initial denaturation	95°C	2 minutes
35 x	Denaturation	95°C	30 seconds
	Annealing	60°C	60 seconds
	Elongation	68°C	45 seconds
1 x	Final elongation	68°C	7 minutes
	Cooling	4°C	∞

6.2.3. Gel electrophoresis

PCR was done as described above (**see section 2.6.3**). The expected band size for $CB_2R^{-/-}$ mice is 400 bp, while for WT it is 639 bp.

6.3. Behavioural experiments

Mice were single-housed in standard laboratory cages under reversed 12 hour light-dark cycle (lights off at 09:00 pm) a week before the first behavioural test.

6.3.1. Partner recognition test (PR)

PR paradigm was used to asses social memory as described above (**see section 2.8.1**). In trial 1, a metal cage was used instead of an empty grid cage. Intertrial interval (ITI) of 1 hour was used for 3-month old mice and of 30 minutes for 12- and 18-month old mice. Mouse

activity was analyzed and recorded with the Ethiovision XT 8.5 and 13 (Noldus). Mice with sociability equal to or lower than 55 % were removed from the analysis.

6.3.2. Home - cage activity measurement

Home - cage activity was measured using “Mouse E-Motion” infrared sensor on the lid of the cage (Infra-E-Motion GmbH, Hamburg, Germany). The number of beam breaks per hour was detected and reported as a measure of home-cage activity.

6.3.3. Olfaction test

The olfaction test protocol was modified from “Simple Behavioral Assessment of Mouse Olfaction”; The Olfactory Habituation/Dishabituation Test (M. Yang & Crawley, 2009). This test was performed only on the male group after all behavioral tests were conducted.

In brief: a cotton swab was inserted around 2-3 cm from the grid top. In trial 1, 10µl of water was placed on the cotton swab and the interaction time of the mouse with a cotton swab was recorded for 2 minutes. The cotton swab was then removed from the cage for 1 minute and another cotton swab was inserted with a 10 µl drop of female urine. Once again, the interaction time was recorded for 2 minutes. The test time was counted from the moment that the mouse first interacts with the cotton swab. The time taken for the mouse to approach the cotton swab in each trial was measured and reported as latency. Interaction time and latency were manually counted.

A proper sense and intact sense of smell would cause no change, or an increase in interaction time in the second trial. Decrease in the interaction time would suggest a habituation to the cotton swab and olfactory disfunction.

6.3.4. y-maze

This paradigm was used to asses working memory as described before. The maze consists of three arms (30 cm long). Mice were allowed a free exploration period of 3 minutes. The activity of the mice was recorded with the Ethiovision XT software (Noldus). Entries to single arms were noted manually. Entries to single arms were noted when all four paws were within that arm. Alternation was defined as a consecutive entry to three different arms. Increased number of alternations indicated a better working memory.

6.3.5. Novel object location recognition test (NOLR).

NOLR was used to asses short-term spatial memory. The activity of the mice was recorded with the Ethiovision software 8.5 (Noldus). The test was performed in an open-field box (44 cm x 44 cm) containing a thin (around 1 cm) layer of sawdust. Similar to the PR, mice had a 3-day habituation period, during which they freely explored the box for 10 minutes. NOLR consisted of two trials. In trial 1, mouse was placed on an arena containing three identical objects (LEGO® constructions, each containing two colors, roughly 3 cm x 3 cm x 4 cm) inter-spaced alongside one wall (around 4 cm from the walls and 8 cm from each other). The mouse was allowed to explore the arena freely for 9 minutes. Interaction was noted when the mouse nose point was within approximately 2 cm from an object. Afterwards, mice were put back to their respective cages for 30 minutes, 1 hour or 2 hours. In trial 2, one of the outer objects was moved to the opposite wall. Again, the time of interaction was measured while the mouse was freely exploring for 3 minutes. Change in preference for the displaced object between trial 1 (before relocation) and trial 2 (after relocation) were calculated as follows:

$$\text{preference T1} = Ta1/(Ta1+Tb1+Tc1)$$

$$\text{preference T2} = Ta2/(Ta2+Tb2+Tc2)$$

where Ta - time of interaction with object that is going to be moved/was moved; Tb – time of interaction with the second object; Tc – time of interaction with the third object.

Mice that remembered the setting have an increase in preference for the moved object in trial 2. The novelty preference is calculated as follows:

$$\text{novelty preference (\%)} = (\text{preference (trial 2)}/\text{preference (trial 1)} - 1) * 100$$

The value should be > 0 if mice exhibit an increased preference for the moved object in trial 2. Each group was tested with a one-sample t-test against a hypothetical mean (0 %) to detect if the mean novelty preference of the group was greater than the chance level. Mice with an initial preference (in trial 1) higher than 50 % for one object were excluded.

6.3.6. Morris water maze (MWM)

This test is commonly used to asses long-term spatial memory (Morris, 1981). Mice learned the position of an invisible platform based on spatial cues. Activity of the mice was recorded with the Ethiovision XT software (Noldus). The platform was immersed around 1 cm under the water level in a round maze (diameter 120 cm). The water was stained white with paint

(Staedtler, Noris Club). Spatial cues (different shapes and colors, around 14 x 14 cm) were placed around 5 cm above the water level. The experiment consisted of three phases: acquisition (day 1-5), probe trial (day 6) and reversal phase (day 7-9). During the acquisition phase the hidden platform remained in a fixed location and animals swam four times per day from different entry points. Inter-trial interval time was 1 hour. The cut-off time for each swim was 90 seconds. If the mouse found the platform within the time limit, then it remained on it for additional 5 seconds before being taken out of the maze. Otherwise, after the time limit passed, the mouse was guided to swim to the platform and remained there for additional 20 seconds. The decrease of latency to find the hidden platform indicated the learning process. In the probe trial memory retrieval was assessed. The platform was removed and the time spent in the platform-associated quadrant was measured for 90 seconds. For the reversal phase, the platform was placed in a new position and the flexibility of the memory was evaluated. Similar to the acquisition phase mice were swimming four times daily and the latency to the platform was recorded. One mouse that stayed close to the wall at all times was excluded from the analysis.

6.3.7. Light-dark test (LD test)

The test arena consists of two boxes (22 cm x 44 cm) connected through a 5 cm hole. One box was completely covered (dark compartment), while the other one had transparent walls and was brightly lit (3300 lx; light compartment). Mice were placed in the dark compartment and their activity throughout the whole arena was recorded for 5 minutes using the ActiMot software (TSE systems GmbH, Germany). Increased time spent in the dark compartment suggests an increased anxiety.

6.3.8. Elevated zero maze (o-maze)

The zero maze is elevated 30 cm above the ground. It has an O-shape (diameter 47 cm, width of the path 5.6 cm) with two open compartments inter-spaced with two closed compartments. Mouse was allowed to explore the maze freely for 5 minutes. Light intensity was around 200 lx. Activity of the mice was recorded with the Ethiovision XT 8.5 and 13 (Noldus). “Head dipping” in the open compartment and “stretched-attend posture” were counted manually as described previously (Shepherd et al., 1994).

6.3.9. Nestlet test

This test was used to assess the stress level of the animals as described above (**see section 2.8.3**). Nest was scored and the remaining nestlet was weight after 3 hours and after 24 hours.

6.4. Transcardial perfusion

If the mice were part of behavioural experiments, then approximately 24 hours after the last behavioral experiment mice were transcardially perfused with phosphate-buffered saline (PBS). Prior to that, mice were deeply anesthetized by isoflurane inhalation until all reflexes were gone (negative paw pinch). Briefly: abdomen cavity was open; diaphragm was cut and chest cavity was exposed. Rib cage was cut to enable access to the heart and needle was inserted into the left ventricle of the heart. Pericardial sac was cut and around 40 ml PBS solution was pumped through the needle (pump flow rate 4 ml per minute). Brains were isolated and hemisected. One of the hemispheres was postfixed in 4% formaldehyde (pH = 6.9; Sigma- Aldrich) for 3.5 - 4 hours on ice with shaking. They were cryoprotected using overnight incubation in 10% sucrose followed by an overnight incubation in 30% sucrose.

Mice that were not subjected to behavioural tests were transcardially perfused with 4% formaldehyde. Brains were frozen in dry-ice cold isopentane and stored at -80°C prior to sectioning. Cortex and hippocampus were dissected from the other hemisphere and they were snap-frozen frozen in liquid nitrogen alongside with the remnants of the hemisphere. Tail tips were obtained from the mice for DNA isolation and genotyping.

6.5. Immunohistochemistry (IHC)

6.5.1. Syn1, RGS14, vGLUT1, vGAT stainings (prCB2b)

Frozen fixed hemispheres were cut with a cryostat (Microm HM500) into 20 µm sections and stored at −20 °C. Prior to the staining, slices were thawed on a 37°C hot plate for 30 minutes. They were then permeabilized for 10 minutes in 0.3% Triton X-100 in Tris- buffered saline (1M TBS, pH = 7.5), followed by three 5 minutes washings in TBS. Then antigen retrieval in citrate buffer pH = 6 for 20 minutes at 65°C was performed. The slides were washed three times with TBS and blocked for 1 hour in blocking buffer (2% BSA, 10% normal goat serum, 0.3% Triton X-100 in TBS). Afterwards, the slides were incubated overnight with primary antibodies in the blocking buffer: rabbit anti-Synapsin-I; guinea pig anti-vesicular glutamate

transporter 1 (vGLUT1); guinea pig anti-vGAT; mouse anti- Regulator Of G Protein Signaling 14 (RGS14) (**see 2.3**). The next day, the slides were incubated for 20 minutes at room temperature and washed three times in TBS. Then they were blocked for 1 hour and incubated with secondary antibodies in blocking solution: goat anti-mouse AlexaFluor®568; goat anti-rabbit AlexaFluor®488; goat anti-guinea pig AlexaFluor®647 (**see 2.3**). Afterwards the slices were washed three time in TBS, stained with DAPI, washed once in TBS and mounted using Prolonged Diamond mounting medium (Life technologies) with cover slips No. 1.5 H and stored in 4 °C, in the dark.

6.5.2. Image acquisition

IHC staining's were imaged with Leica TCS SP8 confocal microscope as described above (**see section 2.10.2**).

For synaptic proteins staining (Syn1, vGLUT1, vGAT, RGS14) 3 – 4 single plane images were obtained per animal using 20x objective (resolution 2048 x 2048 px; 0.2835 µm/px) and using 63x objective (resolution 2048 x 2048 px; 0.09 µm/px).

6.5.3. Image analysis

Part of the analysis was done by Kishore Aravind Ravichandran. Image analysis was performed in Fiji (ImageJ v2.1.0/1.53c). Subsequently, the results were exported and further analysed with Microsoft Excel (v 16.43).

All regions of interest (ROI) were delineated manually using RGS14/DAPI/synapsin-I merged image. In 20X and 63X images mean grey value was measured within each ROI. For particle analysis images were thresholded using a fixed mean grey value threshold to obtain a binary image. Appropriate threshold per staining was determined as arithmetical average of manually set thresholds for each of the pictures. The same threshold was applied to all images and genotypes within a staining. The number and average size of puncta per ROI was counted using Image J's 'Analyze Particles' function (minimum punctate size: 0.005 µm). For each animal 3-4 images were analysed. Data were normalized as % of mean of control group (stratum oriens). Data from immunohistological groups were pooled together per gender.

6.6. Statistical analysis and data presentation

Microsoft Excel (v 16.43) was used for data analysis followed by statistical analysis and data visualization in GraphPad Prism version 7.0.0 and 9.1.2 for Mac, GraphPad Software, San Diego, California USA, www.graphpad.com. Figures were created in Adobe Illustrator (v 24.0.2). Graphical parts of the figures were prepared using Biorender (biorender.com) and Microsoft Powerpoint (v 16.43). For presentation, representative images were post-processed in Fiji (ImageJ v2.1.0/1.53c) to adjust brightness and contrast. Behavioral data analysis was done using Ethiovision XT 8.5 and 13 (Noldus).

Datasets with two independent groups, one dependent variable were first checked for normal distribution using D’Agostino & Pearson normality test. If both datasets distribution did not significantly differ from a normal distribution, then unpaired t-test was used, otherwise Mann-Whitney test (U-test) was used.

For datasets consisting of more than 2 groups with two independent variables (e. g. Genotype and Age; Genotype and Layer or Genotype and Gender) two-way analysis of variance (ANOVA) was used followed by Sidak’s multiple comparison test.

For time-series experiments with 2 groups (e. g**.** Time and Genotype) repeated-measurement ANOVA (based on general linear model) was used followed by Sidak’s multiple comparison test.

For PR and NOLR, with one-sample t-test the mean of the group was tested against a theoretical mean of 50 to detect significant difference of each group from the chance level.

Statistical significance was stated when p-value < 0.05 at a 95% confidence interval. For the figures (Figure 2-9; 11; 12; 15; 18; 19) in which ANOVA was used the p-values were reported as * $p < 0.05$, ** $p < 0.01$; *** $p < 0.001$; **** $p < 0.0001$. The corresponding exact p-values were reported in the statistics table (**see 10.1**). For all the other figures the exact p-values were reported directly on the graphs. If not possible, then p-values were included in the statistics table (**see 10.1**).

All graphs are presented with standard error of the mean (SEM) unless indicated otherwise.

7. RESULTS: "Cannabinoid receptor 2 and cognition"

7.1. "CB_2R in aging"

7.1.1. Age-dependent alterations in basic behaviours after $CB_2R^{-/-}$ deletion

Due to a known accelerated aging phenotype of $CB_1R^{-/-}$ mice, we asked if CB_2R deletion has similar consequences in the context of aging. In order to investigate that we designed a series of behavioural experiments including memory (Partner Recognition – PR; Morris Water Maze - MWM) and anxiety tests (o-maze; **Figure 6.1a**). To distinguish the aging effect, we tested three independent age groups: young (3-month old mice), adult (12-month old mice), and old (18-month old mice).

Over the course of the experiment, we monitored the weight of the animals. We detected a significant genotype effect exclusively in the 12-month old mice. Subsequent post hoc analysis did not reveal any significant differences (**Figure 6.1b**).

We also wanted to know if $CB_2R^{-/-}$ deletion caused any changes in basic behaviours that could have potentially influenced the outcome of the memory tests. First, we used a nestlet shredding test to investigate self-care behaviour of mice during a baseline (habituation for PR) and stressful situation (MWM Probe trial). During the test, mice received a fresh nestlet material and after 3 h we assessed their nest giving a score from 1 to 5. In 3-month old mice, we detected a significant decrease in the nest score already at baseline (**Figure 6.1c**). In agreement with that, the decrease was still there when the mice were tested after a stressful situation, so following a probe trial of MWM. In 18-month old mice, we did not detect any genotype effect neither during baseline nor under stress conditions.

Next, we investigated if CB_2R deletion causes any olfaction deficits that could impair mice performance in the PR. To test that we used a two-trail test. In the first trial we measured mice interaction time with cotton swab scented with water, in the second trial with cotton swab scented with female urine. Decrease in interaction time between trial 1 to 2 would mean that the mice cannot smell and habituated to the presence of a cotton swab. In 3-month old mice we detected a significant increase in the interaction time when exposed to urine-scented cotton swab in both WT and $CB_2R^{-/-}$ mice (**Figure 6.1d**). The cumulative interaction time in both trials was significantly decreased in 3-month old $CB_2R^{-/-}$ mice compared to WT mice by almost 70%. The cumulative latency, so the time that it took for the mice to first approach the cotton swab was not significantly altered.

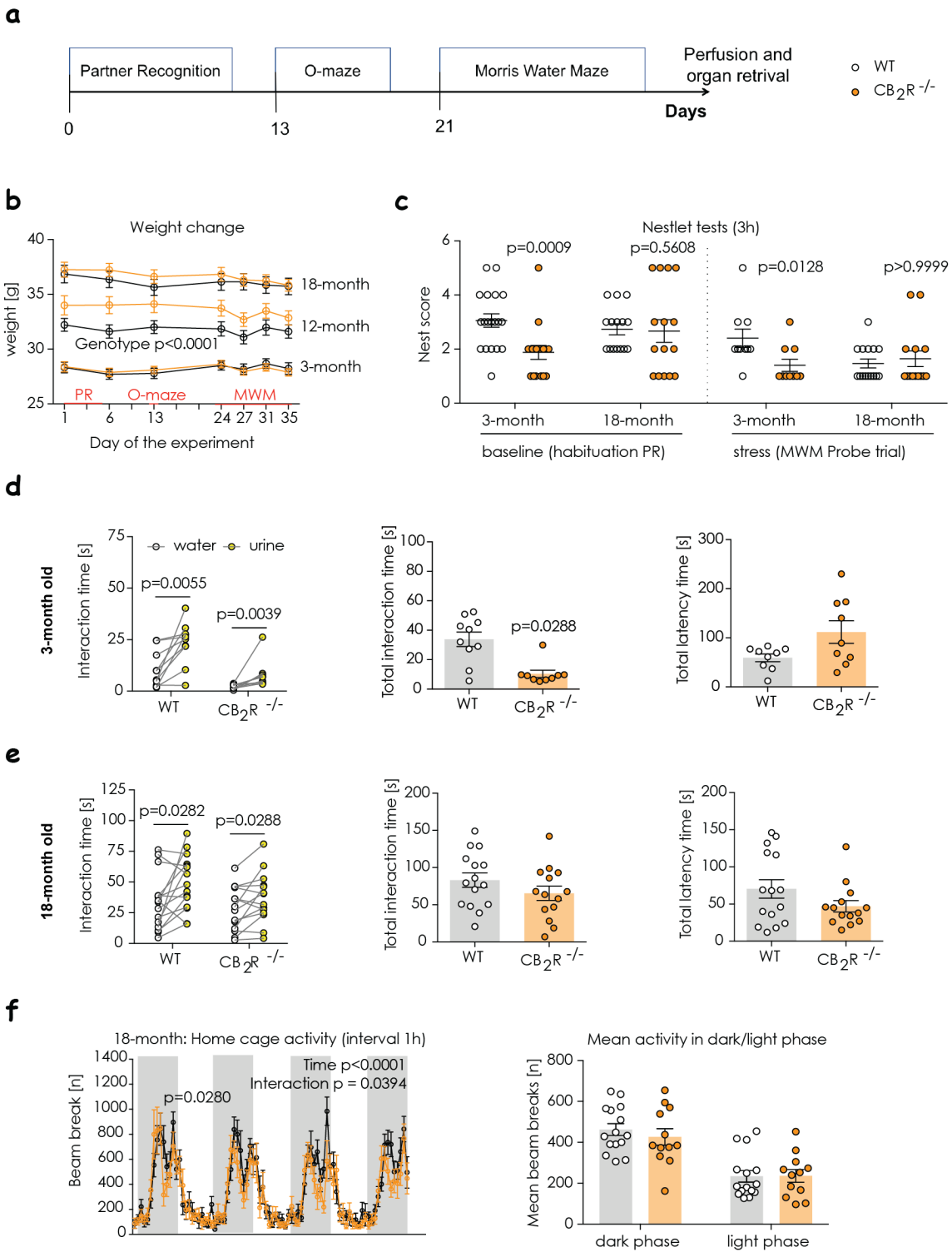

Figure 6.1. Age-dependent alterations in basic behaviours after CB_2R deletion. (**a**) Experimental setup for “CB2 in aging” project. Short-term social memory test (PR), anxiety test (o-maze) and long-term spatial memory test (MWM). (**b**) weight change over the course of the experiments. Each age group is presented separately (N = 14-15 mice / genotype / age group). The timing of each tests is indicated in red on the horizontal axes. Data are displayed as mean value ± SEM. Data was analysed per age group with Two-way ANOVA. (**c**) Nest building behaviour at two different conditions: low stress level (during habituation of the PR) and high stress level (Probe trial of MWM). Each point represents a single mouse. Data are displayed as mean value ± SEM. Data was analysed by U-test. (**d,e**) Olfaction test. Each point represents a single mouse. Right panel – interaction time with water- or urine-scented cotton swab; water – white; urine - yellow; Middle panel – cumulative interaction time from both trials; Right panel – cumulative latency. (**d**) 3-month old mice. Data analysed by paired t-test or

Wilcoxon matched-pairs signed rank test for WT and CB2R-/- respectively (N = 9-10 mice / genotype). (**e**) 18-month old mice. Data analysed by paired t-test (N = 14-15 mice / genotype). (**f**) Home-cage activity measurement by infrared sensors. Activity measured as the number of beam breaks. Left panel – mean cumulative number of beam breaks from 1h per group. Data are displayed as mean value ± SEM. Grey box indicates the duration of the dark phase. Right panel – mean number of beam breaks per mouse calculated separately in the light and dark phase. Each point represents a single mouse. Data was analysed by two-way ANOVA. The exact p-values are reported on each graph. WT mice – white circle; $CB_2R^{-/-}$ mice – orange circles.

In 18-month old mice, we also measured a significant increase in the interaction time between water- and urine-scented cotton swab suggesting that neither aging nor CB_2R deletion did not cause any olfactory deficits (**Figure 6.1e**). We did not detect any significant differences between genotypes in cumulative interaction or latency times. The mean cumulative interaction time was on average twice longer in the 18-month old group then in the 3-month old group. Taken together, we concluded that both young and old $CB_2R^{-/-}$ were able to smell.

Lastly, in 18-month old animals, we investigated changes in home-cage activity using an automated infrared sensor system. We detected a significant effect of time and interaction (**Figure 6.1f**). Post hoc analysis revealed a slight decrease of the activity during the dark phase on the first day of the observation. Subsequent analysis of the mean activity on the light and the dark phase did not show any differences between the genotypes.

Overall, it seems like CB_2R deletion did not majorly effect basic behaviours of mice. However, it did alter nest building and total interaction time in the olfactory test in 3-month old mice. These differences were not detected in 18-month old mice.

7.1.2. CB_2R deletion decreases anxiety in an age-independent manner

Another aspect that can potentially affect mice performance in memory tests is anxiety. Since CB_2R deletion has been reported to cause schizophrenia-like phenotype with increased anxiety-like behaviours, we conducted an o-maze anxiety test in between our memory tests (**Figure 6.2**).

For the % of time spent in the closed compartment we detected a significant age and genotype effect (**Figure 6.2a**). Following post hoc test revealed a significant increase between 3-month and 12-month old WT mice. The increase was also significant between 3-month and 12-month as well as 12-month and 18-month old mice in $CB_2R^{-/-}$mice. We did not detect any significant differences between genotypes within the same age-group, but we noted a trend for a decreased % of time spent in the closed compartment in the 18-month old $CB_2R^{-/-}$ mice.

Furthermore, we detected a significant age and genotype effect for the distance travelled in the open compartment. We detected a significant decrease between 3- and 18-month old WT mice and 3- and 12-month old as well as 3- and 18-month old $CB_2R^{-/-}$ mice (**Figure 6.2b**). Post hoc analysis did not reveal any significant differences between genotypes within the same age group, but we noted a trend for increased distance travelled in the open compartment in $CB_2R^{-/-}$ mice.

Regarding the head dipping behaviour, we detected a genotype effect and a significant increase in $CB_2R^{-/-}$ mice in all age-groups (**Figure 6.2c**). Also, we detected a genotype and age effect for the number of stretched postures. Following post hoc analysis revealed a significant decrease in $CB_2R^{-/-}$ mice in 3- and 18-month old groups in relation to WT mice. Moreover, we detected an age-related decrease in the number of stretched postures between 12- and 18-month in $CB_2R^{-/-}$ mice (**Figure 6.2d**).

Taken together, we did not observe an increased anxiety-like phenotype in $CB_2R^{-/-}$ mice. On a contrary, we detected a decreased age-independent anxiety-like phenotype as indicated by the increased number of head dips and decreased number of stretched postures across all ages.

7.1.3. CB_2R deletion has a moderate age-dependent effect on cognition

To investigate wherever CB_2R deletion causes any cognitive deficits we first used PR test to asses age-related changes in short-term social memory of the $CB_2R^{-/-}$ mice. All the groups had an intact sociability (**Figure 6.3a**). We used 1 hour inter-trial interval (ITI) to detect learning differences in 3-month old mice, but as we detected no learning in older groups with this ITI (data not shown), for those we used a shorter, 30 minutes ITI. In WT animals, we detected an above-chance-level preference for the novel partner in 3-month and 12-month old group, but not in 18-month old group (**Figure 6.3b**). In contrast, in $CB_2R^{-/-}$ mice, the preference did not differ from the chance level for 3-month and 12-month old groups, but it was above the chance level in the 18-month old group. The alterations in social memory did not arise from the novelty avoidance as there was no difference between genotypes in cumulative interaction time (**Figure 6.3c**). Thus, CB_2R deletion caused a moderate age-dependent change in social memory.

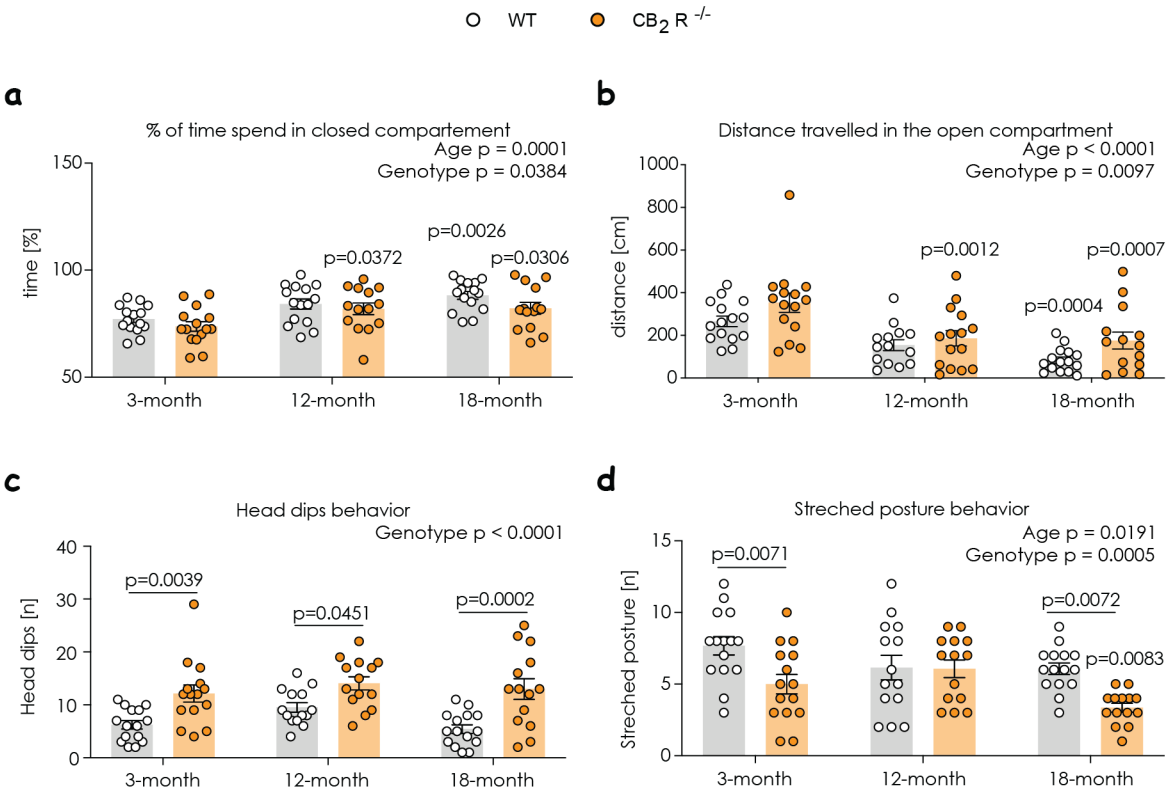

Figure 6.2. CB_2R deletion results in a decreased anxiety phenotype in o-maze. (**a**) % of time spend in the closed compartment. Increased % of time indicates higher anxiety. Significances presented in relation to 3-month old group from each genotype. (**b**) Distance travelled in the open compartment. Decreased distance indicates higher anxiety. Significances presented in relation to 3-month old group from each genotype. (**c**) Number of head dipping behaviours in the open compartment. Decreased number of head dips indicates higher anxiety. (**d**) Number of stretched posture behaviours. Increased number of stretched postures indicates higher anxiety. Significance presented in relation to 12-month old group from each genotype.
Each point represents a single mouse; N = 14-15 mice / genotype / age group. Data are displayed as mean value ± SEM. Data was analysed with two-way ANOVA followed by Sidak's multiple comparison test. The exact p-values are reported on each graph. WT mice – white circle; $CB_2R^{-/-}$ mice – orange circles.

Then we assessed the consequence of the CB_2R deletion on the long-term spatial memory using MWM. In MWM paradigm mice learn to locate the position of an invisible submerged escape platform based on external spatial cues. MWM consisted of three phases: acquisition (day 1-7), probe trial (day 8) and retrieval (day 9-11) phase (**Figure 6.3d**). 3-month old $CB_2R^{-/-}$ mice and WT controls showed a similar improvement during the acquisition phase and a similar performance during the reversal phase of the test (**Figure 6.3e**). They also showed an increased preference for the target quadrant during the probe trial. 12-month old $CB_2R^{-/-}$ mice and WT controls showed a similar improvement during the acquisition phase, but during reversal phase on day 10, $CB_2R^{-/-}$ mice showed a trend for a decreased performance in contrast to WT mice. Both groups spent the biggest amount of time during the probe trial in the platform-associated quadrant.

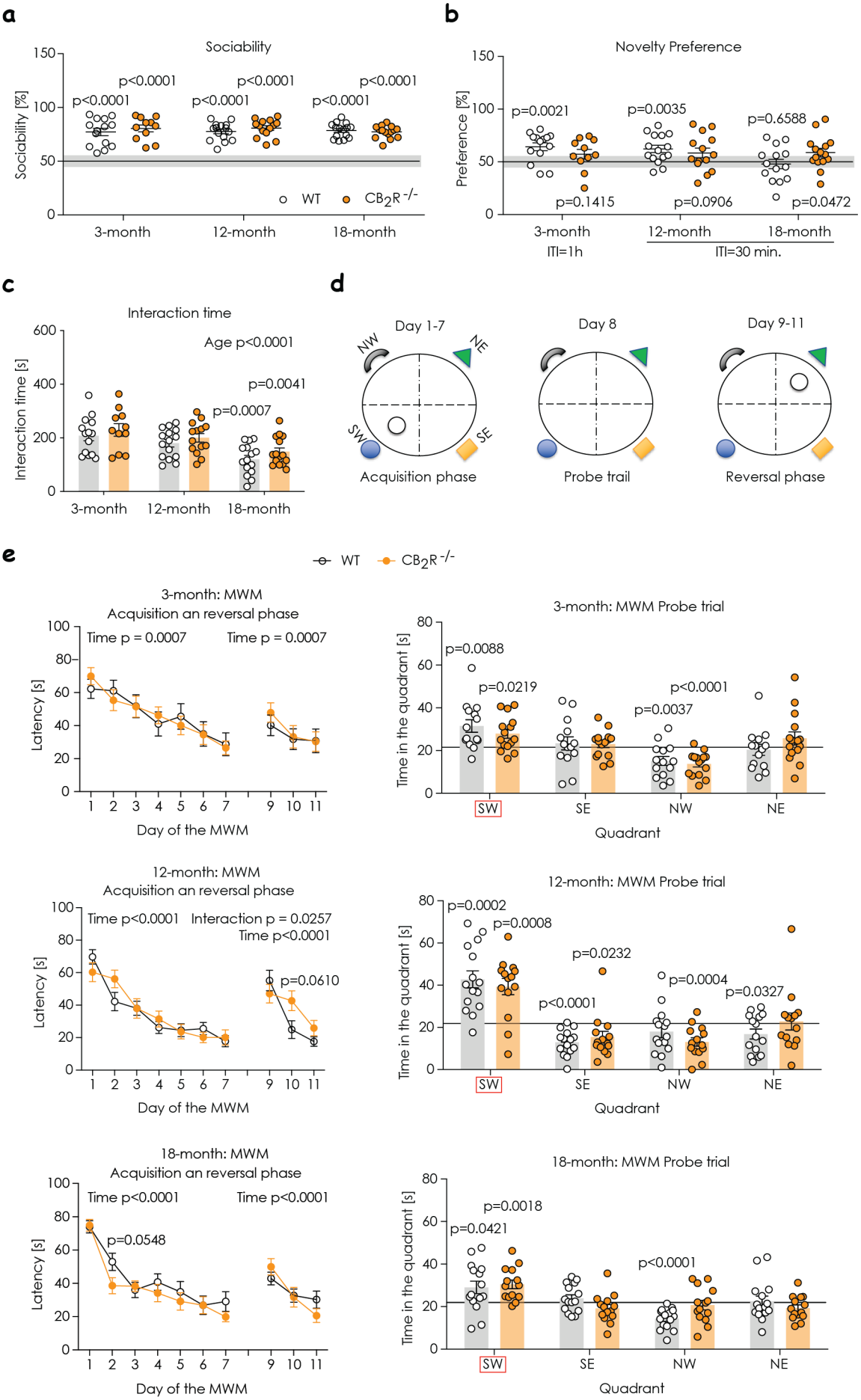
a
Sociability
Sociability [%]
p<0.0001
WT
CB2R -/-
3-month
12-month
18-month
b
Novelty Preference
Preference [%]
p=0.0021
p=0.1415
p=0.0035
p=0.0906
p=0.6588
p=0.0472
ITI=1h
ITI=30 min.
c
Interaction time
Interaction time [s]
Age p<0.0001
p=0.0041
p=0.0007
d
Day 1-7
Day 8
Day 9-11
NW
NE
SW
SE
Acquisition phase
Probe trail
Reversal phase
e
WT
CB2R -/-
3-month: MWM
Acquisition an reversal phase
Time p = 0.0007
Latency [s]
Day of the MWM
3-month: MWM Probe trial
Time in the quadrant [s]
p=0.0088
p=0.0219
p=0.0037
p<0.0001
SW
SE
NW
NE
Quadrant
12-month: MWM
Acquisition an reversal phase
Time p<0.0001
Interaction p = 0.0257
Time p<0.0001
p=0.0610
12-month: MWM Probe trial
p=0.0002
p=0.0008
p=0.0232
p<0.0001
p=0.0004
p=0.0327
18-month: MWM
Acquisition an reversal phase
Time p<0.0001
p=0.0548
18-month: MWM Probe trial
p=0.0018
p=0.0421
p<0.0001

Figure 6.3. CB_2R deletion has a moderate age-dependent effect on cognition. (**a**) Sociability was calculated as interaction time with a partner mouse over total interaction time. A mean value above 50% indicates that the mice are social. Mice with sociability lower than 55% were removed from the analysis. (**b**) Preference for the novel partner was calculated as time with the novel partner mouse over total interaction time. Significant difference from the chance level (50%) indicates learning. (**a-b**) Each point represents a single mouse. Each group was analysed individually by one-sample t-test (hypothetical mean = 50). Differences between groups were analysed by unpaired t-test. Line indicates a 50% chance level. Grey box indicates 5% variance around the chance level. (**c**) Cumulative interaction time from both trails of the PR test. Each point represents a single mouse. Data was analysed with two-way ANOVA followed by Sidak's multiple comparison test. (**d**) Experimental setup for MWM experiment. Drawing of the maze with spatial cues displayed on the walls of the maze. Dotted line delineates different quadrants associated with each cue. Circle indicates the position of the platform. (**e**) Panels from top to bottom: 3-, 12- and 18-month old mice. Left panel: acquisition and reversal phase. The mean latency to reach the platform is indicated for each day. Data are displayed as mean value $\pm$ SEM. Data was analysed with two-way ANOVA followed by Sidak's multiple comparison test. Right panel: probe trial. During the probe trial day, the platform was removed and the time spent in the platform-associated quadrant, was measured. Platform-associated quadrant is indicated with a red box. Line indicates a 22.5 s chance level. Data analyzed per genotype per quadrant by one-sample t-test (hypothetical mean = 22.5).
The exact p-values are reported on each graph. WT mice – white circle; $CB_2R^{-/-}$ mice – orange circles.

$CB_2R^{-/-}$ and WT 18-month mice showed similar improvements in the acquisition and reversal phases as well a strong preference to the platform-associated quadrant in the probe trial. In agreement with the PR results, we also detected a trend for a faster improvement of the $CB_2R^{-/-}$ mice on day 2 of the acquisition phase.

Taken together, we saw that spatial learning and memory performance was not changed in constitutive $CB_2R^{-/-}$ mice in neither of the age-groups. Similarly, we observed only moderate effects of CB_2R deletion on the social memory. Here, we detected that young and adult $CB_2R^{-/-}$ mice performed slightly worse than their age-matched WT controls, while in old mice the findings were the opposite.

7.1.4. CB2R deletion in 3-month old mice does not alter spatial and working memory, but increases the time that mice spent light compartment of the LD test

To further investigate the effect of CB_2R deletion on cognition, we tested an independent group of 3-month old mice in a different experimental setup consisting of two memory tests (novel object location recognition test – NOLR; y-maze, **Figure 6.4a**) and an anxiety test (light-dark test - LD test). As we observed moderate effects of CB_2R deletion in the short-term social memory test (PR, **Figure 6.4b**), but none in the long-term spatial memory test (MWM, **Figure 6.4e**) we decided to include a short-term spatial memory test (NOLR) to see if the observed effects are short-term memory specific. Moreover, since it was reported that $CB_2R^{-/-}$ mice have an improved working memory, we also included an y-maze

in our paradigm. Finally, due to previous reports about the role of CB_2R an anxiety and our findings from the o-maze (**Figure 6.4**), we also included a LD test.

$CB_2R^{-/-}$ mice had a higher than chance level novelty preference after 30 minutes and after 1 hour, while WT mice only after 1 hour (**Figure 6.4c**). Neither of the genotypes had a significant novelty preference for the displaced object after 2 hours. Hence, neither WT nor $CB_2R^{-/-}$ mice remembered the position of the object after 2 hours ITI.

Following investigation of anxiety-related behaviours in $CB_2R^{-/-}$ mice once again failed to show an increased anxiety-like phenotype in these mice. On a contrary, $CB_2R^{-/-}$ mice spent significantly more time in the light compartment of the LD test (**Figure 6.4d**).

We did not detect any differences between genotypes in the % of alterations in the y-maze (**Figure 6.4e**). Also, we did not detect any changes related to overall motility of the mice as the overall number of entries did not differ between genotypes.

Taken together, we observed that CB_2R deletion, aside from social memory, has only minor effects on the behaviour of male mice. Working memory and short-term spatial memory were not affected by the CB_2R deletion.

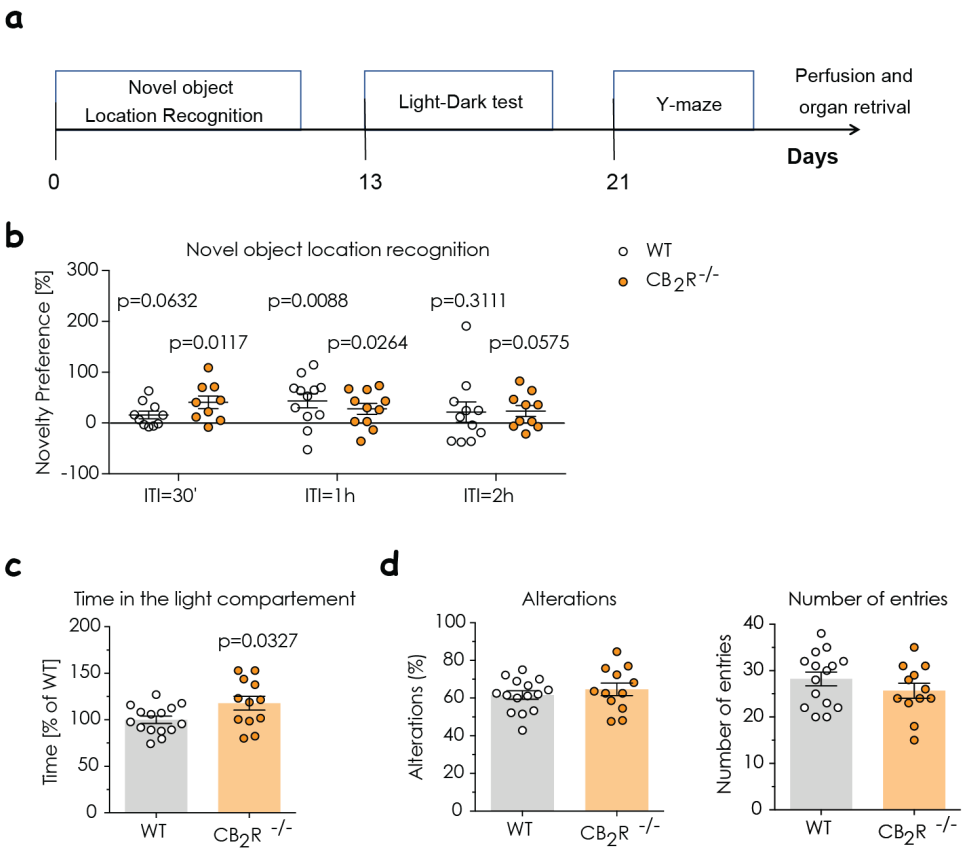

Figure 6.4. CB_2R deletion in 3-month old mice does not alter spatial and working memory, but increases the time that mice spend in light compartment of the LD test. (**a**) Experimental setup. Short-term spatial memory test (NOLR), anxiety test (LD test) and working memory test (y-maze). (**b**) Novelty preference (%), calculated by dividing preference for the moved object in trial 2 over the initial preference for this object in trial 1. A novelty

preference (%) above 0 indicates learning. Each group was analysed individually by one-sample t-test (hypothetical mean = 0). Line indicates a 0% chance level. Mice with initial preference for the moved object > 50% were removed from the analysis. (**c**) Time spent in the light compartment of the LD test. (**d**) Y-maze results. Left panel: % of alterations. An alternation is counted when a mouse consecutively explores three different arms. Right panel: overall number of arm entries. Data was checked against normal distribution using D'Augostino &Pearson normality test and groups were compared to each other using unpaired t-test/U-test. Each point represents a single mouse; N = 9-15 mice / genotype. Data are displayed as mean value ± SEM. The exact p-values are reported on each graph. WT mice – white circle; $CB_2R^{-/-}$ mice – orange circles.

7.1.5. CB_2R deletion decreases social memory in both male and female mice

Next, we investigated if CB_2R role in social memory is gender-specific. In order to check that, we investigated short-term social memory in male and female $CB_2R^{-/-}$ mice using the partner recognition test (PR). All mice had sociability above the 50% chance level (**Figure 6.5a, left panel**).

$CB_2R^{-/-}$ mice and controls displayed similar social behavior. However, only WT mice preferred to interact with a novel partner, indicating that they remembered the familiar mouse from the previous trial. In contrast, for $CB_2R^{-/-}$ mice the preference for the novel partner did not differ from chance level, indicating a social memory impairment in these mice (**Figure 6.5a, middle panel**).

To exclude that the observed effect was due to differences in exploratory behavior, we next calculated the total interaction time during the PR test. We did not detect any genotype effect, but we detected a significant gender effect (**Figure 6.5a, right panel**). Following post hoc analysis revealed a significant increase in the interaction time exclusively between male and female $CB_2R^{-/-}$ mice (**Figure 6.5a, right panel**).

To investigate if the genotype effect in PR was due to a sensory defect, we performed an olfaction test. Mice from both genotypes showed a significant increase in the exploration of a urine-stained cotton swab over a water-stained swab (**Figure 6.5b**). Overall, these data suggest that $CB_2R^{-/-}$ impairs social memory in the PR test in both male and female mice. This effect is neither not due to an olfactory deficit nor decrease in the exploratory drive.

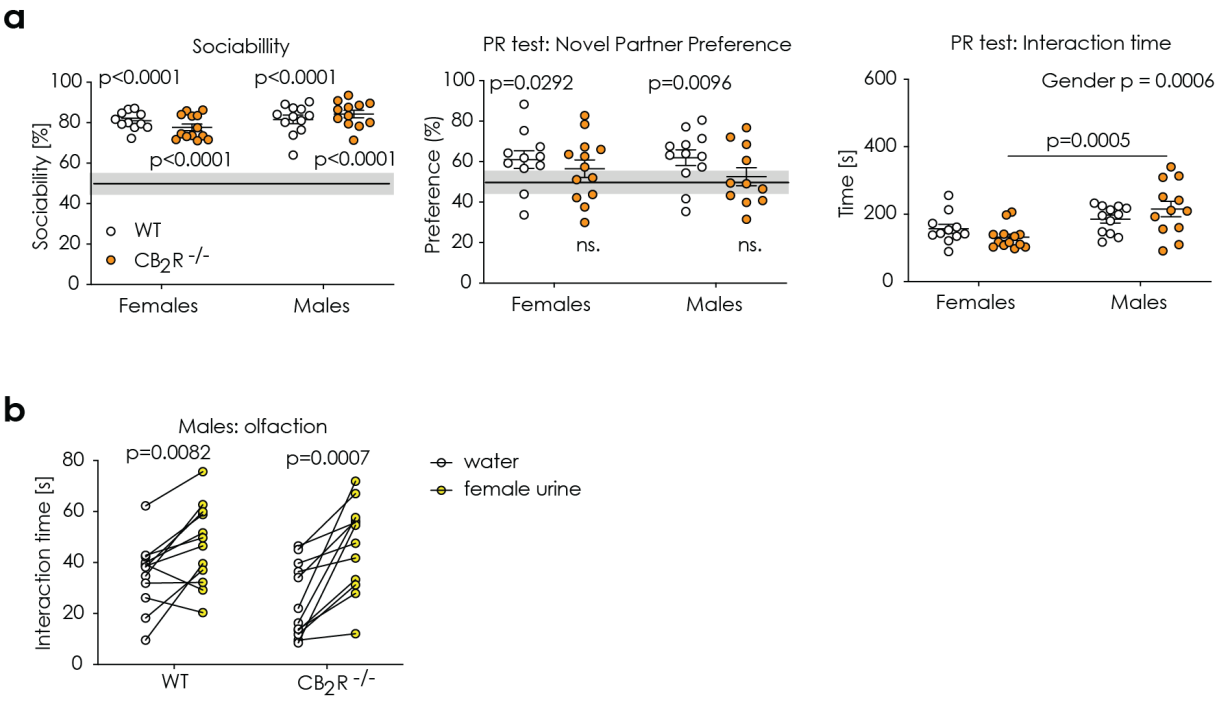

Figure 6.5. CB_2R deletion decreases social memory in both male and female mice. (**a**) Left panel - Sociability (%) was calculated as interaction time with a partner mouse over total interaction time. A mean value above 50% indicates that the mice are social. Middle panel - Preference (%) for the novel partner was calculated as time with the novel partner mouse over total interaction time. Significant difference from the chance level (50%) indicates learning. Each group was analyzed individually by one-sample t-test (hypothetical mean = 50). Right panel – Cumulative interaction time from both trails of the PR test. Data was analyzed by two-way ANOVA followed by Sidak’s multiple comparison test. WT – white circles; $CB_2R^{-/-}$ mice – orange circles.
(**b**) Interaction time of mice with water-stained (white circle) or female urine-stained (yellow circle) cotton swab. Increase in the interaction time suggests lack of olfactory deficits. Data was analyzed separately for each genotype by paired t-test.
Each datapoint represents one mouse; N = 11–13 mice / gender / genotype. Data are displayed as mean value ± SEM. The exact p-values are indicated on the graph.

7.1.6. Sex-specific alterations in basic behaviours after CB_2R deletion.

We further examined if CB_2R deletion causes any gender-specific alterations in mice basic behaviors. In order to do that on top of the PR test we performed a nestlet shredding test, weight measurements and monitored home-cage activity along with food and water intake (**Figure 6.6a**).

In agreement with our previous findings, we detected a significant genotype effect in the weight measurement in both genders. 6-month old $CB_2R^{-/-}$ female mice were approximately 1 g heavier than their WT controls with mean weight at 24.24 g and 23.21 g, respectively. 6-month old $CB_2R^{-/-}$ male mice were approximately 3 g heavier with mean weight at 33.58 g in comparison to 30.69 g mean weight of the WT mice (**Figure 6.6b**).

We did not detect any effects when it comes to the food intake, but for water intake we detected a significant gender, genotype and interaction effect (**Figure 6.6c**). Following post hoc analysis revealed that $CB_2R^{-/-}$ female mice drank almost 30% more than the WT female mice, while there was no genotype-related difference in male mice.

To observe changes induced by mild stress we performed two nestlet shredding tests – before and during habituation. In contrast to our 3-month male group, we did not detect any significant difference in nestlet building neither before nor after habituation in any of the genders (**Figure 6.6d**).

For home-cage activity measurement we detected a significant interaction effect only for female mice (**Figure 6.6e**).

Overall, similarly as in our age-related study, the basic behaviours were not drastically affected by the CB_2R deletion in neither females nor in male mice.

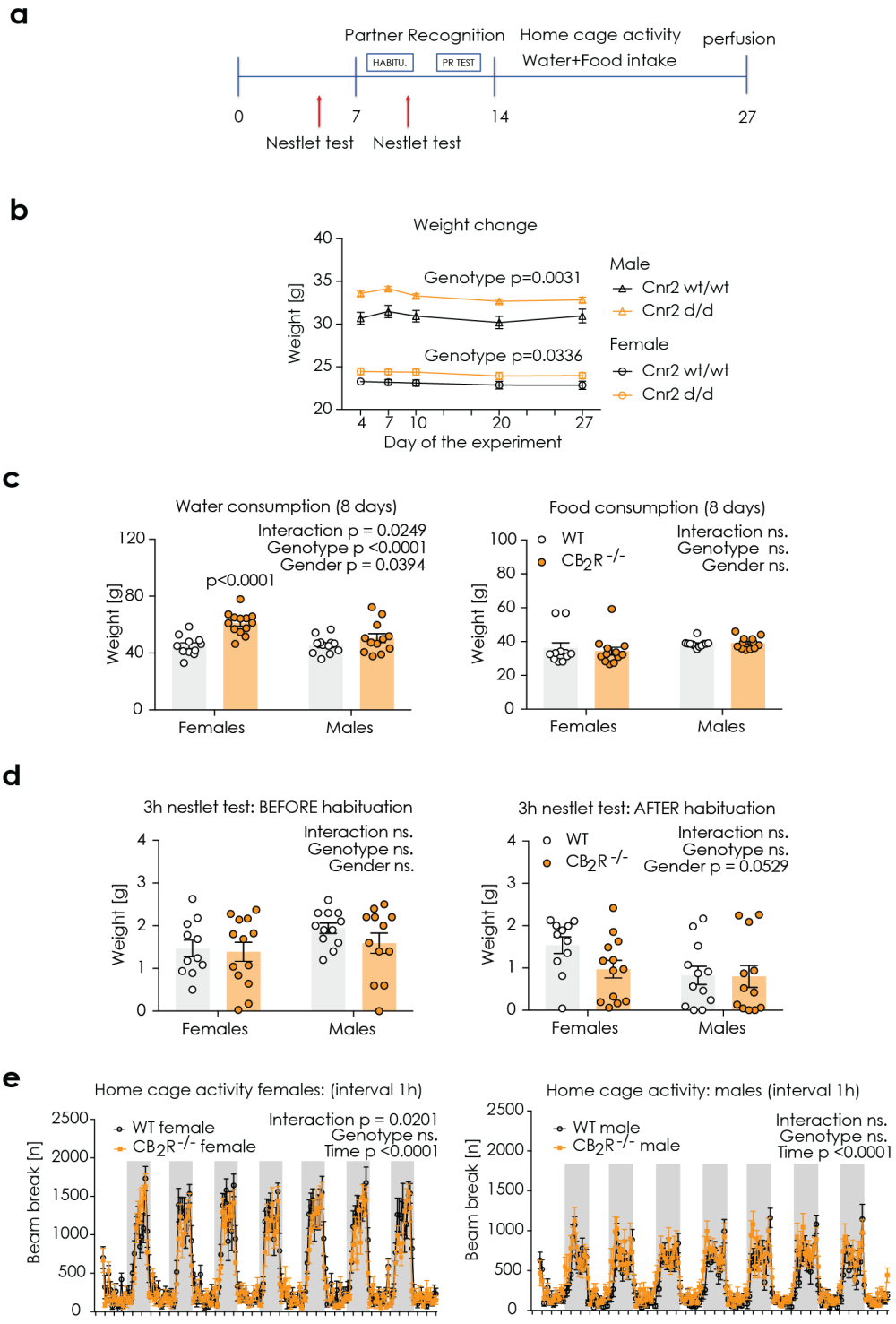

Figure 6.6. Sex-specific alterations in basic behaviours after CB_2R deletion. (**a**) Experimental setup. (**b**) weight change over the course of the experiments. Each age group is presented individually (N = 11-13 mice / genotype / gender). Data are displayed as mean value ± SEM. Data was analysed per gender with Two-way ANOVA. (**c**) Left panel: water consumption; right panel: food consumption over 8 days. (**d**) Results of nestlet shredding tests. Nest score; possible nest scores 1-5. Left panel: test before habituation; right panel: after habituation for the PR. Each point represents a single mouse. Data shown as mean per group ± SEM. (**f**) Home-cage activity measurement by infrared sensors. Activity measured as the number of beam breaks. Left panel – female mice; Right panel: male mice. Data are displayed as cumulative activity per group within 1 hour ± SEM. Grey box indicates the duration of the dark phase.
Data was analysed by two-way ANOVA followed by Sidak’s multiple comparison test. The exact p-values are reported on each graph. WT – white circles; $CB_2R^{-/-}$ - orange circles.

7.1.7. Increased synapsin-I levels and puncta size in the hippocampus after CB_2R deletion in females, but not in males.

Next, we investigated what are the molecular consequences of CB_2R deletion regarding the synaptic architecture in the hippocampal CA1, CA2, and CA3 area. Since CA2 area cannot be distinguish based on neuronal nuclei alone, in order to study this area we first established RGS14 staining, a marker for CA2 principal cells (**Figure 6.7**).

To assess general changes in synapse density and size in the hippocampus we investigated synapsin-I immunostainings in the CA1, CA2 and CA3 area. The areas were discriminated based on a staining with an antibody against RGS14 (**Figure 6.8a**). First, we analyzed the mean grey value in all hippocampal areas (**Figure 6.8b**). As expected, we detected a significant effect of hippocampal layer in all areas with the highest density of synapsin-I in stratum lucidum. Furthermore, we found a significant genotype effect in females in all areas of the hippocampus (**Figure 6.8c**). Post hoc analysis revealed significantly increased synapsin-I levels in all areas and all layers. In male mice a genotype effect was present in the CA3 area, but post hoc analysis did not reveal any layer-specific genotype difference.

To address if the increased synapsin-I signal in females was due to an increase in the size of synaptic clusters we analyzed the average size of synapsin-I puncta specifically in the CA2 and CA3 area (**Figure 6.9a**). Our analysis showed an overall genotype effect in both CA2 and CA3, exclusively in females (**Figure 6.9b**). The following post hoc analysis did not reveal any specific changes in any of the CA2 layers. However, we observed a significant increase in stratum lucidum of the CA3 hippocampal area. In contrast, no genotype effect was present in male mice.

Furthermore, we detected a layer effect in both males and females in the CA2 and CA3 area of the hippocampus with the biggest puncta size in stratum lucidum (**Figure 6.9b**).

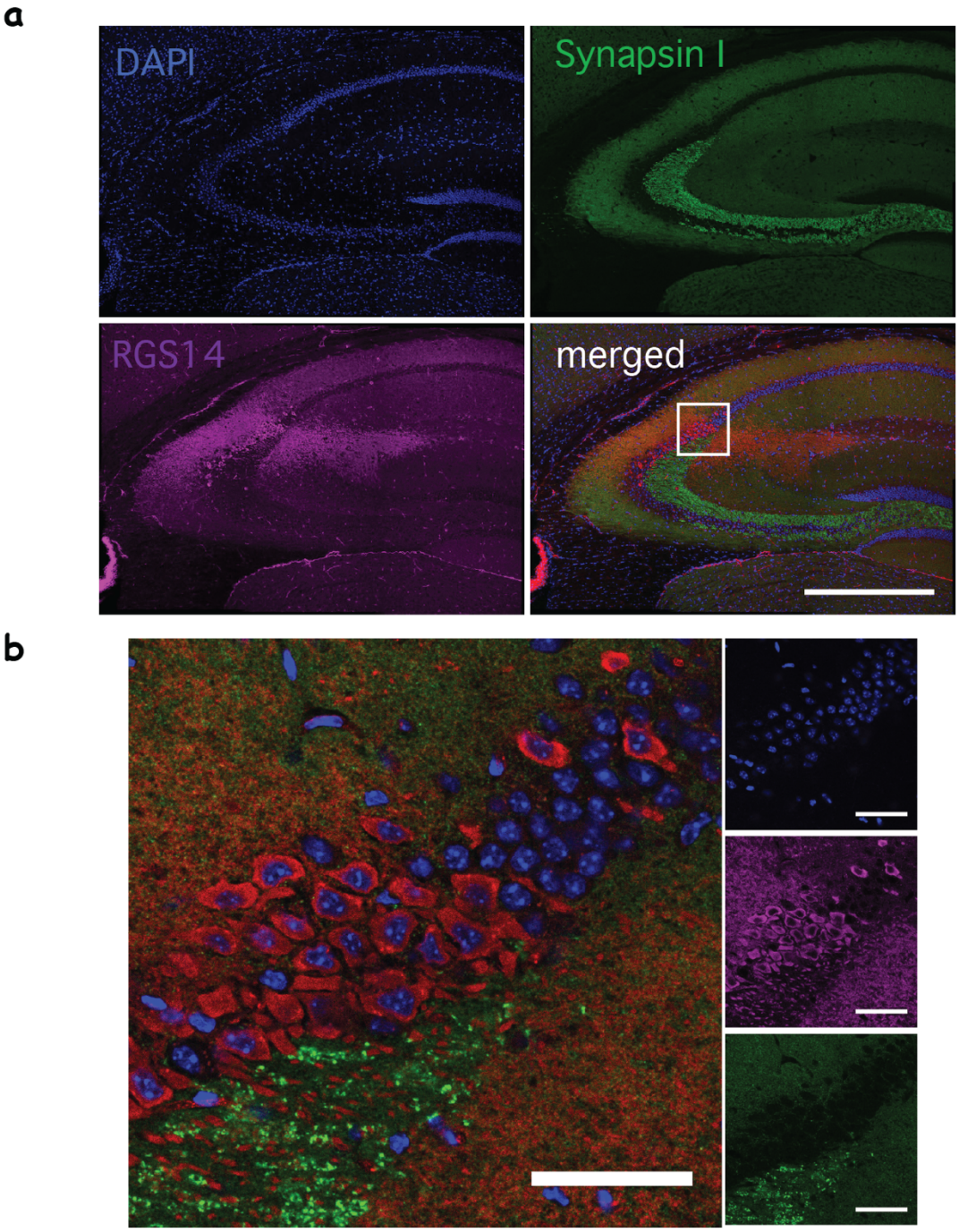

Figure 6.7. RGS14 and synapsin-I staining. (a) Example tilescan image taken with a 20x objective of the hippocampal CA1, CA2, CA3 areas. The white box within the left panel indicates the section that is displayed in higher magnification below. Scale bar represents 500 µm. (**b**) Inset showing a clear border between CA2 and CA1 areas. Scale bar: 50 µm. Single channels: DAPI – blue; synapsin-I – green; RGS14 – magenta. Merged image: DAPI – blue; synapsin I – green; RGS14 – red.

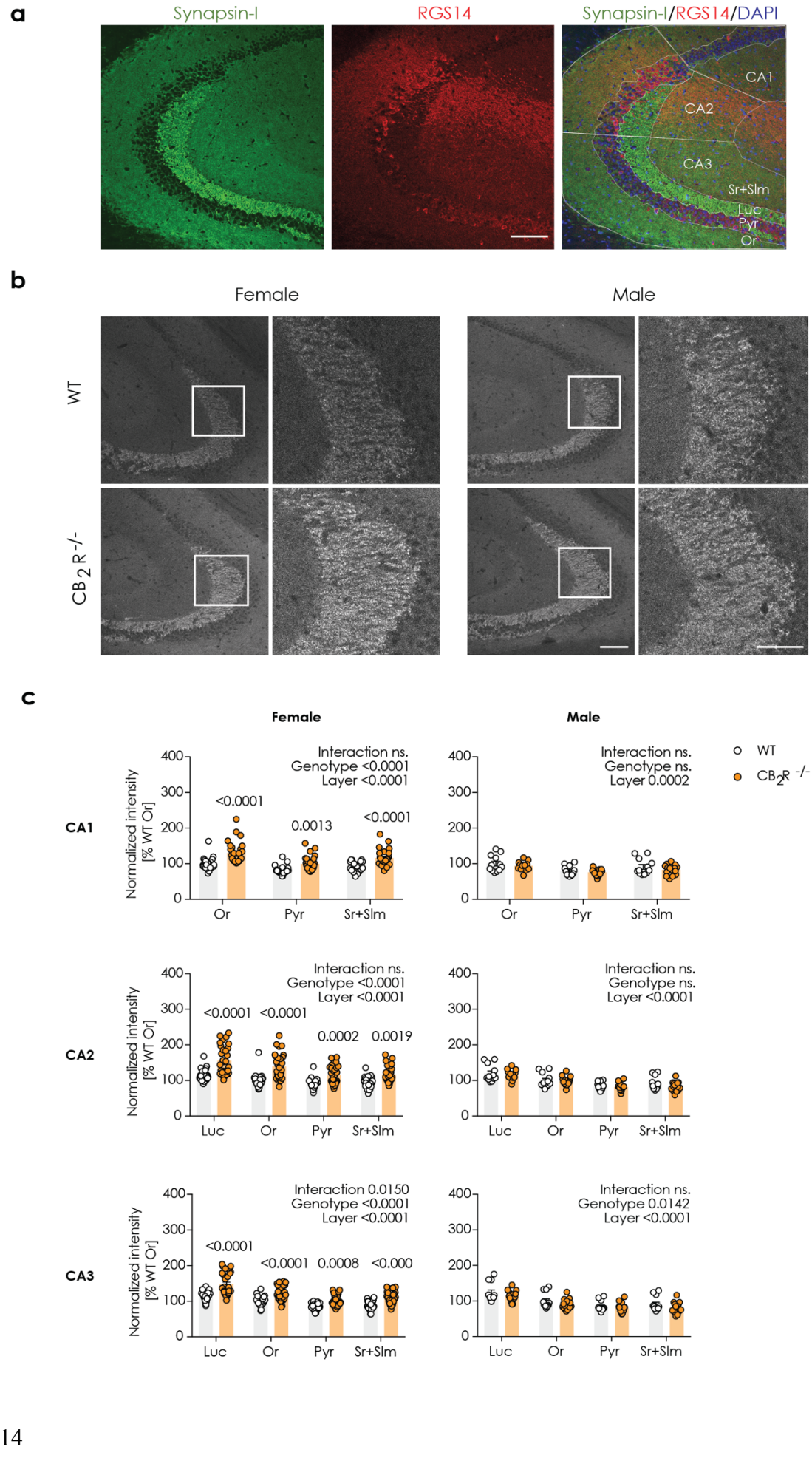
a
Synapsin-I
RGS14
Synapsin-I/RGS14/DAPI
CA1
CA2
CA3
Sr+Slm
Luc
Pyr
Or
b
Female
Male
WT
CB2R -/-
c
Female
Male
WT
CB2R -/-
CA1
CA2
CA3
Normalized intensity [% WT Or]
Interaction ns.
Genotype <0.0001
Layer <0.0001
Interaction ns.
Genotype ns.
Layer 0.0002
Interaction ns.
Genotype ns.
Layer <0.0001
Interaction 0.0150
Genotype <0.0001
Layer <0.0001
Interaction ns.
Genotype 0.0142
Layer <0.0001
<0.0001
0.0013
<0.0001
0.0002
0.0019
0.0008
<0.000
Luc
Or
Pyr
Sr+Slm

Figure 6.8. Synapsin-I levels are increased in the hippocampus after CB_2R deletion in female mice. (**a**) Example images show synapsin-I – green; RGS14 - red and DAPI - blue. White lines indicate manual delineation of CA regions and layers in the hippocampus. Scale bar represents 100µm. (**b**) Example images of synapsin-I immunoreactivity in male and female from WT and $CB_2R^{-/-}$mice. The white box within the left panel indicates the section that is displayed in higher magnification on the right. Scale bars represent: 100µm, 50 µm (inset). (**c**) Quantification of synapsin-I mean grey value within each hippocampal layer normalized to the result from stratum oriens (Or). Or- stratum oriens; Luc – stratum lucidum; Pyr – stratum pyramidale; Sr+Slm – stratum radiatum and stratum lacunosum-moleculare. WT mice – white circle; $CB_2R^{-/-}$ mice – orange circle. Each datapoint represents one image. Left panel – female mice (WT: n = 30 images from N = 9 mice; $CB_2R^{-/-}$: n = 31 images from N = 9 mice); right panel - male mice (WT: n = 12 images from N = 3 mice; $CB_2R^{-/-}$: n = 16 images from N = 4 mice). Top panel – CA1 region; middle panel – CA2 region; bottom panel – CA3 region. Data is displayed as mean value $\pm$ SEM. Data was analyzed by two-way ANOVA followed by Sidak’s multiple comparison test. The exact p-values are indicated on each graph.

7.1.8. CB_2R deletion alters excitatory and inhibitory synapses in a gender-specific manner

We then investigated excitatory synapses in the CA areas of the hippocampus using vGLUT1 as a marker. Co-staining with vGLUT1 and synapsin-I revealed a high degree of colocalization between those markers (**Figure 6.10a**). As for synapsin-I, we found an overall layer effect and a main genotype effect in the CA2 and CA3 areas in female mice (**Figure 6.10bc**). However, we detected no genotype effect in the CA1 region.

The subsequent post hoc analysis in CA2 and CA3 did not reveal any layer-specific effect. In males, there was no genotype effect. Our data indicate that vGLUT1 expression was altered in female $CB_2R^{-/-}$ mice, but the effects were not as pronounced as the changes observed for synapsin-I.

We next investigated inhibitory synapses in the hippocampus using vGAT as a marker. The extend of colocalization between synapsin-I and vGAT staining is smaller compared to what we observed for synpasin-I and vGLUT1 (**Figure 6.11a**). Consistent with the other synaptic markers we analyzed, we found a significant layer effect across all groups. Furthermore, we detected a main effect of the genotype in both female and male mice (**Figure 6.11bc**). Although an increase in vGAT mean gray values was observed in both genders of CB_2 knockout mice, the effect was again much more pronounced in females. Here, a significant genotype effect was present for all areas and regions after post hoc analysis. Whereas in male mice only the increase in CA1 stratum pyramidale reached statistical significance in the postdoc analysis.

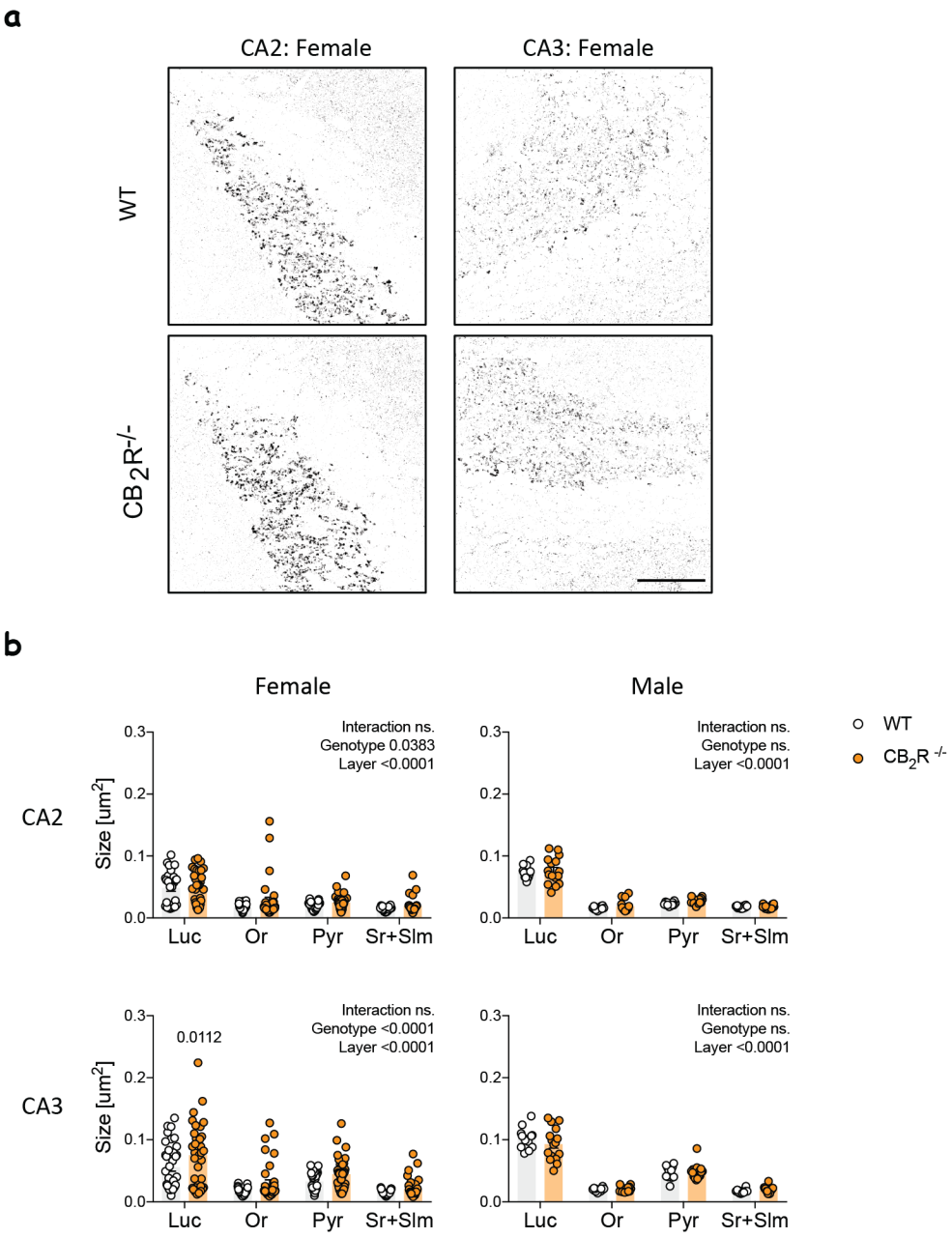

Figure 6.9. Average size of Syn1 particles is increased after CB_2R deletion in females. (**a**) Example images show binary image of synapsin-I. Scale bar represents 50µm. (**b**) Quantification of synapsin-I mean puncta size (detected puncta > 0.005 µm). Or- stratum oriens; Luc – stratum lucidum; Pyr – stratum pyramidale; Sr+Slm – stratum radiatum and stratum lacunosum-moleculare. WT mice – white circle; $CB_2R^{-/-}$ mice – orange circle. Each datapoint represents one image. Left panel – female mice (WT: n = 28-35 images from N = 9 mice; $CB_2R^{-/-}$: n = 31-36 images from N = 9 mice); right panel - male mice (WT: n = 12 images from N = 3 mice; $CB_2R^{-/-}$: n = 16 images from N = 4 mice). Top panel – CA2 region; bottom panel – CA3 region. Data is displayed as mean value ± SEM. Data was analyzed by two-way ANOVA followed by Sidak's multiple comparison test. The exact p-values are indicated on each graph.

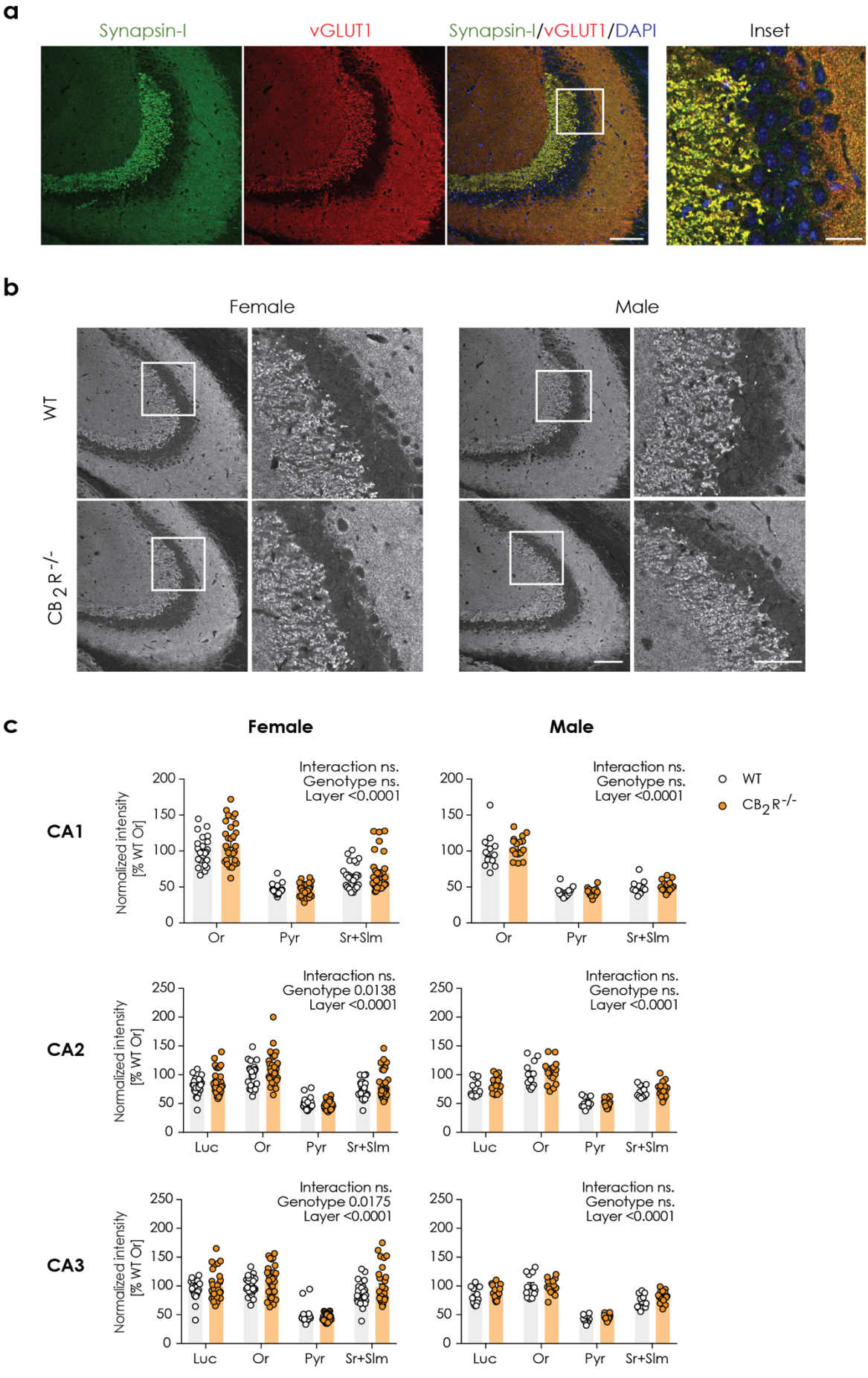
a
Synapsin-I
vGLUT1
Synapsin-I/vGLUT1/DAPI
Inset
b
Female
Male
WT
CB2R-/-
c
Female
Male
WT
CB2R-/-
CA1
CA2
CA3
Normalized intensity [% WT Or]
Interaction ns.
Genotype ns.
Layer <0.0001
Interaction ns.
Genotype 0.0138
Layer <0.0001
Interaction ns.
Genotype 0.0175
Layer <0.0001
Luc
Or
Pyr
Sr+Slm

Figure 6.10. vGLUT1 levels are slightly altered in female $CB_2R^{-/-}$ mice. (**a**) Example images show synapsin-I – green; vGLUT1 - red and DAPI - blue. Scale bar represents 100 µm, 25 µm (inset). (**b**) Example images of vGLUT1 immunoreactivity in male and female from WT and $CB_2R^{-/-}$mice. The white box within the left panel indicates the section that is displayed in higher magnification on the right. Scale bar: 100µm, 50 µm (inset). (**c**) Quantification of vGLUT1 mean grey value within each hippocampal layer normalized to the result from stratum oriens (Or). Or- stratum oriens; Luc – stratum lucidum; Pyr – stratum pyramidale; Sr+Slm – stratum radiatum and stratum lacunosum-moleculare. WT – white circles; $CB_2R^{-/-}$ mice – orange circles. Each datapoint represents one image. Left panel – female mice (WT: n = 30 images from N = 9 mice; $CB_2R^{-/-}$: n = 31 images from N = 9 mice); right panel - male mice (WT: n = 12 images from N = 3 mice; $CB_2R^{-/-}$: n = 16 images from N = 4 mice). Top panel – CA1 region; middle panel – CA2 region; bottom panel – CA3 region. Data is displayed as mean value ± SEM. Data was analyzed by two-way ANOVA followed by Sidak's multiple comparison test. The exact p-values are indicated on the graph.

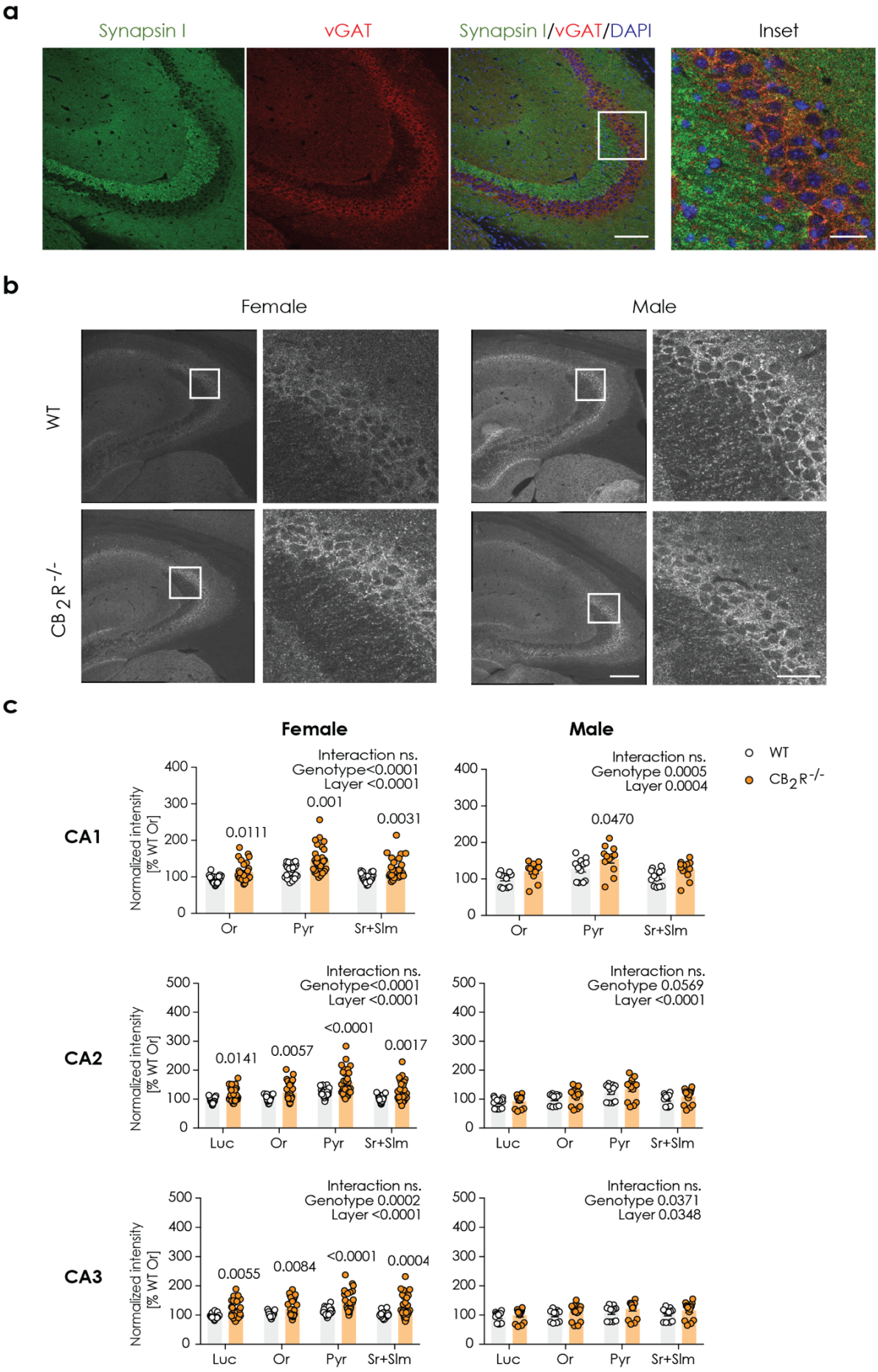
a
Synapsin I
vGAT
Synapsin I/vGAT/DAPI
Inset
b
Female
Male
WT
CB2R-/-
c
Female
Male
WT
CB2R-/-
CA1
CA2
CA3
Normalized intensity [% WT Or]
Interaction ns.
Genotype<0.0001
Layer <0.0001
0.0111
0.001
0.0031
Interaction ns.
Genotype 0.0005
Layer 0.0004
0.0470
Interaction ns.
Genotype<0.0001
Layer <0.0001
0.0141
0.0057
<0.0001
0.0017
Interaction ns.
Genotype 0.0569
Layer <0.0001
Interaction ns.
Genotype 0.0002
Layer <0.0001
0.0055
0.0084
<0.0001
0.0004
Interaction ns.
Genotype 0.0371
Layer 0.0348
Luc
Or
Pyr
Sr+Slm

Figure 6.11. vGAT levels are increased in female $CB_2R^{-/-}$ mice, but not in male. (**a**) Example images show synapsin-I – green; vGAT - red and DAPI - blue. Scale bar represents 100 µm, 25 µm (inset). (**b**) Example images of vGAT immunoreactivity in male and female from WT and $CB_2R^{-/-}$mice. The white box within the left panel indicates the section that is displayed in higher magnification on the right. Scale bar: 200 µm, 25 µm (inset). (**c**) Quantification of vGAT mean grey value within each hippocampal layer normalized to the result from stratum oriens (Or). Or- stratum oriens; Luc – stratum lucidum; Pyr – stratum pyramidale; Sr+Slm – stratum radiatum and stratum lacunosum-moleculare. White circle – WT; orange circle – $CB_2R^{-/-}$ mice. Each datapoint represents one image. Left panel – female mice (WT: n = 30 images from N = 9 mice; $CB_2R^{-/-}$: n = 31 images from N = 9 mice); right panel - male mice (WT: n = 12 images from N = 3 mice; $CB_2R^{-/-}$: n = 16 images from N = 4 mice). Top panel – CA1 region; middle panel – CA2 region; bottom panel – CA3 region. Data is displayed as mean value ± SEM. Data was analyzed by two-way ANOVA followed by Sidak's multiple comparison test. The exact p-values are indicated on each graph.

8. DISCUSSION: “Cannabinoid receptor 2 and cognition”

It is known that the ECS tone decreases with age and that CB_1R deletion causes an accelerated aging phenotype accompanied by premature cognitive decline (A. Bilkei-Gorzo et al., 2005; Andras Bilkei-Gorzo et al., 2012; Piyanova et al., 2015). Due to recent reports confirming the presence of functional CB_2R on neurons, we first asked the question if CB_2R deletion has similar consequences regarding cognition in the context of aging. We observed that CB_2R deletion, in contrast to CB_1R deletion, did not cause any accelerated age-related cognitive impairments. On the contrary, we detected a slight decrease in social memory in young animals, while old $CB_2R^{-/-}$ mice retained their cognitive abilities in comparison to the age-matched controls. In addition, contrary to previous reports, we detected an age-independent decrease in anxiety-like behaviour in $CB_2R^{-/-}$ mice (Ortega-Alvaro et al., 2011).

Second, we asked if CB_2R plays a different role in memory and synaptic architecture in female and male mice. Analysis of synaptic proteins in male and female mice confirmed that despite the low level of expression of CB_2Rs in neurons, their signaling plays an important role in synaptic functions. Our results indicated a pronounced gender effect, with female $CB_2R^{-/-}$ mice showing significant alterations in the expression of hippocampal synaptic markers in contrast to male mice. Consistent with our previous findings we detected a social memory impairment in $CB_2R^{-/-}$ mice that was present both in male and female mice.

Furthermore, we did not detect any major changes in basic behaviours in $CB_2R^{-/-}$ mice neither in the context of aging nor gender-specific alterations.

8.1.1. CB_2R plays a role in social memory in an age-dependent and gender-independent manner

Recent development of new technologies confirmed presence of the CB_2R on neurons and its functional relevance in the CA2/3 area of the hippocampus and somatosensory cortex (Y. Li & Kim, 2015; Stempel et al., 2016; Stumpf et al., 2018). In young mice, CB_2R stimulation caused a cell-intrinsic specific hyperpolarization that resulted in altered gamma oscillations (Stempel et al., 2016). It is known that changes in gamma oscillations are related to changes in cognition (Mably & Colgin, 2018). This together with a known role of the CA2 hippocampal area in social memory, led us to speculate that CB_2R may play a role in short-term social memory (Hitti & Siegelbaum, 2014). Indeed, we observed that young (3-month old) and adult

(12-month old) $CB_2R^{-/-}$ mice had a slight decrease in short-term social memory. Surprisingly, old (18-monthd old) $CB_2R^{-/-}$ mice performed better than their age-matched controls. We confirmed our results and also found a memory impairment in young adult (6-month) female and male $CB_2R^{-/-}$ mice suggesting that CB_2R plays a similar role in social memory in both genders.

$CB_2R^{-/-}$ deletion in old mice seemed to be slightly beneficial. This indicates age-related changes in the CA2 region and/or CB_2R itself. Up to date, not much is known about aging-dependent changes in the CA2 region, but it has been shown this area is uniquely affected during pathologies like schizophrenia and dementia (Benes et al., 1998; Chevaleyre & Piskorowski, 2016; Ishizawa et al., 2002; Piskorowski et al., 2016). Whereas until now, CB_2R age-related changes were exclusively studied in the context of AD and in regard to its function in microglia regulation (Aso et al., 2013; A. C. Schmöle, Lundt, Ternes, et al., 2015). Despite contrasting results, modulation of CB_2R activity did impact cognitive abilities of AD-related model mice. If this influence was due to a direct modulation of the CB_2R on neurons or indirectly through microglia activity regulation, remains elusive.

In agreement with our findings, other studies using young $CB_2R^{-/-}$ mice revealed a decrease in hippocampus-dependent fear memory (García-Gutiérrez et al., 2013; Yong Li & Kim, 2016a). In contrast, activation of the CB_2R with a specific agonist JWH-133 did not alter cognition in neither 5-7 months nor 11-month old mice (Aso et al., 2013; Martín-moreno et al., 2012). This raises a concern of possible developmental effects in the constitutive $CB_2R^{-/-}$ mice. Future studies using inducible knockout mice will help in distinguishing developmental effects.

On a molecular level, CB_2R deletion resulted in a decreased spine density in the hippocampus (García-Gutiérrez et al., 2013; Yong Li & Kim, 2016b). The synaptic changes might underlie the cognitive deficits that we and others observed in younger $CB_2R^{-/-}$ mice.

It has been also shown that aging changes excitatory/inhibitory balance (E/I) in the brain. In the PFC aging decreases excitation and increases inhibition (Legon et al., 2016; Luebke et al., 2004). Many studies suggested that age-related cognitive impairment is associated with altered inhibitory transmission in the hippocampus (Leal & Yassa, 2015; Rozycka & Liguz-Lecznar, 2017). Since CB_2R deletion results in a decreased excitatory synaptic transmission in young animals, the different memory phenotype in young and old $CB_2R^{-/-}$ mice may be related to changes in the E/I (Yong Li & Kim, 2016b).

Moreover, we have proven that social memory impairment did not arise due to an olfactory deficit or novelty avoidance, as both young and old $CB_2R^{-/-}$ and WT mice could smell and had the total same interaction time during the PR.

Taken together our results further support an important role of the CB_2R in memory. Moreover, for the first time, we showed that CB_2R is also involved in social memory and in an age-dependent manner. Further studies deleting CB_2R specifically in the CA2 principle neurons (by using B6.Cg-Tg(Amigo2-cre)1Sieg/J line for instance), are necessary to elucidate CB_2R functions in hippocampal networks in more detail. Furthermore, studies looking into CA2-specific age-related changes will shed some light on the possible underlying molecular mechanism.

8.1.2. Possible role of CB_2R in memory consolidation under specific conditions

To get a comprehensive overview of the age-related changes in the cognitive abilities of $CB_2R^{-/-}$ mice, we also tested other types of memory including short-term and long-term spatial memory as well as working memory. We did not detect any genotype-related alterations in any of the tests. However, we revealed a trend for worse performance in MWM in adult and slightly better performance of old $CB_2R^{-/-}$ mice. This was in contrast to previous reports that showed an increased performance of young $CB_2R^{-/-}$ mice in MWM and y-maze (Yong Li & Kim, 2016a; A. C. Schmöle, Lundt, Ternes, et al., 2015). Opposed to our study that included only male mice, both studies mentioned above were conducted on a gender-mixed group, so it is probable that the differences arose mostly due specific alterations in females (**see 7.1.6**).

The decrease in fear memory in $CB_2R^{-/-}$ mice was speculated to arise from an impairment in memory consolidation (García-Gutiérrez et al., 2013; Ratano et al., 2017, 2018). We did not observe any deficits in long-term spatial memory in $CB_2R^{-/-}$ mice suggesting that CB_2R might be involved in memory consolidation of certain memory types or under specific conditions. Although, the magnitude of the aversive stimuli differed between our experiment (water) and previous studies (electric shock), the aversive character of the stimuli was the same (García-Gutiérrez et al., 2013; Yong Li & Kim, 2016a). This decreases the possibility that CB_2R might only be important for memory consolidation under an aversive stimulus, but does not exclude that it might be important specifically for fear memory. Moreover, CA2 has been proposed as an interface between emotion and cognition, since the ventral CA2 also receives

input from the basal nuclei of Amygdala (Chevaleyre & Piskorowski, 2016; Pikkarainen et al., 1999). Thus, it is possible that CB_2R in CA2 hippocampal region regulates specifically social and fear memory.

8.1.3. CB_2R effects anxiety-like behaviour

Since anxiety and stress levels can influence the performance in memory tests and $CB_2R^{-/-}$ mice have been shown to have increased anxiety- and depressive-like behaviour, we included anxiety tests in our behavioural paradigms (Ortega-Alvaro et al., 2011). In our hands CB_2R deletion did not increase anxiety-like behaviours in any of the tests. On the contrary, we detected a genotype effect and a trend for a decrease in the time spent in the closed arms of the o-maze. Correspondingly, we also detected a genotype effect and a trend for an increased in the distance travelled in the open arms of the o-maze. Furthermore, we detected an age-independent increase in risk taking behaviour and slight decrease in stretched posture behaviour. An independent investigation confirmed a decreased anxiety phenotype as young $CB_2R^{-/-}$ mice spent more time in the lit compartment of the LD test. Altogether, we conclude that CB_2R deletion decreased anxiety-like behaviours in an age-independent fashion.

The schizophrenia-like phenotype was detected in mice, where $CB_2R^{-/-}$, on a C57BL6/J background were crossed to an outbred CD1 mice strain (Ortega-Alvaro et al., 2011). Following investigations by the same group showed that mice with an overexpression of the CB_2R had a decreased vulnerability to anxiogenic and depression-like stimuli (García-Gutiérrez & Manzanares, 2011). However, neither our data nor other studies were able to replicate those findings hinting that there might be over factors involved (Yong Li & Kim, 2016a; Liu et al., 2017).

It was proposed that $CB_2R^{-/-}$ mice are stress-sensitive and this might have impacted the direction on the tests, but we did not make a similar observation. The only observation we made that might support this is the decrease in nestlet building exclusively in 3-month old mice. One cannot also exclude the possibility that a mixed genetic background with CD1 strain could have introduced additional differences in previous investigations. Nevertheless, we confirmed that CB_2R does play a role in anxiety-like behaviours and showed that the role does not change during aging.

In agreement with previous reports, we detected an age-related increase in the time spent in closed arms of the o-maze suggesting that aging enhances anxiety-like behaviours (Singhal et al., 2020). This increase was already prominent in adult $CB_2R^{-/-}$ mice, while in WT mice, it was only prominent in old mice. In parallel, we observed an age-related decrease in distance travelled in the open compartment. However, we did not observe any age-related changes in stretched postures and head dips suggesting that the decline in time and distance might not have arisen due to an increased anxiety, but rather due to an age-related decline in the overall motility.

8.1.4. CB_2R in inflammaging

Aging is accompanied by a low-grade inflammation and a higher susceptibility to an exacerbated inflammatory response (inflammaging) (Franceschi et al., 2000; Franceschi & Campisi, 2014; Kennedy et al., 2014)). *Cnr2* expression increases in many diseases and acute inflammatory states, but also during aging, which might be due to an increased inflammatory status (Komorowska-Müller & Schmöle, 2021; A.-C. Schmöle et al., 2018). Since CB_2R plays a role in switching microglia activity from pro- to an anti-inflammatory, we anticipated that in the context of inflammaging, CB_2R deletion would have negative consequences. We speculated that the deletion would increase ongoing inflammatory processes and thus enhance age-related cognitive decline (Gorelick, 2010). On the contrary, we observed that in old mice CB_2R deletion did not cause any major changes in cognition, but even slightly restored social memory deficits.

The work on how CB_2 deletion influences microglia activity in the context of aging was conducted by Tanushka Rana as a part of her master thesis work “The Role of the CB_2 Receptor in Inflammation Accompanying Aging (Inflammaging)” (2021; inhouse data). This study investigated age-related changes in microglia from $CB_2R^{-/-}$ mice used in our behavioural experiments. Microglia from young $CB_2R^{-/-}$ mice had a slightly increased surface, tree-length, number of branches and ramification index, while their soma size and polarity index were decreased. These morphological changes became less pronounced with aging and were mostly lost in the old mice. These morphological changes were consistent with a less reactive state of the microglia from the young $CB_2R^{-/-}$ mice and a following age-related compensation. An attenuated reactive state of young $CB_2R^{-/-}$ microglia is in agreement with previous findings showing a dampened immune response to a pro-inflammatory stimulus (A. C. Schmöle,

Lundt, Ternes, et al., 2015). Taken together, our findings further indicate an important role that the CB_2R plays not only in the regulation of activated states, but in activation itself. This in turn would mean that $CB_2R^{-/-}$ microglia from young mice have an impaired immune function.

Furthermore, in old mice a subtle decrease in an average branch length as well as increase in whole-cell Iba1 levels and CD68 level was detected. CD68 levels correlated with changes in social memory with slightly lower levels in young and adult $CB_2R^{-/-}$ mice and slightly higher in old $CB_2R^{-/-}$ mice. Thus, it is possible that changes in microglia phagocytic capabilities were reflected in the memory improvement. In support of that, CB_2R deletion reduced inflammation, neuronal loss, plaque-load and decreased cognitive decline in AD Aβ-pathology model (A.-C. Schmöle et al., 2018; A. C. Schmöle, Lundt, Ternes, et al., 2015). Although the underlying molecular mechanisms remain elusive.

8.1.5. CB_2R deletion does not alter basic behaviours

Consistent with the literature we found that 6 and 12-month old $CB_2R^{-/-}$ mice were heavier than their age-matched controls (Agudo et al., 2010; Schmitz et al., 2016). However, we did not detect any major impact of their increased weight on their overall locomotion or home-cage activity.

Moreover, lack of CB_2R decreased nest-building ability in 3-month old male mice already at baseline which might point to a higher stress-sensitivity of $CB_2R^{-/-}$ mice, similarly as $CB_1R^{-/-}$ mice (Beins et al., 2021). However, we neither detected any similar changes in 6-month old male or in female mice, nor in 18-month old male mice. Young $CB_2R^{-/-}$ mice also did not display any anxiety- or stress-like behaviours during other investigations suggesting that a decreased nest building might be a result of a fine motor deficit. In support of this, young $CB_2R^{-/-}$ mice took more time during a marble burring test (inhouse data). Therefore, possible motor deficits after CB_2R should be further investigated.

Interestingly, lack of the CB_2R increased water consumption exclusively in female mice, while food intake remained unaltered. It has been shown before that oestrogens regulates fluid intake (Santollo & Daniels, 2015). In grouped-housed male mice, CB_2R deletion increased alcohol consumption, while CB_1R activation promoted water intake (Pradier et al., 2015; Z. Zhao et al., 2019). Hence, our results highlight a possible role of the ECS and its interaction with sex hormones in the water balance.

8.1.6. CB_2R deletion alters synaptic architecture primarily in female mice

Despite initial contradicting results regarding the CB_2R presence in the brain, recent reports indicate its important role in the modulation of neuronal functions. For instance, acute activation of CB_2R decreased neuronal firing frequency and reduced the excitability of neurons, while chronic activation leads to increased neuronal excitability (den Boon et al., 2012; Stempel et al., 2016).

On a cellular level, CB_2R deletion leads to a decreased excitatory transmission and decreased dendritic spine numbers in the hippocampus (García-Gutiérrez et al., 2013; Yong Li & Kim, 2016b). To further investigate synaptic changes in the hippocampus after CB_2R deletion, we stained for a general presynaptic marker – synapsin-I and observed an increase in synapsin-I levels exclusively in $CB_2R^{-/-}$ female mice. The change in synapsin-I intensity was accompanied by an increase in synapsin-I average puncta size in both CA2 and CA3 area of the hippocampus. It is possible that an increase in the presynaptic vesicle pool is a compensatory mechanism to counter-act the decreased number of dendritic spines. On the other hand, synapsins have been shown to boost synaptic release at high firing rates by recruiting more vesicles from the reserve vesicle pool at excitatory synapses (Gitler et al., 2004). Whether the observed increase comes from an increase in overall vesicle number or an alteration in synaptic facilitation should be addressed in the future. In addition, loss of synapsin-I decreases baseline transmission at inhibitory synapses (Gitler et al., 2004). In agreement with that, decreasing synapsin-I expression also decreases the pool of readily releasable synaptic vesicles and alters short-term synaptic plasticity, while not affecting memory or long-term potentiation in young mice (Baldelli et al., 2007; Corradi et al., 2008; Kushner et al., 2005; Rosahl et al., 1993). Thus, an increase in synapsin-I could explain the improved working memory in $CB_2R^{-/-}$ mice (Yong Li & Kim, 2016a).

Alterations in synapsins are known to affect both excitatory and inhibitory synapses, although in a different capacity. Furthermore, *Cnr2* has been detected on both excitatory and inhibitory cells (Y. Li & Kim, 2015). Following the discovery of increased synapsin-I levels in females, we asked if the increase in presynaptic vesicle staining was due to alterations in glutamatergic or GABAergic synapses. Both vGLUT1 and vGAT intensities were enhanced in $CB_2R^{-/}$ female mice, suggesting that both excitatory and inhibitory synapses are regulated by CB_2R. Although, we observed a stronger effect for inhibitory synapses. It is known that even subtle alterations in perisomatic inhibitory synapses go along with perturbations in gamma

oscillations (Hammer et al., 2015). Thus, our findings might explain the observed CB_2R-dependent alterations of gamma oscillations (Stempel et al., 2016). However, we do see changes in both excitatory and inhibitory synapses and those changes seem to be prominent in all hippocampal layers and most hippocampal regions. Therefore, it is likely that these marker proteins are not directly regulated by CB_2 activity but rather reflect an overall change in the synaptic landscape of the hippocampus. Furthermore, our data indicate that CB_2 modulates hippocampal networks differently in males and females.

In light of these gender-specific phenotypes, it is important to note that most of the previous studies performed on CB_2R knockouts were done using gender-mixed groups (Bouchard et al., 2012; Koppel et al., 2013; Yong Li & Kim, 2016a, 2017; A. C. Schmöle, Lundt, Ternes, et al., 2015) or exclusively with male mice (Aso et al., 2016; García-Gutiérrez et al., 2013; La Porta et al., 2013; Yong Li & Kim, 2016b; Navarrete et al., 2013; Ortega-Alvaro et al., 2011). It is therefore possible that gender-specific phenotypes have been overlooked and that the relevance for CB_2R-dependent processes in the central nervous system have been underestimated. Why females have a stronger CB_2R knockout phenotype remain unclear, but these gender differences may be related to differential CB_2R expression levels. It has been already shown that *Cnr2* expression in the hippocampus, prefrontal cortex and hypothalamus is higher in female than in male mice (Xing et al., 2014).

Taken together our findings not only confirm that, despite its low expression levels, CB_2R plays a role in synaptic architecture, but also add to the growing evidence of important gender-specific differences in endocannabinoid signaling (Wagner, 2016).

9. Bibliography

Agudo, J., Martin, M., Roca, C., Molas, M., Bura, A. S., Zimmer, A., Bosch, F., & Maldonado, R. (2010). Deficiency of CB2 cannabinoid receptor in mice improves insulin sensitivity but increases food intake and obesity with age. *Diabetologia*, *53*(12), 2629–2640. https://doi.org/10.1007/s00125-010-1894-6

Akiyoshi, R., Wake, H., Kato, D., Horiuchi, H., Ono, R., Ikegami, A., Haruwaka, K., Omori, T., Tachibana, Y., Moorhouse, A. J., & Nabekura, J. (2018). Microglia enhance synapse activity to promote local network synchronization. *ENeuro*, *5*(5), 1–13. https://doi.org/10.1523/ENEURO.0088-18.2018

Albayram, O., Alferink, J., Pitsch, J., Piyanova, A., Neitzert, K., Poppensieker, K., Mauer, D., Michel, K., Legler, A., Becker, A., Monory, K., Lutz, B., Zimmer, A., & Bilkei-Gorzo, A. (2011). Role of CB1 cannabinoid receptors on GABAergic neurons in brain aging. *Proceedings of the National Academy of Sciences of the United States of America*, *108*(27), 11256–11261. https://doi.org/10.1073/pnas.1016442108

Albayram, O., Bilkei-gorzo, A., & Zimmer, A. (2012). *Loss of CB1 receptors leads to differential age-related changes in reward-driven learning and memory*. *4*(December), 1–8. https://doi.org/10.3389/fnagi.2012.00034

Ameri, A. (1999). The effect of cannabinoid on the brain. *Progress in Neurobiology*, *58*, 315=348. https://doi.org/10.1080/19386362.2016.1257415

Andó, R. D., Bíró, J., Csölle, C., Ledent, C., & Sperlágh, B. (2012). The inhibitory action of exo- and endocannabinoids on [3H]GABA release are mediated by both CB 1 and CB 2 receptors in the mouse hippocampus. *Neurochemistry International*, *60*(2), 145–152. https://doi.org/10.1016/j.neuint.2011.11.012

Aso, E., Andrés-Benito, P., Carmona, M., Maldonado, R., & Ferrer, I. (2016). Cannabinoid receptor 2 participates in amyloid-β processing in a mouse model of Alzheimer's disease but plays a minor role in the therapeutic properties of a cannabis-based medicine. *Journal of Alzheimer's Disease*, *51*(2), 489–500. https://doi.org/10.3233/JAD-150913

Aso, E., Juvés, S., Maldonado, R., & Ferrer, I. (2013). CB2 cannabinoid receptor agonist ameliorates alzheimer-like phenotype in AβPP/PS1 mice. *Journal of Alzheimer's Disease*, *35*(4), 847–858. https://doi.org/10.3233/JAD-130137

Aso, E., Sánchez-Pla, A., Vegas-Lozano, E., Maldonado, R., & Ferrer, I. (2015). Cannabis-based medicine reduces multiple pathological processes in AβPP/PS1 mice. *Journal of*

Alzheimer's Disease, *43*(3), 977–991. https://doi.org/10.3233/JAD-141014

Ativie, F., Komorowska, J. A., Beins, E., Albayram, Ö., Zimmer, T., Zimmer, A., Tejera, D., Heneka, M., & Bilkei-Gorzo, A. (2018). Cannabinoid 1 Receptor Signaling on Hippocampal GABAergic Neurons Influences Microglial Activity. *Frontiers in Molecular Neuroscience*, *11*. https://doi.org/10.3389/fnmol.2018.00295

Attardo, A., Fitzgerald, J. E., & Schnitzer, M. J. (2015). Impermanence of dendritic spines in live adult CA1 hippocampus. *Nature*, *523*(7562), 592–596. https://doi.org/10.1038/nature14467

Atwood, B. K., & MacKie, K. (2010). CB 2: A cannabinoid receptor with an identity crisis. *British Journal of Pharmacology*, *160*(3), 467–479. https://doi.org/10.1111/j.1476-5381.2010.00729.x

Baek, J. H., Darlington, C. L., Smith, P. F., & Ashton, J. C. (2013). Antibody testing for brain immunohistochemistry: Brain immunolabeling for the cannabinoid CB2 receptor. *Journal of Neuroscience Methods*, *216*(2), 87–95. https://doi.org/10.1016/j.jneumeth.2013.03.021

Baldelli, P., Fassio, A., Valtorta, F., & Benfenati, F. (2007). Lack of synapsin I reduces the readily releasable pool of synaptic vesicles at central inhibitory synapses. *Journal of Neuroscience*, *27*(49), 13520–13531. https://doi.org/10.1523/JNEUROSCI.3151-07.2007

Banks, W. A., Reed, M. J., Logsdon, A. F., Rhea, E. M., & Erickson, M. A. (2021). Healthy aging and the blood–brain barrier. *Nature Aging*, *1*(March). https://doi.org/10.1038/s43587-021-00043-5

Becker, N., Wierenga, C. J., Fonseca, R., Bonhoeffer, T., & Na, U. V. (2008). LTD Induction Causes Morphological Changes of Presynaptic Boutons and Reduces Their Contacts with Spines. *Neuron*, *60*, 590–597. https://doi.org/10.1016/j.neuron.2008.09.018

Befort, K. (2015). Interactions of the opioid and cannabinoid systems in reward: Insights from knockout studies. *Frontiers in Pharmacology*, *6*(FEB), 1–15. https://doi.org/10.3389/fphar.2015.00006

Beins, E. C., Beiert, T., Jenniches, I., Hansen, J. N., & Zimmer, A. (2021). Cannabinoid receptor 1 signalling modulates stress susceptibility and microglial responses to chronic social defeat stress. *Translational Psychiatry*. https://doi.org/10.1038/s41398-021-01283-0

Benes, F. M., Kwok, E. W., Vincent, S. L., & Todtenkopf, M. S. (1998). A reduction of

nonpyramidal cells in sector CA2 of schizophrenics and manic depressives. *Biological Psychiatry*, *44*(2), 88–97. https://doi.org/10.1016/S0006-3223(98)00138-3

Benito, C., Núñez, E., Tolón, R. M., Carrier, E. J., Rábano, A., Hillard, C. J., & Romero, J. (2003). Cannabinoid CB2 receptors and fatty acid amide hydrolase are selectively overexpressed in neuritic plaque-associated glia in Alzheimer's disease brains. *The Journal of Neuroscience*, *23*(35), 11136–11141. https://doi.org/23/35/11136 [pii]

Bessis, A., Béchade, C., Bernard, D., & Roumier, A. (2007). Microglial control of neuronal death and synaptic properties. *Glia*, *55*(3), 233–238. https://doi.org/10.1002/glia.20459

Bijata, M., Labus, J., Guseva, D., Stawarski, M., Butzlaff, M., Dzwonek, J., Schneeberg, J., Böhm, K., Michaluk, P., Rusakov, D. A., Dityatev, A., Wilczyński, G., Wlodarczyk, J., & Ponimaskin, E. (2017). Synaptic Remodeling Depends on Signaling between Serotonin Receptors and the Extracellular Matrix. *Cell Reports*, *19*(9), 1767–1782. https://doi.org/10.1016/j.celrep.2017.05.023

Bilkei-Gorzo, A., Racz, I., Valverde, O., Otto, M., Michel, K., Sarstre, M., & Zimmer, A. (2005). Early age-related cognitive impairment in mice lacking cannabinoid CB1 receptors. *Proceedings of the National Academy of Sciences*, *102*(43), 15670–15675. https://doi.org/10.1073/pnas.0504640102

Bilkei-Gorzo, Andras, Albayram, O., Draffehn, A., Michel, K., Piyanova, A., Oppenheimer, H., Dvir-ginzberg, M., Rácz, I., Ulas, T., Imbeault, S., Bab, I., Schultze, J. L., & Zimmer, A. (2017). A chronic low dose of Δ 9 -tetrahydrocannabinol (THC) restores cognitive function in old mice. *Nature Publishing Group*, *23*(6), 782–787. https://doi.org/10.1038/nm.4311

Bilkei-Gorzo, Andras, Drews, E., Albayram, Ö., Piyanova, A., Gaffal, E., Tueting, T., Michel, K., Mauer, D., Maier, W., & Zimmer, A. (2012). Early onset of aging-like changes is restricted to cognitive abilities and skin structure in Cnr1-/- mice. *Neurobiology of Aging*, *33*(1), 200.e11-200.e22. https://doi.org/10.1016/j.neurobiolaging.2010.07.009

Blinzinger, K., & Kreutzberg, G. (1968). Displacement of synaptic terminals from regenerating motoneurons by microglial cells. *Zeitschrift Für Zellforschung Und Mikroskopische Anatomie*, *85*(2), 145–157. https://doi.org/10.1007/BF00325030

Bonilla-Quintana, M., Wörgötter, F., Tetzlaff, C., & Fauth, M. (2020). Modeling the Shape of Synaptic Spines by Their Actin Dynamics. *Frontiers in Synaptic Neuroscience*, *12*(March). https://doi.org/10.3389/fnsyn.2020.00009

Boros, B. D., Greathouse, K. M., Gearing, M., & Herskowitz, J. H. (2019). Dendritic spine remodeling accompanies Alzheimer's disease pathology and genetic susceptibility in cognitively normal aging. *Neurobiology of Aging*, *73*, 92–103. https://doi.org/10.1016/j.neurobiolaging.2018.09.003.Dendritic

Boros, B. D., Greathouse, K. M., Gentry, E. G., Kendall, A., Birchall, E. L., Gearing, M., & Herskowitz, J. H. (2017). Dendritic spines provide cognitive resilience against Alzheimer's disease. *Annals of Neurology*, *82*(4), 602–614. https://doi.org/10.1002/ana.25049.Dendritic

Bosch, M., Castro, J., Saneyoshi, T., Matsuno, H., Sur, M., & Hayashi, Y. (2014). Article Structural and Molecular Remodeling of Dendritic Spine Substructures during Long-Term Potentiation. *Neuron*, *82*(2), 444–459. https://doi.org/10.1016/j.neuron.2014.03.021

Bouchard, J., Truong, J., Bouchard, K., Dunkelberger, D., Desrayaud, S., Moussaoui, S., Tabrizi, S. J., Stella, N., & Muchowski, P. J. (2012). Cannabinoid Receptor 2 Signaling in Peripheral Immune Cells Modulates Disease Onset and Severity in Mouse Models of Huntington's Disease. *Journal of Neuroscience*. https://doi.org/10.1523/jneurosci.4008-12.2012

Brown, A. J. (2007). Novel cannabinoid receptors. *British Journal of Pharmacology*, *152*(5), 567–575. https://doi.org/10.1038/sj.bjp.0707481

Brown, S. P., Brenowitz, S. D., & Regehr, W. G. (2003). Brief presynaptic bursts evoke synapse-specific retrograde inhibition mediated by endogenous cannabinoids. *Nature Neuroscience*, *6*(10), 1048–1057. https://doi.org/10.1038/nn1126

Brusco, A., Tagliaferro, P. A., Saez, T., & Onaivi, E. S. (2008). Ultrastructural localization of neuronal brain CB2 cannabinoid receptors. *Annals of the New York Academy of Sciences*, *1139*, 450–457. https://doi.org/10.1196/annals.1432.037

Buckley, N. E., McCoy, K. L., Mezey, É., Bonner, T., Zimmer, A., Felder, C. C., Glass, M., & Zimmer, A. (2000). Immunomodulation by cannabinoids is absent in mice deficient for the cannabinoid CB2 receptor. *European Journal of Pharmacology*, *396*(2–3), 141–149. https://doi.org/10.1016/S0014-2999(00)00211-9

Burns, J. C., Cotleur, B., Walther, D. M., Bajrami, B., Rubino, S. J., Wei, R., Franchimont, N., Cotman, S. L., Ransohoff, R. M., & Mingueneau, M. (2020). Differential accumulation of storage bodies with aging defines discrete subsets of microglia in the healthy brain. *ELife*, *9*, 1–71. https://doi.org/10.7554/eLife.57495

Caceres, A., Payne, M. R., Binder, L. I., & Steward, O. (1983). Immunocytochemical localization of actin and microtubule-associated protein MAP2 in dendritic spines. *Proceedings of the National Academy of Sciences of the United States of America*, *80*(6 I), 1738–1742. https://doi.org/10.1073/pnas.80.6.1738

Campisi, J. (2005). Senescent cells, tumor suppression, and organismal aging: Good citizens, bad neighbors. *Cell*, *120*(4), 513–522. https://doi.org/10.1016/j.cell.2005.02.003

Campisi, J., & D'Adda Di Fagagna, F. (2007). Cellular senescence: When bad things happen to good cells. *Nature Reviews Molecular Cell Biology*, *8*(9), 729–740. https://doi.org/10.1038/nrm2233

Cane, M., Maco, B., Knott, G., & Holtmaat, A. (2014). The relationship between PSD-95 clustering and spine stability In Vivo. *Journal of Neuroscience*, *34*(6), 2075–2086. https://doi.org/10.1523/JNEUROSCI.3353-13.2014

Cangalaya, C., Stoyanov, S., Fischer, K. D., & Dityatev, A. (2020). Light-induced engagement of microglia to focally remodel synapses in the adult brain. *ELife*, *9*, 1–16. https://doi.org/10.7554/ELIFE.58435

Cao, C., Li, Y., Liu, H., Bai, G., Mayl, J., Lin, X., Sutherland, K., Nabar, N., & Cai, J. (2014). The potential therapeutic effects of THC on Alzheimer's disease. *Journal of Alzheimer's Disease*, *42*(3), 973–984. https://doi.org/10.3233/JAD-140093

Cardona, A. E., Pioro, E. P., Sasse, M. E., Kostenko, V., Cardona, S. M., Dijkstra, I. M., Huang, D. R., Kidd, G., Dombrowski, S., Dutta, R., Lee, J. C., Cook, D. N., Jung, S., Lira, S. A., Littman, D. R., & Ransohoff, R. M. (2006). Control of microglial neurotoxicity by the fractalkine receptor. *Nature Neuroscience*, *9*(7), 917–924. https://doi.org/10.1038/nn1715

Carlisle, S. J., Marciano-Cabral, F., Staab, A., Ludwick, C., & Cabral, G. A. (2002). Differential expression of the CB2 cannabinoid receptor by rodent macrophages and macrophage-like cells in relation to cell activation. *International Immunopharmacology*, *2*(1), 69–82. https://doi.org/10.1016/S1567-5769(01)00147-3

Castillo, P. E., Younts, T. J., Chavez, A. E., & Hashimotodani, Y. (2012). Endocannabinoid signaling and synaptic function. *Neuron*, *76*(1), 70–81. https://doi.org/10.1016/j.neuron.2012.09.020.Endocannabinoid

Chan, G. C. K., Hinds, T. R., Impey, S., & Storm, D. R. (1998). Hippocampal neurotoxicity of Δ9-tetrahydrocannabinol. *Journal of Neuroscience*, *18*(14), 5322–5332.

https://doi.org/10.1523/jneurosci.18-14-05322.1998

Chavarría, A., & Cárdenas, G. (2013). Neuronal influence behind the central nervous system regulation of the immune cells. *Frontiers in Integrative Neuroscience*, *7*(SEP), 1–6. https://doi.org/10.3389/fnint.2013.00064

Chen, J. L., Villa, K. L., Cha, J. W., So, P. T. C., Kubota, Y., & Nedivi, E. (2012). Clustered Dynamics of Inhibitory Synapses and Dendritic Spines in the Adult Neocortex. *Neuron*, *74*(2), 361–373. https://doi.org/10.1016/j.neuron.2012.02.030

Chen, Y., Dubé, C. M., Rice, C. J., & Baram, T. Z. (2008). Rapid loss of dendritic spines after stress involves derangement of spine dynamics by corticotropin-releasing hormone. *Journal of Neuroscience*, *28*(11), 2903–2911. https://doi.org/10.1523/JNEUROSCI.0225-08.2008

Chen, Z., Jalabi, W., Hu, W., Park, H. J., Gale, J. T., Kidd, G. J., Bernatowicz, R., Gossman, Z. C., Chen, J. T., Dutta, R., & Trapp, B. D. (2014). Microglial displacement of inhibitory synapses provides neuroprotection in the adult brain. *Nature Communications*, *5*(July). https://doi.org/10.1038/ncomms5486

Chevaleyre, V., Heifets, B. D., Kaeser, P. S., Südhof, T. C., & Castillo, P. E. (2007). Endocannabinoid-mediated long-term plasticity requires cAMP/PKA signaling and RIM1alpha. *Neuron*, *54*(5), 801–812. https://www.ncbi.nlm.nih.gov/pmc/articles/PMC3624763/pdf/nihms412728.pdf

Chevaleyre, V., & Piskorowski, R. A. (2016). Hippocampal Area CA2: An Overlooked but Promising Therapeutic Target. *Trends in Molecular Medicine*, *22*(8), 645–655. https://doi.org/10.1016/j.molmed.2016.06.007

Chevaleyre, V., Takahashi, K. A., & Castillo, P. E. (2006). Endocannabinoid-mediated synaptic plasticity in the CNS. *Annual Review of Neuroscience*, *29*, 37–76. https://doi.org/10.1146/annurev.neuro.29.051605.112834

Childs, E., Lutz, J. A., & de Wit, H. (2017). Dose-related effects of delta-9-THC on emotional responses to acute psychosocial stress. *Drug Alcohol Dependence*, *177*, 136–144. https://doi.org/10.1016/j.drugalcdep.2017.03.030.Dose-related

Choudhury, M. E., Miyanishi, K., Takeda, H., Islam, A., Matsuoka, N., Kubo, M., Matsumoto, S., Kunieda, T., Nomoto, M., Yano, H., & Tanaka, J. (2020). Phagocytic elimination of synapses by microglia during sleep. *Glia*, *68*(1), 44–59. https://doi.org/10.1002/glia.23698

Chu, Y., Jin, X., Parada, I., Pesic, A., Stevens, B., Barres, B., & Prince, D. A. (2010). Enhanced synaptic connectivity and epilepsy in C1q knockout mice. *Proceedings of the National Academy of Sciences of the United States of America*, *107*(17), 7975–7980. https://doi.org/10.1073/pnas.0913449107

Colizzi, M., & Bhattacharyya, S. (2018). Cannabis use and the development of tolerance: a systematic review of human evidence. *Neuroscience and Biobehavioral Reviews*, *93*(April), 1–25. https://doi.org/10.1016/j.neubiorev.2018.07.014

Collado, M., Blasco, M. A., & Serrano, M. (2007). Cellular Senescence in Cancer and Aging. *Cell*, *130*(2), 223–233. https://doi.org/10.1016/j.cell.2007.07.003

Corradi, A., Zanardi, A., Giacomini, C., Onofri, F., Valtorta, F., Zoli, M., & Benfenati, F. (2008). Synapsin-I- and synapsin-II-null mice display an increased age-dependent cognitive impairment. *Journal of Cell Science*, *121*(18), 3042–3051. https://doi.org/10.1242/jcs.035063

Costa, B., Parolaro, D., & Colleoni, M. (1996). Chronic cannabinoid, CP-55,940, administration alters biotransformation in the rat. *European Journal of Pharmacology*, *313*(1–2), 17–24. https://doi.org/10.1016/0014-2999(96)00499-2

Crotti, A., & Ransohoff, R. M. (2016). Microglial Physiology and Pathophysiology: Insights from Genome-wide Transcriptional Profiling. *Immunity*, *44*(3), 505–515. https://doi.org/10.1016/j.immuni.2016.02.013

Cunningham, C., Wilcockson, D. C., Campion, S., Lunnon, K., & Perry, V. H. (2005). Central and systemic endotoxin challenges exacerbate the local inflammatory response and increase neuronal death during chronic neurodegeneration. *Journal of Neuroscience*, *25*(40), 9275–9284. https://doi.org/10.1523/JNEUROSCI.2614-05.2005

D'Souza, D. C., Cortes-Briones, J. A., Ranganathan, M., Thurnauer, H., Creatura, G., Surti, T., Planeta, B., Neumeister, A., Pittman, B., Normandin, M. D., Kapinos, M., Ropchan, J., Huang, Y., Carson, R. E., & Skosnik, P. D. (2016). Rapid Changes in Cannabinoid 1 Receptor Availability in Cannabis-Dependent Male Subjects after Abstinence from Cannabis. *Biological Psychiatry: Cognitive Neuroscience and Neuroimaging*, *1*(1), 60–67. https://doi.org/10.1016/j.bpsc.2015.09.008

D'Souza, D. C., Ranganathan, M., Braley, G., Gueorguieva, R., Zimolo, Z., Cooper, T., Perry, E., & Krystal, J. (2008). Blunted psychotomimetic and amnestic effects of Δ-9-tetrahydrocannabinol in frequent users of cannabis. *Neuropsychopharmacology*,

33(10), 2505–2516. https://doi.org/10.1038/sj.npp.1301643

Dailey, M. E., & Smith, S. J. (1996). The dynamics of dendritic structure in developing hippocampal slices. *Journal of Neuroscience*, *16*(9), 2983–2994. https://doi.org/10.1523/jneurosci.16-09-02983.1996

Davidson, A. M., Mejiá-Gómez, H., Jacobowitz, M., & Mostany, R. (2020). Dendritic Spine Density and Dynamics of Layer 5 Pyramidal Neurons of the Primary Motor Cortex Are Elevated with Aging. *Cerebral Cortex*, *30*(2), 767–777. https://doi.org/10.1093/cercor/bhz124

De Fonseca, F. R., Gorriti, M. A., Fernández-Ruiz, J. J., Palomo, T., & Ramos, J. A. (1994). Downregulation of rat brain cannabinoid binding sites after chronic Δ9-tetrahydrocannabinol treatment. *Pharmacology, Biochemistry and Behavior*, *47*(1), 33–40. https://doi.org/10.1016/0091-3057(94)90108-2

Deacon, R. M. J. (2006). Assessing nest building in mice. *Nature Protocols*, *1*(3), 1117–1119. https://doi.org/10.1038/nprot.2006.170

Deeks, S. G. (2011). HIV infection, inflammation, immunosenescence, and aging. *Annual Review of Medicine*, *62*(5), 141–155. https://doi.org/10.1146/annurev-med-042909-093756

DeKosky, S. T., & Scheff, S. W. (1990). Synapse loss in frontal cortex biopsies in Alzheimer's disease: Correlation with cognitive severity. *Annals of Neurology*, *27*(5), 457–464. https://doi.org/10.1002/ana.410270502

Deleidi, M., Jäggle, M., & Rubino, G. (2015). Immune ageing, dysmetabolism and inflammation in neurological diseases. *Frontiers in Neuroscience*, *9*(APR), 1–14. https://doi.org/10.3389/fnins.2015.00172

den Boon, F. S., Chameau, P., Schaafsma-Zhao, Q., van Aken, W., Bari, M., Oddi, S., Kruse, C. G., Maccarrone, M., Wadman, W. J., & Werkman, T. R. (2012). Excitability of prefrontal cortical pyramidal neurons is modulated by activation of intracellular type-2 cannabinoid receptors. *Proceedings of the National Academy of Sciences*, *109*(9), 3534–3539. https://doi.org/10.1073/pnas.1118167109

Denk, W., Strickler, J. H., & Webb, W. W. (1990). Two-Photon Laser Scanning Fluorescence Microscopy. *Science*, *24*(8), 73–76.

Dent, E. W. (2017). Of microtubules and memory: Implications for microtubule dynamics in dendrites and spines. *Molecular Biology of the Cell*, *28*(1), 1–8.

https://doi.org/10.1091/mbc.E15-11-0769

Devane, WA, Dysarz, F. 3rd, Johnson, M., Melvin, L., & AC, H. (1988). Determination and Characterization of a Cannabinoid Receptor in Rat Brain. *Mol Pharmacol.*, *34*(5), 605–613.

Devane, William, Hanus, L., Breuer, A., Pertwee, R., Stevenson, L., Griffin, G., Gibson, D., Mandelbaum, A., Etinger, A., & Mechoulam, R. (1992). Isolation and structure of a brain constituent that binds to the cannabinoid receptor. *Science*, *258*, 1946–1949. https://doi.org/10.1039/CT9120102209

Dickstein, D. L., Kabaso, D., Rocher, A. B., Luebke, J. I., Wearne, S. L., & Hof, P. R. (2007). Changes in the structural complexity of the aged brain. *Aging Cell*, *6*(3), 275–284. https://doi.org/10.1111/j.1474-9726.2007.00289.x

DiPatre, L. P., & Gelman, B. (1997). Microglia Cell Activation in Aging and Alzheimers Disease: Partial Linkage with Neurofibrillary Tangle Burden in the Hippocampus. *Journal of Neuropathology and Experimental Neurology*, *56*(2), 143–149.

Dragt, S., Nieman, D. H., Becker, H. E., Van De Fliert, R., Dingemans, P. M., De Haan, L., Van Amelsvoort, T. A., & Linszen, D. H. (2010). Age of onset of cannabis use is associated with age of onset of high-risk symptoms for psychosis. *Canadian Journal of Psychiatry*, *55*(3), 165–171. https://doi.org/10.1177/070674371005500308

Du, J. J., Liu, Z. Q., Yan, Y., Xiong, J., Jia, X. T., Di, Z. L., & Ren, J. J. (2020). The Cannabinoid WIN 55,212-2 Reduces Delayed Neurologic Sequelae After Carbon Monoxide Poisoning by Promoting Microglial M2 Polarization Through ST2 Signaling. *Journal of Molecular Neuroscience*, *70*(3), 422–432. https://doi.org/10.1007/s12031-019-01429-2

Dumitriu, D., Hao, J., Hara, Y., Kaufmann, J., Janssen, W. G. M., Lou, W., Rapp, P. R., & Morrison, J. H. (2010). Selective Changes in Thin Spine Density and Morphology in Monkey Prefrontal Cortex Correlate with Aging-Related Cognitive Impairment. *The Journal of Neuroscience*, *30*(22), 7507–7515. https://doi.org/10.1523/JNEUROSCI.6410-09.2010

Dvorkin, R., & Ziv, N. E. (2016). Relative Contributions of Specific Activity Histories and Spontaneous Processes to Size Remodeling of Glutamatergic Synapses. *PLoS Biology*, *14*(10), 1–33. https://doi.org/10.1371/journal.pbio.1002572

Eggan, S. M., & Lewis, D. A. (2007). Immunocytochemical distribution of the cannabinoid CB1 receptor in the primate neocortex: A regional and laminar analysis. *Cerebral Cortex*,

17(1), 175–191. https://doi.org/10.1093/cercor/bhj136

Ekdahl, C. T. (2012). Microglial activation-tuning and pruning adult neurogenesis. *Frontiers in Pharmacology*, *3 MAR*(March), 1–9. https://doi.org/10.3389/fphar.2012.00041

Elston, G. N., & DeFelipe, J. (2002). Spine distribution in cortical pyramidal cells: A common organizational principle across species. *Progress in Brain Research*, *136*(1970), 109–133. https://doi.org/10.1016/S0079-6123(02)36012-6

Eyo, U. B., & Wu, L. J. (2013). Bidirectional microglia-neuron communication in the healthy brain. *Neural Plasticity*, *2013*. https://doi.org/10.1155/2013/456857

Feliszek, M., Bindila, L., Lutz, B., Zimmer, A., Bilkei-Gorzo, A., & Schlicker, E. (2016). Lack of hippocampal CB1 receptor desensitization by Δ9-tetrahydrocannabinol in aged mice and by low doses of JZL 184. *Naunyn-Schmiedeberg's Archives of Pharmacology*, *389*(6), 603–612. https://doi.org/10.1007/s00210-016-1226-6

Feng, G., Mellor, R. H., Bernstein, M., Keller-Peck, C., Nguyen, Q. T., Wallace, M., Nerbonne, J. M., Lichtman, J. W., & Sanes, J. R. (2000). Neurotechnique Imaging Neuronal Subsets in Transgenic Mice Expressing Multiple Spectral Variants of GFP variants with altered spectral properties and improved translational efficiency, thermostability, and quantum yield. As a result of these favorable pro. *Neuron*, *28*, 41–51.

Fernandez-Cabrera, M., Higuera-matas, A., Fernaud-espinosa, I., Defelipe, J., Ambrosio, E., & Migue, M. (2018). Selective effects of Δ 9 -tetrahydrocannabinol on medium spiny neurons in the striatum. *PLoS ONE*, *13*(7), 1–20.

Flanary, B. E., & Streit, W. J. (2004). Progressive Telomere Shortening Occurs in Cultured Rat Microglia, but Not Astrocytes. *Glia*, *45*(1), 75–88. https://doi.org/10.1002/glia.10301

Franceschi, C., Bonafè, M., Valensin, S., Olivieri, F., De Luca, M., Ottaviani, E., & De Benedictis, G. (2000). Inflamm-aging. An evolutionary perspective on immunosenescence. *Annals of the New York Academy of Sciences*, *908*, 244–254. https://doi.org/10.1111/j.1749-6632.2000.tb06651.x

Franceschi, C., & Campisi, J. (2014). Chronic inflammation (Inflammaging) and its potential contribution to age-associated diseases. *Journals of Gerontology - Series A Biological Sciences and Medical Sciences*, *69*, S4–S9. https://doi.org/10.1093/gerona/glu057

Freire, M. (1978). Effects of dark rearing on dendritic spines in layer IV of the mouse visual cortex. A quantitative electron microscopical study. *Journal of Anatomy*, *126*(Pt 1), 193–201.

http://www.ncbi.nlm.nih.gov/pubmed/649498%0Ahttp://www.pubmedcentral.nih.gov/articlerender.fcgi?artid=PMC1235723

Fuhrmann, M., Bittner, T., Jung, C. K. E., Burgold, S., Page, R. M., Mitteregger, G., Haass, C., LaFerla, F. M., Kretzschmar, H., & Herms, J. (2010). Microglial Cx3cr1 knockout prevents neuron loss in a mouse model of Alzheimer's disease. *Nature Neuroscience*, *13*(4), 411–413. https://doi.org/10.1038/nn.2511

Gabrielli, M., Battista, N., Riganti, L., Prada, I., Antonucci, F., Cantone, L., Lombardi, M., Matteoli, M., Maccarrone, M., & Verderio, C. (2015). Active endocannabinoids are secreted on the surface of microglial microvesicles. *EMBO Reports*, *4*(2), 1–32. https://doi.org/10.1186/2193-1801-4-S1-L29

Gao, S., Zhang, S., Zhou, H., Tao, X., Ni, Y., Pei, D., Kang, S., Yan, W., & Lu, J. (2021). Role of mTOR-Regulated Autophagy in Synaptic Plasticity Related Proteins Downregulation and the Reference Memory Deficits Induced by Anesthesia/Surgery in Aged Mice. *Frontiers in Aging Neuroscience*, *13*(April), 1–12. https://doi.org/10.3389/fnagi.2021.628541

Gaoni, Y., & Mechoulam, R. (1964). Isolation, Structure, and Partial Synthesis of an Active Constituent of Hashish. *Journal of the American Chemical Society*, *86*(8), 1646–1647. https://doi.org/10.1021/ja01062a046

García-Gutiérrez, M. S., & Manzanares, J. (2011). Overexpression of CB2 cannabinoid receptors decreased vulnerability to anxiety and impaired anxiolytic action of alprazolam in mice. *Journal of Psychopharmacology*, *25*(1), 111–120. https://doi.org/10.1177/0269881110379507

García-Gutiérrez, M. S., Ortega-Álvaro, A., Busquets-García, A., Pérez-Ortiz, J. M., Caltana, L., Ricatti, M. J., Brusco, A., Maldonado, R., & Manzanares, J. (2013). Synaptic plasticity alterations associated with memory impairment induced by deletion of CB2 cannabinoid receptors. *Neuropharmacology*, *73*, 388–396. https://doi.org/10.1016/j.neuropharm.2013.05.034

Gehrmann, J., Matsumoto, Y., & Kreutzberg, G. W. (1995). Microglia: Intrinsic immuneffector cell of the brain. *Brain Research Reviews*, *20*(3), 269–287. https://doi.org/10.1016/0165-0173(94)00015-H

Gemma, C., & Bachstetter, A. D. (2013). The role of microglia in adult hippocampal neurogenesis. *Frontiers in Cellular Neuroscience*, *7*(NOV), 1–5. https://doi.org/10.3389/fncel.2013.00229

Gems, D., & Partridge, L. (2013). Genetics of longevity in model organisms: Debates and paradigm shifts. *Annual Review of Physiology*, *75*(November), 621–644. https://doi.org/10.1146/annurev-physiol-030212-183712

Gil-Pagés, M., Stiles, R. J., Parks, C. A., Neier, S. C., Radulovic, M., Oliveros, A., Ferrer, A., Reed, B. K., Wilton, K. M., & Schrum, A. G. (2013). Slow angled-descent forepaw grasping (SLAG): An innate behavioral task for identification of individual experimental mice possessing functional vision. *Behavioral and Brain Functions*, *9*(1). https://doi.org/10.1186/1744-9081-9-35

Gitler, D., Takagishi, Y., Feng, J., Ren, Y., Rodriguiz, R. M., Wetsel, W. C., Greengard, P., & Augustine, G. J. (2004). Different presynaptic roles of synapsins at excitatory and inhibitory synapses. *Journal of Neuroscience*, *24*(50), 11368–11380. https://doi.org/10.1523/JNEUROSCI.3795-04.2004

Gorelick, P. B. (2010). Role of inflammation in cognitive impairment: Results of observational epidemiological studies and clinical trials. *Annals of the New York Academy of Sciences*, *1207*, 155–162. https://doi.org/10.1111/j.1749-6632.2010.05726.x

Grabert, K., Michoel, T., Karavolos, M. H., Clohisey, S., Kenneth Baillie, J., Stevens, M. P., Freeman, T. C., Summers, K. M., & McColl, B. W. (2016). Microglial brain region-dependent diversity and selective regional sensitivities to aging. *Nature Neuroscience*, *19*(3), 504–516. https://doi.org/10.1038/nn.4222

Gray, B. E. G. (1959). Axo-somatic and axo-dendritic synapses ofthe cerebral cortex: an electron microscope study. *Journal of Anatomy*, *93*(4), 420–433. https://doi.org/10.1016/B978-0-12-801426-4.05001-X

Grutzendler, J., Kasthuri, N., & Gan, W. B. (2002). Long-term dendritic spine stability in the adult cortex. *Nature*, *420*(6917), 812–816. https://doi.org/10.1038/nature01276

Gyoneva, S., Hosur, R., Gosselin, D., Zhang, B., Ouyang, Z., Cotleur, A. C., Peterson, M., Allaire, N., Challa, R., Cullen, P., Roberts, C., Miao, K., Reynolds, T. L., Glass, C. K., Burkly, L., & Ransohoff, R. M. (2019). Cx3cr1-deficient microglia exhibit a premature aging transcriptome. *Life Science Alliance*, *2*(6), 1–16. https://doi.org/10.26508/lsa.201900453

Hammer, M., Krueger-Burg, D., Tuffy, L. P., Cooper, B. H., Taschenberger, H., Goswami, S. P., Ehrenreich, H., Jonas, P., Varoqueaux, F., Rhee, J. S., & Brose, N. (2015). Perturbed Hippocampal Synaptic Inhibition and γ-Oscillations in a Neuroligin-4 Knockout Mouse

Model of Autism. *Cell Reports*, *13*(3), 516–523. https://doi.org/10.1016/j.celrep.2015.09.011

Harry, G. J., & Kraft, A. (2012). Microglia in the developing brain: a potential target with lifetime effects. *Neurotoxicology*, *33*(2), 191–206. https://doi.org/10.1016/j.neuro.2012.01.012.Microglia

Hart, A. D., Wyttenbach, A., Hugh Perry, V., & Teeling, J. L. (2012). Age related changes in microglial phenotype vary between CNS regions: Grey versus white matter differences. *Brain, Behavior, and Immunity*, *26*(5), 754–765. https://doi.org/10.1016/j.bbi.2011.11.006

Hayashi-takagi, A., Nakamura, M., Shirai, F., Wu, Y., Loshbaugh, A. L., Kuhlman, B., Hahn, K. M., Kasai, H., Hill, C., Hill, C., Carolina, N., Hill, C., Agency, T., & Agency, T. (2016). Labelling and optical erasure of synaptic memory traces in the motor cortex. *Nature*, *525*(7569), 333–338. https://doi.org/10.1038/nature15257.Labelling

Hayashi, Y., & Majewska, A. K. (2005). Dendritic spine geometry: Functional implication and regulation. *Neuron*, *46*(4), 529–532. https://doi.org/10.1016/j.neuron.2005.05.006

Heifets, B. D., & Castillo, P. E. (2009). Endocannabinoid signaling and long-term synaptic plasticity. *Annual Review of Physiology*, *71*, 283–306. https://doi.org/10.1146/annurev.physiol.010908.163149

Herkenham, M., Lynn, A. B., Little, M. D., Johnson, M. R., Melvin, L. S., De Costa, B. R., & Rice, K. C. (1990). Cannabinoid receptor localization in brain. *Proceedings of the National Academy of Sciences of the United States of America*, *87*(5), 1932–1936. https://doi.org/10.1073/pnas.87.5.1932

Hickman, S., Izzy, S., Sen, P., Morsett, L., & El Khoury, J. (2018). Microglia in neurodegeneration. *Nature Neuroscience*, *21*(10), 1359–1369. https://doi.org/10.1038/s41593-018-0242-x

Hitti, F. L., & Siegelbaum, S. A. (2014). The hippocampal CA2 region is essential for social memory. *Nature*, *508*(1), 88–92. https://doi.org/10.1038/nature13028

Hoek, R. H., Ruuls, S. R., Murphy, C. A., Wright, G. J., Goddard, R., Zurawski, S. M., Blom, B., Homola, M. E., Streit, W. J., Brown, M. H., Barclay, A. N., & Sedgwick, J. D. (2000). Down-regulation of the macrophage lineage through interaction with OX2 (CD200). *Science*, *290*(5497), 1768–1771. https://doi.org/10.1126/science.290.5497.1768

Holtmaat, A., Bonhoeffer, T., Chow, D. K., Chuckowree, J., De Paola, V., Hofer, S. B., Hübener,

M., Keck, T., Knott, G., Lee, W. C. A., Mostany, R., Mrsic-Flogel, T. D., Nedivi, E., Portera-Cailliau, C., Svoboda, K., Trachtenberg, J. T., & Wilbrecht, L. (2009). Long-term, high-resolution imaging in the mouse neocortex through a chronic cranial window. *Nature Protocols*, *4*(8), 1128–1144. https://doi.org/10.1038/nprot.2009.89

Holtmaat, A., & Svoboda, K. (2009). Experience-dependent structural synaptic plasticity in the mammalian brain. *Nature Reviews Neuroscience*, *10*(9), 647–658. https://doi.org/10.1038/nrn2699

Holtmaat, A., Trachtenberg, J. T., Wilbrecht, L., Shepherd, G. M., Zhang, X., Knott, G. W., & Svoboda, K. (2005). Transient and Persistent Dendritic Spines in the Neocortex In Vivo. *Neuron*, *45*, 279–291. https://doi.org/10.1016/j.neuron.2005.01.003

Holtmaat, A., Wilbrecht, L., Knott, G. W., Welker, E., & Svoboda, K. (2006). Experience-dependent and cell-type-specific spine growth in the neocortex. *Nature*, *441*(7096), 979–983. https://doi.org/10.1038/nature04783

Hopperton, K. E., Mohammad, D., Trépanier, M. O., Giuliano, V., & Bazinet, R. P. (2018). Markers of microglia in post-mortem brain samples from patients with Alzheimer's disease: A systematic review. *Molecular Psychiatry*, *23*(2), 177–198. https://doi.org/10.1038/mp.2017.246

Hotulainen, P., & Hoogenraad, C. C. (2010). Actin in dendritic spines : connecting dynamics to function. *The Journal of Cell Biology*, *189*(4), 619–629. https://doi.org/10.1083/jcb.201003008

Howlett, A. C., Barth, F., Bonner, T. I., Cabral, G., Casellas, P., Devane, W. A., Felder, C. C., Herkenham, M., Mackie, K., Martin, B. R., Mechoulam, R., & Pertwee, R. G. (2002). International Union of Pharmacology. XXVII. Classification of cannabinoid receptors. *Pharmacological Reviews*, *54*(2), 161–202. https://doi.org/10.1124/pr.54.2.161

Hu, X., Viesselmann, C., Nam, S., Merriam, E., & Dent, E. W. (2008). Activity-dependent dynamic microtubule invasion of dendritic spines. *Journal of Neuroscience*, *28*(49), 13094–13105. https://doi.org/10.1523/JNEUROSCI.3074-08.2008

Huang, L., Zhou, H., Chen, K., Chen, X., Yang, G., & Chen, S. (2020). Learning-Dependent Dendritic Spine Plasticity Is Reduced in the Aged Mouse Cortex. *Frontiers in Neural Circuits*, *14*(November), 1–11. https://doi.org/10.3389/fncir.2020.581435

Hutsler, J. J., & Zhang, H. (2010). Increased dendritic spine densities on cortical projection neurons in autism spectrum disorders. *Brain Research*, *1309*, 83–94.

https://doi.org/10.1016/j.brainres.2009.09.120

Iida, T., Tanaka, S., & Okabe, S. (2019). Spatial impact of microglial distribution on dynamics of dendritic spines. *European Journal of Neuroscience*, *49*(11), 1400–1417. https://doi.org/10.1111/ejn.14325

Ishizawa, T., Ko, L. W., Cookson, N., Davies, P., Espinoza, M., & Dickson, D. W. (2002). Selective neurofibrillary degeneration of the hippocampal CA2 sector is associated with four-repeat tauopathies. *Journal of Neuropathology and Experimental Neurology*, *61*(12), 1040–1047. https://doi.org/10.1093/jnen/61.12.1040

Jacobs, B., Schall, M., Prather, M., Kapler, E., Driscoll, L., Baca, S., Jacobs, J., Ford, K., Wainwright, M., & Treml, M. (2001). Regional dendritic and spine variation in human cerebral cortex: A quantitative golgi study. *Cerebral Cortex*, *11*(6), 558–571. https://doi.org/10.1093/cercor/11.6.558

Jaworski, J., Kapitein, L. C., Gouveia, S. M., Dortland, B. R., Wulf, P. S., Grigoriev, I., Camera, P., Spangler, S. A., Di Stefano, P., Demmers, J., Krugers, H., Defilippi, P., Akhmanova, A., & Hoogenraad, C. C. (2009). Dynamic Microtubules Regulate Dendritic Spine Morphology and Synaptic Plasticity. *Neuron*, *61*(1), 85–100. https://doi.org/10.1016/j.neuron.2008.11.013

Jordan, C. J., & Xi, Z.-X. (2019). Progress in brain cannabinoid CB2 receptor research: From genes to behavior. *Neuroscience and Biobehavioral Reviews*, *98*, 208–220. https://doi.org/10.1016/j.neubiorev.2018.12.026

Jurga, A. M., Paleczna, M., & Kuter, K. Z. (2020). Overview of General and Discriminating Markers of Differential Microglia Phenotypes. *Frontiers in Cellular Neuroscience*, *14*(August), 1–18. https://doi.org/10.3389/fncel.2020.00198

Kano, M., Ohno-Shosaku, T., Hashimotodani, Y., Uchigashima, M., & Watanabe, M. (2009). Endocannabinoid-mediated control of synaptic transmission. *Physiological Reviews*, *89*(1), 309–380. https://doi.org/10.1152/physrev.00019.2008

Kasai, H., Matsuzaki, M., Noguchi, J., Yasumatsu, N., & Nakahara, H. (2003). Structure-stability-function relationships of dendritic spines. *Trends in Neurosciences*, *26*(7), 360–368. https://doi.org/10.1016/S0166-2236(03)00162-0

Kawamura, Y., Fukaya, M., Maejima, T., Yoshida, T., Miura, E., Watanabe, M., Ohno-Shosaku, T., & Kano, M. (2006). The CB1 cannabinoid receptor is the major cannabinoid receptor at excitatory presynaptic sites in the hippocampus and cerebellum. *Journal of*

Neuroscience, *26*(11), 2991–3001. https://doi.org/10.1523/JNEUROSCI.4872-05.2006

Keller-Peck, C. R., Walsh, M. K., Gan, W. B., Feng, G., Sanes, J. R., & Lichtman, J. W. (2001). Asynchronous synapse elimination in neonatal motor units: Studies using GFP transgenic mice. *Neuron*, *31*(3), 381–394. https://doi.org/10.1016/S0896-6273(01)00383-X

Kennedy, B. K., Berger, S. L., Brunet, A., Campisi, J., Cuervo, A. M., Epel, E. S., Franceschi, C., Lithgow, G. J., Morimoto, R. I., Pessin, J. E., Rando, T. A., Richardson, A., Schadt, E. E., Wyss-Coray, T., & Sierra, F. (2014). Geroscience: Linking aging to chronic disease. *Cell*, *159*(4), 709–713. https://doi.org/10.1016/j.cell.2014.10.039

Kettenmann, H., Kirchhoff, F., & Verkhratsky, A. (2013). Microglia: New Roles for the Synaptic Stripper. *Neuron*, *77*(1), 10–18. https://doi.org/10.1016/j.neuron.2012.12.023

Kim, H. J., Cho, M. H., Shim, W. H., Kim, J. K., Jeon, E. Y., Kim, D. H., & Yoon, S. Y. (2017). Deficient autophagy in microglia impairs synaptic pruning and causes social behavioral defects. *Molecular Psychiatry*, *22*(11), 1576–1584. https://doi.org/10.1038/mp.2016.103

Kloft, L., Otgaar, H., Blokland, A., Monds, L. A., Toennes, S. W., Loftus, E. F., & Ramaekers, J. G. (2020). Cannabis increases susceptibility to false memory. *Proceedings of the National Academy of Sciences of the United States of America*, *117*(9), 4585–4589. https://doi.org/10.1073/pnas.1920162117

Knott, G. W., Holtmaat, A., Wilbrecht, L., Welker, E., & Svoboda, K. (2006). Spine growth precedes synapse formation in the adult neocortex in vivo. *Nature Neuroscience*, *9*(9), 1117–1124. https://doi.org/10.1038/nn1747

Kolb, B. (2018). THC alters alters morphology of neurons in medial prefrontal cortex , orbital prefrontal cortex , and nucleus accumbens and alters the ability of later experience to promote structural plasticity. *Synapse*. https://doi.org/10.1002/syn.

Koleske, A. J. (2013). Molecular mechanisms of dendrite stability. *Nature Reviews Neuroscience*, *14*(8), 536–550. https://doi.org/10.1038/nrn3486

Komorowska-Müller, J. A., & Schmöle, A. C. (2021). CB2 receptor in microglia: The guardian of self-control. *International Journal of Molecular Sciences*, *22*(1), 1–27. https://doi.org/10.3390/ijms22010019

Koppel, J., Vingtdeux, V., Marambaud, P., d'Abramo, C., Jimenez, H., Stauber, M., Friedman, R., & Davies, P. (2013). CB2 Receptor Deficiency Increases Amyloid Pathology and Alters

Tau Processing in a Transgenic Mouse Model of Alzheimer's Disease. *Molecular Medicine*, *19*(1), 357–364. https://doi.org/10.2119/molmed.2013.00140

Kreitzer, A. C., & Regehr, W. G. (2001). Retrograde inhibition of presynaptic calcium influx by endogenous cannabinoids at excitatory synapses onto Purkinje cells. *Neuron*, *29*(3), 717–727. https://doi.org/10.1016/S0896-6273(01)00246-X

Kushner, S. A., Elgersma, Y., Murphy, G. G., Jaarsma, D., Van Woerden, G. M., Hojjati, M. R., Cui, Y., LeBoutillier, J. C., Marrone, D. F., Choi, E. S., De Zeeuw, C. I., Petit, T. L., Pozzo-Miller, L., & Silva, A. J. (2005). Modulation of presynaptic plasticity and learning by the H-ras/extracellular signal-regulated kinase/synapsin I signaling pathway. *Journal of Neuroscience*, *25*(42), 9721–9734. https://doi.org/10.1523/JNEUROSCI.2836-05.2005

Kwon, H. B., & Sabatini, B. L. (2011). Glutamate induces de novo growth of functional spines in developing cortex. *Nature*, *474*(7349), 100–104. https://doi.org/10.1038/nature09986

La Porta, C., Bura, S. A., Aracil-Fernández, A., Manzanares, J., & Maldonado, R. (2013). Role of CB1 and CB2 cannabinoid receptors in the development of joint pain induced by monosodium iodoacetate. *Pain*, *154*(1), 160–174. https://doi.org/10.1016/j.pain.2012.10.009

Lawson, L. J., Perry, V. H., & Gordon, S. (1992). Turnover of resident microglia in the normal adult mouse brain. *Neuroscience*, *48*(2), 405–415. https://doi.org/10.1016/0306-4522(92)90500-2

Leal, S., & Yassa, M. (2015). Neurocognitive Aging and the Hippocampus Across Species. *Trends in Neuroscience*, *38*(12), 800–812. https://doi.org/10.1016/j.tins.2015.10.003.Neurocognitive

Legon, W., Punzell, S., Dowlati, E., Adams, S. E., Stiles, A. B., & Moran, R. J. (2016). Altered Prefrontal Excitation/Inhibition Balance and Prefrontal Output: Markers of Aging in Human Memory Networks. *Cerebral Cortex*, *26*(11), 4315–4326. https://doi.org/10.1093/cercor/bhv200

Li, W., Ma, L., Yang, G., & Gan, W. B. (2017). REM sleep selectively prunes and maintains new synapses in development and learning. *Nature Neuroscience*, *20*(3), 427–437. https://doi.org/10.1038/nn.4479

Li, Y., & Kim, J. (2015). Neuronal expression of CB2 cannabinoid receptor mRNAs in the mouse hippocampus. *Neuroscience*, *311*, 253–267.

https://doi.org/10.1016/j.neuroscience.2015.10.041

Li, Ying, Du, X. F., Liu, C. S., Wen, Z. L., & Du, J. L. (2012). Reciprocal Regulation between Resting Microglial Dynamics and Neuronal Activity In Vivo. *Developmental Cell*, *23*(6), 1189–1202. https://doi.org/10.1016/j.devcel.2012.10.027

Li, Yong, & Kim, J. (2016a). CB2 cannabinoid receptor knockout in mice impairs contextual long-term memory and enhances spatial working memory. *Neural Plasticity*, *2016*. https://doi.org/10.1155/2016/9817089

Li, Yong, & Kim, J. (2016b). Deletion of CB2 cannabinoid receptors reduces synaptic transmission and long-term potentiation in the mouse hippocampus. *Hippocampus*, *26*(3), 275–281. https://doi.org/10.1002/hipo.22558

Li, Yong, & Kim, J. (2017). Distinct roles of neuronal and microglial CB2 cannabinoid receptors in the mouse hippocampus. *Neuroscience*, *363*, 11–25. https://doi.org/10.1016/j.neuroscience.2017.08.053

Liston, C., & Gan, W. B. (2011). Glucocorticoids are critical regulators of dendritic spine development and plasticity in vivo. *Proceedings of the National Academy of Sciences of the United States of America*, *108*(38), 16074–16079. https://doi.org/10.1073/pnas.1110444108

Liu, Q. R., Canseco-Alba, A., Zhang, H. Y., Tagliaferro, P., Chung, M., Dennis, E., Sanabria, B., Schanz, N., Escosteguy-Neto, J. C., Ishiguro, H., Lin, Z., Sgro, S., Leonard, C. M., Santos-Junior, J. G., Gardner, E. L., Egan, J. M., Lee, J. W., Xi, Z. X., & Onaivi, E. S. (2017). Cannabinoid type 2 receptors in dopamine neurons inhibits psychomotor behaviors, alters anxiety, depression and alcohol preference. *Scientific Reports*, *7*(1), 1–17. https://doi.org/10.1038/s41598-017-17796-y

Lopes, P. C., Block, P., & König, B. (2016). Infection-induced behavioural changes reduce connectivity and the potential for disease spread in wild mice contact networks. *Nature Publishing Group*, *February*, 1–10. https://doi.org/10.1038/srep31790

López-Otín, C., Blasco, M. A., Partridge, L., Serrano, M., & Kroemer, G. (2013). The Hallmarks of Aging Europe PMC Funders Group. *Cell*, *153*(6), 1194–1217. https://doi.org/10.1016/j.cell.2013.05.039

López, A., Aparicio, N., Pazos, M. R., Grande, M. T., Barreda-Manso, M. A., Benito-Cuesta, I., Vázquez, C., Amores, M., Ruiz-Pérez, G., García-García, E., Beatka, M., Tolón, R. M., Dittel, B. N., Hillard, C. J., & Romero, J. (2018). Cannabinoid CB 2 receptors in the mouse

brain: Relevance for Alzheimer's disease. *Journal of Neuroinflammation*, *15*(1), 1–11. https://doi.org/10.1186/s12974-018-1174-9

Luebke, J. I., Chang, Y. M., Moore, T. L., & Rosene, D. L. (2004). Normal aging results in decreased synaptic excitation and increased synaptic inhibition of layer 2/3 pyramidal cells in the monkey prefrontal cortex. *Neuroscience*, *125*(1), 277–288. https://doi.org/10.1016/j.neuroscience.2004.01.035

Mably, A. J., & Colgin, L. L. (2018). Gamma oscillations in cognitive disorders. *Current Opinion in Neurobiology*, *52*, 182–187. https://doi.org/10.1016/j.conb.2018.07.009

Maccarrone, M., Bab, I., Bíró, T., Cabral, G. A., Dey, S. K., Di Marzo, V., Konje, J. C., Kunos, G., Mechoulam, R., Pacher, P., Sharkey, K. A., & Zimmer, A. (2015). Endocannabinoid signaling at the periphery: 50 years after THC. In *Trends in Pharmacological Sciences* (Vol. 36, Issue 5, pp. 277–296). https://doi.org/10.1016/j.tips.2015.02.008

Majewska, A. K., Newton, J. R., & Sur, M. (2006). Remodeling of synaptic structure in sensory cortical areas In Vivo. *Journal of Neuroscience*, *26*(11), 3021–3029. https://doi.org/10.1523/JNEUROSCI.4454-05.2006

Marchalant, Y., Brothers, H. M., & Wenk, G. L. (2009). Cannabinoid agonist WIN-55,212-2 partially restores neurogenesis in the aged rat brain. *Molecular Psychiatry*, *14*(12), 1068–1071. https://doi.org/10.1038/mp.2009.62

Marchalant, Yannick, Cerbai, F., Brothers, H. M., & Wenk, G. L. (2008). Cannabinoid receptor stimulation is anti-inflammatory and improves memory in old rats. *Neurobiology of Aging*, *29*(12), 1894–1901. https://doi.org/10.1016/j.neurobiolaging.2007.04.028

Maret, S., Faraguna, U., Nelson, A. B., Cirelli, C., & Tononi, G. (2011). Sleep and waking modulate spine turnover in the adolescent mouse cortex. *Nature Neuroscience*, *14*(11), 1418–1420. https://doi.org/10.1038/nn.2934

Martín-moreno, A. M., Brera, B., Spuch, C., Carro, E., García-garcía, L., Delgado, M., Pozo, M. A., Innamorato, N. G., Cuadrado, A., & Ceballos, M. L. De. (2012). Prolonged oral cannabinoid administration prevents neuroinflammation , lowers b -amyloid levels and improves cognitive performance in Tg APP 2576 mice. *Journal of Neuroinflammation*, *9*(1), 8. https://doi.org/10.1186/1742-2094-9-8

Matsuzaki, M., Ellis-Davies, G. C., Nemoto, T., Miyashita, Y., & Kasai, H. (2001). Dendritic spine geometry is critical for AMPA receptor expression in hippocampal CA1 pyramidal neurons. *Nature Neuroscience*, *4*(11), 1086–1092.

https://doi.org/10.1038/nn736.Dendritic

Matsuzaki, M., Honkura, N., Ellis-Davies, G. C., & Kasai, H. (2004). Structural basis of long-term potentiation in single den- dritic spines. *Nature*, *429*(6993), 761–766. https://doi.org/10.1038/nature02617.Structural

Matus, A., Ackermann, M., Pehling, G., Byers, H. R., & Fujiwara, K. (1982). High actin concentrations in brain dendritic spines and postsynaptic densities. *Proceedings of the National Academy of Sciences of the United States of America*, *79*(23 I), 7590–7594. https://doi.org/10.1073/pnas.79.23.7590

Mechoulam, R., Ben-Shabat, S., Hanus, L., Ligumsky, M., Kaminski, N. E., Schatz, A. R., Gopher, A., Almog, S., Martin, B. R., Compton, D. R., Pertwee, R. G., Griffin, G., Bayewitch, M., Barg, J., & Vogel, Z. (1995). Identification of an endogenous 2-monoglyceride, present in canine gut, that binds to cannabinoid receptors. *Biochemical Pharmacology*, *50*(1), 83–90. https://doi.org/10.1016/0006-2952(95)00109-D

Mechoulam, R., & Parker, L. A. (2013). The endocannabinoid system and the brain. *Annual Review of Psychology*, *64*, 21–47. https://doi.org/10.1146/annurev-psych-113011-143739

Meerlo, P., Overkamp, G., Daan, S., Van den Hoofdakker, R. H., & Koolhaas, J. M. (1996). Changes in Behaviour and Body Weight Following a Single or Double Social Defeat in Rats. *Stress*, *1*, 21–32.

Melser, S., Zottola, A. C. P., Serrat, R., Puente, N., Grandes, P., Marsicano, G., & Hebert-Chatelain, E. (2017). Functional Analysis of Mitochondrial CB1 Cannabinoid Receptors (mtCB1) in the Brain. In *Methods in Enzymology* (1st ed., Vol. 593). Elsevier Inc. https://doi.org/10.1016/bs.mie.2017.06.023

Minhas, P. S., Latif-Hernandez, A., McReynolds, M. R., Durairaj, A. S., Wang, Q., Rubin, A., Joshi, A. U., He, J. Q., Gauba, E., Liu, L., Wang, C., Linde, M., Sugiura, Y., Moon, P. K., Majeti, R., Suematsu, M., Mochly-Rosen, D., Weissman, I. L., Longo, F. M., … Andreasson, K. I. (2021). Restoring metabolism of myeloid cells reverses cognitive decline in ageing. *Nature*, *590*(7844), 122–128. https://doi.org/10.1038/s41586-020-03160-0

Mitchell, D. J., & Cusack, R. (2018). Visual short-term memory through the lifespan: Preserved benefits of context and metacognition. *Psychology and Aging*, *33*(5), 841–854. https://doi.org/10.1037/pag0000265

Miyamoto, A., Wake, H., Ishikawa, A. W., Eto, K., Shibata, K., Murakoshi, H., Koizumi, S.,

Moorhouse, A. J., Yoshimura, Y., & Nabekura, J. (2016). Microglia contact induces synapse formation in developing somatosensory cortex. *Nature Communications*, *7*. https://doi.org/10.1038/ncomms12540

Miyamoto, A., Wake, H., Moorhouse, A. J., & Nabekura, J. (2013). Microglia and synapse interactions: Fine tuning neural circuits and candidate molecules. *Frontiers in Cellular Neuroscience*, *7*(MAY), 1–6. https://doi.org/10.3389/fncel.2013.00070

Molinari, C., Morsanuto, V., Ruga, S., Notte, F., Farghali, M., Galla, R., & Uberti, F. (2020). The role of BDNF on aging-modulation markers. *Brain Sciences*, *10*(5). https://doi.org/10.3390/brainsci10050285

Montagne, A., Barnes, S., Sweeney, M., Halliday, M., Sagare, A., Zhao, Z., Toga, A., Jacobs, R., Liu, C., Amezcua, L., Harrington, M., Chui, H., Law, M., & Zlokovic, B. (2015). Blood-Brain Barrier Breakdown in the Aging Human Hippocampus. *Neuron*, *85*(2), 296–302. https://doi.org/10.1016/j.neuron.2014.12.032.Blood-Brain

Morris, R. G. M. (1981). Spatial localization does not require the presence of local cues. *Learning and Motivation*, *12*(2), 239–260. https://doi.org/10.1016/0023-9690(81)90020-5

Mostany, R., Anstey, J. E., Crump, K. L., Maco, B., Knott, G., & Portera-cailliau, C. (2013). Altered Synaptic Dynamics during Normal Brain Aging data suggest that age-related deficits in sensory perception are not associated with synapse loss in somatosensory cortex (as might be expected). *Journal of Neuroscience*, *33*(9), 4094–4104. https://doi.org/10.1523/JNEUROSCI.4825-12.2013

Munro, S., Thomas, K. L., & Abu-Shaar, M. (1993). Molecular characterization of a peripheral receptor for cannabinoids. *Nature*, *365*(6441), 61–65. https://doi.org/10.1038/365061a0

Nahas, G. G. (2001). The pharmacokinetics of THC in fat and brain: Resulting functional responses to marihuana smoking. *Human Psychopharmacology*, *16*(3), 247–255. https://doi.org/10.1002/hup.258

Navarrete, F., Rodríguez-Arias, M., Martín-García, E., Navarro, D., García-Gutiérrez, M. S., Aguilar, M. A., Aracil-Fernández, A., Berbel, P., Miñarro, J., Maldonado, R., & Manzanares, J. (2013). Role of CB2 cannabinoid receptors in the rewarding, reinforcing, and physical effects of nicotine. *Neuropsychopharmacology*, *38*(12), 2515–2524. https://doi.org/10.1038/npp.2013.157

Nelson, G., Wordsworth, J., Wang, C., Jurk, D., Lawless, C., Martin-Ruiz, C., & von Zglinicki, T. (2012). A senescent cell bystander effect: Senescence-induced senescence. *Aging Cell*, *11*(2), 345–349. https://doi.org/10.1111/j.1474-9726.2012.00795.x

Nguyen, P. T., Dorman, L. C., Pan, S., Vainchtein, I. D., Han, R. T., Nakao-Inoue, H., Taloma, S. E., Barron, J. J., Molofsky, A. B., Kheirbek, M. A., & Molofsky, A. V. (2020). Microglial Remodeling of the Extracellular Matrix Promotes Synapse Plasticity. *Cell*, *182*(0), 1–16. https://doi.org/10.1016/j.cell.2020.05.050

Nicaise, A. M., Willis, C. M., Crocker, S. J., & Pluchino, S. (2020). Stem Cells of the Aging Brain. *Frontiers in Aging Neuroscience*, *12*(August), 1–23. https://doi.org/10.3389/fnagi.2020.00247

Nimmerjahn, A., Kirchhoff, F., & Helmchen, F. (2005). Resting microglial cells are highly dynamic surveillants of brain parenchyma in vivo. *Neuroforum*, *11*(3), 95–96. https://doi.org/10.1515/nf-2005-0304

Niraula, A., Sheridan, J. F., & Godbout, J. P. (2017). Microglia Priming with Aging and Stress. *Neuropsychopharmacology*, *42*(1), 318–333. https://doi.org/10.1038/npp.2016.185

Njoo, C., Agarwal, N., Lutz, B., & Kuner, R. (2015). *The Cannabinoid Receptor CB1 Interacts with the WAVE1 Complex and Plays a Role in Actin Dynamics and Structural Plasticity in Neurons*. 1–36. https://doi.org/10.1371/journal.pbio.1002286

Oh, W. C., Lutzu, S., Castillo, P. E., & Kwon, H. B. (2016). De novo synaptogenesis induced by GABA in the developing mouse cortex. *Science*, *353*(6303), 1037–1040. https://doi.org/10.1126/science.aaf5206

Ohno-Shosaku, T., Maejima, T., & Kano, M. (2001). Endogenous cannabinoids mediate retrograde signals from depolarized postsynaptic neurons to presynaptic terminals. *Neuron*, *29*(3), 729–738. https://doi.org/10.1016/S0896-6273(01)00247-1

Olah, M., Biber, K., Vinet, J., & W.G.M. Boddeke, H. (2011). Microglia Phenotype Diversity. *CNS & Neurological Disorders - Drug Targets*, *10*(1), 108–118. https://doi.org/10.2174/187152711794488575

Onaivi, E. S. (2007). Neuropsychobiological evidence for the functional presence and expression of cannabinoid CB2 receptors in the brain. *Neuropsychobiology*, *54*(4), 231–246. https://doi.org/10.1159/000100778

Ortega-Alvaro, A., Aracil-Fernández, A., García-Gutiérrez, M. S., Navarrete, F., & Manzanares, J. (2011). Deletion of CB2 cannabinoid receptor induces schizophrenia-related behaviors

in mice. *Neuropsychopharmacology*, *36*(7), 1489–1504. https://doi.org/10.1038/npp.2011.34

Oviedo, A., Glowa, J., & Herkenham, M. (1993). Chronic cannabinoid administration alters cannabinoid receptor binding in rat brain: a quantitative autoradiographic study. *Brain Research*, *616*(1–2), 293–302. https://doi.org/10.1016/0006-8993(93)90220-H

Padmashri, R., Reiner, B. C., Suresh, A., Spartz, E., & Dunaevsky, A. (2013). Altered structural and functional synaptic plasticity with motor skill learning in a mouse model of fragile X syndrome. *Journal of Neuroscience*, *33*(50), 19715–19723. https://doi.org/10.1523/JNEUROSCI.2514-13.2013

Paolicelli, R. C., Bolasco, G., Pagani, F., Maggi, L., Scianni, M., Panzanelli, P., Giustetto, M., Ferreira, T. A., Guiducci, E., Dumas, L., Ragozzino, D., & Gross, C. T. (2011). Synaptic pruning by microglia is necessary for normal brain development. *Science*, *333*(6048), 1456–1458. https://doi.org/10.1126/science.1202529

Parkhurst, C. N., Yang, G., Ninan, I., Savas, J. N., III, J. R. Y., Lafaille, J. J., Hempstead, B. L., Littman, D. R., & Gan, W.-B. (2013). Microglia promote learning-dependent synapse formation through BDNF. *Cell*, *155*(7), 1596–1609. https://doi.org/10.1016/j.cell.2013.11.030.Microglia

Pertwee, R. G. (2008). The diverse CB 1 and CB 2 receptor pharmacology of three plant cannabinoids: Δ 9-tetrahydrocannabinol, cannabidiol and Δ 9-tetrahydrocannabivarin. *British Journal of Pharmacology*, *153*(2), 199–215. https://doi.org/10.1038/sj.bjp.0707442

Peters, A., & Kaiserman-Abramof, I. R. (1970). The small pyramidal neuron of the rat cerebral cortex. The perikaryon, dendrites and spines. *American Journal of Anatomy*, *127*(4), 321–355. https://doi.org/10.1002/aja.1001270402

Pfeiffer, T., Avignone, E., & Nägerl, U. V. (2016). Induction of hippocampal long-term potentiation increases the morphological dynamics of microglial processes and prolongs their contacts with dendritic spines. *Scientific Reports*, *6*(September), 1–9. https://doi.org/10.1038/srep32422

Pfeiffer, T., Poll, S., Bancelin, S., Angibaud, J., Inavalli, V. V. G. K., Keppler, K., Mittag, M., Fuhrmann, M., & Nägerl, U. V. (2018). Chronic 2P-STED imaging reveals high turnover of dendritic spines in the hippocampus in vivo. *ELife*, *7*, 1–17. https://doi.org/10.7554/eLife.34700

Pikkarainen, M., Ronkko, S., Savander, V., Insausti, R., & Pitkanen, A. (1999). Projections from the lateral, basal, and accessory basal nuclei of the amygdala to the entorhinal cortex in the macaque monkey. *The Journal of Comparative Neurology*, *403*, 229–260. https://doi.org/10.1002/hipo.1099

Piskorowski, R. A., Nasrallah, K., Diamantopoulou, A., Mukai, J., Hassan, S. I., Siegelbaum, S. A., Gogos, J. A., & Chevaleyre, V. (2016). Age-Dependent Specific Changes in Area CA2 of the Hippocampus and Social Memory Deficit in a Mouse Model of the 22q11.2 Deletion Syndrome. *Neuron*, *89*(1), 163–176. https://doi.org/10.1016/j.neuron.2015.11.036

Piyanova, A., Lomazzo, E., Bindila, L., Lerner, R., Albayram, O., Ruhl, T., Lutz, B., Zimmer, A., & Bilkei-Gorzo, A. (2015). Age-related changes in the endocannabinoid system in the mouse hippocampus. *Mechanisms of Ageing and Development*, *150*, 55–64. https://doi.org/10.1016/j.mad.2015.08.005

Plescher, M., Seifert, G., Hansen, J. N., Bedner, P., Steinhäuser, C., & Halle, A. (2018). Plaque-dependent morphological and electrophysiological heterogeneity of microglia in an Alzheimer's disease mouse model. *Glia*, *66*(7), 1464–1480. https://doi.org/10.1002/glia.23318

Pologruto, T. A., Sabatini, B. L., & Svoboda, K. (2003). ScanImage Flexible software for operating laser scanning. *BioMedical Engineering OnLine*, *2*(13), 1–9.

Pradier, B., Erxlebe, E., Markert, A., & Rácz, I. (2015). Interaction of cannabinoid receptor 2 and social environment modulates chronic alcohol consumption. *Behavioural Brain Research*, *287*, 163–171. https://doi.org/10.1016/j.bbr.2015.03.051

Prini, P., Federica, P., Emanuele, S., Tiziana, A., & Rubino, T. (2017). Chronic Δ 9 -THC Exposure Differently Affects Histone Modifications in the Adolescent and Adult Rat Brain. *International Journal of Molecular Sciences*. https://doi.org/10.3390/ijms18102094

Puighermanal, E., Marsicano, G., Busquets-garcia, A., Lutz, B., & Maldonado, R. (2009). Cannabinoid modulation of hippocampal long-term memory is mediated by mTOR signaling. *Nature Neuroscience*, *12*(9), 1152–1160. https://doi.org/10.1038/nn.2369

Radley, J. J., Anderson, R. M., Hamilton, B. A., Alcock, J. A., & Romig-Martin, S. A. (2013). Chronic stress-induced alterations of dendritic spine subtypes predict functional decrements in an hypothalamo-pituitary-adrenal-inhibitory prefrontal circuit. *Journal of Neuroscience*, *33*(36), 14379–14391. https://doi.org/10.1523/JNEUROSCI.0287-

13.2013

Ramirez, B. G., Blazquez, C., Gomez del Pulgar, T., Guzman, M., & de Ceballos, M. L. (2005). Prevention of Alzheimer's Disease Pathology by Cannabinoids: Neuroprotection Mediated by Blockade of Microglial Activation. *Journal of Neuroscience*, *25*(8), 1904–1913. https://doi.org/10.1523/JNEUROSCI.4540-04.2005

Ransohoff, R. M. (2016). A polarizing question: Do M1 and M2 microglia exist. *Nature Neuroscience*, *19*(8), 987–991. https://doi.org/10.1038/nn.4338

Ratano, P., Palmery, M., Trezza, V., & Campolongo, P. (2017). Cannabinoid Modulation of Memory Consolidation in Rats : Beyond the Role of Cannabinoid Receptor Subtype 1. *Frontiers in P*, *8*(April), 1–13. https://doi.org/10.3389/fphar.2017.00200

Ratano, P., Petrella, C., Forti, F., Passeri, P. P., Morena, M., Palmery, M., Trezza, V., Severini, C., & Campolongo, P. (2018). Pharmacological inhibition of 2-arachidonoilglycerol hydrolysis enhances memory consolidation in rats through CB2 receptor activation and mTOR signaling modulation. *Neuropharmacology*, *138*, 210–218. https://doi.org/10.1016/j.neuropharm.2018.05.030

Reshef, R., Kudryavitskaya, E., Shani-Narkiss, H., Isaacson, B., Rimmerman, N., Mizrahi, A., & Yirmiya, R. (2017). The role of microglia and their CX3CR1 signaling in adult neurogenesis in the olfactory bulb. *ELife*, *6*, 1–30. https://doi.org/10.7554/eLife.30809

Rex, C. S., Lauterborn, J. C., Lin, C. Y., Kramár, E. A., Rogers, G. A., Gall, C. M., & Lynch, G. (2006). Restoration of long-term potentiation in middle-aged hippocampus after induction of brain-derived neurotrophic factor. *Journal of Neurophysiology*, *96*(2), 677–685. https://doi.org/10.1152/jn.00336.2006

Robertson, J. M., Achua, J. K., Smith, J. P., Prince, M. A., Staton, C. D., Ronan, P. J., Summers, T. R., & Summers, C. H. (2017). Anxious behavior induces elevated hippocampal Cb 2 receptor gene expression. *Neuroscience*, *352*, 273–284. https://doi.org/10.1002/cncr.27633.Percutaneous

Rogers, J. T., Morganti, J. M., Bachstetter, A. D., Hudson, C. E., Peters, M. M., Grimmig, B. A., Weeber, E. J., Bickford, P. C., & Gemma, C. (2011). CX3CR1 deficiency leads to impairment of hippocampal cognitive function and synaptic plasticity. *Journal of Neuroscience*, *31*(45), 16241–16250. https://doi.org/10.1523/JNEUROSCI.3667-11.2011

Romero, J., Berrendero, F., Garcia-Gil, L., De La Cruz, P., Ramos, J. A., & Fernandez-Ruiz., J. J.

(1998). *LOSS OF CANNABINOID RECEPTOR BINDING AND MESSENGER RNA LEVELS AND CANNABINOID AGONIST-STIMULATED [35S] GUANYLYL-5 ' -O- (THIO) -TRIPHOSPHATE BINDING IN THE BASAL GANGLIA OF AGED RATS *. 84*(4), 1075–1083.

Rosahl, T. W., Geppert, M., Spillane, D., Herz, J., Hammer, R. E., Malenka, R. C., & Südhof, T. C. (1993). Short-term synaptic plasticity is altered in mice lacking synapsin I. *Cell*, *75*(4), 661–670. https://doi.org/10.1016/0092-8674(93)90487-B

Rozycka, A., & Liguz-Lecznar, M. (2017). The space where aging acts: focus on the GABAergic synapse. *Aging Cell*, *16*(4), 634–643. https://doi.org/10.1111/acel.12605

Rubino, T., Realini, N., Braida, D., Guidi, S., Capurro, V., Guidali, C., Pinter, M., Sala, M., Bartesaghi, R., & Parolaro, D. (2009). *Changes in Hippocampal Morphology and Neuroplasticity Induced by Adolescent THC Treatment are Associated With Cognitive Impairment in Adulthood*. *772*, 763–772. https://doi.org/10.1002/hipo.20554

Runge, K., Cardoso, C., & de Chevigny, A. (2020). Dendritic Spine Plasticity: Function and Mechanisms. *Frontiers in Synaptic Neuroscience*, *12*(August). https://doi.org/10.3389/fnsyn.2020.00036

Sadanandan, S. M., Kreko-Pierce, T., Khatri, S. N., & Pugh, J. R. (2020). Cannabinoid type 2 receptors inhibit GABAA receptor-mediated currents in cerebellar Purkinje cells of juvenile mice. *PLoS ONE*, *15*(5), 1–14. https://doi.org/10.1371/journal.pone.0233020

Santollo, J., & Daniels, D. (2015). Control of fluid intake by estrogens in the female rat: Role of the hypothalamus. *Frontiers in Systems Neuroscience*, *9*(MAR), 1–11. https://doi.org/10.3389/fnsys.2015.00025

Sarne, Y., Toledano, R., Rachmany, L., Sasson, E., & Doron, R. (2018). Reversal of age-related cognitive impairments in mice by an extremely low dose of tetrahydrocannabinol. *Neurobiology of Aging*, *61*, 177–186. https://doi.org/10.1016/j.neurobiolaging.2017.09.025

Schafer, D. P., Lehrman, E. K., Kautzman, A. G., Koyama, R., Mardinly, A. R., Yamasaki, R., Ransohoff, R. M., Greenberg, M. E., Barres, B. A., & Stevens, B. (2012). Microglia Sculpt Postnatal Neural Circuits in an Activity and Complement-Dependent Manner. *Neuron*, *74*(4), 691–705. https://doi.org/10.1016/j.neuron.2012.03.026

Schmitz, K., Mangels, N., Häussler, A., Ferreirós, N., Fleming, I., & Tegeder, I. (2016). Pro-inflammatory obesity in aged cannabinoid-2 receptor-deficient mice. *International Journal of Obesity*, *40*, 366–379. https://doi.org/10.1038/ijo.2015.169

Schmöle, A.-C., Lundt, R., Toporowski, G., Hansen, J. N., Beins, E., Halle, A., & Zimmer, A. (2018). Cannabinoid Receptor 2-Deficiency Ameliorates Disease Symptoms in a Mouse Model with Alzheimer's Disease-Like Pathology. *Journal of Alzheimer's Disease*, *64*(2), 379–392. https://doi.org/10.3233/JAD-180230

Schmöle, A. C., Lundt, R., Gennequin, B., Schrage, H., Beins, E., Krämer, A., Zimmer, T., Limmer, A., Zimmer, A., & Otte, D. M. (2015). Expression analysis of CB2-GFP BAC transgenic mice. *PLoS ONE*, *10*(9), 1–16. https://doi.org/10.1371/journal.pone.0138986

Schmöle, A. C., Lundt, R., Ternes, S., Albayram, Ö., Ulas, T., Schultze, J. L., Bano, D., Nicotera, P., Alferink, J., & Zimmer, A. (2015). Cannabinoid receptor 2 deficiency results in reduced neuroinflammation in an Alzheimer's disease mouse model. *Neurobiology of Aging*, *36*(2), 710–719. https://doi.org/10.1016/j.neurobiolaging.2014.09.019

Sheng, J. G., Mrak, R. E., & Griffin, W. S. T. (1998). Enlarged and phagocytic, but not primed, interleukin-1α-immunoreactive microglia increase with age in normal human brain. *Acta Neuropathologica*, *95*(3), 229–234. https://doi.org/10.1007/s004010050792

Sheng, M., & Kim, E. (2011). The postsynaptic organization of synapses. *Cold Spring Harbor Perspectives in Biology*, *3*(12), 1–20. https://doi.org/10.1101/cshperspect.a005678

Shepherd, J. K., Grewal, S. S., Fletcher, A., Bill, D. J., & Dourish, C. T. (1994). Behavioural and pharmacological characterisation of the elevated "zero-maze" as an animal model of anxiety. *Psychopharmacology*, *116*(1), 56–64. https://doi.org/10.1007/BF02244871

Shobin, E., Bowley, M. P., Estrada, L. I., Heyworth, N. C., Orczykowski, M. E., Eldridge, S. A., Calderazzo, S. M., Mortazavi, F., Moore, T. L., & Rosene, D. L. (2017). Microglia activation and phagocytosis: relationship with aging and cognitive impairment in the rhesus monkey. *GeroScience*, *39*(2), 199–220. https://doi.org/10.1007/s11357-017-9965-y

Shrivastava, A., Johnston, M., & Tsuang, M. (2011). Cannabis use and cognitive dysfunction. *Indian Journal of Psychiatry*, *53*(3), 187–191. https://doi.org/10.4103/0019-5545.86796

Sierra, A., Gottfried-Blackmore, A., McEwen, B., & Bulloch, K. (2007). Microglia Derived from Aging Mice Exhibit an Altered Inflammatory Profil. *Glia*, *55*, 412–424. https://doi.org/10.1002/glia

Singhal, G., Morgan, J., Jawahar, M. C., Corrigan, F., Jaehne, E. J., Toben, C., Breen, J., Pederson, S. M., Manavis, J., Hannan, A. J., & Baune, B. T. (2020). Effects of aging on the motor, cognitive and affective behaviors, neuroimmune responses and hippocampal gene expression. *Behavioural Brain Research*, *383*(January), 112501.

https://doi.org/10.1016/j.bbr.2020.112501

Singla, S., Kreitzer, A. C., & Malenka, R. C. (2007). Mechanisms for synapse specificity during striatal long-term depression. *Journal of Neuroscience*, *27*(19), 5260–5264. https://doi.org/10.1523/JNEUROSCI.0018-07.2007

Smith, K. L., Kassem, M. S., Clarke, D. J., Kuligowski, M. P., Bedoya-Pérez, M. A., Todd, S. M., Lagopoulos, J., Bennett, M. R., & Arnold, J. C. (2019). Microglial cell hyper-ramification and neuronal dendritic spine loss in the hippocampus and medial prefrontal cortex in a mouse model of PTSD. *Brain, Behavior, and Immunity*, *80*(May), 889–899. https://doi.org/10.1016/j.bbi.2019.05.042

Solas, M., Francis, P. T., Franco, R., & Ramirez, M. J. (2013). CB2 receptor and amyloid pathology in frontal cortex of Alzheimer's disease patients. *Neurobiology of Aging*. https://doi.org/10.1016/j.neurobiolaging.2012.06.005

Solowij, N., Michie, P. T., & Fox, A. M. (1995). Differential impairments of selective attention due to frequency and duration of cannabis use. *Biological Psychiatry*, *37*(10), 731–739. https://doi.org/10.1016/0006-3223(94)00178-6

Špaček, J. (1985). Three-dimensional analysis of dendritic spines - II. Spine apparatus and other cytoplasmic components. *Anatomy and Embryology*, *171*(2), 235–243. https://doi.org/10.1007/BF00341418

Stella, N. (2009). Endocannabinoid signaling in microglial cells. *Neuropharmacology*, *56*(Suppl 1), 244–253. https://doi.org/10.1016/j.neuropharm.2008.07.037

Stempel, A. V., Stumpf, A., Zhang, H. Y., Özdoğan, T., Pannasch, U., Theis, A. K., Otte, D. M., Wojtalla, A., Rácz, I., Ponomarenko, A., Xi, Z. X., Zimmer, A., & Schmitz, D. (2016). Cannabinoid Type 2 Receptors Mediate a Cell Type-Specific Plasticity in the Hippocampus. *Neuron*, *90*(4), 795–809. https://doi.org/10.1016/j.neuron.2016.03.034

Streit, W. J., & Xue, Q. S. (2014). Human CNS immune senescence and neurodegeneration. *Current Opinion in Immunology*, *29*(1), 93–96. https://doi.org/10.1016/j.coi.2014.05.005

Stumpf, A., Parthier, D., Sammons, R. P., Stempel, A. V., Breustedt, J., Rost, B. R., & Schmitz, D. (2018). Cannabinoid type 2 receptors mediate a cell type-specific self-inhibition in cortical neurons. *Neuropharmacology*, *139*, 217–225. https://doi.org/10.1016/j.neuropharm.2018.07.020

Subramanian, J., Michel, K., Benoit, M., & Nedivi, E. (2019). CPG15/Neuritin Mimics

Experience in Selecting Excitatory Synapses for Stabilization by Facilitating PSD95 Recruitment. *Cell Reports*, *28*(6), 1584-1595.e5. https://doi.org/10.1016/j.celrep.2019.07.012

Tanaka, J. I., Horiike, Y., Matsuzaki, M., Miyazaki, T., Ellis-Davies, G. C. R., & Kasai, H. (2008). Protein synthesis and neurotrophin-dependent structural plasticity of single dendritic spines. *Science*, *319*(5870), 1683–1687. https://doi.org/10.1126/science.1152864

Tang, Y., & Le, W. (2016). Differential Roles of M1 and M2 Microglia in Neurodegenerative Diseases. *Molecular Neurobiology*, *53*(2), 1181–1194. https://doi.org/10.1007/s12035-014-9070-5

Tapia-Arancibia, L., Aliaga, E., Silhol, M., & Arancibia, S. (2008). New insights into brain BDNF function in normal aging and Alzheimer disease. *Brain Research Reviews*, *59*(1), 201–220. https://doi.org/10.1016/j.brainresrev.2008.07.007

Terry, R. D., Masliah, E., Salmon, D. P., Butters, N., Deteresa, R., Hill, R., Hansen, L. A., & Katzman, R. (1991). Physical Basis of Cognitive Alterations in Major Correlate of Cognitive Impairment Alzheimer's Disease: Synapse Loss Is the Major Correlate of Cognitive Impairment. *Annals of Neurology*, *4*, 572–580.

Tjia, M., Yu, X., Jammu, L. S., Lu, J., & Zuo, Y. (2017). Pyramidal neurons in different cortical layers exhibit distinct dynamics and plasticity of apical dendritic spines. *Frontiers in Neural Circuits*, *11*(June), 1–10. https://doi.org/10.3389/fncir.2017.00043

Tønnesen, J., Katona, G., Rózsa, B., & Nägerl, U. V. (2014). Spine neck plasticity regulates compartmentalization of synapses. *Nature Neuroscience*, *17*(5), 678–685. https://doi.org/10.1038/nn.3682

Trachtenberg, J. T., Chen, B. E., Knott, G. W., Feng, G., Sanes, J. R., Walker, E., & Svoboda, K. (2002). Long-term in vivo imaging of experience-dependent synaptic plasticity in adult cortex. *Nature*, *420*(19/26). https://doi.org/10.1111/j.1528-1157.1986.tb03495.x

Tremblay, M. É. (2012). The role of microglia at synapses in the healthy CNS: Novel insights from recent imaging studies. *Neuron Glia Biology*, *7*(1), 67–76. https://doi.org/10.1017/S1740925X12000038

Tremblay, M. Ě., Lowery, R. L., & Majewska, A. K. (2010). Microglial interactions with synapses are modulated by visual experience. *PLoS Biology*, *8*(11). https://doi.org/10.1371/journal.pbio.1000527

Uchigashima, M., Narushima, M., Fukaya, M., Katona, I., Kano, M., & Watanabe, M. (2007).

Subcellular arrangement of molecules for 2-arachidonoyl-glycerol-mediated retrograde signaling and its physiological contribution to synaptic modulation in the striatum. *Journal of Neuroscience*, *27*(14), 3663–3676. https://doi.org/10.1523/JNEUROSCI.0448-07.2007

Van Sickle, M. D., Duncan, M., Kingsley, P. J., Mouihate, A., Urbani, P., Mackie, K., Stella, N., Makriyannis, A., Piomelli, D., Davison, J. S., Marnett, L. J., Di Marzo, V., Pittman, Q. J., Patel, K. D., & Sharkey, K. A. (2005). Neuroscience: Identification and functional characterization of brainstem cannabinoid CB2 receptors. *Science*, *310*(5746), 329–332. https://doi.org/10.1126/science.1115740

Villa, K. L., Berry, K. P., Subramanian, J., Cha, J. W., Oh, W. C., Kwon, H. B., Kubota, Y., So, P. T. C., & Nedivi, E. (2016). Inhibitory Synapses Are Repeatedly Assembled and Removed at Persistent Sites In Vivo. *Neuron*, *89*(4), 756–769. https://doi.org/10.1016/j.neuron.2016.01.010

Villeda, S. A., Luo, J., Mosher, K. I., Zou, B., Britschgi, M., Bieri, G., Stan, T. M., Fainberg, N., Ding, Z., Eggel, A., Lucin, K. M., Czirr, E., Park, J. S., Couillard-Després, S., Aigner, L., Li, G., Peskind, E. R., Kaye, J. A., Quinn, J. F., … Wyss-Coray, T. (2011). The ageing systemic milieu negatively regulates neurogenesis and cognitive function. *Nature*, *477*(7362), 90–96. https://doi.org/10.1038/nature10357

Wagner, E. J. (2016). Sex differences in cannabinoid-regulated biology: A focus on energy homeostasis. *Frontiers in Neuroendocrinology*, *40*(January), 101–109. https://doi.org/10.1016/j.yfrne.2016.01.003

Wake, H., Moorhouse, A. J., Jinno, S., Kohsaka, S., & Nabekura, J. (2009). Resting microglia directly monitor the functional state of synapses in vivo and determine the fate of ischemic terminals. *Journal of Neuroscience*, *29*(13), 3974–3980. https://doi.org/10.1523/JNEUROSCI.4363-08.2009

Walker, C. K., & Herskowitz, J. H. (2020). Dendritic Spines : Mediators of Cognitive Resilience in Aging and Alzheimer ' s Disease. *The Neuroscientist*. https://doi.org/10.1177/1073858420945964

Wang, C., Yue, H., Hu, Z., Shen, Y., Li, J., Wang, X., Wang, L., Sun, B., Shi, P., Wang, L., & Gu, Y. (2020). *Microglia mediate forgetting via complement- dependent synaptic elimination*. *367*, 688–694.

Wang, F., Flanagan, J., Su, N., Wang, L. C., Bui, S., Nielson, A., Wu, X., Vo, H. T., Ma, X. J., &

Luo, Y. (2012). RNAscope: A novel in situ RNA analysis platform for formalin-fixed, paraffin-embedded tissues. *Journal of Molecular Diagnostics*, *14*(1), 22–29. https://doi.org/10.1016/j.jmoldx.2011.08.002

Weinhard, L., Di Bartolomei, G., Bolasco, G., Machado, P., Schieber, N. L., Neniskyte, U., Exiga, M., Vadisiute, A., Raggioli, A., Schertel, A., Schwab, Y., & Gross, C. T. (2018). Microglia remodel synapses by presynaptic trogocytosis and spine head filopodia induction. *Nature Communications*, *9*(1). https://doi.org/10.1038/s41467-018-03566-5

Welch, K. A., McIntosh, A. M., Job, D. E., Whalley, H. C., Moorhead, T. W., Hall, J., Owens, D. G. C., Lawrie, S. M., & Johnstone, E. C. (2011). The impact of substance use on brain structure in people at high risk of developing schizophrenia. *Schizophrenia Bulletin*, *37*(5), 1066–1076. https://doi.org/10.1093/schbul/sbq013

Wes, P. D., Holtman, I. R., Boddeke, E. W. G. M., Möller, T., & Eggen, B. J. L. (2016). Next generation transcriptomics and genomics elucidate biological complexity of microglia in health and disease. *Glia*, *64*(2), 197–213. https://doi.org/10.1002/glia.22866

White, M. C., Holman, D. M., Boehm, J. E., Peipins, L. A., Grossman, M., & Jane Henley, S. (2014). Age and cancer risk: A potentially modifiable relationship. *American Journal of Preventive Medicine*, *46*(3 SUPPL. 1), 1–16. https://doi.org/10.1016/j.amepre.2013.10.029

Wilson, R. I., & Nicoll, R. A. (2001). Endogenous cannabinoids mediate retrograde signalling at hippocampal synapses. *Nature*, *410*(6828), 588–592. https://doi.org/10.1038/35069076

Wilson, Rachel I., Kunos, G., & Nicoll, R. A. (2001). Presynaptic specificity of endocannabinoid signaling in the hippocampus. *Neuron*, *31*(3), 453–462. https://doi.org/10.1016/S0896-6273(01)00372-5

Xing, G., Carlton, J., Jiang, X., Wen, J., Jia, M., & Li, H. (2014). Differential expression of brain cannabinoid receptors between repeatedly stressed males and females may play a role in age and gender-related difference in traumatic brain injury: Implications from animal studies. *Frontiers in Neurology*, *5 AUG*(August), 1–12. https://doi.org/10.3389/fneur.2014.00161

Xu, H. T., Pan, F., Yang, G., & Gan, W. B. (2007). Choice of cranial window type for in vivo imaging affects dendritic spine turnover in the cortex. *Nature Neuroscience*, *10*(5), 549–551. https://doi.org/10.1038/nn1883

Xu, T., Yu, X., Perlik, A. J., Tobin, W. F., Zweig, J. A., Tennant, K., Jones, T., & Zuo, Y. (2009). Rapid formation and selective stabilization of synapses for enduring motor memories. *Nature*, *462*(7275), 915–919. https://doi.org/10.1038/nature08389

Yagishita, S., Hayashi-Takagi, A., Ellis-Davies, G. C. R., Urakubo, H., Ishii, S., & Kasai, H. (2014). A critical time window for dopamine actions on the structural plasticity of dendritic spines. *Science*, *345*(6204), 1616–1620. https://doi.org/10.1126/science.1255514

Yang, G., Lai, C. S. W., Cichon, J., Ma, L., Li, W., & Gan, W.-B. (2014). Sleep promotes branch-specific formation of dendritic spines after learning. *Science*, *344*(6188), 1173–1178. http://www.ncbi.nlm.nih.gov/pubmed/24904169%5Cnhttp://www.pubmedcentral.nih.gov/articlerender.fcgi?artid=PMC4447313

Yang, G., Pan, F., & Gan, W. B. (2009). Stably maintained dendritic spines are associated with lifelong memories. *Nature*, *462*(7275), 920–924. https://doi.org/10.1038/nature08577

Yang, M., & Crawley, J. N. (2009). Simple Behavioral Assessment of Mouse Olfaction Mouse Olfaction. *Current Protocols in Neuroscience*, *CHAPTER: Unit–8.24*, 1–14. https://doi.org/10.1002/0471142301

Yang, Y., Wang, X., Frerking, M., & Zhou, Q. (2008). Spine Expansion and Stabilization Associated with Long- Term Potentiation. *The Journal of Neuroscience*, *28*(22), 5740–5751. https://doi.org/10.1523/JNEUROSCI.3998-07.2008

Yasumatsu, N., Matsuzaki, M., Miyazaki, T., Noguchi, J., & Kasai, H. (2008). Principles of long-term dynamics of dendritic spines. *Journal of Neuroscience*, *28*(50), 13592–13608. https://doi.org/10.1523/JNEUROSCI.0603-08.2008

Young, M. E., Ohm, D. T., Dumitriu, D., Rapp, P. R., & Morrison, J. H. (2014). Differential effects of aging on dendritic spines in visual cortex and prefrontal cortex of the rhesus monkey. *Neuroscience*, *274*, 33–43. https://doi.org/10.1016/j.neuroscience.2014.05.008.Differential

Yuste, R., Majewska, A., & Holthoff, K. (2000). From form to function: Calcium compartmentalization in dendritic spines. *Nature Neuroscience*, *3*(7), 653–659. https://doi.org/10.1038/76609

Zhan, Y., Paolicelli, R. C., Sforazzini, F., Weinhard, L., Bolasco, G., Pagani, F., Vyssotski, A. L., Bifone, A., Gozzi, A., Ragozzino, D., & Gross, C. T. (2014). Deficient neuron-microglia signaling results in impaired functional brain connectivity and social behavior. *Nature Neuroscience*, *17*(3), 400–406. https://doi.org/10.1038/nn.3641

Zhang, H.-Y., Gao, M., Liu, Q.-R., Bi, G.-H., Li, X., Yang, H.-J., Gardner, E. L., Wu, J., & Xi, Z.-X. (2014). Cannabinoid CB $_2$ receptors modulate midbrain dopamine neuronal activity and dopamine-related behavior in mice. *Proceedings of the National Academy of Sciences*, *111*(46), E5007–E5015. https://doi.org/10.1073/pnas.1413210111

Zhang, H. Y., Bi, G. H., Li, X., Li, J., Qu, H., Zhang, S. J., Li, C. Y., Onaivi, E. S., Gardner, E. L., Xi, Z. X., & Liu, Q. R. (2015). Species differences in cannabinoid receptor 2 and receptor responses to cocaine self-administration in mice and rats. *Neuropsychopharmacology*, *40*(4), 1037–1051. https://doi.org/10.1038/npp.2014.297

Zhang, Hai-ying, Gao, M., Shen, H., Bi, G., Yang, H., Liu, Q., Wu, J., Gardner, E. L., Bonci, A., Xi, Z., Targets, M., Branch, M. D., & Section, P. (2017). Expression of Functional Cannabinoid CB2 Receptor in VTA Dopamine Neurons in Rats. *Addict Biol.*, *22*(3), 752–765. https://doi.org/10.1111/adb.12367.Expression

Zhang, Hai ying, Shen, H., Jordan, C. J., Liu, Q. rong, Gardner, E. L., Bonci, A., & Xi, Z. xiong. (2019). CB 2 receptor antibody signal specificity: correlations with the use of partial CB 2 -knockout mice and anti-rat CB 2 receptor antibodies. *Acta Pharmacologica Sinica*, *40*(3), 398–409. https://doi.org/10.1038/s41401-018-0037-3

Zhao, X., Liao, Y., Morgan, S., Mathur, R., Feustel, P., Mazurkiewicz, J., Qian, J., Chang, J., Mathern, G. W., Adamo, M. A., Ritaccio, A. L., Gruenthal, M., Zhu, X., & Huang, Y. (2018). Noninflammatory Changes of Microglia Are Sufficient to Cause Epilepsy. *Cell Reports*, *22*(8), 2080–2093. https://doi.org/10.1016/j.celrep.2018.02.004

Zhao, Z., Soria-Gómez, E., Varilh, M., Julio-Kalajzić, F., Cannich, A., Castiglione, A., Vanhoutte, L., Duveau, A., Zizzari, P., Beyeler, A., Cota, D., Bellocchio, L., Busquets-Garcia, A., & Marsicano, G. (2019). Top-down control of water intake by the endocannabinoid system. *BioRxiv*, *33*(0), 1–40. https://doi.org/10.1101/729970

Zhou, Q., Homma, K. J., & Poo, M. M. (2004). Shrinkage of dendritic spines associated with long-term depression of hippocampal synapses. *Neuron*, *44*(5), 749–757. https://doi.org/10.1016/j.neuron.2004.11.011

Ziv, N. E., & Smith, S. J. (1996). Evidence for a role of dendritic filopodia in synaptogenesis and spine formation. *Neuron*, *17*(1), 91–102.

Ziv, Y., & Schwartz, M. (2008). Immune-based regulation of adult neurogenesis: Implications for learning and memory. *Brain, Behavior, and Immunity*, *22*(2), 167–176. https://doi.org/10.1016/j.bbi.2007.08.006

Zuo, Y., Yang, G., Kwon, E., & Gan, W. B. (2005). Long-term sensory deprivation prevents dendritic spine loss in primary somatosensory cortex. *Nature*, *436*(7048), 261–265. https://doi.org/10.1038/nature03715

10. Appendix

10.1. Detailed statistics table

		Statistical test		Post hoc test	
Figure	**Panel**	**Test name**	**result**	**Test name**	**result**
3.1. Basic behaviors	**3.1b:** 3-month old	RM Anova (Mixed-effects model (REML))	time: "F (18, 89) = 66.39", p < 0.0001; treatment "F (1, 5) = 0.7080", p = 0.4385	Šídák's multiple comparisons test	-
	3.1b: 18-month old	RM Anova (Mixed-effects model (REML))	time "F (18, 264) = 9.215", p < 0.0001; treatment "F (1, 16) = 0.1900, p = 0.6687"	Šídák's multiple comparisons test	-
3.2. Long-term low-dosage THC-treatment increases spine density in old, but not in young mice.	**3.2b:** 3-month old	RM Anova (Mixed-effects model (REML))	time "F (14, 181) = 1.941", p = 0.0249; treatment "F (1, 19) = 0.1795", p = 0.6765; time x treatment "F (14, 181) = 3.324", p <0.0001	Šídák's multiple comparisons test	-
	3.2b: 18-month old	RM Anova (Mixed-effects model (REML))	treatment "F (1, 38) = 12.37", p = 0.0011; time x treatment "F (14, 410) = 5.152", p <0.0001	Šídák's multiple comparisons test	day 25 p = 0.0146; day 35 p = 0.0031; day 42 p = 0.0085; day 49 p <0.0001; day 56 <0.0001
3.3. Spine dynamics changes	**3.3a:** density dynamic spines	RM Anova (Mixed-effects model (REML))	time "F (9, 117) = 3.664", p = 0.0005; treatment "F (1, 20) = 10.11", p = 0.0047; time x treatment "F (9, 117) = 2.793", p = 0.0053	Šídák's multiple comparisons test	day 7 p = 0.0007; day 10 p = 0.0005; day 13 p =0.0020
	3.3a: Turnover ratio	RM Anova (Mixed-effects model (REML))	time "F (9, 118) = 4.423", p < 0.0001; treatment "F (1, 20) = 13.41", p = 0.0016; time x treatment "F (9, 118) = 2.593", p = 0.0091	Šídák's multiple comparisons test	day 7 p = 0.0001; day 10 p = 0.0005; day 13 p = 0.0014
	3.3b: lost spines	RM Anova (Mixed-effects model (REML))	time "F (9, 118) = 2.078", p = 0.0368; treatment "F (1, 20) = 13.45", p = 0.0015; time x treatment "F (9, 118) = 1.373", p = 0.2078	Šídák's multiple comparisons test	day 10 p = 0.0087; day 13 p = 0.0020
	3.3b: gained spines	RM Anova (Mixed-effects model (REML))	time "F (9, 118) = 3.572", p = 0.0006; treatment "F (1, 20) = 9.914", p = 0.0051; time x treatment "F (9, 118) = 2.565", p = 0.0099	Šídák's multiple comparisons test	day 7 p <0.0001; day 10 p = 0.0358

		Statistical test		Post hoc test	
Figure	**Panel**	**Test name**	**result**	**Test name**	**result**
	3.3: stable spines	RM Anova (Mixed-effects model (REML))	time "F (9, 118) = 2.078", p = 0.0368; treatment "F (1, 20) = 13.45", p = 0.0015; time x treatment "F (9, 118) = 1.373", p = 0.2078	Šídák's multiple comparisons test	day 10 p = 0.0087; day 13 p = 0.0020
	3.3b: transient spines	RM Anova (Mixed-effects model (REML))	time "F (9, 108) = 4.509", p <0.0001; treatment "F (1, 19) = 12.93", p = 0.0019; time x treatment "F (9, 108) = 2.944", p = 0.0036	Šídák's multiple comparisons test	day 7 p <0.0001; day 10 p = 0.0254
	3.3c: density dynamic spines	RM Anova (Mixed-effects model (REML))	time "F (9, 272) = 2.190", p = 0.0230; treatment "F (1, 37) = 4.118", p = 0.0497	Šídák's multiple comparisons test	-
	3.3c: Turnover ratio	RM Anova (Mixed-effects model (REML))	time "F (9, 272) = 2.937", p = 0.0024; treatment "F (1, 37) = 5.763", 0.0215; time x treatment "F (9, 272) = 1.141", p = 0.3339	Šídák's multiple comparisons test	day 16 p = 0.0459
	3.3d: lost spines	RM Anova (Mixed-effects model (REML))	treatment "F (1, 37) = 6.495", p = 0.0151	Šídák's multiple comparisons test	day 25 p =0.0477
	3.3d: gained spines	RM Anova (Mixed-effects model (REML))	time "F (9, 272) = 2.327", p = 0.0154; treatment "F (1, 37) = 4.573", 0.0392	Šídák's multiple comparisons test	day 28 p = 0.0346
	3.3d: stable spines	RM Anova (Mixed-effects model (REML))	treatment "F (1, 37) = 6.495", p = 0.0151	Šídák's multiple comparisons test	day 25 p =0.0477
	3.3d: transient spines	RM Anova (Mixed-effects model (REML))	time "F (9, 250) = 2.134", p = 0.0273; treatment "F (1, 37) = 7.381", p = 0.0100	Šídák's multiple comparisons test	day 28 p = 0.0499
3.4. Long-term low-dosage THC-treatment differently alters synaptic dynamics in old and young mice even after	**3.4a:** Turnover ratio	RM Anova (Mixed-effects model (REML))	time "F (13, 167) = 4.361", p <0.0001; treatment "F (1, 20) = 11.11", p = 0.0033; time x treatment "F (13, 167) = 2.234", p = 0.0102	Šídák's multiple comparisons test	day 7 p = 0.0003; day 10 p = 0.0008; day 13 p = 0.0027
	3.4a: lost spines	RM Anova (Mixed-effects model (REML))	time "F (13, 167) = 2.726", p = 0.0016; treatment "F (1, 20) = 9.372", p = 0.0062; time x treatment "F (13, 167) = 2.584", p = 0.0028	Šídák's multiple comparisons test	day 10 p =0.0128; day 13 p =0.0028

		Statistical test		Post hoc test	
Figure	**Panel**	**Test name**	**result**	**Test name**	**result**
treatment termination.	**3.4a:** gained spines	RM Anova (Mixed-effects model (REML))	time "F (13, 167) = 3.480", p <0.0001; treatment "F (1, 20) = 10.19", p = 0.0046; time x treatment "F (13, 167) = 3.674", p <0.0001	Šídák's multiple comparisons test	day 7 <0.0001; day 35 p = 0.0002
	3.4b: Turnover ratio	RM Anova (Mixed-effects model (REML))	time "F (13, 351) = 4.844", p <0.0001; treatment "F (1, 37) = 4.551", p = 0.0396	Šídák's multiple comparisons test	-
	3.4b: lost spines	RM Anova (Mixed-effects model (REML))	time "F (13, 351) = 2.533", p = 0.0024; treatment "F (1, 37) = 6.611", p = 0.0143	Šídák's multiple comparisons test	-
	3.4b: gained spines	RM Anova (Mixed-effects model (REML))	time "F (13, 351) = 3.153", p = 0.0002	Šídák's multiple comparisons test	day 28 p = 0.0454
3.5. THC treatment decreases spine survival in 3-month old mice.	First panel from the top (day -1)	RM Anova (Mixed-effects model (REML))	time "F (12, 133) = 154.4", p <0.0001 , time x treatment "F (12, 133) = 2.161", p = 0.0170	Šídák's multiple comparisons test	-
	First panel from the top (day 7)	RM Anova (Mixed-effects model (REML))	time "F (11, 146) = 173.0", p <0.0001; treatment "F (1, 17) = 7.344", p = 0.0149; time x treatment "F (11, 146) = 3.945", p <0.0001	Šídák's multiple comparisons test	day 13 p = 0.0122; day 16 p = 0.0075; day 19 p = 0.0049; day 22 p = 0.0195; day 25 p = 0.0425
	First panel from the top (day 10)	RM Anova (Mixed-effects model (REML))	time "F (10, 123) = 154.3", p <0.0001; treatment "F (1, 17) = 5.321", p = 0.0339; time x treatment "F (10, 123) = 2.759", p = 0.0042	Šídák's multiple comparisons test	-
	First panel from the top (day 13)	RM Anova (Mixed-effects model (REML))	time "F (9, 115) = 139.6", p <0.0001 , time x treatment "F (9, 115) = 2.385", p = 0.0163	Šídák's multiple comparisons test	-
	First panel from the top (day 16)	RM Anova (Mixed-effects model (REML))	time "F (8, 106) = 188.8", p <0.0001	Šídák's multiple comparisons test	-
	First panel from the top (day 28)	RM Anova (Mixed-effects model (REML))	time "F (4, 46) = 166.1", p <0.0001	Šídák's multiple comparisons test	-

		Statistical test		Post hoc test	
Figure	**Panel**	**Test name**	**result**	**Test name**	**result**
	First panel from the top (day 42)	RM Anova (Mixed-effects model (REML))	time "F (2, 22) = 146.7", p <0.0001	Šídák's multiple comparisons test	-
3.6. THC treatment decreases spine survival of gained spines in 3-month old mice.	First panel from the top (day -1)	RM Anova (Mixed-effects model (REML))	time "F (12, 134) = 58.56", p <0.0001	Šídák's multiple comparisons test	-
	First panel from the top (day 10)	RM Anova (Mixed-effects model (REML))	time "F (10, 120) = 164.6", p <0.0001; treatment "F (1, 16) = 7.438", p = 0.0149	Šídák's multiple comparisons test	day 13 p = 0.0023
	First panel from the top (day 13)	RM Anova (Mixed-effects model (REML))	time "F (9, 106) = 110.1", p <0.0001; treatment "F (1, 14) = 5.976", p = 0.0283; time x treatment "F (9, 106) = 3.582", p = 0.0006	Šídák's multiple comparisons test	day 22 p = 0.0113; day 25 p = 0.0190; day 28 p = 0.0109
	First panel from the top (day 16)	RM Anova (Mixed-effects model (REML))	time "F (1.674, 15.07) = 41.79", p <0.0001	Šídák's multiple comparisons test	-
	First panel from the top (day 22)	RM Anova (Mixed-effects model (REML))	time "F (6, 72) = 160.8", p <0.0001	Šídák's multiple comparisons test	-
	First panel from the top (day 28)	RM Anova (Mixed-effects model (REML))	time "F (4, 46) = 178.7", p <0.0001	Šídák's multiple comparisons test	-
	First panel from the top (day 42)	RM Anova (Mixed-effects model (REML))	time "F (2, 20) = 229.6", p <0.0001	Šídák's multiple comparisons test	-
3.7. THC treatment increases spine survival in 18-month old mice.	First panel from the top (day -1)	RM Anova (Mixed-effects model (REML))	time "F (12, 347) = 221.4", p <0.0001; treatment "F (1, 37) = 7.980", p = 0.0076; time x treatment "F (12, 347) = 2.754", p = 0.0014	Šídák's multiple comparisons test	day 10 p = 0.0114; day 19 p = 0.0455
	First panel from the top (day 7)	RM Anova (Mixed-effects model (REML))	time "F (11, 282) = 438.6", p <0.0001; treatment "F (1, 34) = 7.972", p = 0.0079; time x treatment "F (11, 282) = 2.699", p = 0.0025	Šídák's multiple comparisons test	day 19 p = 0.0443; day 25 p = 0.0186; day 49 p = 0.0298

		Statistical test		Post hoc test	
Figure	**Panel**	**Test name**	**result**	**Test name**	**result**
	First panel from the top (day 10)	RM Anova (Mixed-effects model (REML))	time "F (10, 235) = 363.7", p <0.0001; treatment "F (1, 31) = 4.517", p = 0.0416	Šídák's multiple comparisons test	-
	First panel from the top (day 13)	RM Anova (Mixed-effects model (REML))	time "F (9, 221) = 379.9", p <0.0001; treatment "F (1, 34) = 5.125", p = 0.0301; time x treatment "F (9, 221) = 2.071", p = 0.0332	Šídák's multiple comparisons test	-
	First panel from the top (day 16)	RM Anova (Mixed-effects model (REML))	time "F (8, 213) = 311.7", p <0.0001; treatment "F (1, 34) = 5.508", p = 0.0249; time x treatment "F (8, 213) = 2.434", p = 0.0154	Šídák's multiple comparisons test	day 25 p = 0.0344
	First panel from the top (day 28)	RM Anova (Mixed-effects model (REML))	time "F (4, 82) = 293.8", p <0.0001; treatment "F (1, 30) = 6.530", p = 0.0159; time x treatment "F (4, 82) = 2.965", p = 0.0243	Šídák's multiple comparisons test	day 49 p = 0.0094
	First panel from the top (day 42)	RM Anova (Mixed-effects model (REML))	time "F (2, 33) = 288.6", p <0.0001; treatment "F (1, 20) = 4.485", p = 0.0469	Šídák's multiple comparisons test	-
3.8. THC treatment increases spine survival of gained spines in 18-month old mice.	First panel from the top (day -1)	RM Anova (Mixed-effects model (REML))	time "F (12, 305) = 229.6", p <0.0001	Šídák's multiple comparisons test	-
	First panel from the top (day 10)	RM Anova (Mixed-effects model (REML))	time "F (10, 209) = 268.9", p <0.0001; treatment"F (1, 28) = 5.146", p = 0.0312; time x treatment "F (10, 209) = 3.506", p = 0.0003	Šídák's multiple comparisons test	day 13 p <0.0001; day 16 p = 0.0091
	First panel from the top (day 13)	RM Anova (Mixed-effects model (REML))	time "F (9, 196) = 279.8", p <0.0001	Šídák's multiple comparisons test	
	First panel from the top (day 16)	RM Anova (Mixed-effects model (REML))	time "F (8, 190) = 87.03", p <0.0001	Šídák's multiple comparisons test	-
	First panel from the top (day 22)	RM Anova (Mixed-effects model (REML))	time "F (6, 145) = 357.4", p <0.0001	Šídák's multiple comparisons test	-

		Statistical test		Post hoc test	
Figure	**Panel**	**Test name**	**result**	**Test name**	**result**
	First panel from the top (day 28)	RM Anova (Mixed-effects model (REML))	time "F (4, 82) = 285.4", p <0.0001	Šídák's multiple comparisons test	-
	First panel from the top (day 42)	RM Anova (Mixed-effects model (REML))	time "F (2, 33) = 297.0", p <0.0001	Šídák's multiple comparisons test	-
3.10. THC effect does not depend on the initial spine density or weight of the animals	**3.10a:** Correlation of turnover at day 7 to initial spine denisty	Pearson	vehicle r = 0.3878, p = 0.3025; THC r = -0.1764, p = 0.7051		
	3.10a: Correlation of turnover at day 10 to initial spine denisty	Pearson	vehicle r = 0.4856, p = 0.1548; THC r = 0.1775, p = 0.6478		
	3.10b: Correlation of turnover at day 10 to initial weight	Pearson	vehicle r = -0.1009, p = 0.8991; THC r = 0.6302, p = 0.3698		
	3.10c: Correlation of density % at day 35 to initial spine denisty	Pearson	vehicle r = -0.4404, p = 0.1519; THC r = -0.4873, p = 0.0555		
	3.10c: Correlation of density % at day 56 to initial spine denisty	Pearson	vehicle r = -0.1337, p = 0.7316; THC r = -0.6672, p = 0.0707		

		Statistical test		Post hoc test	
Figure	**Panel**	**Test name**	**result**	**Test name**	**result**
	3.10d: Correlation of denisty % at day 35 to initial weight	Spearman	vehicle r = -0.08571, p = 0.9194; THC r = -0.02395, p = 0.9640		
3.11. THC treated 18-month old mice resemble 3-month old mice on the level of spine dynamics	**3.11a:** density of spines	unpaired t-test	all vs Vehicle: p = 0.0075; Vehicle vs THC p = 0.0260; all vs THC p <0.0001		
	3.11b: Turnover ratio	unpaired t-test	all vs Vehicle: p = 0.0001; Vehicle vs THC p = 0.0292; all vs THC p = 0.0291		
	3.11c: lost spines	unpaired t-test	all vs Vehicle: p = 0.0010; Vehicle vs THC p = 0.0445; all vs THC p = 0.0780		
	3.11d: gained spines	unpaired t-test	all vs Vehicle: p = 0.0007; Vehicle vs THC p = 0.0522; all vs THC p = 0.0333		
	3.11e: transient spines	unpaired t-test	all vs Vehicle: p = 0.0810; Vehicle vs THC p = 0.0545; all vs THC p = 0.6957		
	3.11f: stable spines	unpaired t-test	all vs Vehicle: p = 0.0013; Vehicle vs THC p = 0.0445; all vs THC p = 0.1063		
	3.11g: gained spines	RM Anova (Mixed-effects model (REML))	3-month vehicle vs 18-month vehicle: time "F (10, 145) = 174.7", p <0.0001; age "F (1, 22) = 8.760", p = 0.0072; time x age "F (10, 145) = 2.049", p = 0.0324	Šídák's multiple comparisons test	day 13 p <0.0001
		RM Anova (Mixed-effects model (REML))	3-month vehicle vs 18-month THC: time "F (10, 160) = 181.9", p <0.0001; age "F (1, 22) = 0.6486", p = 0.4292; time x age "F (10, 160) = 1.386", p =0.1911	Šídák's multiple comparisons test	-
	3.11g: present spines	RM Anova (Mixed-effects model (REML))	3-month vehicle vs 18-month vehicle: time "F (10, 209) = 268.9", p <0.0001; age "F (1, 23) = 7.448", p = 0.0120; time x age "F (10, 154) = 2.568", p = 0.0067	Šídák's multiple comparisons test	day 25 p = 0.0199

		Statistical test		Post hoc test	
Figure	**Panel**	**Test name**	**result**	**Test name**	**result**
		RM Anova (Mixed-effects model (REML))	3-month vehicle vs 18-month THC: time "F (10, 177) = 232.5", p <0.0001; age "F (1, 24) = 1.561", p = 0.2236; time x age "F (10, 177) = 0.8534", p = 0.5780	Šídák's multiple comparisons test	-
3.14. THC treatment does not change microglia density	**3.14b:** cortex: microglia cell denisty	two-way ANOVA	layer "F (3, 116) = 6.841", p = 0.0003		
	3.14b: cortex: % of area covered	two-way ANOVA	layer "F (3, 116) = 12.08", p <0.0001		
	3.14c: CA1: microglia cell denisty	two-way ANOVA	layer "F (3, 120) = 8.252", p <0.0001		
	3.14d. CA3: microglia cell denisty	two-way ANOVA	layer "F (3, 116) = 2.638", p = 0.0529		
3.17. THC treatment decreased the colocalization of GFP x Iba1 in dendrites with higher spine density	**3.17b:** left panel	two-way ANOVA	treatment "F (1, 101) = 9.763", p = 0.0023	Šídák's multiple comparisons test	0.6 p = 0.0007
	3.17b: right panel	two-way ANOVA	treatment "F (1, 113) = 7.148", p = 0.0086; bin x treatment "F (1, 113) = 7.182", p = 0.0085	Šídák's multiple comparisons test	>=0.6 p = 0.0002
3.18. Repeated imaging and testing decrease mice sociability and thus prevents a proper assessment of memory performance.	**3.18c:** sociability: 3-month old	one-sample t-test (hypothetical mean = 50)	vehicle PR1 p =0.0413; THC PR1 p = 0.0529; THC PR3 p = 0.0055; Veh+THC PR1 p = 0.0027; veh+THC PR2 p = 0.0394		
	3.18c: sociability: 18-month old	one-sample t-test (hypothetical mean = 50)	Vehicle PR1 p = 0.0010; THC PR5 p = 0.0417; veh+THC PR1 p = 0.0009		
	3.18d: novelty preference: 3-month old	one-sample t-test (hypothetical mean = 50)	vehicle PR1 = 0.0160; veh+THC PR1 p = 0.0050; veh+THC PR2 p = 0.0243		

		Statistical test		Post hoc test	
Figure	**Panel**	**Test name**	**result**	**Test name**	**result**
	3.18d: novelty preference: 18-month old	one-sample t-test (hypothetical mean = 50)	vehicle PR1 = 0.0010; vehicle PR2 = 0.0222; vehicle PR3 = 0.0053; veh+THC PR1 p = 0.0197; veh+THC PR2 p = 0.0153		
	3.18d: novelty preference: 18-month old (without mice with sociability <50%)	one-sample t-test (hypothetical mean = 50)	vehicle PR1 p = 0.0003; veh+THC p = 0.0385		
	3.18f: interaction time: 18-month old	two-way ANOVA	time "F (4, 115) = 3.993", p = 0.0045		
	3.18g: distance: 18-month old	two-way ANOVA	time "F (4, 115) = 4.878", p = 0.0011	Šídák's multiple comparisons test	Vehicle PR1-PR2 p = 0.0435
6.1. Age-dependent alterations in basic behaviours after CB2R-/- deletion.	**6.1b:** 12-month old group	two-way ANOVA	genotype "F (1, 189) = 24.51", p <0.0001	Šídák's multiple comparisons test	-
	6.1f: home-cage activity	two-way ANOVA	time "F (85, 2210) = 17.76", p <0.0001; time x genotype "F (85, 2210) = 1.293", p = 0.0394	Šídák's multiple comparisons test	17:00 at Day1: p = 0.0280
6.2. CB2R deletion results in a decreased anxiety phenotype in o-maze.	**6.2a:** % of time in the closed compartment	two-way ANOVA	age "F (2, 82) = 10.26", p = 0.0001; genotype "F (1, 82) = 4.427" p = 0.0384	Šídák's multiple comparisons test	WT: 3 vs 18-months: p = 0.0026; CB2R-/-: 3 vs 12 months: p = 0.0372; 12 vs 18-months: p = 0.0306
	6.2b: distance travelled in the open compartment	two-way ANOVA	age "F (2, 82) = 17.00", p <0.0001; genotype "F (1, 82) = 7.009" p = 0.0097	Šídák's multiple comparisons test	WT: 3 vs 18-months: p = 0.0004; CB2R-/-: 3 vs 12 months: p = 0.0012; 3 vs 18-months: p = 0.0007
	6.2c: head dips behavior	two-way ANOVA	genotype "F (1, 81) = 33.24" p <0.0001	Šídák's multiple comparisons test	3-month p = 0.0039; 12-month p = 0.0451; 18-

		Statistical test		Post hoc test	
Figure	**Panel**	**Test name**	**result**	**Test name**	**result**
					month p = 0.0002
	6.2d: streched posture behavior	two-way ANOVA	age "F (2, 81) = 4.152", p = 0.0192; genotype "F (1, 81) = 13.24" p = 0.0005	Šídák's multiple comparisons test	CB2R-/-: 12 vs 18-months: p = 0.0083 ;; 3-month p = 0.0071; 18-month p = 0.0072
6.3. CB2R deletion has a moderate age-dependent effect on cognition.	**6.3c:** interaction time in PR test	two-way ANOVA	age "F (2, 78) = 13.51", p <0.0001	Šídák's multiple comparisons test	WT: 3 vs 18-months: p = 0.0007; 12 vs 18-month: p = 0.0286; CB2R-/-: 3 vs 18-month p = 0.0041
	6.3e: 3-month old acquisition	RM ANOVA	time "F (6, 162) = 17.85", p <0.0001		
	6.3e: 3-month old reversal	RM ANOVA	time "F (2, 54) = 8.366", p = 0.0007		
	6.3e: 12-month old acquisition	RM ANOVA	time "F (6, 162) = 35.52", p <0.0001		
	6.3e: 12-month old reversal	RM ANOVA	time "F (2, 54) = 20.04", p <0.0001; time x genotype "F (2, 54) = 3.920", p = 0.0257	Šídák's multiple comparisons test	-
	6.3e: 18-month old acquisition	RM ANOVA	time "F (6, 162) = 33.56", p <0.0001		
	6.3e: 18-month old reversal	RM ANOVA	time "F (2, 54) = 12.82", p <0.0001		
6.5. CB2R deletion decreases social memory in both male and female mice.	**6.5a:** interaction time	two-way ANOVA	gender "F (1, 44) = 13.51", p = 0.0006		CB2R-/- males vs females p = 0.0005
6.6. Sex-specific alterations in basic behaviours after CB2R deletion	**6.6e:** females	RM ANOVA (based on GLM model)	time "F (181, 3801) = 32.71", p <0.0001; genotype x time "F (181, 3801) = 1.234", p = 0.0201		

		Statistical test		Post hoc test	
Figure	**Panel**	**Test name**	**result**	**Test name**	**result**
6.8. Synapsin-I levels are increased in the hippocampus after CB2R deletion in female mice.	**6.8c: females: CA1**	two-way ANOVA	layer "F (2, 171) = 25.16", p < 0.0001; genotype "F (1, 171) = 64.42", p < 0.0001	Šídák's multiple comparisons test	Or p < 0.00001; Pyr p = 0.0013; Sr+Slm p <0.0001
	6.8c: males: CA1	two-way ANOVA	layer "F (2, 75) = 9.820", p = 0.0002		
	6.8c: females: CA2	two-way ANOVA	layer "F (3, 236) = 22.06", p < 0.0001; genotype "F (1, 236) = 102.4", p < 0.0001	Šídák's multiple comparisons test	Luc p < 0.0001; Or p < 0.00001; Pyr p = 0.0002; Sr+Slm p = 0.0019
	6.8c: males: CA2	two-way ANOVA	layer "F (3, 104) = 27.58", p < 0.0001		
	6.8c: females: CA3	two-way ANOVA	layer "F (3, 236) = 51.37", p < 0.0001; genotype "F (1, 236) = 110.2", p < 0.0001; layer x genotype "F (3, 236) = 3.557", p = P=0.0150	Šídák's multiple comparisons test	Luc p < 0.0001; Or p < 0.00001; Pyr p = 0.0008; Sr+Slm p <0.0001
	6.8c: males: CA3	two-way ANOVA	layer "F (3, 104) = 27.58", p < 0.0001		
6.9. Average size of Syn1 particles is increased after CB2R deletion in females.	**6.9b:** females: CA2	two-way ANOVA	layer "F (3, 228) = 31.96", p < 0.0001; genotype "F (1, 228) = 4.343", p = 0.0383	Šídák's multiple comparisons test	-
	6.9b: males: CA2	two-way ANOVA	layer "F (3, 104) = 214.0", p < 0.0001		
	6.9b: females: CA3	two-way ANOVA	layer "F (3, 276) = 43.86", p < 0.0001; genotype "F (1, 276) = 16.07", p < 0.0001	Šídák's multiple comparisons test	Luc p = 0.0112
	6.9b: males: CA3	two-way ANOVA	layer "F (3, 104) = 220.4", p < 0.0001		
6.10. vGLUT1 levels are slightly increased in female CB2R-/- mice.	**6.10c:** females: CA1	two-way ANOVA	layer "F (2, 162) = 130.6", p < 0.0001		
	6.10c: males: CA1	two-way ANOVA	layer "F (2, 78) = 172.2", p < 0.0001		
	6.10c: females: CA2	two-way ANOVA	layer "F (3, 224) = 94.36", p < 0.0001; genotype "F (1, 224) = 6.166", p = 0.0138	Šídák's multiple comparisons test	-
	6.10c: males: CA2	two-way ANOVA	layer "F (3, 104) = 61.08", p < 0.0001		
	6.10c: females: CA3	two-way ANOVA	layer "F (3, 224) = 91.73", p < 0.0001; genotype "F	Šídák's multiple	-

		Statistical test		Post hoc test	
Figure	**Panel**	**Test name**	**result**	**Test name**	**result**
			(1, 224) = 5.725", p = 0.0175	comparisons test	
	6.10c: males: CA3	two-way ANOVA	layer "F (3, 104) = 104.0", p < 0.0001		
6.11. vGAT levels are increased in female CB2R-/- mice, but not in male.	**6.11c:** females: CA1	two-way ANOVA	layer "F (2, 155) = 18.93", p < 0.0001; genotype "F (1, 155) = 36.59", p < 0.0001	Šídák's multiple comparisons test	Or p = 0.0111; Pyr p = 0.0001; Sr+Slm p = 0.0031
	6.11c: males: CA1	two-way ANOVA	layer "F (2, 66) = 8.762", p = 0.0004; genotype "F (1, 66) = 13.55", p = 0.0005	Šídák's multiple comparisons test	Pyr p = 0.0470
	6.11c: females: CA2	two-way ANOVA	layer "F (3, 216) = 17.29", p < 0.0001; genotype "F (1, 216) = 55.13", p < 0.0001	Šídák's multiple comparisons test	Luc p = 0.0141; Or p = 0.0057; Pyr p <0.0001; Sr+Slm p = 0.0017
	6.11c: males: CA2	two-way ANOVA	layer "F (3, 100) = 11.19", p < 0.0001; genotype "F (1, 100) = 3.711", p = 0.0569		
	6.11c: females: CA3	two-way ANOVA	layer "F (3, 216) = 6.922", p = 0.0002; genotype "F (1, 216) = 53.83", p < 0.0001	Šídák's multiple comparisons test	Luc p = 0.0055; Or p = 0.0084; Pyr p <0.0001; Sr+Slm p = 0.0004
	6.11c: males: CA3	two-way ANOVA	layer "F (3, 100) = 2.986", p = 0.0348; genotype "F (1, 100) = 4.463", p = 0.0371		

10.2. Acknowledgments

I would like to thank **Prof. Dr. Andreas Zimmer** for his constant trust, patience and support throughout the years. I was very privileged to be your student and to learn from you. Thank you for making me a better scientist.

I would like to thank my second supervisor **Prof. Dr. Gerhard von der Emde** for his continued support since my master studies. I would like to thank also other members of my thesis advisory committee members - **Prof. Dr. Christian Henneberger** and **Prof. Dr. Ryohei Yasuda,** for their support, time, and great discussions.

I would also like to thank **Prof. Dr. Valentin Stein** for his trust and support. Thank you for believing in me and helping me with all the 'challenges' no matter if big or small.

I would like to thank **Dr. Anne-Kathrin Gellner** for teaching me everything I know about in vivo imaging, but most of all for being a great friend and a supporter. Your humor, people-skills, knowledge, and know-how are very inspiring and made me a better person.

I would like to thank everyone at the **Institute of Molecular Psychiatry**. Thank you for the family-like atmosphere that always made me feel safe and appreciated. For all your good advices, critical discussions and assistance in times of need. I enjoyed my time very much with each one of you! Especially, I would like to thank **Dr. Anne-Caroline Schmöle** for her support and friendship. Thank you for always finding time for me and thank you for all our collaborations. I would like to thank **Dr. Este Leidmaa** for all the discussions – scientific and non-scientific ones and sharing with me her positive vibe. I would like to thank **Dr. Andras Bilkei-Gorzo** for all his cheers and reality-checks. Thank you for your support, honesty and always having time for me. I would like to thank **Hanna Schrage, Edda Erxlebe, Anne Zimmer, Kirsten Krengel** and **Kerstin Nicolai** for their technical support with genotyping and perfusions. I would like to thank **Dr. Eva Drews** for her assistance with animal protocols and all the last-minute corrections of my texts. I would like to thank all the students in the lab, former and present. Especially: **Bolanle Fatima Olabiyi, Lena-Louise Schüle, Alessandra Gargano** and **Michela Palmisano** for lifting up my spirit and keeping me sane throughout the years. I would also like to thank **Kishore Aravind Ravichandran** for his help with the calculation of synaptic stainings (CB_2R project) and help with the calculation of spines (THC in vivo project). I would also like to thank **Kishore** and **Tanushka Rana** for English correction of the thesis.

I would like to thank everyone in the **Institute of Physiology II**. Thank you for making me feel like a part of the lab and not just a visitor. I would also like to thank **Michael Döngi** and **Ulf Einsfelder** for the help with the 2P microscope and **Dorit Glass** and **Isa Lehmann** for the technical assistance.

I would like to thank **International Max Planck Research School for Brain and Behavior**. Especially, **Ezgi Bulca** and **Dr. Paul Evans** for all their assistance and organization of the graduate school events.

I would like to thank all my extended family – **all my friends** from all around the world. Thank you for being there for me during this crazy ride. I would like to especially thank **Eleonora Ambrad Giovannetti, Ilkin Özer** and **Cátia Domingos** for all the mental support, fun adventures and going through this journey together.

Chciałbym z całego serca podziękować **wszystkim moim drogim przyjaciołom z Polski**. Dziękuję, że zawsze mnie wspieracie pomimo dzielącej nas odległości. Dziękuję, że zawsze we mnie wierzyliście, zwłaszcza w tych trudnych czasach.

Z całego serca dziękuję mojej rodzinie - **mamie**, **tacie**, **Krzysztofowi** i **babci** za bezwarunkową miłość i niesłabnące wsparcie moich szalonych pomysłów. Dziękuję, że dajecie mi możliwość rozwoju i spełniania marzeń. Ta praca powstała tylko dzięki Wam.

I would like to thank my husband **Daniel Müller-Komorowska** for always supporting me - being the best fan and critic of my work. Thank you for always believing in me. I cannot wait to see what awaits us. I love you.